Unraveling TRIM71-mediated RNA regulatory mechanisms during developmental and oncogenic processes

Dissertation

zur

Erlangung des Doktorgrades (Dr. rer. nat.)

der

Mathematisch-Naturwissenschaftlichen Fakultät

der

Rheinischen Friedrich-Wilhelms-Universität Bonn

vorgelegt von

Lucia Anaís Torres Fernández

aus Valencia, Spanien

Bonn, 2019

Angefertigt mit Genehmigung der Mathematisch-Naturwissenschaftlichen Fakultät der Rheinischen Friedrich-Wilhelms-Universität Bonn

1. Gutachter: Prof. Dr. Waldemar Kolanus

2. Gutachter: Prof. Dr. Michael Pankratz

Tag der Promotion: 30.04.2020

Erscheinungsjahr: 2020

Contents

Preliminary Remarks

I hereby declare that I wrote the present dissertation without sources other than indicated in the main text and without help from third parties. I have designed and conducted all the experiments described in this thesis, except for the computational modeling of the human TRIM71 NHL domain native structure, which was kindly provided by Prof. Dr. Matthias Geyer (Institute of Structural Biology, University of Bonn). According to the common practice in English scientific writing, the present dissertation is drafted using the first-person plural.

Parts of this dissertation, present in the section 4.2. Results, Chapter II: TRIM71-mediated mRNA regulation, have been published:

The mRNA repressor TRIM71 cooperates with Nonsense-Mediated Decay factors to destabilize the mRNA of CDKN1A/p21 (2019). Lucia A Torres-Fernández, Bettina Jux, Maximilian Bille, Yasmine Port, Karin Schneider, Matthias Geyer, Günter Mayer, Waldemar Kolanus. *Nucleic Acids Res.* gkz105.

Abbreviation List

A	Adenine
aa	Amino acid
AML	Acute myeloid leukemia
ANOVA	Analysis of variance
AP	Alkaline phosphatase
APS	Ammonium persulfate
AUC	Area under curve
BB	B-Box domain
BCA	Bicinchoninic acid
bp	Base pair(s)
BSA	Bovin serum albumin
C	Cytosine
C. elegans	Caenorhabditis elegans (nematode)
CC	Coiled-coil domain
CDKs	Cyclin-dependent kinases
cDNA	Complementary deoxyribonucleic acid
CDS	Coding sequence
CH	Congenital Hydrocephalus
CKIs	Cyclin-dependent kinase inhibitor
CNS	Central nervous system
cpm	Counts per minute
CSCs	Cancer stem cells
CSD	Cold shock domain
CSF	Cerebrospinal fluid
Ct	Threshold cycle value
D. melanogaster	Drosophila melanogaster (fruitfly)
D. rerio	Danio rerio (zebrafish)
DABCO	1, 4-diazabicyclo[2.2.2]octane
DAPI	4’, 6-diamidino-2-phenylindole

ddH2O	Double-distilled water
DECID	Decay-inducing complex
DMEM	Dulbecco's modified Eagle medium
DMSO	Dimethyl sulfoxide
DNA	Deoxyribonucleic acid
DNase	Desoxyribonuclease
dNTPs	Deoxyribonucleotides triphosphate
dpf	Days post-fertilization
dsRNA	Double-stranded ribonucleic acid
DTT	Dithiothreitol
E. coli	Escherichia coli (bacteria)
EC	Embryonic Carcinoma
ECL	Enhanced chemiluminescence
EDTA	Ethylenediaminetetraacetic acid
EGTA	Ethyleneglycotetraacetic acid
EJC	Exon-junction complex
ESCs	Embryonic stem cells
et al.	*et alia* (and others)
EtOH	Ethanol
FACS	Fluorescence-activated cell sorting
FBS	Fetal bovine serum
Fig.	Figure
FLN	Filamin domain
For	Forward primer
G	Guanine
GFP	Green fluorescent protein
GOI	Gene of interest
HBS	HEPES buffered saline
HCC	Hepatocellular carcinoma
HEPES	4-(2-hydroxyethyl)-1-piperazineethanesulfonic acid
hpt	Hours post-transfection
HRP	Horseradish peroxidase

ICM	Inner cell mass
IF	Immunofluorescence
Ig	Immunoglobulin
IP	Immunoprecipitation
iPSCs	Induced pluripotent stem cells
KD	Knockdown
kDa	Kilo Daltons
KO	Knockout
LIF	Leukemia inhibitory factor
mESCs	Mouse/murine embryonic stem cells
MFI	Median fluorescence intensity
miRNA	Micro-ribonucleic acid
MPA	Mycophenolic acid
mRNA	Messenger ribonucleic acid
MS	Mass spectrometry
NMD	Nonsense-mediated decay
NPCs	Neural progenitor cells
NSCs	Neural stem cells
NSCLC	Non-small cell lung cancer
nt	Nucleotide(s)
NTPs	Nucleotide(s) triphosphate
OD	Optical density
Oligo(s)	Oligonucleotide(s)
ON	Overnight
ORF	Open reading frame
PAGE	Polyacrylamide gel electrophoresis
PBS	Phosphate buffered saline
PCR	Polymerase chain reaction
Pen/Strep	Penicillin and Streptomycin
PFA	Paraformaldehyde
PLL	Poly-L-lysine
PMSF	Phenylmethylsulfonyl fluoride

pre-miRNA	Precursor micro-ribonucleic acid
pri-miRNA	Primary micro-ribonucleic acid
PTC	Premature termination codon
PTMs	Post-translational modification(s)
RA	Retinoic acid
RBPs	Ribonucleic acid-binding protein(s)
Rev	Reverse primer
RFP	Red Fluorescent protein
RING	Really interesting new gene
RISC	Ribonucleic acid-inducing silencing complex
RNA	Ribonucleic acid
rpm	Rounds per minute
RPMI	Roswell Park Memorial Institute
rRNA	Ribosomic ribonucleic acid
RT	Room temperature
SD	Standard deviation
SDS	Sodium dodecyl sulfate
SEM	Standard error of the mean
siRNA	Small interfering ribonucleic acid
SMD	Staufen-mediated decay
snRNA	Small nuclear ribonucleic acid
ssRNA	Single-stranded ribonucleic acid
SURF	Surveillance Complex (SMG1-UPF1-eRF1-eRF3)
T	Thymine
TAE	Tris acetate EDTA
TBS	Tris buffered saline
TBST	Tris buffered saline with Tween
TEMED	Tetramethylethylendiamine
TGCT	Testicular germ cell tumor
TK	Thymidine kinase
TRIM	Tripartite motif
TSSCs	Tissue-specific stem cells

U	Uracil
uORF	Upstream open reading frame
UTR	Untranslated region
UV	Ultraviolet
WB	Western blot
WT	Wild type
λP	Lambda phosphatase

1. Introduction

1.1. An overview of stem cell types, characteristics and their use in clinics and research

Stem cells are characterized by the capability of self-renewal and differentiation into specialized cell types. Self-renewal refers to the ability of stem cells to continuously divide while maintaining an undifferentiated state, whereas differentiation involves the ability of stem cells to commit to specific linages in order to produce a mature functional progeny. In mammals, there are two major types of stem cells: embryonic stem cells (ESCs), which tightly coordinate the development of an organism, and adult stem cells, also known as tissue-specific stem cells (TSSCs), which enable the homeostatic renewal and damage repair of a given tissue. Stem cells can be further classified according to their niche (localization or tissue of origin) and their potency (differentiation potential)[1] (Fig. 1.1).

During mammal development, when a sperm cell fertilizes an oocyte, the single diploid cell known as zygote undergoes several mitotic divisions with no significant growth in a process called cleavage, in order to form a cluster of sixteen cells called morula (3-4 days post-fertilization (dpf)). The cells within a morula are called blastomeres and are totipotent ESCs which can give rise to all embryonic and extraembryonic tissues. These cells undergo then a blastulation process which involves the earliest segregation of lineages in the developing embryo, concluding with the formation of a blastocyst (4-5 dpf). The blastocyst contains an outer layer of cells called the trophoblast, surrounding the blastocyst cavity or blastocoel, which shelters the inner cell mass (ICM) located at the so-called embryonic pole. While the cells of the trophoblast are committed to form extraembryonic tissues such as placenta and umbilical cord to nourish the embryo, the cells from the ICM are pluripotent ESCs which can differentiate into all three embryonic layers (ectoderm, mesoderm and endoderm). The different embryonic layers give rise to all cell types in the embryo proper, including somatic and germ cells. Although differentiation of stem cells into their committed linages is immediately associated with a loss of potency, the cells of each embryonic layer are also considered pluripotent ESCs. Each embryonic layer can give rise to several types of multipotent TSSCs, endowed with self-renewal capacity and able to differentiate into multiple cell types of a specific tissue. Differentiation of TSSCs usually occurs through the formation of committed progenitor cells with a more limited self-renewal capacity. Progenitor cells further differentiate into precursor cells, which are slow-dividing, undifferentiated but linage-committed cells, which ultimately differentiate terminally into a specialized cell type. Progenitor and precursor cells are typically oligo- or unipotent[1] (Fig. 1.1).

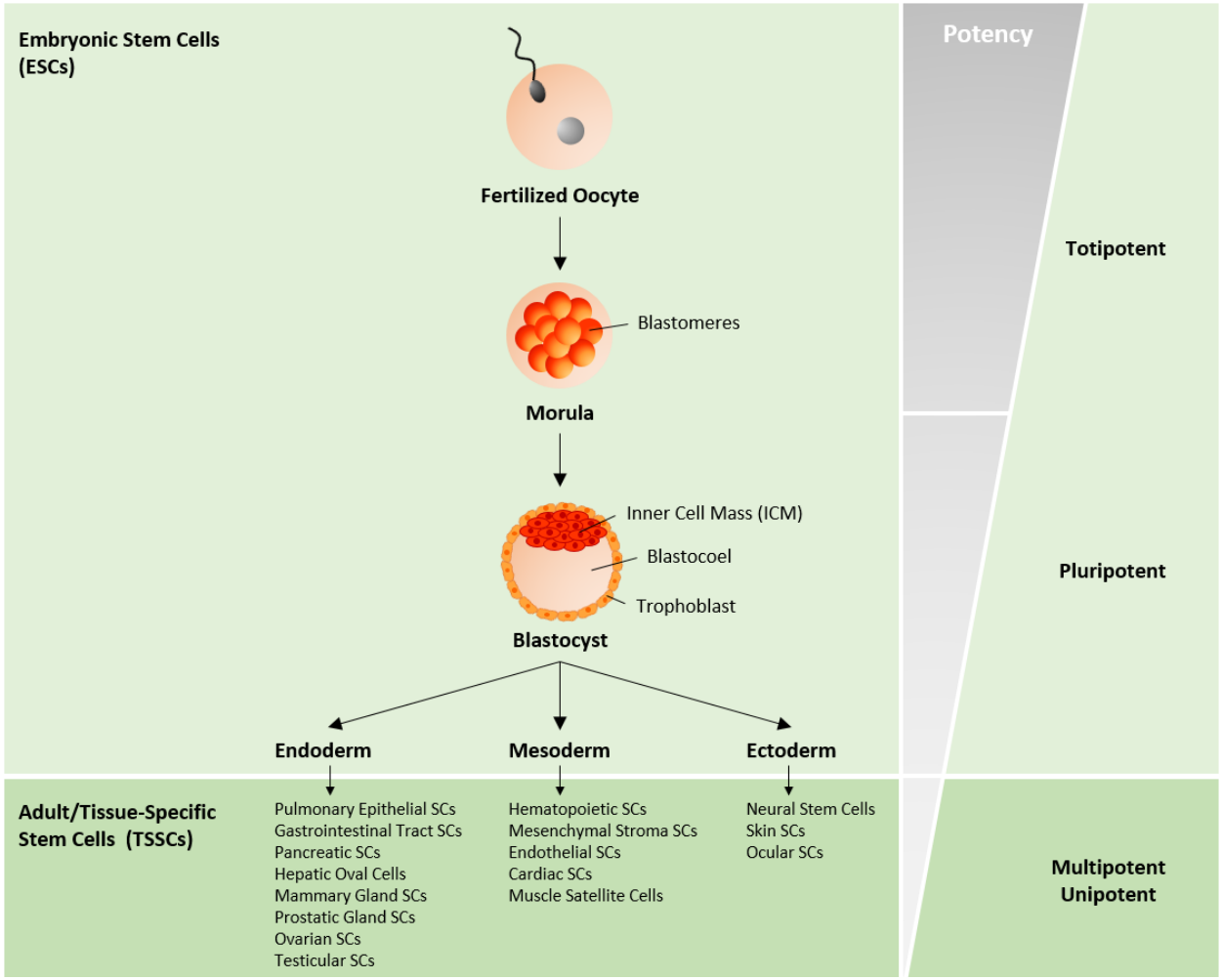

Figure 1.1. Stem cell types in the developing embryo and the adult organism. Embryonic stem cells (ESC) refer to all totipotent and pluripotent stem cells present during early embryonic development, which can differentiate into all somatic and germ cells within the embryo proper. Tissue-specific stem cells (TSSCs) refer to all multipotent and unipotent stem, progenitor and precursor cells present in the adult organism, which retain their capability of self-renewal and differentiation within a given tissue.

Because of their enormous potential for clinical applications in the fields of organ transplantation and tissue engineering, stem cells are being widely investigated in recent years. ESCs can be isolated from the ICM of an embryo and propagated *in vitro* indefinitely under specific conditions, as well as differentiated into multiple adult cell types. However, the use of human embryo material is highly controversial due to ethical reasons. Furthermore, controlling ESCs differentiation *in vivo* is specially challenging and usually results in teratoma formation[2]. Besides, ESCs transplantation has been shown to be highly immunogenic, thereby requiring immunosuppression to avoid rejection[3]. For all these reasons, there are no current treatments based on ESCs transplantation. Adult stem cell therapy is however widely accepted and has been successfully used for the treatment of several diseases, but the sources of adult stem cells are limited (bone marrow, blood and adipose tissue), and so is their potency. Overcoming the limitations of ESCs and TSSCs, induced pluripotent stem cells (iPSCs) can be generated by somatic cell reprogramming, and are used for several purposes in clinics and research[1] (Fig. 1.2).

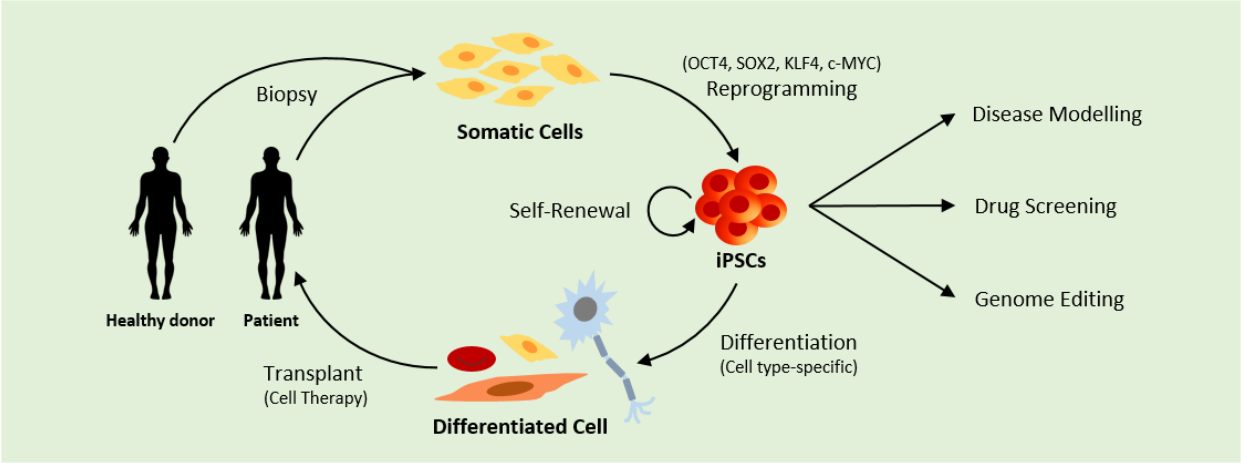

Figure 1.2. Generation and uses of induced pluripotent stem cells (iPSCs). Somatic cells can be obtained from the patient or a healthy donor and reprogrammed to iPSCs by the addition of specific pluripotency factor cocktails. iPSCs have the capability of self-renewal and differentiation into the required cell type by the addition of specific differentiation cocktails. Differentiated cells can be then transplanted into the patient. iPSCs can be subjected to genome editing before transplantation. Besides being used for cell therapy, iPSCs can be used for disease modelling and drug screening in order to develop new non-cell-based treatments.

iPSCs were first generated by Yamanaka and colleagues (Kyoto University) though the overexpression of stem cell-specific transcription factors (OCT4, SOX2, KLF4 and c-MYC) in mouse fibroblasts[4]. Later research identified alternative reprogramming cocktails for the generation of iPSCs from human somatic cells[5]. iPSCs are similar to ESCs in self-renewal and differentiation potential, but they can be derived from the patient's cells and differentiated *in vitro* prior to their transplantation, reducing the risks of rejection and teratoma formation, as well as overcoming ethical issues. TSSCs and iPSCs are currently under heavy investigation for the development of treatments for some of the most devastating human diseases, including neurodegenerative diseases such as Alzheimer or Parkinson, as well as heart disease and diabetes[6,7].

Despite the fact that they cannot be used in clinics, murine ESCs (mESCs) are widely used in research, as they offer a unique opportunity to understand the basics of embryonic development and the mechanisms underlying human developmental diseases. Furthermore, stem cell biology and cancer biology cannot be separated from one another, since oncogenic transformation reflects the reprogramming or dedifferentiation of somatic cells into an earlier and more potent stage, which uncontrolledly proliferate driving tumorigenesis, and even differentiate into several cancer cell types to form solid heterogeneous tumors[8]. Indeed, although their existence has been in debate for years, cancer stem cells (CSCs) are now known to be the cells able to self-renew and differentiate into multiple cell types within a tumor, resembling very much ESCs during development[9]. CSCs constitute only a small subpopulation of all tumor cells, and are responsible for tumor initiation and maintenance, as well as for tumor relapse and metastasis after conventional therapies[10] (Fig. 1.3). Therefore, new therapies aim at targeting molecules specifically controlling proliferation and survival of CSCs. In this regard, the identification of stem cell-specific cues and the investigation of their functional mechanisms constitutes one of the most promising avenues for the development of high-efficiency cancer-targeted therapies with minimal side effects.

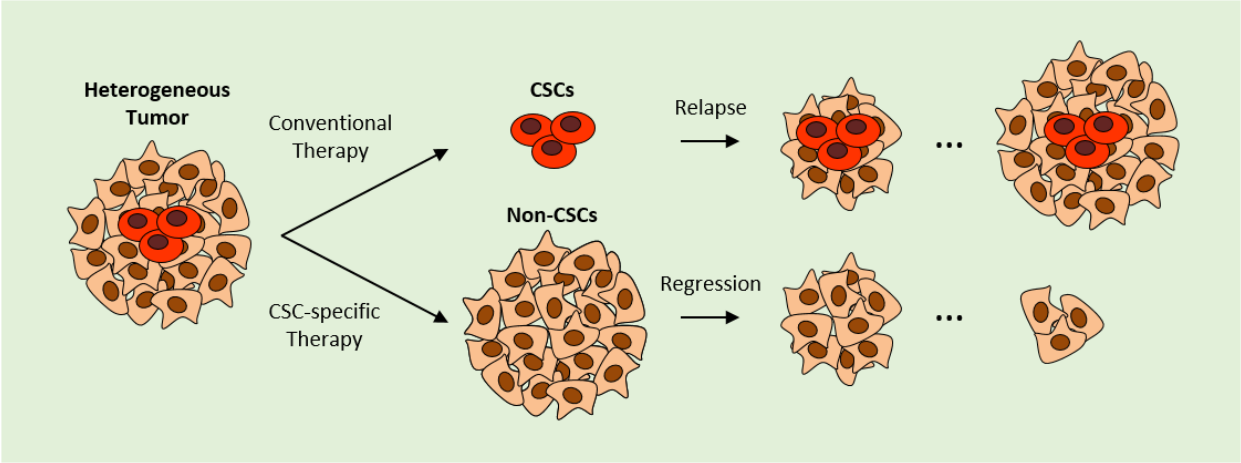

Figure 1.3. Cancer stem cells (CSCs) are responsible for tumor initiation and maintenance. Conventional therapies targeting general tumor cell characteristics can result in tumor relapse due to the capability of CSCs to self-renew and differentiate into multiple tumor types. Therefore, therapies based on the specific targeting of CSCs could successfully lead to tumor regression.

Understanding the molecular regulation of pluripotency is fundamental, not only for the development of CSCs-targeting therapies, but also for the safe and efficient application of stem cell therapies. Stem cells are not merely characterized by the expression of pluripotency-promoting factors such as OCT4, SOX2 or NANOG, but by a whole network of stem cell-specific cues such as surface markers, RNA-binding proteins and miRNAs, as it will be discussed later. Furthermore, the identity of a stem cell relies on a specific chromatin architecture and specific metabolic profiles that together sustain the pluripotent state.

Pluripotency is characterized by a globally "open-chromatin" state with abundant levels of epigenetic marks that are indicative of active transcription[11]. At this stage, lineage-specific genes contain bivalent histone marks and remain in a poised state, locally repressed by specific regulators until differentiation is triggered. In the course of differentiation, lineage-specific genes are rapidly activated while chromatin remodelers start "closing" specific chromatin domains in order to shape the transcriptional profile which is programmed for the committed linage[11]. A histone mark commonly associated with transcriptional repression is methylation of histone H3K9, which is known to increase upon differentiation[12]. OCT4 activates the expression of several histone demethylases which maintain the low methylation levels of H3K9 characteristic of undifferentiated ESCs[13]. In the course of differentiation, the histone methyl transferase G9a is upregulated and binds to the promoter of target genes, including OCT4, leading to H3K9 methylation and repressing their expression[14]. These examples superficially illustrate how the cross-talk between pluripotency factors and chromatin remodelers tightly regulate the open-close chromatin switch in the proliferation-differentiation balance. Conversely, the process of reprogramming somatic cells into iPSCs is accompanied by a remodeling of the epigenome[11,15].

The metabolic profile also distinguishes the pluripotent from the differentiated state[16]. Stem cells show an upregulation of glycolytic key enzymes which sustain a glucose-based metabolism, enabling their rapid growth[17]. Upon differentiation, an increase in mitochondrial DNA accompanied by changes in mitochondrial morphology drive the shift to an oxidative metabolism[16,18]. Stem cells are also characterized by a high content of unsaturated lipids which enhance membrane fluidity to facilitate subsequent division

rounds[19]. Indeed, lipid unsaturation has been reported to be a hallmark of CSCs and the inhibition of lipid desaturases was shown to impair CSCs stemness and to prevent tumor formation[20]. Furthermore, the abundance of proteins associated with RNA processing and protein folding is higher in ESCs, whereas proteins associated with redox and vitamin metabolism have been found to be more abundant in differentiated cells[21]. All these mechanisms illustrate how the biology of stem cells is tightly coordinated to orchestrate the fulfilment of their two main functions, self-renewal and differentiation, which are ultimately driven by progressive changes occurring in the regulation of their cell cycle.

1.2. Cell cycle regulation during embryonic development and cancer

The cell cycle is defined as the group of progressive stages that a mother cell undergoes to achieve cell division into two daughter cells[22] (Fig. 1.4A). In eukaryotes, the cell cycle is divided into two major stages: the interphase, which is a preparatory phase during which cell growth, DNA replication and nutrient accumulation are sustained, and the mitotic phase (M), in which the separation of the replicated genetic material occurs, and the cytoplasm, organelles and cell membrane are divided into two daughter cells by a process called cytokinesis. The interphase itself is divided in three phases. The first intervening gap phase (G1) starts after the previous M phase and is therefore also known as post-mitotic gap phase. G1 is a growth phase in which a highly active metabolism enables an increase in protein supply and organelle number. The G1 phase concludes with a G1/S checkpoint control mechanism that ensures that everything is ready for the coming synthesis phase (S), in which DNA replication occurs resulting in each chromosome having two sister chromatids. The interphase concludes with a second intervening gap phase (G2) in which the cell continues to grow, and ends with a G2/M checkpoint control mechanism that ensures that everything is ready for mitosis. The core engines that drive eukaryotic cell cycle progression are protein heterodimeric complexes of Cyclins and associated kinases known as Cyclin-dependent kinases (CDKs). Cyclin-CDK complexes can be inhibited by inactivating phosphorylation or upon binding to CDK inhibitors (CKIs), thereby preventing cell cycle progression and promoting the entrance in the G0 phase. G0 is a quiescent state enabling temporary cell cycle exit under unfavorable conditions or long-term cell cycle arrest upon terminal differentiation or senescence[22] (Fig. 1.4A).

Embryonic development is a tightly regulated process requiring the generation of large numbers of cells, which at the appropriate times acquire specialized functions and specific morphologies, while assembling into defined tissues and organs. Most cells follow a gradual process of specialization accompanied by a progressive potency loss, which concludes with the acquisition of a terminally differentiated state. Cell cycle phases and their duration are shaped during subsequent developmental stages[23] (Fig. 1.4B). The proper temporal coupling of these changes along with the proliferation-differentiation balance is crucial for normal growth and development, and continues to be critical for tissue homeostasis and cell replacement throughout life. A failure in the control of cell cycle progression and cell cycle arrest mechanisms can lead to a variety of developmental diseases, as well as resulting in oncogenic transformation[24] and neurodegenerative diseases[25] in the adult organism.

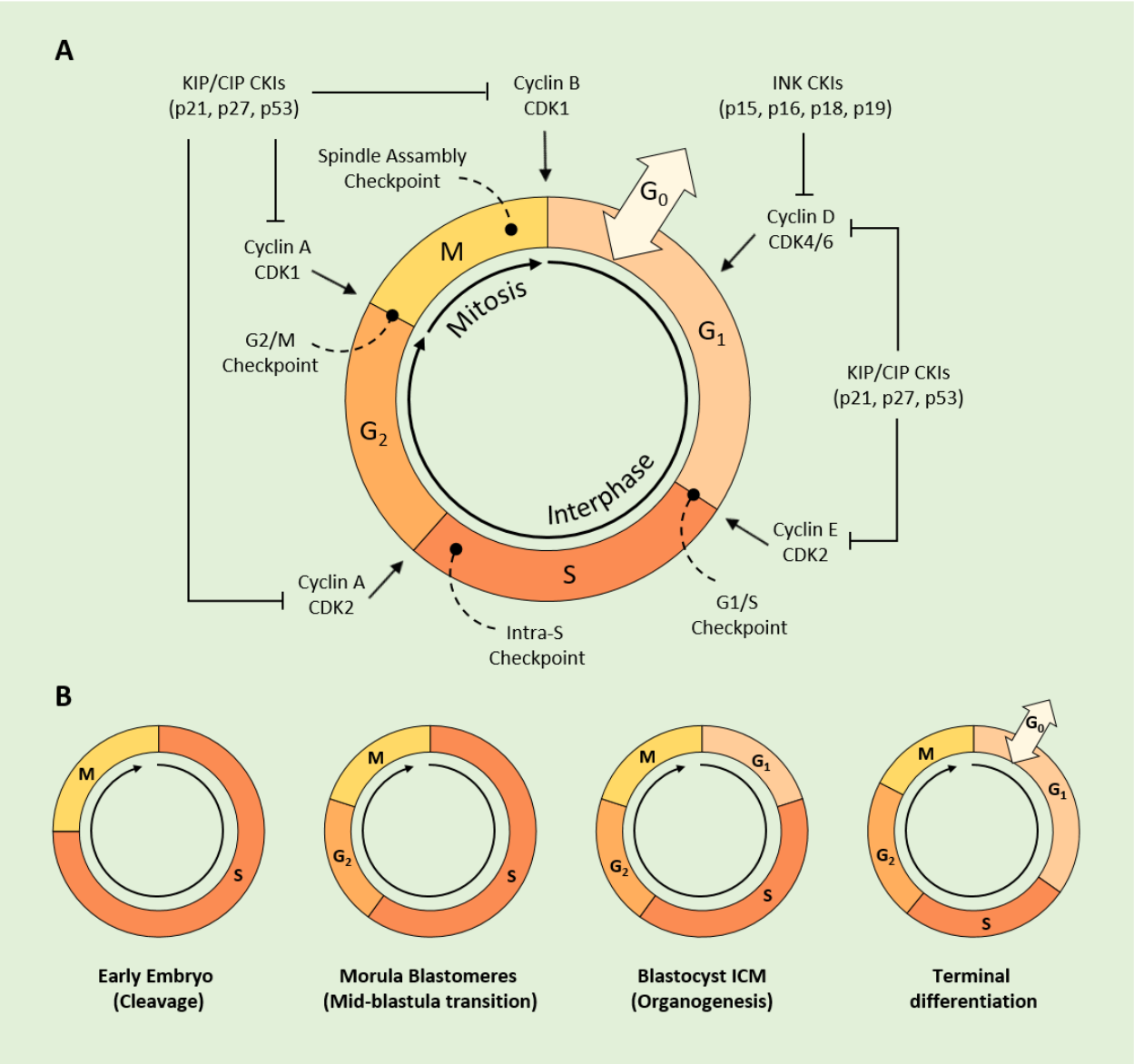

Figure 1.4. Cell cycle phases and their modulation during development. A) Cell cycle phases of a proliferating cell in a developed organism. As specified in the main text, cell cycle progression is driven by several Cyclin-CDK heterodimeric complexes, controlled by cell cycle checkpoints at various stages, and can be specifically inhibited by different families of CKIs. **B)** Modulation of the cell cycle during development (adapted from [23]). In the early embryo, during the cleavage process, the cell cycle is driven by maternal components and alternates between S and M phases. At the mid-blastula transition, there is a switch from maternal to zygotic transcription and a G2 phase is introduced in the cell cycle of the blastomeres (totipotent ESCs within a morula). After the first event of linage segregation, pluripotent ESCs of the blastocyst ICM incorporate a short G1 phase in their cell cycle that enables rapid but controlled cell divisions in order to drive differentiation, first into the three embryonic layers and later organogenesis. In the course of differentiation, there is a progressive prolongation of the G1 phase[26], and in the last stages of organogenesis, the G0 phase is introduced and terminal differentiation results in cell cycle exit. Terminally differentiated cells undergoing malignant transformation re-enter the cell cycle and drive tumorigenesis[24]. Cell cycle re-entry has also been observed in neurons during neurodegenerative diseases[25].

In order to exert a proper control of cell cycle progression and cell cycle arrest, positive and negative cell cycle regulators are differentially expressed during development or even during different cell cycle phases[27]. This is the case of cyclins for instance, which are synthesized and degraded in periodic oscillations, ensuring unidirectional cell cycle progression[23]. During cell cycle progression, if cells commit in the G1 phase to enter the S phase, the Cyclin D-CDK4/6 complex phosphorylates the tumor suppressor retinoblastoma protein pRB. Unmodified pRB sequesters the transcription factor E2F1, whereas pRB phosphorylation results in the release of E2F1, which activates the transcription of genes required for the G1/S transition, including Cyclin E. The Cyclin E-CDK2 complex further phosphorylates pRB, whereas E2F1 stimulates its own transcription, creating a positive-feedback loop that promotes S phase entry[28].

Inhibition of cell cycle progression from G1 into S leads to cell cycle arrest in G0 and can occur due to nutrient unavailability, DNA damage, or be signalized by cell fate determinants that trigger terminal differentiation. In this regard, members of two different families of CKIs play an essential role. CKIs of the INK protein family (p15, p16, p18 and p19) bind specifically to CDK4/6 preventing their interaction with D-type cyclins, whereas CKIs of the CIP/KIP family (p21, p27, p53) associate with CDK-cyclin complexes and block their activity[29] (Fig. 1.4A). Proteins of both CKI families contribute to cell cycle exit upon terminal differentiation, and therefore pluripotent cells have several mechanisms that ensure their absence or maintain their expression at minimal levels[30]. The expression of CKIs increases in the course of differentiation, reaching maximal levels upon terminal differentiation[31,32]. Conversely, functional inactivation of CKIs, specially p16, p21 and p53, has been observed in most cancer types[33]. Therefore, cell cycle positive and negative regulators play an essential role in both, embryonic development and cancer, and the cross-talk between cell cycle regulators and cell fate determinants generates robust regulatory networks that ensure a tight control of the proliferation-differentiation balance[27] (Fig. 1.5).

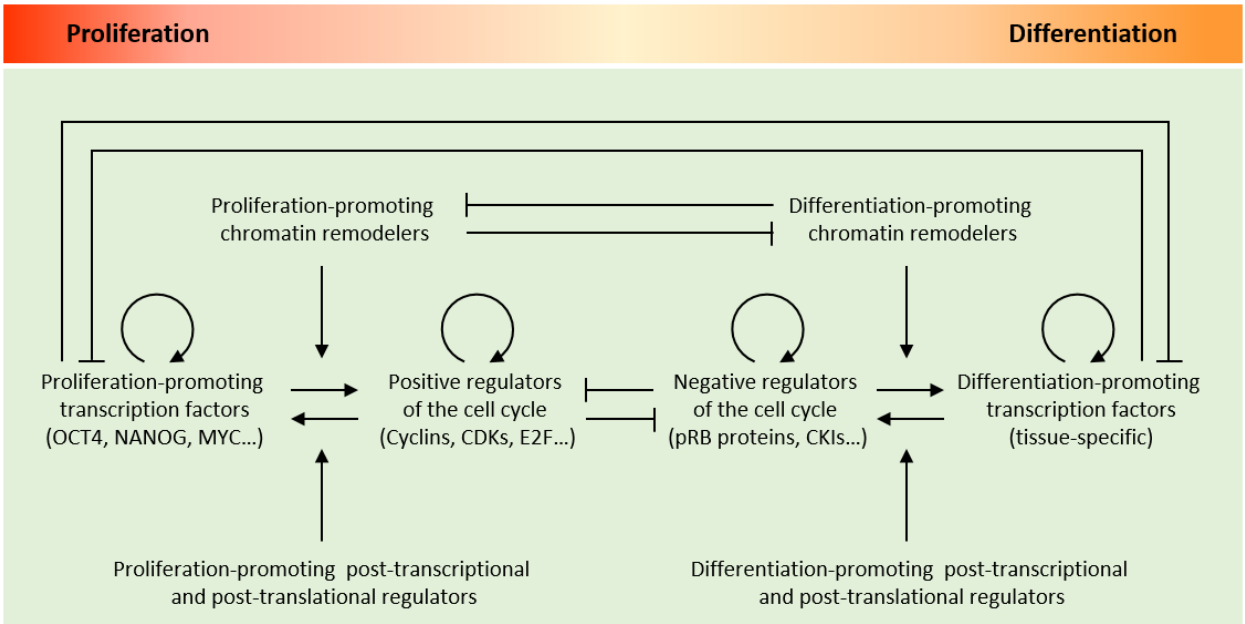

Figure 1.5. Regulation of the proliferation-differentiation balance. Major components participating in the regulatory networks controlling the balance between proliferation and differentiation during embryonic development and cancer (adapted from[27]).

1.3. RNA surveillance mechanisms in the control of proliferation and differentiation

A great number of ESCs-specific miRNAs and RNA-binding proteins reinforce the pluripotency network established by the aforementioned mechanisms. Therefore, post-transcriptional regulatory mechanisms add another layer of complexity to the maintenance of pluripotency in ESCs. In this regard, two major RNA surveillance pathways, namely the miRNA-mediated mRNA silencing pathway and the Nonsense-mediated mRNA decay pathway, will be discussed.

1.3.1. The microRNA-mediated mRNA silencing pathway

MicroRNAs (miRNAs) are small non-coding RNA molecules which function as post-transcriptional regulators via mRNA silencing. The biogenesis of miRNAs is a multi-step process involving several protein complexes that assist miRNA expression, transport, maturation and activity[34] (Fig. 1.6).

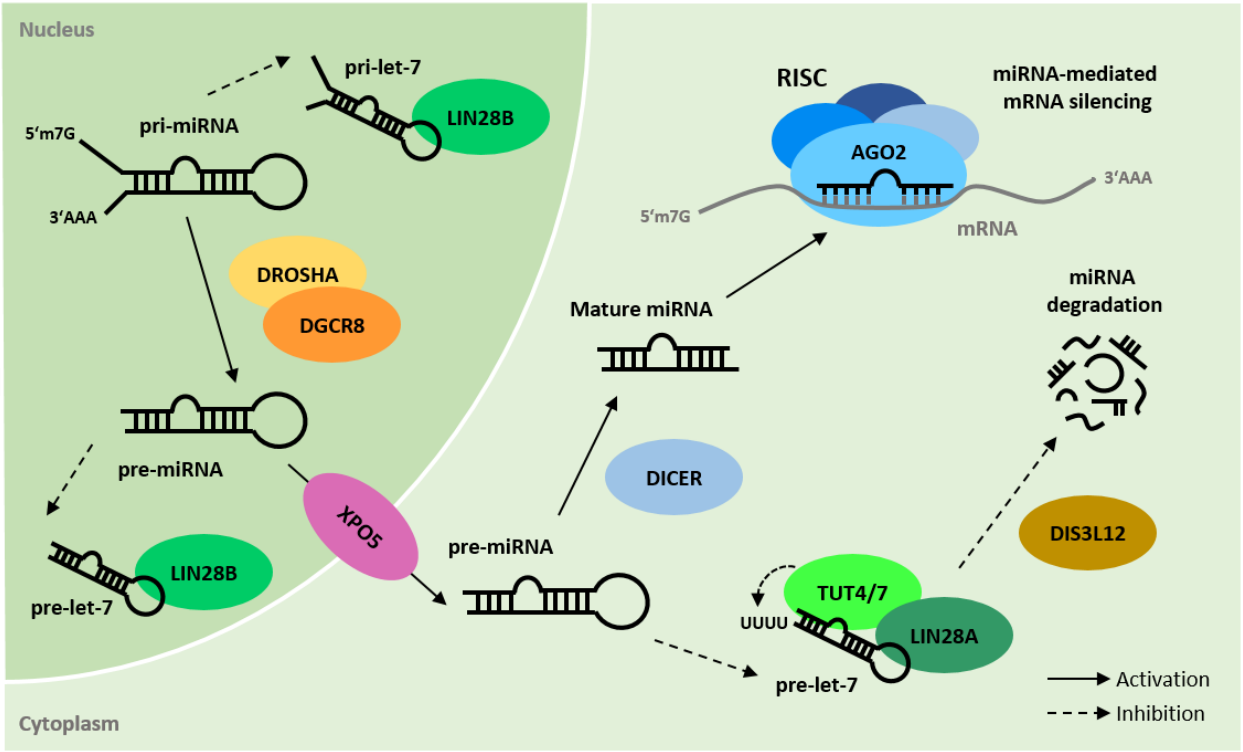

Figure 1.6. The miRNA pathway. During miRNA biogenesis, several proteins (discussed in the main text) assist their synthesis, maturation and function, promoting the activation of miRNA-mediated silencing. The inhibition of this pathway is highly cell- and miRNA-dependent. Here is depicted the specific inhibition of the pro-differentiation miRNA let-7 exerted by the stem cell-specific LIN28 proteins, which interfere at various stages of let-7 biogenesis to block its maturation and promote its degradation[35].

MiRNAs-encoding genes are transcribed by the RNA-polymerase II/III, resulting in the formation of a hairpin-looped primary miRNA molecule (pri-miRNA) of about 70 nt which undergoes conventional 5' capping and 3' poly-A-tailing. The stem-loop structure of the pri-miRNA is recognized by the microprocessor complex formed by the RNA-binding protein DGCR8 (Pasha in invertebrates) and the

ribonuclease DROSHA, which cleaves the pri-miRNA short after the hairpin base, resulting in the formation of a precursor miRNA molecule (pre-miRNA) with short overhangs. The 3' overhang of the pre-miRNA is then recognized by Exportin-5 (XPO5), which assists pre-miRNAs nuclear export. Once transported to the cytoplasm, pre-miRNAs are further processed by the endoribonuclease DICER, which interacts with the 5' and 3' overhangs of the hairpin and cuts the loop away, yielding a mature miRNA duplex of about 22 nt[34]. Usually, only one of the two strands in the duplex, the so-called guide strand, is biologically active and will be loaded on the RNA-induced silencing complex (RISC), whereas the other one, known as the passenger strand, is rapidly degraded. The major effector of the RISC complex is Argonaute protein 2 (AGO2), which directly binds the miRNA guide strand, orients it for interaction with the target mRNA, and cleaves the target mRNA directly upon complementary binding (Fig. 1.6). Other AGO proteins from the same family exert similar functions in miRNA-mediated silencing with the difference that only AGO2 mediates target mRNA cleavage, while the other AGO proteins recruit additional factors to achieve either degradation or translational repression of the target mRNA[36]. Perfect pairing of the so-called seed sequence, a highly conserved 7 nt sequence shared by all members of the same miRNA family, is usually required for miRNA-mediated silencing. Other parts of the miRNA confer further target specificity and stabilize the interaction, as well as influencing whether silencing is achieved through target degradation or translational repression, based on the degree of complementarity[37].

Whereas the above-mentioned mechanisms assisting miRNA synthesis and function operate ubiquitously and apply for most miRNAs, regulation of specific miRNAs is highly context-dependent, and therefore the miRNome is very characteristic of a specific cell type or developmental stage. The expression of ESC-specific miRNA families such as the miR-290/302 or miR-17/20/106 clusters is induced by pluripotency factors such as OCT4, SOX2 and NANOG[38,39]. These miRNAs support the rapid cell cycle of ESCs characterized by short G1 phases by targeting mRNAs encoding for cell cycle inhibitors such as CDKN1A/p21, as well as by indirectly promoting pRB hyperphosphorylation[40–42]. Furthermore, ESC-specific miRNAs counteract the activity of several pro-differentiation miRNAs like the members of the let-7 miRNA family[43]. In the undifferentiated state, DGCR8 and DICER knockout ESCs lacking mature miRNAs proliferate slower than wild type ESCs. These proliferation defects could be rescued by overexpression of the ESC-specific miR-290[42]. Upon induction of differentiation, DGCR8 and DICER knockout ESCs failed to differentiate unless ectopic let-7 miRNA expression was provided[43–45]. Apart of being counteracted by ESC-specific miRNAs, the expression of pro-differentiation miRNAs like let-7 is regulated by several other manners. For instance, the promoters of some pro-differentiation miRNAs are bound by ESCs-specific transcription factors but simultaneously repressed by Polycomb group complexes in undifferentiated ESCs[46], indicating that these miRNAs are constantly kept in a poised state in order to rapidly increase upon induction of differentiation.

Besides specific transcription factors and chromatin remodeling proteins, other negative regulators of pro-differentiation miRNAs play important roles in the maintenance of stemness. For example, the stem cell-specific RNA-binding protein LIN28 is a well-known repressor of let-7 miRNA species. Although pri- and pre-let7 miRNAs are indeed expressed in undifferentiated cells, their maturation is inhibited by LIN28 proteins, which interfere at various stages of let-7 biogenesis[35] (Fig. 1.6). There are two paralog proteins present in mammals, LIN28A and LIN28B, which are known to recognize a conserved GGAG motif within pri- and pre-let-7 stem-loop[47]. The binding of LIN28 proteins to pre-let-7 prevents further processing by

sequestration from DICER, and triggers pre-let-7 uridylation by the recruitment of the terminal uridyltransferases TUT4/7[48], tagging the precursor for degradation by the exonuclease DIS32L[49]. The LIN28B paralog protein has a nuclear localization sequence (NLS) and can additionally bind pri-let-7 and pre-let-7 miRNAs in the nucleus, preventing further processing and export, respectively[50]. These mechanisms strongly contribute to keeping low mature let-7 levels in ESCs while ensuring fast let-7 upregulation upon differentiation. LIN28A has been used in exchange of c-MYC in combination with OCT4, SOX2 and NANOG for the reprograming of somatic cells into iPSCs[5]. Interestingly, the transcription factor c-MYC negatively regulates the expression of let-7 by direct transcriptional repression[51] as well as indirectly by transcriptional activation of LIN28 expression[52]. Furthermore, both c-MYC and LIN28 are let-7 targets, thereby being downregulated as let-7 expression increases upon differentiation. Indeed, inhibiting let-7 in human cells promoted their reprogramming to iPSCs to a comparable extent to c-MYC or LIN28 when combined with OCT4, SOX2, and KLF4[53]. Altogether, these findings highlight the importance of the LIN28/let-7 axis the control of proliferation and differentiation, as well as illustrating that the proper regulation of the miRNA pathway is critical for the functionality of ESCs.

1.3.2. The Nonsense-Mediated mRNA Decay pathway

Nonsense-Mediated Decay (NMD) is well known as a quality control pathway for the detection and elimination of transcripts containing a premature termination codon (PTC)[54]. However, in the last years, it has become evident that many functional transcripts are also degraded by NMD[55,56], although such "non-canonical" functions remain poorly understood. Thereby, NMD not only plays an essential role preventing the production of aberrant truncated proteins, but also participates in the regulation of various physiological and pathological processes, including embryonic development and cancer[57,58].

The canonical NMD pathway is activated upon an aberrant or premature translation termination during the pioneer round of translation[59] (Fig. 1.7). Discerning between a PTC and the normal stop codon is crucial for NMD initiation. After splicing, the mature mRNA is exported to the cytoplasm and contains several exon junction complexes (ECJs) bound 20-25 nt upstream of each exon-exon boundary[60]. Since EJCs are displaced by the ribosome during the first round of translation, usually no EJCs remain bound to the mRNA when the ribosome stalls at the normal stop codon, which is typically present in the last exon[60,61]. Therefore, a PTC is signaled by the presence of an EJC located downstream of the terminating ribosome[62]. In this context, UPF1 – the major NMD effector – and its activating kinase SMG1, are recruited together with the release factors eRF1 and eRF3 to form the surveillance complex (SURF). The SURF complex then interacts with other NMD effectors present in the EJC – UPF2 and UPF3b – to form the decay-inducing complex (DECID), resulting in SMG1 activation and subsequent UPF1 phosphorylation. Phosphorylated UPF1 recruits other proteins assisting target mRNA degradation, namely the SMG5-SMG7 dimer, which trigger CCR4-NOT-mediated deadenylation and DCP2-mediated decapping, and the endonuclease SMG6, which cleaves the mRNA in the vicinity of the PTC. The downstream RNA products are then subjected to 3'-5' and 5'-3' exonucleolytic decay by the exosome complex and XRN1, respectively[57] (Fig. 1.7).

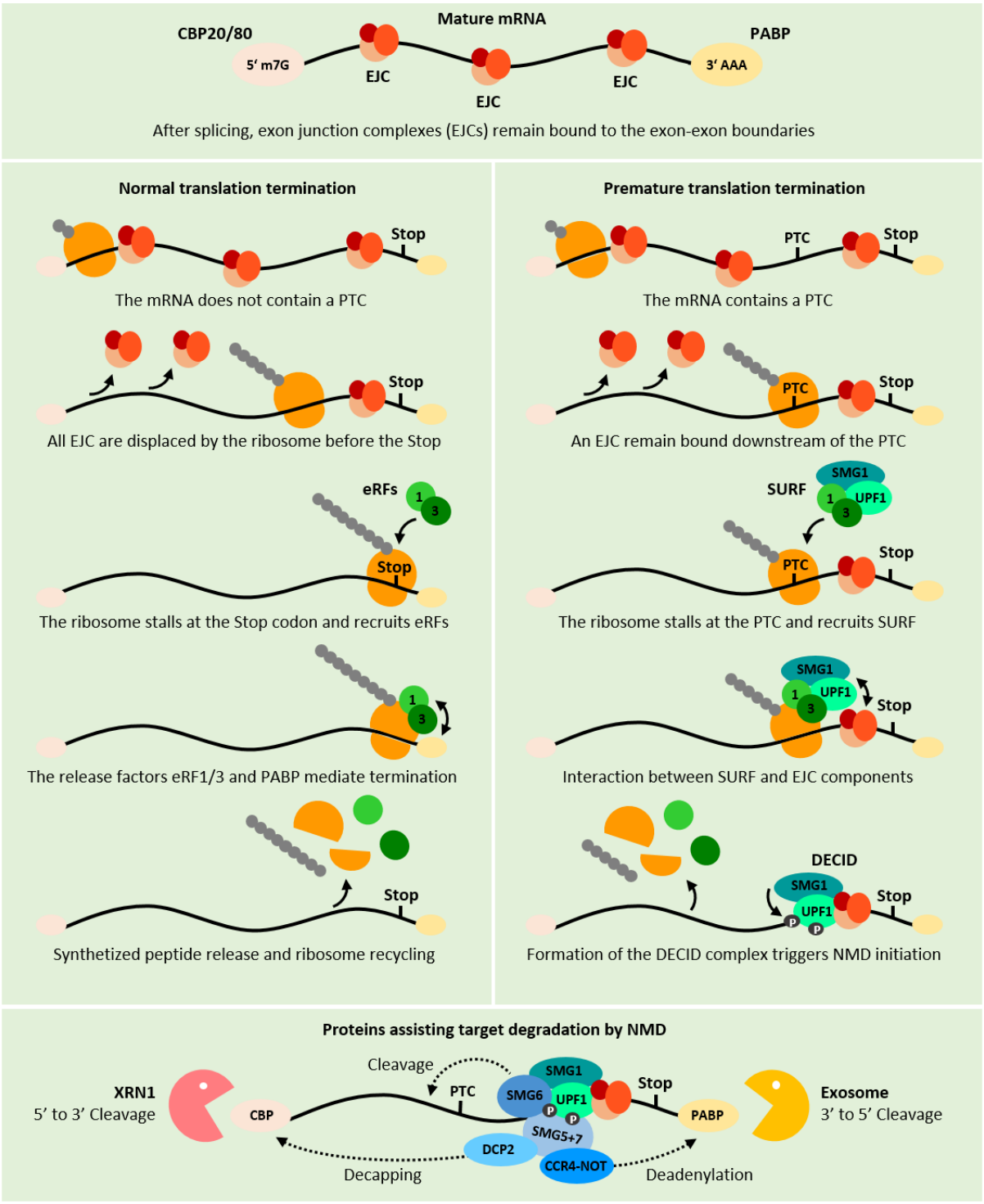

Figure 1.7. The Nonsense-Mediated Decay (NMD) pathway. In the pioneer round of translation, a normal termination (left panel) is driven by the recruitment of the release factors eRF1/3 to the terminating ribosome and their interaction with the downstream poly-A-binding protein (PABP). In contrast, a premature or aberrant termination (right panel) is triggered by the presence of an exon junction complex (EJC) downstream of the terminating ribosome, mediating the recruitment of UPF1 and SMG1 together with the release factors to form the surveillance complex (SURF). The interaction between SURF and the EJC results in the formation of a decay-inducing complex (DECID), which triggers NMD initiation by SMG1-mediated UPF1 phosphorylation. Phosphorylated UPF1 act as a platform recruiting other proteins assisting target mRNA degradation (down panel).

The so-called EJC model explains how NMD triggers the degradation of PTC-containing transcripts (canonical pathway), which include not only aberrant transcripts with nonsense mutations, but also transcripts with upstream reading frames (uORF) resulting from alternative splicing, transcripts encoding for selenoproteins, in which the stop codon UGA can be redefined to encode for selenocysteine in a high-selenium environment, and transcripts with introns in their 3'UTR, which lack a PTC but contain an EJC bound downstream of the normal stop codon[58]. However, NMD is known to regulate many transcripts lacking any of these features[63], and EJC-independent NMD mechanisms (non-canonical pathway) have been previously reported[64]. An atypically long 3'UTR is one of the most common features of PTC-lacking NMD targets[65,66]. However, neither UTR length nor any of the aforementioned RNA features *per se* guarantees a reliable prediction of NMD targets[63,67], suggesting that non-canonical NMD may be highly target-specific. Hence, the signals and factors triggering NMD of PTC-lacking mRNAs remain to be investigated for specific targets and cellular contexts.

Most NMD components are essential for embryonic development[68] and NMD has been shown to play crucial roles in the regulation of proliferation and differentiation, thereby controlling stem cell fates[69]. Specifically, ESCs rely on NMD for their proliferation, while differentiation is typically associated with a downregulation of NMD activity. For instance, UPF1 promotes the self-renewal of mESCs[70] as well as neural stem cells (NSCs)[71]. Knockdown of UPF1 results in a reduced expression of the pluripotency markers NANOG and OCT4, and a simultaneous upregulation of the neuronal lineage markers SOX1 and NESTIN[71]. Furthermore, proper differentiation of NSCs requires the upregulation of the brain-specific pro-differentiation miR-128, which targets UPF1 mRNA, thereby decreasing NMD activity[72]. Similarly, NMD activity is attenuated during myogenesis. Specifically, differentiating myoblasts upregulate the expression of STAU1 and STAU2, the major effectors of another RNA surveillance pathway called Staufen-mediated decay (SMD). SMD is triggered by the binding of STAU proteins to STAU-binding sites within the 3'UTR of target mRNAs[73]. Both STAU1 and STAU2 interact directly with UPF1, enhancing its helicase activity to promote effective SMD. Therefore, SMD and NMD are competitive pathways, and the upregulation of STAU proteins in developing myoblasts result in the downregulation of NMD and the consequent upregulation of the NMD target myogenin, which drives differentiation of myoblasts into myotubes[74]. A similar mechanism involving NMD downregulation at expenses of SMD upregulation operates in the differentiation process of adipocytes[75]. NMD is also involved in lymphocyte development[76], granulocyte differentiation[77] and spermatogenesis[78]. Altogether, these findings illustrate how deregulation of NMD can affect development, and furthermore highlight the importance of understanding how NMD influences and is influenced by pluripotency-sustaining networks in ESCs and cancer cells.

1.4. The stem cell-specific protein TRIM71/LIN41

1.4.1. The TRIM-NHL protein family

TRIM71, also known as LIN41, is a stem cell-specific protein which belongs to the TRIM-NHL protein family. The TRIM (Tripartite motif) family of proteins is characterized by the presence of the so-called RBCC domain in its N-terminus, consisting of a RING finger domain followed by one or two B-box (BB) zinc finger domains and a coiled-coil (CC) region[79]. Intrinsic E3 ligase activity of the RING domain provides TRIM

proteins with ubiquitylation capability[80], whereas the CC region mediates protein-protein interactions allowing the formation of high-order homo- and heteromeric structures[81]. TRIM-NHL proteins are a highly-conserved subclass of the TRIM family which contain in their C-terminus several copies (2-6) of a 44-aa sequence denominated NHL repeat, in some cases preceded by a Filamin domain (FLN)[82] (Fig. 1.8). The NHL domain has been reported to mediate RNA interaction[83–85], suggesting an involvement of TRIM-NHL proteins in RNA surveillance pathways. Therefore, based on their structural domain organization, TRIM-NHL proteins can potentially act as post-transcriptional regulators via RNA binding, or as post-translational regulators via protein ubiquitylation.

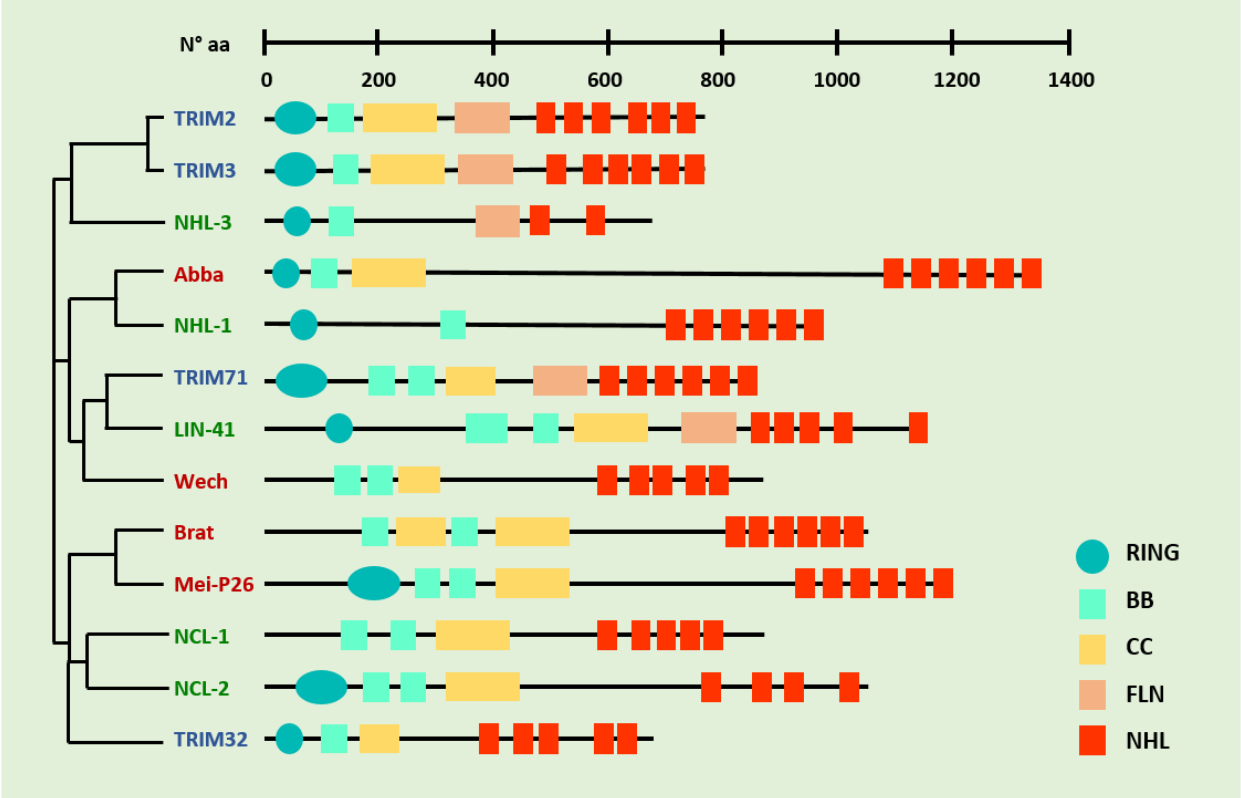

Figure 1.8. Overview of the TRIM-NHL protein family members in different species. A neighbor-joining phylogenetic tree was generated by ClustalW multiple alignment of the C-terminal protein sequences (RING domain not included) of distinct TRIM-NHL proteins from several species, including *M. musculus* (blue), *C. elegans* (green) and *D. melanogaster* (red). (Adapted from[86]).

There are four TRIM-NHL proteins expressed in mammals (TRIM2, TRIM3, TRIM32 and TRIM71), and all of them are known to play important roles in the developing or adult central nervous system (CNS). TRIM2 is dispensable for embryonic development, but adult mice lacking TRIM2 presented a neurodegenerative phenotype characterized by tremor, ataxia and seizures[87]. TRIM3 is strongly expressed in the mouse brain and it is involved in the transport of cargos along microtubules of motor neurons[88]. Furthermore, *TRIM3* has been identified as a tumor suppressor gene in glioma[89] and glioblastoma[90]. Supporting the role of TRIM3 as a tumor suppressor protein, the *D. melanogaster* orthologues Brat and Mei-P26 also act as tumor suppressors in stem cell lineages, since mutations in these two proteins result in tumor formation in the brain and the germline, respectively[91,92]. TRIM32 is mostly expressed in skeletal muscle and it has

been proposed to participate in muscle regeneration, as mutations in the *TRIM32* gene are associated with muscular dystrophy[93]. In the brain, TRIM32 was reported to prevent proliferation and promote differentiation of NSCs during mouse cortical development[94]. This was achieved, on one hand, by promoting c-MYC protein proteasomal degradation via ubiquitylation, a function that Brat also fulfilled in Drosophila NSCs[95]; and on the other hand, TRIM32 enhanced let-7a miRNA activity via AGO1 binding. In this regard, most TRIM-NHL proteins have been found to interact with AGO proteins[86]. For instance, the *C. elegans* orthologue protein NHL-2 was found to enhance repression of several miRNA targets as a result of such interaction, including let-7 targets, and NHL-2 mutants resembled let-7 family mutants[96].

Of all TRIM-NHL mammalian proteins, TRIM71 is the only stem cell-specific protein. Opposing TRIM32 function and that of its orthologue counterparts Brat and NHL-2, TRIM71 has been shown to promote proliferation and prevent differentiation of ESCs and NSCs, as well as driving tumorigenesis in several cancer types[97]. The role of TRIM71 in embryonic development and cancer will be discussed in detail in the following sections.

1.4.2. The role of TRIM71 as a proliferation-promoting factor

The heterochronic gene *lin-41* was first identified in *C. elegans* as a major target of the pro-differentiation *let-7* miRNA[98,99]. Later studies confirmed the conservation of *lin-41* and its repression by *let-7* miRNAs among many species[99–104], highlighting the importance of this TRIM-NHL protein and its proper regulation in the control of developmental events. The name TRIM71 was adopted for the homolog protein in mammals, although LIN41 is also widely accepted.

TRIM71 is expressed in mouse early embryonic development and its transcript levels start to decrease around E9.5-10.5, when let-7a and miR-125 miRNAs increase during differentiation to mediate TRIM71 mRNA repression[102]. Therefore, TRIM71 expression is restricted to undifferentiated cells, with an expression pattern that correlates temporally with proliferative processes and spatially with the distribution of the pluripotency factor OCT4[105]. Although it is clear that let-7 plays a major role in shaping TRIM71 expression during development, it is by no means the only regulator of TRIM71. FGF signaling was shown to induce TRIM71 expression[103], which in turns activates FGF signaling in a positive feedback regulatory loop[106], thereby stimulating its own expression. The pluripotency factor c-MYC can also activate TRIM71 expression directly by binding to its promoter[107], and indirectly through the activation of LIN28 expression[52], which is a well-known repressor of let-7a biogenesis. Like LIN28A, TRIM71 has been used in exchange of c-MYC in combination with OCT4, SOX2 and NANOG for the reprograming of somatic cells into iPSCs[53], highlighting its important role in the restoration of pluripotency. Accordingly, TRIM71 has been described as an oncogene in several cancer types[107–109], and previous studies in our lab showed a significant reduction of DMBA/TPA-induced skin carcinogenesis in skin-specific TRIM71 knockout mice as compared to wild type mice (unpublished data).

Despite its short expression window, TRIM71 is completely essential for embryonic development, being TRIM71 mutants embryonically lethal in several vertebrate and invertebrate species[97]. Embryonic lethality in mouse occurs at E12.5 and is accompanied by neural tube closure defects, highlighting also an essential role of TRIM71 in the development of the CNS[110]. Recurrent TRIM71 mutations have been recently

identified in a cohort of congenital hydrocephalus (CH) patients[111], a brain developmental disease which is associated with neural tube closure defects, among other causes. TRIM71 expression is also observed in muscle and gonads of the developing mouse embryo[99]. Accordingly, the deficiency of the Drosophila orthologue protein Wech/Dappled results in loss of muscle attachment[112] and LIN-41 deficiency in *C. elegans* induces sterility[99]. Furthermore, RNA sequencing of TRIM71-deficient mESCs showed an overall downregulation of genes associated with reproductive processes[113] and current studies in our lab with gonad-specific TRIM71 knockout mice show that TRIM71 deficiency causes a dramatic reduction of the testis size accompanied by sterility (unpublished data). Thus, TRIM71 is not only essential for embryonic development, but also for the proper function of the aforementioned organs in the adult organism.

The observed phenotypes in TRIM71-deficient animals are attributed to the general function of TRIM71 in the promotion of proliferation and the prevention of premature differentiation in stem and progenitor cells[97]. However, the causes of embryonic lethality remain to date unknown, and the molecular mechanisms underlying brain and gonad developmental defects remain to be elucidated. Given the functional complexity of TRIM71 distinct domains, the association of an observed phenotype with the regulation of a given target, either through its RNA-binding and repression function or through its protein ubiquitylation function, is particularly challenging. Furthermore, such complex phenotypes are probably not resulting from a single deregulated target, but rather from multiple deregulated pathways in the absence of TRIM71. Therefore, elucidating the functions of TRIM71 in developmental and oncogenic processes demands a better understanding of the molecular mechanisms underlying TRIM71 roles as an E3 ligase and an mRNA repressor, as well as the identification of new TRIM71 mRNA and protein targets.

1.4.3. The role of TRIM71 as an E3 ligase

TRIM-NHL proteins have been reported to have an E3 ligase role conferred by their RING domain, and the ubiquitylation of various proteins has been shown to contribute to their specific functions[114]. Autoubiquitylation of TRIM71 was found *in vitro* and in cell culture[105,115], although there is no evidence that this is used as an autoregulatory mechanism *in vivo*. However, several TRIM71 ubiquitylation substrates have been shown to contribute to the role of TRIM71 in the development of the CNS. For instance, TRIM71 was shown to promote proliferation of NSCs through its E3 ligase function. Specifically, TRIM71-mediated ubiquitylation of the adaptor protein SHCBP1 enhanced its stability, thereby promoting FGF signaling in ESCs and NSCs[106,116]. Furthermore, TRIM71-mediated ubiquitylation of p53 in mESCs cells undergoing neural differentiation resulted in p53 proteasomal degradation, antagonizing p53-dependent pro-apoptotic and pro-differentiation functions[117]. The authors proposed that this mechanism is connected with TRIM71-associated brain developmental defects, since the loss of TRIM71 resulted in aberrant p53 activation and enhanced cell death in the brain during neural tube closure stages[117].

The role of TRIM71 as an oncogene has also been supported by the ubiquitylation of several proteins. For example, TRIM71 has been shown to promote non-small cell lung cancer (NSCLC) by inducing the ubiquitylation-dependent degradation of the NF-κB inhibitor IκB-α, resulting in activation of the NF-κB pathway and promoting proliferation[109]. Furthermore, TRIM71 was reported to mediate ubiquitylation and proteasomal degradation of AGO2, thereby decreasing overall miRNA activity[105]. This mechanism was later claimed to be involved in the development of hepatocellular carcinoma[107], since impairment of

miRNA activity had previously been linked to enhanced proliferation and tumorigenesis[118]. Interaction with AGO proteins has been described for several TRIM-NHL proteins, such as *D. melanogaster* Mei-P26, Brat, and Wech/Dappled[119], *C. elegans* NHL-2[96] and mammalian TRIM32[94]. The interaction between TRIM71 and AGO2 was confirmed in later studies and extended to other AGO proteins, although regulation of AGO2 protein stability by TRIM71 could not be reproduced[41,105,115] and has neither been reported for other TRIM71 orthologues[86]. Therefore, the existence of a TRIM71-mediated AGO2 protein degradation mechanism remains controversial, and the functional outcome of the TRIM71-AGO2 interaction remains to be further investigated.

Although TRIM71 can act as an E3 ligase, several facts argue against ubiquitylation being the main TRIM71 function in the control of proliferation and differentiation during development. First, most of mutations causing loss of function and phenotypic alterations in *C. elegans* clustered in the NHL domain of LIN-41, whereas no mutations affecting the RING domain were identified in a screening of heterochronic mutants[99]. Second, the two recurrent mutations identified in CH patients – R608H and R796H – are present in the NHL domain and are predicted to disrupt TRIM71 RNA-binding function[85,111]. Third, both the putative Drosophila TRIM71 protein Wech/Dappled and the orthologue protein Brat lack a RING domain[120], indicating that the ancestral function of TRIM71 does not rely on its E3 ligase activity, but that this capability has been acquired rather later in evolution. Last, a TRIM71 mutant merely lacking the last NHL repeat of the NHL domain phenocopied the total loss of TRIM71 during mice development, causing embryonic lethality and neural tube closure defects[110]. Collectively, these findings highlight the major importance of TRIM71 function as an RNA binding and repressor protein.

1.4.4. The role of TRIM71 as an mRNA repressor

TRIM71 has been shown to repress the expression of several mRNA targets which collectively justify its role promoting proliferation and preventing differentiation in developmental and oncogenic processes. For instance, TRIM71 was found to repress the mRNA of several cell cycle inhibitors such as CDKN1A[41], which encodes for the CKI p21; the retinoblastoma-like proteins pRBL-1 and pRBL-2[115], which like pRB proteins, sequester the master cell cycle-promoter transcription factor E2F1; and the cell cycle repressor E2F7[115], a transcription factor whose expression is induced by p53[121] and which represses the expression of E2F1[122]. TRIM71 has also been reported to repress the mRNA of several pro-differentiation factors, such as HOXA5[115], a morphogenesis transcription factor whose expression is also induced by p53[123]; PLXNB2 and INHBB[113], involved in brain and testis development, respectively[124,125]; and EGR1[53], a differentiation-promoter transcription factor which has been found to impair the reprogramming of human fibroblasts into iPSCs[53]. Interestingly, one of the first LIN-41 targets identified in *C. elegans* was the EGR1 homolog *lin-29*[99,126], a transcription factor whose activity is required for terminal differentiation in last larval stages[127]. Altogether, these examples not only show how TRIM71 functions as an mRNA repressor to control the proliferation-differentiation balance through the regulation of multiple targets, but also highlights the requirement of these mechanisms in developmental and oncogenic processes, based on their conservation among species.

TRIM71 has been described as a mRNA[128] and miRNA[129] binding protein. Specific RNA binding brings TRIM71 in close proximity to other RNA-binding proteins (RBPs) which may assist TRIM71-mediated mRNA

repression in various manners. Indeed, TRIM71 interacts with several proteins in a RNA-dependent manner[105,115]. Interaction with RNA is an essential requirement for its mRNA repression function. In this regard, the CC, FLN and NHL domains have been found to be required for mRNA repression while the RING and BB domains were dispensable for such a function[115]. The NHL domain structurally resembles the β-propeller WD40 domain present in other RNA binding proteins[84,128,130], and has been reported to mediate direct interaction with RNA in *D. melanogaster* Brat, *C. elegans* LIN-41 and *D. rerio* Lin41[83,85,126]. Whether the mammalian TRIM71 NHL domain can also mediate direct RNA interaction remains to be elucidated.

Although it is clear that TRIM71 is a mRNA repressor protein, little is known about how such a repression is achieved upon target recognition. TRIM71 has been reported to repress its mRNA targets in most cases through UTR recognition[97]. Two distinct repression mechanisms, namely mRNA degradation and translational inhibition, were found to be employed by TRIM71 for target downregulation, depending on its capability to bind either the 3'UTR or the 5'UTR of the given target, respectively[126]. A previous study postulated that for a given target, TRIM71-mediated mRNA silencing resulted from combined mRNA degradation and translational inhibition[115]. Interestingly, the "ratio" between these two molecular mechanisms seems to vary in distinct cellular contexts, since mRNA degradation was more pronounced in HEK293T cells as compared to mESCs, where translational inhibition was found to be a preferred mechanism[115]. In contrast, a recent study combining transcriptomics and ribosome profiling reported low levels of TRIM71-mediated translational inhibition in mESCs, and postulated mRNA degradation to be the preferred mRNA repression mechanism in these cells[131].

Regarding its subcellular localization, TRIM71 localizes within P-bodies[105], which are organelles hosting several RNA surveillance pathways, including the miRNA pathway and the NMD pathway[132,133]. Based on TRIM71 localization in these organelles, as well as its interaction with several proteins involved in the miRNA pathway, including AGO1, AGO2, AGO4 and DICER[41,105,115], TRIM71-mediated mRNA repression was proposed to be assisted by miRNAs[41]. Furthermore, TRIM71-deficient mESCs had an altered miRNA landscape, with reduced ESC-specific miRNAs and increased differentiation-promoting miRNAs – namely brain- and gonad-specific miRNAs – as compared to wild type mESCs[113]. This highlights a role for TRIM71 in the regulation of miRNA biogenesis, possibly impacting on miRNA targets as well, but whether TRIM71 requires miRNA assistance for specific mRNA target repression remains elusive. Indeed, several mRNAs were found to be repressed by TRIM71 in an AGO2- and miRNA-independent manner[115]. Altogether, these findings underscore the requirement of further research to clarify the involvement of TRIM71 in the regulation of miRNA expression and activity, and to elucidate which factors other than miRNAs cooperate with TRIM71 in the repression of its mRNA targets.

1.4.5. The role of TRIM71 in the LIN28/let-7 axis

The *let-7* (*lethal-7*) gene was first discovered in *C. elegans* as a key developmental regulator and became one of the first two known miRNAs together with *lin-4*[98]. Let-7 family members are highly conserved and have been described as pro-differentiation and tumor suppressor miRNAs[134]. During let-7 biogenesis, proteins like DGCR8, DICER or AGO2 assist its processing, maturation and function, promoting let-7-mediated mRNA silencing, whereas LIN28 proteins inhibit let-7 maturation and promote its degradation (see again Fig. 1.6). Although pri- and pre-let-7 are present during the whole developmental process,

mature let-7 is only detectable upon differentiation and tissue development[35], opposing the expression pattern of its targets, which include several mitogens and oncogenes (c-MYC, MYCN, RAS, HMGA2), cell cycle progression factors (CCNA2, CCND1, CCND2, E2F1, E2F2), and the stem cell-specific RNA-binding proteins TRIM71 and LIN28A/B, among others[135]. Opposing let-7 tumor suppressor functions, many let-7 targets have been shown to promote tumorigenesis. Like TRIM71, LIN28 is upregulated in several tumor types, including germ cell tumors[136], breast cancer[137], hepatocellular carcinoma[138] and Wilms tumor[139]. Therefore, both LIN28 and TRIM71 are stem cell-specific RNA binding proteins abundantly expressed in undifferentiated cells and whose expression is downregulated in the course of differentiation by let-7 miRNAs.

The parallelisms between these two proteins has been extended by the fact that not only LIN28 is both a target and a repressor of let-7, but also TRIM71 has been reported to exert a feedback regulation on let-7 miRNAs. However, TRIM71 has been involved in the LIN28/let-7a axis in quite controversial manners (Fig. 1.9A). On one hand, TRIM71 overexpression in HEK293 cells led to let-7a activity repression in luciferase reporter assays[105]. In light of these results, a cooperation between LIN28A and TRIM71 in the repression of let-7 expression was proposed, but to no extent proven (Fig. 1.9A_I). In contrast, another publication claimed that TRIM71 negatively regulates LIN28B stability via its E3 ligase function, thereby upregulating let-7 expression[140] (Fig. 1.9A_II). Through such a mechanism, TRIM71 was claimed to act as a tumor suppressor gene in a later study[141], opposing all previous findings regarding the role of TRIM71 in the control of proliferation[97]. Last, TRIM71 was reported to promote AGO2 proteasomal degradation via ubiquitylation, leading to a general decrease of miRNA activity, including let-7 activity[105] (Fig. 1.9A_III). Although, as mentioned before, the results regarding AGO2 stability regulation remain controversial, a global impairment of miRNA activity had been previously linked with enhanced cell proliferation[118]. Altogether, several studies revealed the possibility of a feedback regulation exerted by TRIM71 on let-7, but the direction and mechanism of such a regulation remain to be further investigated.

In order to clarify this issue, previous studies in our lab conducted miRNA sequencing in TRIM71-deficient mESCs. These studies revealed an upregulation of differentiation-promoting miRNAs upon TRIM71 deficiency[113]. Let-7 family members were some of the most significantly upregulated miRNAs in TRIM71-deficient mESCs, supporting a role of TRIM71 as a repressor of let-7 expression. Interestingly, mature let-7 levels were significantly upregulated whereas pri- and pre-miRNAs remained unaltered, indicating that TRIM71 affects the last processing stage of let-7 biogenesis (unpublished data). Because LIN28A interferes with let-7 biogenesis at the very same stage, Dr. Mitschka generated LIN28A knockout mESCs, as well as double LIN28-TRIM71 knockout mESCs, in order to evaluate whether TRIM71 assisted LIN28A in the repression of let-7 expression, or whether both proteins could achieve the same function via rather independent mechanisms. Both TRIM71- and LIN28A-deficient mESCs showed upregulated let-7 miRNA levels, albeit to different extents, being let-7 upregulation more dramatic in LIN28A knockout mESCs. However, the double LIN28-TRIM71 knockout did not show any additional let-7 upregulation in comparison to the single LIN28A knockout (unpublished data, Fig. 1.9B). These findings strongly suggested that TRIM71 cooperates with LIN28A in the repression of let-7 maturation, and highlighted a role for TRIM71 in the regulation of miRNA biogenesis beyond its role as an mRNA repressor.

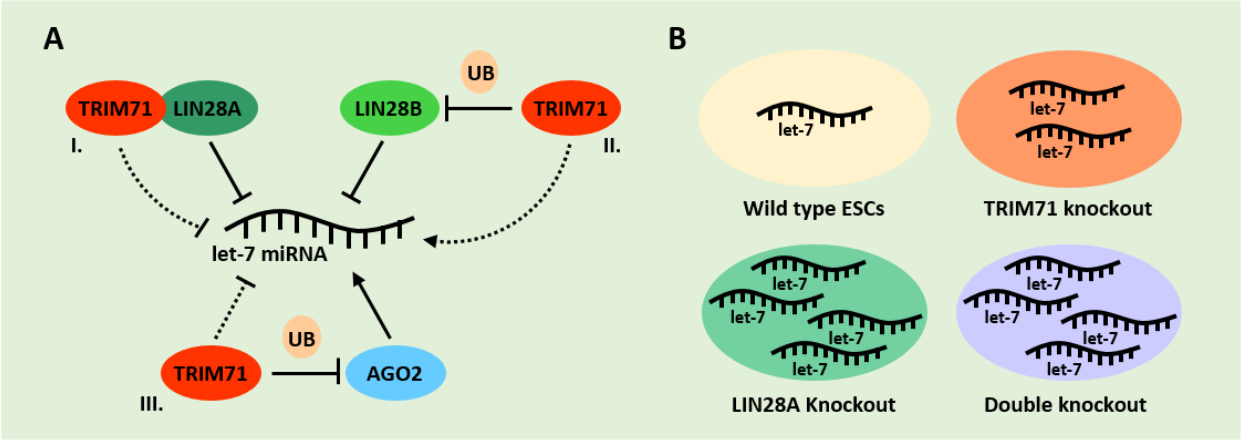

Figure 1.9. TRIM71-mediated let-7 miRNA regulation. A) Reported mechanisms of TRIM71-mediated let-7 miRNA regulation are controversial. **(I)** TRIM71 has been found to repress let-7 activity and it has been speculated that such a function could be achieved in cooperation with LIN28A[105]. **(II)** TRIM71 has been claimed to indirectly enhance let-7 expression by mediating LIN28B ubiquitylation (UB) and proteasomal degradation[140]. **(III)** TRIM71 was claimed to indirectly repress overall miRNA activity by mediating AGO2 ubiquitylation (UB) and proteasomal degradation[105]. **B)** Levels of mature let-7 miRNA quantified in different mES cell lines showed no additional let-7 upregulation in LIN28A-TRIM71 double knockout mESCs, as compared to the upregulation of let-7 observed in single LIN28A knockout mESCs (unpublished data; experiments performed by Dr. Mitschka). These results indicated that the upregulation of let-7 observed in TRIM71 knockout mESCs is achieved by TRIM71 in cooperation with LIN28A, as proposed in A (I).

2. Aims of the present work

The stem cell-specific factor TRIM71 is essential for embryonic development and plays a role in controlling the proliferation-differentiation balance of ESCs and cancer cells. Its restricted expression makes TRIM71 an ideal target for the development of cancer-specific therapies. However, the causes of embryonic lethality are still unknown, and many aspects of the molecular mechanisms underlying TRIM71 various functions remain to be investigated.

The main aim of the present work was to unravel mechanistic aspects of TRIM71-mediated RNA regulation, including both miRNA and mRNA targets with important roles in developmental and oncogenic processes.

Regarding TRIM71-mediated miRNA regulation, and particularly focusing on the regulation of the pro-differentiation and tumor suppressor miRNA let-7, we tried to shed light on the involvement of TRIM71 in the miRNA pathway, both concerning the regulation of miRNA synthesis and miRNA activity. In this context, we further investigated the controversial role of TRIM71 in the LIN28/let-7 axis, and tried to elucidate the functional outcome of the long-known but yet-enigmatic interaction between TRIM71 and AGO2.

Regarding TRIM71-mediated mRNA regulation, and particularly focusing on the repression of the cell cycle inhibitor and tumor suppressor CDKN1A/p21, we aimed at elucidating TRIM71 molecular requirements for target recognition and repression. In this context, we further investigated whether the role of TRIM71 as an mRNA repressor was assisted by the miRNA pathway, or by other RNA surveillance mechanisms through the interaction of TRIM71 with specific RNA-binding proteins.

Although we often investigated miRNAs other than let-7 and mRNAs other than CDKN1A, the present work focuses mainly on these two targets, not only for simplification purposes, but also because these miRNA and mRNA molecules are well-described anti-proliferative and pro-differentiation cues, which play major roles in developmental and oncogenic processes. Therefore, we considered their regulation by TRIM71 to be of strong physiological and pathological relevance.

3. Materials and Methods

3.1. Materials

3.1.1. Laboratory equipment

Device and Model	Company (Office, Land)
Autoclave DX-150	Systec (Linden, Germany)
Centrifuge (caps) 5415R	Eppendorf (Hamburg, Germany)
Centrifuge (falcon tubes and plates) 5810R	Eppendorf (Hamburg, Germany)
Centrifuge (Ultracentrifugation) Optima LE-80K	Beckman Coulter (Munich, Germany)
Centrifuge Avanti J-20XP	Beckman Coulter (Munich, Germany)
Controlled atmosphere incubator C150	Binder (Great River, USA)
Controlled atmosphere incubator C200	Labotect (Rosdorf, Germany)
Electrophoresis chambers (agarose gels)	Polymehr (Paderborn, Germany)
Electrophoresis chambers (native PAGE gels)	Peqlab VWR (Radnor, USA)
Electrophoresis chambers (SDS-PAGE gels)	Bio-Rad (Munich, Germany)
Electroporator Gene Pulser Xcell	Bio-Rad (Munich, Germany)
Flow cytometer BD Canto II	BD Biosciences (Heidelberg, Germany)
Freezing container Cryo -1°C/min Nalgene	Thermo Fisher Scientific (Waltham, USA)
Geiger radiation counter	Berthold (Cologne, Germany)
Heating block Thermomixer Compact	Eppendorf (Hamburg, Germany)
Heating cabinet EcoCell 55 MMM	Medcenter (Munich, Germany)
Heating magnetic stirrer ARE	VELP Scientifica (Usmate, Italy)
Laminar flow hood BioFlow	BDK (Sonnenbühl-Genkingen, Germany)
Laminar flow hood HeraSafe KS	Thermo Fisher Scientific (Waltham, USA)
Liquid scintillation analyzer Tri-Carb 2810TR	Perkin Elmer (Waltham, USA)
Luminometer MicroLumat Plus LB96V	Berthold (Cologne, Germany)
Magnetic rack DynaMag-2	Thermo Fisher Scientific (Waltham, USA)
Microscope (confocal) LSM 880+ Airyscan	Zeiss (Jena, Germany)
Microscope (confocal) LSM FV-1000	Olympus (Tokyo, Japan)
Microscope Eclipse TS100	Nikon (Tokyo, Japan)
Neubauer cell counting chamber	Marienfeld (Lauda-Königshofen, Germany)
Orbital shaker New Brunswick innova44	Eppendorf (Hamburg, Germany)
pH meter MP220	Mettler Toledo (Greifensee, Switzerland)

Device and Model	Company (Office, Land)
Pipette controler AccuJet Pro	Brand (Wertheim, Germany)
Pipette multi-channel (300 µl)	ErgoLine StarLab (Helsinki, Finland)
Pipette set (2.5 - 1000 µl)	Pipetman Classic Gilson (Middleton, USA)
Plate reader Infinite M200	Tecan (Männedorf, Switzerland)
Plate reader Synergy HT	BioTek (Bad Friedrichshall, Germany)
Plate reader Tecan Ultra	Tecan (Männedorf, Switzerland)
Power supplies PowerPac 200	Bio-Rad (Munich, Germany)
Rocker WS-10	Edmund Bühler (Hechingen, Germany)
Roller mixer RS-TR05	Phoenix Instrument (Garbsen, Germany)
Rotating wheel Neolab Rotator	Neolab (Heidelberg, Germany)
Scales AG285 and JB2002-G (micro-precision)	Mettler Toledo (Greifensee, Switzerland)
Sonicator bath Sonorex RK-100H	Bandelin Electronic (Berlin, Germany)
Spectrophotometer NanoDrop 2000	Thermo Fisher Scientific (Waltham, USA)
Thermocycler C1000 Touch Thermal Cycler	Bio-Rad (Munich, Germany)
Thermocycler CFX96 Touch Deep Well (qPCR)	Bio-Rad (Munich, Germany)
Thermocycler T100 MyCycler	Bio-Rad (Munich, Germany)
UV transiluminator Systeme	Intas (Göttingen, Germany)
UV crosslinker CL-1000 UVP	Analytik Jena (California, USA)
Vacuum gel dryer 583	Bio-Rad (Munich, Germany)
Vacuum pump AC02 HLC	BioTech (Bovenden, Germany)
Vortex mixer UNIMAG ZX3	VELP Scientifica (Usmate, Italy)
Water bath WNE	Memmert (Schwabach, Germany)

3.1.2. Plastic ware and consumables

Material	Company (Office, Land)
Cell culture dishes 6/10/15 cm Cellstar	Greiner Bio-one (Frickenhausen, Germany)
Cell culture flasks 40/200 ml Cellstar	Greiner Bio-one (Frickenhausen, Germany)
Cell scaper 25 cm 2-Positions Blade	Sarstedt (Nümbrecht, Germany)
Centrifugal filter units 10K Amicon	Merk Millipore (Darmstadt, Germany)
Coverslips (glass) 15 mm	Marienfeld (Lauda-Königshofen, Germany)
Cryotubes CryoPure 2ml	Sarstedt (Nümbrecht, Germany)
Electroporation cuvettes 4 mm	Biozym (Vienna, Austria)
Filter paper Whatman	GE Healthcare (Chicago, USA)
Filter tips 10/200/1000 µl	Sarstedt (Nümbrecht, Germany)
Flow cytometry tubes 5 ml	Sarstedt (Nümbrecht, Germany)
Glass Pasteur pipettes	Brand (Wertheim, Germany)
Microscope slides	Marienfeld (Lauda-Königshofen, Germany)
Multilwell plate 96 Black Fluotrac (polarization)	Greiner Bio-one (Frickenhausen, Germany)
Multiwell plate 96 White Lumitrac (luminiscence)	Greiner Bio-one (Frickenhausen, Germany)
Multiwell plates 6/12/24/96 wells Cellstar (cell culture)	Greiner Bio-one (Frickenhausen, Germany)
Nitrocellulose membrane BioTrace NT	Pall-Corporation (New Xork, USA)

Material	Company (Office, Land)
Paraffin laboratory film Parafilm M	Bemis (Neenah, USA)
PCR tubes 200 µl Thin Wall	Axygen (Tewksbury, USA)
Petri dishes 10 cm	Greiner Bio-one (Frickenhausen, Germany)
Plastic tips 10/200/1000 µl	Carl Roth (Karlsruhe, Germany)
ProbeQuant G-50 MicroColumns	GE Healthcare (Chicago, USA)
Radiographic films Amersham hyperfilm ECL	GE Healthcare (Chicago, USA)
Reaction tubes 0.5/1/2 ml	Starlab (Ahrensburg, Germany)
Serological pipettes 5/10/25 ml	Greiner Bio-one (Frickenhausen, Germany)
Syringes Injekt 10 ml	Braun Melsungen (Melsungen, Germany)
Ultracentrifugation tubes QuickSeal Polypropylene	Beckman (Munich, Germany)

3.1.3. Chemical reagents

Name	Company (Office, Land)
^{32}P-YATP	Hartmann Analytic (Braunschweig, Germany)
Acetic acid	Carl Roth (Karlsruhe, Germany)
Acrylamide/Bisacrylamide solution	Carl Roth (Karlsruhe, Germany)
Agar	BD (Heidelberg, Germany)
Agarose	Thermo Fisher Scientific (Waltham, USA)
Ammonium acetate	Carl Roth (Karlsruhe, Germany)
Ammonium persulfate (APS)	Carl Roth (Karlsruhe, Germany)
Ampicillin	Carl Roth (Karlsruhe, Germany)
Antipain	Sigma-Aldrich (Taufkirchen, Germany)
Aprotinin	Sigma-Aldrich (Taufkirchen, Germany)
Benzamidin	Sigma-Aldrich (Taufkirchen, Germany)
Boric acid	Carl Roth (Karlsruhe, Germany)
Bovine serum albumin (BSA)	Carl Roth (Karlsruhe, Germany)
Bromophenol blue	Carl Roth (Karlsruhe, Germany)
Butyl alcohol (1-butanol)	Merck (Darmstadt, Germany)
Cesium chloride	Carl Roth (Karlsruhe, Germany)
Calcium chloride	Carl Roth (Karlsruhe, Germany)
Chloroform	Carl Roth (Karlsruhe, Germany)
Coomassie Blue PageBlue	Thermo Fisher Scientific (Waltham, USA)
Deoxynucleotides (dNTPs)	Thermo Fisher Scientific (Waltham, USA)
Developing solution (Adefo Citroline2000)	Adefo-Chemie (Neu-Isenburg, Germany)
Diamidinophenylindole (DAPI)	Sigma-Aldrich (Taufkirchen, Germany)
Diazabicyclooctan (DABCO)	Sigma-Aldrich (Taufkirchen, Germany)
Dimethyl sulfoxide (DMSO)	Carl Roth (Karlsruhe, Germany)
Disodium Edetate	Carl Roth (Karlsruhe, Germany)
Disodium phosphate	Carl Roth (Karlsruhe, Germany)
Dithiothreitol (DTT)	Carl Roth (Karlsruhe, Germany)
DNA loading dye 6x	Thermo Fisher Scientific (Waltham, USA)

Name	Company (Office, Land)
Double-distilled water	In-house production (LIMES, Germany)
Ethanol, 96 % (EtOH)	Werner Hoffman (Düsseldorf, Germany)
Ethidium bromide (EtBr)	Carl Roth (Karlsruhe, Germany)
Ethylenediaminetetraacetic acid (EDTA)	Carl Roth (Karlsruhe, Germany)
Ethyleneglycotetraacetic acid (EGTA)	Sigma-Aldrich (Taufkirchen, Germany)
Gelatin solution, type B	Sigma-Aldrich (Taufkirchen, Germany)
Glucose	Carl Roth (Karlsruhe, Germany)
Glycerol	Carl Roth (Karlsruhe, Germany)
Glycerophosphate	Sigma-Aldrich (Taufkirchen, Germany)
Glycine	Carl Roth (Karlsruhe, Germany)
Glycogen	Roche (Mannheim, Germany)
heparin	Sigma-Aldrich (Taufkirchen, Germany)
HEPES	Carl Roth (Karlsruhe, Germany)
Hydrochloric acid	Carl Roth (Karlsruhe, Germany)
Hydrogen peroxide	Merck (Darmstadt, Germany)
Hypoxanthine	Sigma-Aldrich (Taufkirchen, Germany)
Igepal/NP-40 CA-630	Sigma-Aldrich (Taufkirchen, Germany)
Isopropanol	Merck (Darmstadt, Germany)
Kanamycin	Carl Roth (Karlsruhe, Germany)
LB medium	Thermo Fisher Scientific (Waltham, USA)
Leupeptin	Sigma-Aldrich (Taufkirchen, Germany)
Lithium chloride	Carl Roth (Karlsruhe, Germany)
Magnesium chloride	Carl Roth (Karlsruhe, Germany)
Methanol	Carl Roth (Karlsruhe, Germany)
Mycophenolic acid (MPA)	Sigma-Aldrich (Taufkirchen, Germany)
Milk powder	Carl Roth (Karlsruhe, Germany)
MOPS	Carl Roth (Karlsruhe, Germany)
Mounting media for IF (FluoroShield)	ImmunoBioScience (Mukilteo, USA)
Paraformaldehyde (PFA)	AppliChem (Darmstadt, Germany)
Phenol	AppliChem (Darmstadt, Germany)
Phenylmethylsulfonyl fluoride (PMSF)	Carl Roth (Karlsruhe, Germany)
Ponceau S	Carl Roth (Karlsruhe, Germany)
Potassium acetate	Carl Roth (Karlsruhe, Germany)
Potassium bicarbonate	Sigma-Aldrich (Taufkirchen, Germany)
Potassium chloride	Sigma-Aldrich (Taufkirchen, Germany)
RNA loading dye (2x)	New England Biolabs (Ipswich, USA)
Saccharose/Sucrose	Carl Roth (Karlsruhe, Germany)
Sodium acetate	Carl Roth (Karlsruhe, Germany)
Sodium azide	Carl Roth (Karlsruhe, Germany)
Sodium chloride	Carl Roth (Karlsruhe, Germany)
Sodium deoxycholate	Sigma-Aldrich (Taufkirchen, Germany)
Sodium dodecyl sulfate (SDS)	Carl Roth (Karlsruhe, Germany)

Name	Company (Office, Land)
Sodium fluoride	Carl Roth (Karlsruhe, Germany)
Sodium hydroxide	Carl Roth (Karlsruhe, Germany)
Sodium pyrophosphate	Sigma-Aldrich (Taufkirchen, Germany)
Sodium vanadate	Sigma-Aldrich (Taufkirchen, Germany)
Tetramethylethylendiamine (TEMED)	Sigma-Aldrich (Taufkirchen, Germany)
Tris	Carl Roth (Karlsruhe, Germany)
Triton X-100	Carl Roth (Karlsruhe, Germany)
Trizol reagent	Thermo Fisher Scientific (Waltham, USA)
Tween 20	Carl Roth (Karlsruhe, Germany)
Water, nuclease-free	Sigma-Aldrich (Taufkirchen, Germany)
Xanthine	Sigma-Aldrich (Taufkirchen, Germany)
Yeast tRNA	Thermo Fisher Scientific (Waltham, USA)
β-mercaptoethanol	Carl Roth (Karlsruhe, Germany)

3.1.4. Cell reagents

Name	Company	Product ID
Actinomycin D	Sigma-Aldrich	A9415-2MG
B27 supplement	Gibco	17504044
Bafilomycin A1	Sigma-Aldrich	B1793
Cell cuture water	PAN Biotech	PA04-991000
Cell proliferation dye eFluor670	Thermo Fisher Scientific	65-0840-85
DMEM/F-12 media	Gibco	11514436
DMEM knockout media	Gibco	10389172
DMEM media	PAN Biotech	P04-01549
Fetal bovine serum (FBS)	Sigma-Aldrich	F2442
G418-BC/Neomycin	Biochrom	A2912
GlutaMAX	Thermo Fisher Scientific	35050061
Lipofectamine 2000	Thermo Fisher Scientific	11668027
Lipofectamine RNAiMAX	Thermo Fisher Scientific	13778075
MG132	Sigma-Aldrich	M7449
N2 supplement	Gibco	17502048
Neurobasal media	Gibco	21103049
Non-essential aminoacids (NEAA)	Sigma-Aldrich	M7145
OPTI-MEM	Gibco	31985047
PANfect	PAN Biotech	P02-8010
PBS	PAN Biotech	P04-35500
Penicillin-Streptomycin	PAN Biotech	P06-07100
Poly-L-Lysine	Sigma-Aldrich	P8920
RPMI 1640 media	PAN Biotech	P04-17500
StemCell Pro Accutase	Thermo Fisher Scientific	A1110501
Trypsin-EDTA 0.05% Phenol Red	Thermo Fisher Scientific	25300054

3.1.5. Commercial kits and enzymes

Name	Company	Product ID
Anti-FLAG M2 magnetic beads	Sigma-Aldrich	M8823
AP detection kit (BCIP/NBT solution)	Sigma-Aldrich	B6404
DNase I kit (RNase-free)	Thermo Fisher Scientific	EN0523
Dual-Luciferase Reporter Assay System kit	Promega	E1910
Dynabeads His-Tag Isolation and Pulldown	Thermo Fisher Scientific	10104D
Dynabeads Protein G	Thermo Fisher Scientific	10004D
Fast Alkaline Phosphatase kit (AP)	Thermo Fisher Scientific	EF0651
Gene Ruler 100 bp DNA ladder	Thermo Fisher Scientific	SM0241
Gene Ruler 1 kb DNA ladder	Thermo Fisher Scientifci	SM0311
High-Capacity cDNA Reverse Transcription kit	Thermo Fisher Scientific	4368814
iTaq Universal Probes Supermix	Bio-Rad	172-5132
iTaq Universal SYBR Green Supermix	Bio-Rad	172-5122
Lamda Phosphatase kit (λP)	New England Biolabs (NEB)	P0753S
NEB buffer 2 (10x)	New England Biolabs (NEB)	B7202S
NucleoSpin Gel and PCR Clean-up kit	Macherey-Nagel	740609.240C
peqGOLD Proteinase K	Peqlab	04-1071
peqGOLD TriFast	PeqLab	30-2010
Phusion DNA polymerase kit	New England Biolabs (NEB)	E0553S
Pierce BCA Protein Assay Kit	Thermo Fisher Scientific	23225
Pierce ECL Western Blotting Substrate	Thermo Fisher Scientific	32106
Precision Plus Protein All Blue Standard	Bio-Rad	1610373
Restriction enzyme kit DpnI	Thermo Fisher Scientific	ER1701
Restriction enzyme kit HindIII	Thermo Fisher Scientific	ER0501
Restriction enzyme kit MluI	Thermo Fisher Scientific	ER0561
Restriction enzyme kit NotI	Thermo Fisher Scientific	ER0591
Restriction enzyme kit XhoI	Thermo Fisher Scientific	ER0691
RiboLock RNase inhibitor	Thermo Fisher Scientific	EO0381
RNase A	Thermo Fisher Scientific	EN0531
T4 DNA Ligase kit	Thermo Fisher Scientific	EL0014
T4 PNK phosphorylation kit	Roche Diagnostics	10709557001

3.1.6. Primary antibodies

Name	Company	Product ID
Goat anti-IgG (39.7 kDa)	Jackson ImmunoResearch	109-005-098
Mouse anti-FLAG M2 (1 kDa)	Sigma-Aldrich	F1804
Mouse anti-FLAG M2 AP-conjugated	Sigma-Aldrich	A9469
Mouse anti-GAPDH (36 kDa)	Acris	ACP001P
Mouse anti-GFP (32.7 kDa)	Santa Cruz Biotechnology	sc-9996
Mouse anti-TUBULIN (50 kDa)	Sigma-Aldrich	T9026
Mouse anti-VINCULIN (123.8 kDa)	Sigma-Aldrich	V9131
Rabbit anti-ACTIN (41.7 kDa)	Sigma-Aldrich	A2066
Rabbit anti-AKT (60 kDa)	Cell Signaling Technology	9272
Rabbit anti-p-AKT (Ser473)	Cell Signaling Technology	4060
Rabbit anti-CDKN1A/p21 (18 kDa)	Cell Signaling Technology	2947
Rabbit anti-DGCR8 (86 kDa)	Proteintech Group	10996-1-AP
Rabbit anti-eIF4E (25 kDa)	Cell Signaling Technology	2067
Rabbit anti-ERK1/2 (44/42 kDa)	Cell Signaling Technology	9102
Rabbit anti-p-ERK1/2 (Thr202/Tyr204)	Cell Signaling Technology	9101
Rabbit anti-HA tag (1.1 kDa)	Proteintech	51064-2-AP
Rabbit anti-HMGA2 (12 kDa)	Thermo Fisher Scientific	PA5-25276
Rabbit anti-LIN28A (23 kDa)	Cell Signaling Technology	8641
Rabbit anti-LIN28B (30 kDa)	Cell Signaling Technology	4196
Rabbit anti-OCT4 (45 kDa)	Cell Signaling Technology	2750
Rabbit anti-P53 (43.6 kDa)	Cell Signaling Technology	2527
Mouse anti-p-P53 (Ser15)	Cell Signaling Technology	9286
Rabbit anti-p-H2AX (Ser139) (15.8 kDa)	Cell Signaling Technology	2577
Rabbit anti-SMG1 (410 kDa)	Cell Signaling Technology	4993
Rabbit anti-SMG7 (127 kDa)	Bethyl	A302-170A-M
Rabbit anti-SMG7 (for IP)	Bethyl	A302-170A
Rabbit anti-SOX1 (39 kDa)	Cell Signaling Technology	4194
Rabbit anti-TRIM71 (93.4 kDa)	Sigma-Aldrich	HPA038142
Rabbit anti-Ubiquitin (UBI)	Cell Signaling Technology	3933
Rabbit anti-UPF1 (123 kDa)	Cell Signaling Technology	9435S
Rabbit anti-p-UPF1 (Ser1127)	Sigma-Aldrich	07-1016
Rabbit anti-ZCCHC11/TUT4 (185 kDa)	Proteintech Group	18980-1-AP
Rat-anti-AGO2 (93.6 kDa)	Sigma-Aldrich	SAB4200085
Sheep anti-TRIM71/LIN-41 (93.4 kDa)	R & D Systems	AF5104

3.1.7. Secondary antibodies

Name	Company	Product ID
Rabbit anti-goat HRP-conjugated	Santa Cruz Biotechnology	sc-2768
Goat anti-mouse HRP-conjugated	Jackson ImmunoResearch	115-035-166
Goat anti-rabbit HRP-conjugated	Jackson ImmunoResearch	111-035-144
Mouse anti-rat HRP-conjugated	Jackson ImmunoResearch	212-035-168
Donkey anti-sheep HRP-conjugated	Santa Cruz Biotechnology	sc-2473
Donkey anti-rabbit Alexa647-conjugated	Jackson ImmunoResearch	711-606-152

3.1.8. Recombinant proteins

Name	Company	Product ID
Flag-NHL human protein (33 kDa)	In-house produced	-
Myc-LIN28A human protein (23 kDa)	OriGene	TP303397
3xFLAG peptide (3 kDa)	Sigma-Aldrich	F4799

3.1.9. Plasmids

Overexpression vectors		Luciferase vectors
pRK5-Flag-empty	pN1-GFP-empty	psiCHECK2-Renilla-empty
pRK5-Flag-TRIM71	pN1-GFP-TRIM71	psiCHECK2-Renilla-8xlet-7 (Addgene #20931)
pRK5-Flag-C12LC15A	pN1-GFP-C12LC15A	psiCHECK2-Renilla-3xlet-7a
pRK5-Flag-RBB	pN1-GFP-RBB	psiCHECK2-Renilla-3xlet-7g
pRK5-Flag-CCNHL	pN1-GFP-CCNHL	psiCHECK2-Renilla-3xmiR-128
pRK5-Flag-RBCC_WT	pN1-GFP-RBCC	psiCHECK2-Renilla-3xmiR-16
pRK5-Flag-RBCC_C12LC15A	pN1-GFP-FLNNHL	psiCHECK2-Renilla-3xmiR-19
pRK5-Flag-FLNNHL	pN1-GFP-FLN	psiCHECK2-Renilla-CDKN1A CDS
pRK5-Flag-FLN	pN1-GFP-NHL	psiCHECK2-Renilla-CDKN1A 3'UTR (FL)
pRK5-Flag-NHL	pN1-GFP-TRIM71-ΔCC	psiCHECK2-Renilla-CDKN1A 3'UTR-3xBoxB
pRK5-Flag-TRIM71-ΔNHL6	pN1-Ig-empty	psiCHECK2-Renilla-F1_CDKN1A 3'UTR
pRK5-Flag-TRIM71-ΔCC	pN1-Ig-TRIM71	psiCHECK2-Renilla-F2_0-500-CDKN1A 3'UTR (F2)
pRK5-Flag-TRIM71-SY/AF	pN1-Ig-C12LC15A	psiCHECK2-Renilla-F2_0-400-CDKN1A 3'UTR
pRK5-Flag-TRIM71-STS/AAA	pN1-Ig-RBB	psiCHECK2-Renilla-F2_0-300-CDKN1A 3'UTR
pRK5-Flag-TRIM71-SS/VV	pN1-Ig-CCNHL	psiCHECK2-Renilla-F2_0-200-CDKN1A 3'UTR
pRK5-Flag-TRIM71-14xS/V	pN1-Ig-RBCC	psiCHECK2-Renilla-F2_0-100-CDKN1A 3'UTR
pRK5-Flag-R608H	pN1-Ig-FLNNHL	psiCHECK2-Renilla-F2_100-200-CDKN1A 3'UTR (WT)
pRK5-Flag-R796H	pN1-Ig-NHL	psiCHECK2-Renilla-F2_100-200_M#1-CDKN1A 3'UTR
pRK5-Flag-TRIM71-λN	pN1-Ig-TRIM71-ΔNHL6	psiCHECK2-Renilla-F2_100-200_M#2-CDKN1A 3'UTR
pRK5-Flag-R796H-λN	pN1-Ig-R608H	psiCHECK2-Renilla-F2_100-200_M#3-CDKN1A 3'UTR
pRK5-Flag-LIN28A	pN1-Ig-R796H	psiCHECK2-Renilla-F2_100-200_M#4-CDKN1A 3'UTR
pRK5-Flag-UPF1	pN1-Ig-LIN28A	psiCHECK2-Renilla-F3_CDKN1A 3'UTR
pRK5-Flag-TRIM32	pN1-Ig-AGO2	pTkg-Flag-NHL (Vaccinia Virus Expression vector)
pRK5-HA-6xUBI (Addgene #17608)	pN1-Ig-TRIM32	
pRK5-HIS-6xUBI	pN1-RFP-DCP1A	

3.1.10. DNA oligonucleotides

3.1.10.1. Cloning primers

Construct	Primers (5'-3')	
TRIM71[1]	For	GGGGCGACGCGTATGGCTTCGTTCCCCGAGACC
	Rev	GGGGCGGCGGCCGCTTTAGAAGACGAGGATTCGATTGTTGCC
C12LC15A[2]	For	CCGATTTCCAGATCTTATTGCTGGCAAAGGAGATGTGCGGC
	Rev	GCCGCACATCTCCTTTGCCAGCAATAAGATCTGGAAATCGG
RBB[1]	For	GGGGCGACGCGTATGGCTTCGTTCCCCGAGACC
	Rev	GGGGCGGCGGCCGCTTAGCGGATCTTTTCTACCTTCCACAG
CCNHL[1]	For	GGGGCGACGCGTCAGGAGGCACTGCAGGACTC
	Rev	GGGGCGGCGGCCGCTTTAGAAGACGAGGATTCGATTGTTGCC
RBCC_WT[1]	For	GGGGCGACGCGTATGGCTTCGTTCCCCGAGACC
	Rev	GCGGGGGCGGCCGCTTTAGATGTCTAGCGCTCTACCCTCC
RBCC_C12LC15A[2]	For	CCGATTTCCAGATCTTATTGCTGGCAAAGGAGATGTGCGGC
	Rev	GCCGCACATCTCCTTTGCCAGCAATAAGATCTGGAAATCGG
FLNNHL[1]	For	GGGGCGACGCGTTTTGTTAGCAGCGGGGCCT
	Rev	GGGGCGGCGGCCGCTTTAGAAGACGAGGATTCGATTGTTGCC
FLN[1]	For	GGGGCGACGCGTATGTTTGTTAGCAGCGGGGC
	Rev	GGGGCGGCGGCCGCTTACTTGACCACGACCTTGAAGGG
NHL[1]	For	GGGGCGACGCGTAAGTCAGGCCGCAGC
	Rev	GGGGCGGCGGCCGCTTTAGAAGACGAGGATTCGATTGTTGCC
TRIM71-ΔNHL6[1]	For	GGGGCGACGCGTATGGCTTCGTTCCCCGAGACC
	Rev	GGGGCGGCGGCCGCTTAGTTGGATTCAAACATCTGTACCCGA
TRIM71-ΔCC[3]	For	GTAGAAAAGATCCGCCTAGACATCCTACTGGCCCG
	Rev	CAGTAGGATGTCTAGGCGGATCTTTTCTACCTTCCAC
TRIM71-SY/AF[2]	For	GAAAGCCAAGGCTCTGTTCCTGCAGGTGG
	Rev	CCACCTGCAGGAACAGAGCCTTGGCTTTC
TRIM71-STS/AAA[2]	For	CTCAACAAGCTTGAGGCCGCCATCGCTGCCGTGCAGCAGGTC
	Rev	GACCTGCTGCACGGCAGCGATGGCGGCCTCAAGCTTGTTGAG
TRIM71-SS/VV[2]	For	GGCTCGCCGGCGCCGCTCGTCGTCAACTCGTCCGCGTCGTCG
	Rev	CGACGACGCGGACGAGTTGACGACGAGCGGCGCCGGCGAGCC
R608H[2]	For	ATGGCAAGCTCTGCCACCCTTGGGGTGTGAG
	Rev	CTCACACCCCAAGGGTGGCAGAGCTTGCCAT
R796H[2]	For	ATGGGCAGTTCCTGCACCCACAAGGGGTAGC
	Rev	GCTACCCCTTGTGGGTGCAGGAACTGCCCAT
λN insert (C-ter)[1]	For	GGGGCGGCGGCCGCATGAACGCAAGAACACGAC
	Rev	GGGGCGGCGGCCGCTTAGTTTGCAGCTTTCCATTGAG
TRIM71-λN/R796H-λN (ΔSTOP)[2]	For	CGAATCCTCGTCTTC_AGCGGCCGCATGAACGCA
	Rev	TGCGTTCATGCGGCCGCT_GAAGACGAGGATTCG
LIN28A[1]	For	GCGGGGACGCGTATGGGCTCCGTGTCCAACC
	Rev	GGGGCGGCGGCCGCTCAATTCTGTGCCTCCGGGAG

Construct	Primers (5'-3')	
UPF1[1]	For	GGGGCGACGCGTATGAGCGTGGAGGCGTACG
	Rev	GGGGCGGCGGCCGCTTAATACTGGGACAGCCCCGTC
TRIM32[1]	For	GGGGCGACGCGTATGGCTGCAGCAGCAGCTTC
	Rev	GGGGCGGCGGCCGCCTATGGGGTGGAATATCTTCTCAGATGG
AGO2[1]	For	GCGGGGACGCGTATGTACTCGGGAGCCGGCC
	Rev	GCGGGGGCGGCCGCTCAAGCAAAGTACATGGTGCGCAGA
DCP1A[1]	For	GGGGCGACGCGTATGGAGGCGCTGAGTCGAG
	Rev	GGGGCGGCGGCCGCTCATAGGTTGTGGTTGTCTTTGTTCTTGG
Renilla-empty (New NotI site)[2]	For	CAGTAATTCTAGGCGGCCGCTCGAGCGCCAAC
	Rev	GTTGGCGCTCGAGCGGCCGCCTAGAATTACTG
CDKN1A CDS[1]	For	GGGGCGCTCGAGATGTGGGGAGTATTCAGGAGACAG
	Rev	GGGGCGGCGGCCGCTTAGGGCTTCCTCTTGGAGAAGAT
CDKN1A 3'UTR (FL)[1]	For	GGGGCGCTCGAGTCCGCCCACAGGAAGCCTGCAGTC
	Rev	GGGGCGCGGCCGCACAAGTAAAGTCACTAAGAATCATTTATTGAG
F1_CDKN1A 3'UTR[1]	For	GGGGCGCTCGAGTCCGCCCACAGGAAGCCTGCAGTC
	Rev	GGGGCGGCGGCCGCTTTGATGATGCCCCCACTCGG
F2_0-500-CDKN1A 3'UTR (F2)[1]	For	GGGGCGCTCGAGAACTTTGGAGTCCCCTCACCTC
	Rev	GGGGCGGCGGCCGCCCTGTGCCACCACATGGGA
F2_0-400-CDKN1A 3'UTR[1]	For	GGGGCGCTCGAGAACTTTGGAGTCCCCTCACCTC
	Rev	GGGGCGGCGGCCGCCCTTCCAGTCCATTGAGCTGG
F2_0-300-CDKN1A 3'UTR[1]	For	GGGGCGCTCGAGAACTTTGGAGTCCCCTCACCTC
	Rev	GGGGCGGCGGCCGCGGAATTGCAGAGCCCAGCTG
F2_0-200-CDKN1A 3'UTR[1]	For	GGGGCGCTCGAGAACTTTGGAGTCCCCTCACCTC
	Rev	GGGGCGGCGGCCGCCTCAACACTGAGACGGGCTCC
F2_0-100-CDKN1A 3'UTR[1]	For	GGGGCGCTCGAGAACTTTGGAGTCCCCTCACCTC
	Rev	GGGGCGGCGGCCGCGTATCAAGAGCCAGGAGGGTACC
F2_100-200-CDKN1A 3'UTR (WT)[1]	For	GGGGCGCTCGAGGGTACCCTCCTGGCTCTTGATAC
	Rev	GGGGCGGCGGCCGCCTCAACACTGAGACGGGCTCC
F2_100-200_M#1-CDKN1A 3'UTR[2]	For	GCTCTTGATACCCCCCTCT_AGGGGGAAGGTGGGG
	Rev	CCCCACCTTCCCCCTAGA_GGGGGGTATCAAGAGC
F2_100-200_M#2-CDKN1A 3'UTR[2]	For	CCCCCTCTGTCTTGTAAAGGCAGGGGGAAGG
	Rev	CCTTCCCCCTGCCTTTACAAGACAGAGGGGG
F2_100-200_M#3-CDKN1A 3'UTR[2]	For	CCCCCTCTGTCTTGTCAAGGCAGGGGGAAGG
	Rev	CCTTCCCCCTGCCTTGACAAGACAGAGGGGG
F2_100-200_M#4-CDKN1A 3'UTR[2]	For	CCCCCTCTGTCTTGTGCAGGCAGGGGGAAGG
	Rev	CCTTCCCCCTGCCTGCACAAGACAGAGGGGG
F3_CDKN1A 3'UTR[1]	For	GGGGCGCTCGAGCCCCCTTGAGTGGGGTTATCT
	Rev	GGGGCGCGGCCGCACAAGTAAAGTCACTAAGAATCATTTATTGAG

Construct	Primers (5'-3')	
CDKN1A 3'UTR-3xBoxB[4]	For	GGCCGCGGGCCCTGAAGAAGGGCCCAGGGCCCTGAAGAAGGGCCCAGGGCCCTGAAGAAGGGCCCGC
	Rev	GGCCGCGGGCCCTTCTTCAGGGCCCTGGGCCCTTCTTCAGGGCCCTGGGCCCTTCTTCAGGGCCCGC
3xlet-7a binding sites[4]	For	TCGAGAACTATACAACCTACTACCTCAAAACTATACAACCTACTACCTCAAAACTATACAACCTACTACCTCAGC
	Rev	GGCCGCTGAGGTAGTAGGTTGTATAGTTTTGAGGTAGTAGGTTGTATAGTTTTGAGGTAGTAGGTTGTATAGTTC
3xlet-7g binding sites[4]	For	TCGAGAACTGTACAAACTACTACCTCAAAACTGTACAAACTACTACCTCAAAACTGTACAAACTACTACCTCAGC
	Rev	GGCCGCTGAGGTAGTAGTTTGTACAGTTTTGAGGTAGTAGTTTGTACAGTTTTGAGGTAGTAGTTTGTACAGTTC
3xmiR-128 binding sites[4]	For	TCGAGAAAGAGACCGGTTCACTGTGAAAAAGAGACCGGTTCACTGTGAAAAAGAGACCGGTTCACTGTGAGC
	Rev	GGCCGCTCACAGTGAACCGGTCTCTTTTTCACAGTGAACCGGTCTCTTTTTCACAGTGAACCGGTCTCTTTC
3xmiR-16 binding sites[4]	For	TCGAGCGCCAATATTTACGTGCTGCTAACGCCAATATTTACGTGCTGCTAACGCCAATATTTACGTGCTGCTAGC
	Rev	GGCCGCTAGCAGCACGTAAATATTGGCGTTAGCAGCACGTAAATATTGGCGTTAGCAGCACGTAAATATTGGCGC
3xmiR-19 binding sites[4]	For	TCGAGAGTTTTGCATAGTTGCACTACAAAGTTTTGCATAGTTGCACTACAAAGTTTTGCATAGTTGCACTACAGC
	Rev	GGCCGCTGTAGTGCAACTATGCAAAACTTTGTAGTGCAACTATGCAAAACTTTGTAGTGCAACTATGCAAAACTC

[1] Conventional cloning (restriction sites underlined; MluI: A^CGCGT, XhoI: C^TCGAG; NotI: GC^GGCCGC).
[2] Site-directed mutagenesis cloning (mutation/deletion underlined).
[3] SOEing PCR of independently-amplified fragments (overlapping region underlined).
[4] Artificial oligo-annealing cloning (restriction sites after-digestion mimic underlined).

3.1.10.2. Primers for SYBR Green qPCR

Target	Primers (5'-3')	
Hs 18S rRNA	For	GTAACCCGTTGAACCCCATTC
	Rev	CCATCCAATCGGTAGTAGCGAC
Hs ATF3	For	CACTGGTGTTTGAGGATTTTGCTAA
	Rev	GCAGCTGCAATCTTATTTCTTTCTC
Hs CCNE2	For	TAGCTGGTCTGGCGAGGTTT
	Rev	ACAGGTGGCCAACAATTCCT
Hs CDH1	For	GAAAACAGCAAAGGGCTTGGA
	Rev	TTAGGGCTGTGTACGTGCTG
Hs CDKN1A_TV1-5	For	ATGTCAGAACCGGCTGGG
	Rev	TTAGGGCTTCCTCTTGGAGAAGAT
Hs CDKN1A_TV3	For	ATGTGGGGAGTATTCAGGAGACAG
	Rev	TTAGGGCTTCCTCTTGGAGAAGAT

Target	Primers (5'-3')	
Hs GADD45B	For	GCAGAAGATGCAGACGGTGAC
	Rev	CACGATGTTGATGTCGTTGTCAC
Hs HOXA5	For	AAAACTCCCTAAGCAACTCC
	Rev	ATGTTGTCATGACTTATGTGC
Hs MYB	For	GGAGACCCCGACACAGC
	Rev	CCAAGTGACGCTTTCCAGATTTG
Hs pre-CDKN1A	For	ACTCTCAGGGTCGAAAACGG
	Rev	GCCTGGCATAATGAACATTCCC
Hs PUM2	For	ATGTCCCAGCCTATTATGGTACAG
	Rev	CCTTTCTCAGGTCCATCTGTTTCAG
Hs SMG1	For	TACTTATGGTCGGAAGTCGTTGG
	Rev	GCCAATCTTCGGTCTCTGTCG
Hs SMG6	For	CGGGAGCAGAGAAAACATGAA
	Rev	AGCAGAGCAATCTCGGTCAT
Hs SMG7	For	TACCTCCGGCAGGCAGAA
	Rev	CTGGCCTTGCAGTGTTGTGA
Hs STATB5	For	CCCAGCGCAGGCAACT
	Rev	AGCGGTCATACGTGTTCTGG
Hs TBL2	For	CATCTGGAGCACCAAGGACTTC
	Rev	GTGCTTTTTAGGGAAGTCCTCTGG

3.1.10.3. Probes for TaqMan qPCR (products from Thermo Fisher Scientific, Expression Assays)

Target	Product ID
Hs CDKN1A	Hs00355782_m1
Hs E2F7	Hs00171569_m1
Hs FOXJ1	Hs00230964_m1
Hs GADD45A	Hs01003267_m1
Hs GAPDH	4352934
Hs HMGA2	Hs00171569_m1
Hs HPRT1	Hs01003267_m1
Hs INHHB	Hs00173582_m1
Hs LIN28B	Hs01013729_m1
Hs TRIM71	Hs01394933_m1
Hs UPF1	Hs00161289_m1
Hs U6 snRNA	001973
Hs let-7a	000377
Hs let-7g	002282
Hs miR-16a	000391
Mm miR-294	001056
Mm Cdkn1a	Mm04205640_g1
Mm Trim71	Mm01341471_m1

3.1.11. RNA oligonucleotides

3.1.11.1. siRNAs

Name	Sequence (5'-3')
siCtrl (Renilla)	AAACAUGCAGAAAAUGCUGTT
siTRIM71#1	CCGUGUGCGACCAGAAAGUATT
siTRIM71#2	AGAAAGUAGUGCUAGCCGATT
siDGCR8	AUCCGUUGAUCUCGAGGAAUUTT
siAGO2	GCACGGAAGUCCAUCUGAAUUTT
siPUM2	GCAUGGUAGAAUAUGUAUUTT
siTUT4 (ZCCHC11)	GGAGCACAUAAACAUAUAATT
siUPF1#1	GAUGCAGUUCCGCUCCAUUTT
siUPF1#2	AAUUUCUGUAACUUGUUUCCUTT
siSMG1	GUGAAGAUGUUCCCUAUGATT
siSMG6	GGGUCACAGUGCUGAAGUATT
siSMG7	CAGCACAGUCUACAAGCCATT
siLIN28B	GGAAGGAUUUAGAAGCCUAAA

3.1.11.2. miRNAs (products from Thermo Fisher Scientific, mirVana miRNA mimics)

Name	Product ID
miR Ctrl/siCtrl (Negative control #1 miRNA mimic)	4464058
Let-7a (hs-let-7a-5p miRNA mimic)	4464066
pre-let7a (hs-let-7a-5p miRNA precursor)	PM10050
pre-mir-16 (hs-miR-16-5p miRNA precursor)	PM10339

3.1.11.3. ssRNA (products from Elle Biotech, 5’Cy3-conjugated)

Name	Sequence (5'-3')
TRE WT	GCUUUGUGAAGGC
TRE M#3	GUCUUGUCAAGGC

3.1.12. Organisms

Cell line name	Type
mESCs Trim71 fl/fl (WT)	Mouse embryonic stem cells
mESCs Trim71 -/- (KO)	Mouse embryonic stem cells
mESCs Lin28A -/- (KO)	Mouse embryonic stem cells
mESCs wild type (WT)	Mouse embryonic stem cells
mESCs Trim71 R595H	Mouse embryonic stem cells
HEK293T (WT)	Human embryonic kidney tumor cells
HEK293T AGO2 -/- (KO)	Human embryonic kidney tumor cells
HEK293 GFP	Human embryonic kidney tumor cells
HEK293 GFP-TRIM71	Human embryonic kidney tumor cells
NIH3T3	Mouse embryonic fibroblasts
JURKAT E6.1	Human acute leukemia T cells
NCCIT	Human embryonic carcinoma (non-seminoma)
TCam-2	Human embryonic carcinoma (seminoma)
HepG2	Human hepatocellular carcinoma
CV1	Monkey embryonic kidney
DH5α E. Coli	Competent Gram-negative bacteria
Vaccinia Virus	DNA enveloped Poxvirus

3.1.13. Software and online tools

Name	Company/URL Direction
CFX Manager Software (qPCR data analysis)	BIO-RAD
FACS Diva Software (FACS data recording)	BD Biosciences
FlowJo V10 Software (FACS data analysis)	FlowJo
Fluoview Olympus FV10-ASW Software (imaging)	Olympus
Fiji (Image J) Software (imaging data analysis)	Fiji
Image Studio Lite (Western Blot band densitometry)	LI-COR Biosciences
KC4 Vx (colorimetric measurement and analysis)	BioTek
Prism7 Software (data illustration and analysis)	GraphPad
WinGlow Software (luminiscence measurement)	Berthold Technologies
RNAfold (nucleic acid secondary structure prediction)	http://rna.tbi.univie.ac.at/cgi-bin/RNAWebSuite/RNAfold.cgi
R2 database (genomic analysis and visualization)	https://hgserver1.amc.nl/cgi-bin/r2/main.cgi
GEPIA server (genomic analysis and visualization)	http://gepia.cancer-pku.cn/
Swiss-Model (protein structure modeling)	https://swissmodel.expasy.org/
Coot Software (macromolecular modeling)	https://www2.mrc-lmb.cam.ac.uk/personal/pemsley/coot/
TargetScan (miRNA-binding site prediction)	http://www.targetscan.org/vert72/

3.2. Methods

3.2.1. Molecular cloning

3.2.1.1. Amplification of the gene of interest by PCR

In order to clone a gene of interest (GOI) in a eukaryotic expression vector, a polymerase chain reaction (PCR) was conducted using sequence-specific forward (For) and reverse (Rev) primers targeting homology regions upstream and downstream of the sequence of interest, respectively. For protein overexpression, constructs were cloned into pN1 or pRK5 vectors downstream of a Flag-, GFP-, Ig-, HA- or His-tag, with primers designed to amplify the coding sequence/open reading frame (CDS/ORF), without including regulatory elements such as untranslated regions (UTRs). For luciferase reporter assays, constructs were cloned into psiCHECK2 vectors downstream of the Renilla Luciferase CDS/ORF, with primers designed to amplify specific regulatory elements (either the 3'UTR or an artificial sequence containing miRNA-binding sites). The primers used for the PCR amplification contained restriction sites for subsequent enzymatic digestion prior to ligation into the desired vector. To enable directional cloning of the sequence of interest, all sequences cloned into pN1 or pRK5 vectors were amplified with For/Rev primers containing MluI/NotI restriction sites, whereas all sequences cloned into psiCHECK2 vectors were amplified with For/Rev primers containing XhoI/NotI restriction sites. For the initial cloning of a GOI, a human brain cDNA library was used as source template material, whereas for the subsequent cloning of truncated sequences within the GOI, a vector containing the full length sequence was used as a source template material. The standard PCR reaction mix and cycling conditions were the following:

PCR reaction

Reagent	Vol. (for 50 µl)
Phusion GC buffer (5x)	10 µl
dNTPs (10 mM)	1 µl
Forward primer (10 µM)	2 µl
Reverse primer (10 µM)	2 µl
Template DNA (100 ng/µl)	1 µl
DMSO (100%)	2.5 µl
Phusion DNA polymerase (2.5 U/µl)	0.5 µl
ddH_2O	31 µl

PCR cycling

Cycles	Conditions	Phase
1x	98°C, 2 min	Initial denaturation
15-35x	98°C, 30 sec	Denaturation
	60°C, 20 sec	Annealing
	72°C, 30 sec/kb	Extension
1x	72°C, 10 min	Final extension
1x	4°C, hold	End

3.2.1.2. Purification of PCR products

Successful PCR amplification was confirmed by visualizing the size of the PCR product in agarose gels. Specifically, 5 µl of PCR reaction were mixed with 1 µl of 6x DNA loading dye and loaded in a 1% agarose/1x TAE gel. The gel was run at 100 V for 30 min in 1x TAE buffer (40 mM Tris, 20 mM acetic acid, 1 mM EDTA pH 8) containing ethidium bromide diluted 1:50000. PCR products were visualized under a UV-transilluminator. The remaining PCR reaction volume was brought up to 400 µl with ddH_2O and nucleic acids were extracted by adding 300 µl of phenol-chloroform (1:1), followed by vigorous vortexing and centrifugation at 12000 rpm and 4°C for 5 min. The upper aqueous phase was then recovered, and nucleic acids were precipitated by adding 40 µl of 4 M LiCl salt and 1 ml of cold pure ethanol, followed by incubation at -20°C for 30 min and centrifugation at 12000 rpm and 4°C for 15-30 min. The resultant DNA pellet was washed once with 70% ethanol, dried at 37°C and resuspended in 20 µl ddH_2O.

3.2.1.3. Enzymatic DNA digestion and ligation

The purified DNA and the desired vector backbone were subjected to digestion with specific restriction enzymes for 2 h at 37°C (MluI/NotI for pN1 and pRK5 vectors and XhoI/NotI for psiCHECK2 vectors). The digestion reaction was prepared as follows:

Digestion reaction

Reagent	Vol. (for 30 µl)
purified DNA	20 µl
Fermentas buffer O (10x)	3 µl
MluI or XhoI (10 U/µl)	2 µl
NotI (10 U/µl)	1 µl
ddH_2O	4 µl

After digestion, vector backbones were treated with 1 µl of alkaline phosphatase (FastAP, 1U/µl) at 37°C for 30 min. Digestion reactions were run in 1% agarose gels, in order to separate the desired product from other unspecific-amplified PCR products. The desired bands were cut out of the gel using a scalpel, and the DNA was extracted from the gel using the NucleoSpin Gel and PCR Clean-up kit according to the manufacturer's instructions. The DNA concentration for purified digested PCR products and vector backbones was quantified using a Nanodrop spectrophotometer, and insert and vectors were ligated for 1 h at RT or overnight at 16°C. A ligation reaction with digested-dephosphorylated linear vector and no insert was set as transformation control, since bacteria can only be successfully transformed with circular DNA. The ligation reaction was prepared as follows:

Ligation reaction

Reagent	Vol. (for 20 µl)
Vector : Insert	1:3 molar ratio
Ligase buffer (10x)	2 µl
T4 DNA ligase (5 U/L)	1 µl
ddH_2O	up to 20 µl

3.2.1.4. Bacterial transformation

After ligation, plasmids were transformed in bacteria and amplified by bacterial growth. Chemically competent DH5α *E. Coli* were thawed on ice and mixed with the ligated plasmid (60 µl of bacteria and 7 µl of ligation reaction). After 10 min incubation on ice, bacteria were transformed by a heat shock at 42°C in the water bath for 45 sec. Immediately after the heat shock, bacteria were placed on ice again and diluted in 1 ml LB medium without antibiotics. Bacteria were then incubated for 1 h at 37°C under agitation at 600 rpm in order to recover from the heat shock and to allow the expression of the specific antibiotic resistance gene encoded by the transformed plasmid (kanamycin resistance in pN1 vectors and ampicillin resistance in pRK5 and psiCHECK2 vectors). Bacterial suspensions were then pelleted by centrifugation at 3000 rpm and RT for 2 min and resuspended in 100 µl LB before plating on LB agar plates containing the corresponding selective antibiotic (30 µg/ml kanamycin or 100 µg/ml ampicillin). The bacterial plates were incubated upside-down at 37°C overnight, and successful transformation was confirmed by the appearance of significantly more colonies in the plasmid-transformed plates as compared to the transformation control plate (see previous section). Individual clones were then picked with a pipette tip and inoculated in 4 ml LB medium with the corresponding selective antibiotic in the concentrations specified above, and grown overnight under agitation at 180 rpm and 37°C. Half of the bacterial suspensions were then used for mini-preparation of plasmid DNA in order to confirm the identity of the cloned sequences, whereas the other half was kept for subsequent maxi-preparation of plasmid DNA in case of positive identification of the desired sequence.

3.2.1.5. Mini-preparation of plasmid DNA

After an overnight incubation, 2 ml of bacterial suspension were centrifuged at 3000 rpm and RT for 2 min. Bacterial pellets were then resuspended in 200 µl solution I, and lysed by adding 400 µl of solution II followed by 3 min incubation at RT. The lysate was then neutralized by adding 300 µl of solution III (see Solution I-III composition below), centrifuged at 12000 rpm and 4°C for 10 min, and the supernatant was transferred to a new cap. Nucleic acids were then extracted by adding 400 µl of phenol-chloroform (1:1) followed by vigorous vortexing and centrifugation at 12000 rpm and 4°C for 5min. The upper aqueous phase was transferred to a new cap and plasmid DNA was precipitated by adding 600 µl of isopropanol followed by centrifugation at 12000 and 4°C for 15min. The DNA pellet was then washed once with 70% ethanol, dried at 37°C and resuspended in 50 µl of ddH_2O containing 5 µg of RNaseA. Samples were then subjected to RNase digestion at 37°C for 10 min. Afterwards, 3 µl of each mini-preparation were used to conduct several digestion tests with selected restriction enzymes, generating specific band patterns that allowed the identification of positive clones. Specifically, two digestions were performed per mini-preparation: an “insert release digestion” by using the same enzyme pair whose restriction sites were initially included in the cloning primers (MluI/NotI or XhoI/NotI), and an “identity digestion”, by using a single restriction enzyme chosen for every particular plasmid, containing a single restriction site within the insert and another site within the vector backbone. The resultant digestion products were visualized on a 1% agarose gel and positive clones were then Sanger-sequenced (Eurofins Genomics GATC) to confirm their identity. The remaining 2 ml of the corresponding bacterial suspension were then inoculated in 1 L of LB with antibiotics for maxi-preparation, in order to produce the cloned plasmid in high amounts and high purity.

3.2.1.6. Maxi-preparation of plasmid DNA

For maxi-preparations of plasmid DNA, 1 L of overnight-grown bacterial suspension was centrifuged at 4200 rpm and RT for 20 min and the pellet was resuspended in 40 ml of solution I followed by the addition of 80 ml of solution II and incubation for 5 min at RT to assist alkaline lysis. The pH was then neutralized by adding 40 ml of solution III and lysates were then cleared by centrifugation at 4200 rpm and 4°C for 15 min. The supernatant, containing the plasmid DNA, was filtered through a gauze and mixed with 100 ml isopropanol for DNA precipitation. After centrifugation at 6000 rpm and 4°C for 15 min, the DNA pellet was dried and then resuspended in 4 ml of solution I supplemented with 5.5 g of CsCl salt, 500 µl of ethidium bromide and 100 µl of 10% Igepal detergent. The sample was vigorously mixed until it became homogeneous and then centrifuged at 4500 rpm and RT for 5 min. The supernatant was transferred to an ultracentrifugation tube, and after proper tube sealing, samples were subjected to density gradient ultracentrifugation at 80000 rpm and RT for 4 h. Plasmid DNA was then recovered by aspirating the visible dark-red band in the middle of the tube with a syringe, followed by several washings steps with 1-butanol saturated with 1 M NaCl salt to remove the ethidium bromide. Plasmid DNA was then precipitated by adding 1 volume of 1 NH_4OAc salt and 3 volumes of pure ethanol, followed by centrifugation at 4500 rpm and 4°C for 5 min. The DNA pellet was then washed with 70% ethanol, air-dried and resuspended in 500 µl of ddH_2O, and DNA concentration was quantified using a Nanodrop spectrophotometer.

Solutions for mini- and maxi-preparations of plasmid DNA

Solution I (pH 8)	Solution II (pH 13)	Solution III (pH 5)
25 mM Tris-HCl	0.2 M NaOH	5 M KAc
50 mM Sucrose	1% SDS	2 M HAc
10 mM EDTA		

3.2.1.7. Cloning of miRNA luciferase reporters

In order to investigate TRIM71-mediated regulation of miRNA activity, artificial forward and reverse sequences containing three subsequent copies of the specific miRNA-binding site (BS) were designed and ordered as long oligonucleotides (oligos). These oligos furthermore included specific nucleotides in the 5' and 3' end mimicking the cohesive ends resulting from a double digestion with XhoI/NotI. Of note, miRNA binding sites corresponded to the sequence of the miRNA passenger strand and were present in the forward oligo. Forward and reverse oligos were combined (see annealing reaction below), denatured for 5 min at 95°C, and annealed by progressive temperature lowering while left in the turned-off thermoblock until RT was reached. Annealed oligos were then directly ligated into a non-dephosphorylated XhoI/NotI-digested psiCHECK2 vector, and the cloning process continued from this point on as specified above.

Annealing reaction

Reagent	Vol. (for 50 µl)
NEB buffer 2 (10x)	5 µl
Forward primer (100 µM)	1 µl
Reverse primer (100 µM)	1 µl
ddH_20	43 µl

3.2.1.8. Cloning of point mutants by site-directed mutagenesis

In order to introduce specific point mutations within already-cloned plasmids, completely self-complementary For/Rev primers annealing with the region of interest were designed. Primers were approximately 30-35 bp-long and contained the desired mutation in the middle of their sequence. A specific PCR reaction was used to allow the rolling-circle amplification of the whole plasmid (see PCR reaction and cycling conditions below). As a result, the amplified plasmid contained the desired mutation, while the parental plasmid used as a template was then digested by directly adding to the PCR reaction 1 µl of DpnI (10 U/µl) restriction enzyme, which is able to digest methylated DNA. The digested PCR product was then directly transformed into bacteria. This method did neither require the purification of PCR and digestion products, nor ligation. After bacterial transformation, the cloning process followed as specified above.

Mutagenesis PCR reaction

Reagent	Vol. (for 50 µl)
Pfu Ultra buffer (10x)	5 µl
dNTPs (10 mM)	1 µl
Forward primer (10 µM)	2 µl
Reverse primer (10 µM)	2 µl
plasmid DNA (100 ng/µl)	1 µl
DMSO (100%)	2.5 µl
Pfu DNA polymerase (2.5 U/µl)	1 µl
ddH_2O	36 µl

Mutagenesis PCR cycling

Cycles	Conditions	Phase
1x	98°C, 2 min	Initial denaturation
15x-18x	98°C, 30 sec	Denaturation
	55°C, 1 min	Annealing
	68°C, 1 min/kbp	Extension
1x	72°C, 10 min	Final extension
1x	4°C, hold	End

3.2.2. Cell-based assays

3.2.2.1. Cell culture maintenance

To initially put cells in culture, the vials stored in liquid nitrogen were rapidly thawed in the water bath at 37°C and cells were washed once in suitable pre-warmed culture media to eliminate the DMSO present in the freezing media (50% FBS, 40% complete media, 10% DMSO). Freezing of cells was conducted slowly in cryotubes within freezing containers which allow a constant temperature drop of -1ºC/min when placed closed at -80°C. All cells were grown by incubation at 37℃ in a controlled atmosphere provided with 5% CO_2 and 95% relative humidity. Centrifugation of cells was always performed at 1200 rpm for 5 min. All

cells were periodically washed with PBS before media replacement or before detaching for splitting, and the culture plates/flasks were renewed every week when cells remained longer times in culture, albeit never exceeding 15 splitting generations to avoid the accumulation of spontaneous mutations.

HEK293 cells stably overexpressing GFP or GFP-TRIM71 were kindly provided by Dr. Schneider (LIMES Institute, University of Bonn). For the stable expression of GFP or GFP-TRIM71 in HEK293 cells, which are susceptible to G418/Neomycin antibiotic, cells were transfected by Calcium Phosphate with linearized plasmids (pN1-GFP or pN1-GFP-TRIM71) containing a G418 resistance gene. The expression of GFP was confirmed 48 h post-transfection (hpt) under the fluorescence microscope. Around 50% of the cells were shown to be efficiently transfected (data not shown). The integration of DNA into the genome occurs randomly in approximately 1 of every 100 transfected cells. Stably transfected cells (GFP positive) were then selected by incubation with 600 µg/ml of G418 antibiotic for 8 days, changing the antibiotic-containing media every second day. After selection, 100% of the cells were GFP positive and considered to be stably transfected. Individual clones were grown and the expression of GFP or GFP-TRIM71 was checked by protein extraction followed by western blot analysis with anti-GFP and anti-TRIM71 antibodies. HEK293 cells were maintained in DMEM media supplemented with 10% FBS and 600 µg/ml of G418 antibiotic solution, and split every 2-3 days. HEK293T cells were maintained in DMEM media supplemented with 10% FBS and 1% Penicillin-Streptomycin antibiotic solution, and split every 2-3 days. For splitting, HEK293 and HEK293T cells were detached from the plates by gentle pipetting. AGO2 Knockout (KO) HEK293T cells, generated by Dr. Ebert and kindly provided by Prof. Hornung (Gene Center, Ludwig-Maximilian University of Munich), were maintained under the same conditions. The generation of AGO2 KO HEK293T cells was achieved by transfection with CRISPR/CAS9 vectors targeting the exon 3 of the AGO2 mature mRNA sequence (target sequence: 5'-GGAAGCCCGTGTTTGACGGCAGG-3'). Single clones were grown and deep-sequenced with primers amplifying the target sequence to confirm the presence of an ORF-altering mutation. Positive clones were then checked for AGO2 KO by protein extraction followed by western blot analysis with an anti-AGO2 antibody.

NIH3T3 mouse fibroblasts were maintained in DMEM media supplemented with 10% FBS and 1% Penicillin-Streptomycin antibiotic solution, and split every 2-3 days. HepG2 human hepatocellular carcinoma cells were maintained in RPMI 1640 media supplemented with 10% FBS and 1% Penicillin-Streptomycin antibiotic solution, and split every 4 days. For splitting, NIH3T3 and HepG2 cells were detached from plates by incubation with 0,05% Trypsin-EDTA solution at 37°C for 2-3 min. Jurkat E6.1 human acute leukemia T cells were maintained in RPMI 1640 media supplemented with 10% FBS and 1% Penicillin-Streptomycin antibiotic solution, and split every 2 days. Jurkat E6.1 cells were grown in suspension within flasks and were simply diluted for their splitting. Mouse embryonic stem cells (mESCs) were maintained in DMEM knockout media supplemented with 15% FBS, 1% Penicillin-Streptomycin antibiotic solution, 1% Non-essential amino acids, 1% GlutaMAX, 0.2% Leukemia inhibitory factor (LIF) and 0.1% β-mercaptoethanol. The media of mESCs was replaced every day to avoid that complete consumption of LIF resulted in spontaneous differentiation, and cells were strictly split 1:4 every second day to avoid exceeding 60% confluence, which can also drive spontaneous differentiation. For splitting, mESCs were detached from plates by incubation with in StemCell Pro Accutase solution at 37°C for 1 min. TRIM71 knockout mESCs, LIN28A knockout mESCs and double TRIM71-LIN28A knockout mESCs were

kindly provided by Dr. Mitschka (LIMES Institute, University of Bonn) and their generation is specified elsewhere[113]. TRIM71 homozygous mutant R595H mESCs were a kind gift from Prof. Kahle (Yale School of medicine, Boston) and their generation is specified elsewhere[142]. To induce neural differentiation of mESCs, cells were detached, washed in PBS and plated for 4 days in N2B27 differentiation media (Neurobasal medium mixed with DMEM/F12 medium 1:1, supplemented with 1% Penicillin-Streptomycin, 50 mg/ml BSA, 0.5% GlutaMAX, 1% N2 Supplement and 2% B27 Supplement). The media was renewed every day and samples were taken every second day in order to monitor the course of differentiation.

3.2.2.2. Cell transfections

DNA transfection in HEK293 and HEK293T cells was conducted with the well-established calcium phosphate method, which is based on the formation of salt-DNA precipitates upon mixing DNA with $CaCl_2$ in a phosphate buffered saline solution (2x HBS). When these calcium phosphate-DNA precipitates are in contact with the cell surface, they are incorporated into the cell, presumably by endocytosis. Specifically, the DNA was first solved in 0.25 M $CaCl_2$ and this solution was added dropwise onto a 2x HBS solution while vortexing. The transfection solution was then incubated at 37°C for 5 min or at RT for 30 min, and added dropwise to the cells growing in plates at approximately 60% confluence, preferentially split the day before and containing fresh media. 6 hpt, cells were carefully washed 1-2 times with PBS avoiding cell detaching and fresh media was added. Cells were harvested 48 hpt for further analysis. Although transfections in each specific experiment required different amounts of total DNA (see DNA amounts and transfection volumes below), the final DNA concentration in the transfection solution was always 25 µg DNA/ml of calcium phosphate, and the $CaCl_2$-DNA and 2x HBS solutions were always mixed 1:1.

Calcium phosphate transfection*

Culture dish	N° Cells**	DNA (µg)	$CaCl_2$ (µl)	2x HBS (µl)
12-well plate	0.25×10^6	3	60	60
6-well plate	0.75×10^6	6	120	120
6 cm dish	2×10^6	10	200	200
10 cm dish	5×10^6	25	500	500

*Amounts are specified per well or dish

**approximate numbers of HEK293(T) cells for 60% confluence

2xHBS

42 mM HEPES pH 7.05
274 mM NaCl
10 mM KCl
1.4 mM Na_2HPO_4
15 mM D-glucose

DNA transfection in NIH3T3 and HepG2 cells was conducted with Lipofectamine 2000 reagent following the manufacturer's instructions and using a ratio 1µg:2µL DNA:Lipofectamine 2000. DNA transfection in mESCs was conducted with PANfect reagent following the manufacturer's instructions and using a ratio 1µg:2µL DNA:PANfect. Jurkat E.6 cells were transfected by electroporation in 1:1 RPMI:FBS media using an exponential wave program in a Bio-Rad electroporation system and providing a single pulse of 240 V. All DNA-transfected cells were harvested 48 hpt for further analysis. siRNA/miRNA transfection for all cell lines was conducted with the use of Lipofectamine RNAiMAX reagent following the manufacturer's instructions and using a ratio 10pmol:2µL RNA:Lipofectamine RNAiMAX. Cells transfected with siRNAs/miRNAs were typically harvested 72 hpt for further analysis, since this was the time where efficient knockdown normally reached its maximal effect (data not shown).

3.2.2.3. Proliferation assays

For proliferation assays, a CFSE-like proliferation assay was conducted using the cell proliferation dye eFluor670, which specifically binds to any cellular protein containing primary amines. Upon every cell division, the whole cell content, including proteins available, distributes equally between daughter cells, thereby decreasing by half the fluorescence intensity of single cells. In immortalized cell lines, where the whole population of cells is constantly proliferating, the complete eFluo670 histogram shifts to lower values day after day, without remaining a peak for the – in this case inexistent – non-proliferating population. For this reason, in case of proliferation experiments with cell lines, measuring the initial fluorescence intensity is especially important. The cell proliferation dye eFluor670 has an excitation peak at 647 nm and therefore can be excited by the red laser at 633 nm. Emission at 670 nm was detected with the APC or Alexa647 660/20 band pass filter.

For staining, cells were detached and washed once in PBS to eliminate rests of FBS which may interfere with the procedure. Next, 10^6 cells were stained with eFuo670 diluted to 5 µM in 1 ml of PBS. Staining was conducted at 37°C in the dark for 10 min and stopped by the addition of 4 ml cold FBS and 5 min incubation on ice. Cells were then pelleted at 1200 rpm and 4°C for 5min and washed once with complete media before platting them in triplicates. The fluorescence intensity was measured by FACS directly after staining (day 0), and its decrease upon cell division over time was monitored every 24 h for 4 days after staining. The number of cell divisions was calculated assuming half decrease of the median fluorescence intensity (MFI) upon each cell division with the following formula:

$$\text{Division Number} = \log_2 [(\text{MFI}_{\text{day 0}} - \text{MFI}_{\text{unstained}}) / (\text{MFI}_{\text{day X}} - \text{MFI}_{\text{unstained}})]$$

The length of each cell cycle can be calculated from the number of cell divisions at any time point in the proliferation experiment. Our experiments typically depicted the average cell cycle duration in hours, calculated at the end of the experiment as 96h/Division Number.

For proliferation experiments in TRIM71 knockdown HepG2 cells and mESCs, staining was conducted 24 h after siRNA transfection. In case of HEK293 cells stably expressing GFP or GFP-TRIM71, cells were stained at any desired time point, and proliferation of GFP-positive cells was measured. For proliferation experiments of stable wildtype and TRIM71 knockout mESCs, cells were stained at any desired time point. For proliferation experiments in mESCs undergoing differentiation into neural progenitor cells (NPCs), staining was conducted immediately before their culture in N2B27 differentiation media.

3.2.2.4. Cell Imaging by confocal laser scanning microscopy

For p-body co-localization studies, HEK293T cells were co-transfected with the P-body-specific marker DCP1A (pN1-RFP-DCP1A) and the desired pN1-GFP-TRIM71 construct in a 1:1 ratio, and seeded on glass Poly-L-Lysine-coated coverslips 24 hpt. The coating was done by adding 200 µl of 100 µg/µl Poly-L-Lysine onto the coverslips followed by 1 h incubation at RT. 48 hpt, cells growing in coverslips were washed once with PBS and fixed with 4% Paraformaldehide (PFA) for 20 min at RT. After three PBS washing steps, nuclear staining with DAPI diluted 1:1000 in PBS was performed for 1 h at RT in a dark humid chamber.

Cells were then washed three more times with PBS, and the coverslips were mounted on glass slides with FluoroShield mounting media supplemented with 50 mg/ml Dabco. Images of single Z-stacks were obtained by using an Olympus LSM FV-1000 microscope in confocal mode with a 60x oil immersion objective and laser wavelengths of 405 nm, 488 nm and 594 nm for the excitation of DAPI, GFP and RFP, respectively. For qualitative image analysis, a total of at least 50 double-transfected (GFP-positive and RFP-positive) cells per condition were observed for GFP-RFP co-localization, and the percentage of HEK293T cells in which the given TRIM71 construct localized within P-bodies was calculated.

For DNA damage studies, 72 h after siRNA transfection, cells growing on coverslips were fixed with PFA as specified above, permeabilized with 0.2% Triton X-100 for 15 min at RT, blocked with 1% BSA/PBS for 1 h at RT and stained overnight with anti-phospho-H2AX antibody diluted 1:400 in blocking solution. After three PBS washing steps, simultaneous DAPI (1:1000) and Alexa647-coupled secondary antibody (1:400) staining was performed for 1 h at RT in the dark. Following three more PBS washing steps, coverslips were mounted for imaging as specified above. Images of all Z-stacks were obtained by using a Zeiss LSM 880 microscope in confocal mode with a 60x oil immersion objective and laser wavelengths of 405 nm and 594 nm for the excitation of DAPI and Alexa647, respectively. For quantitative image analysis, maximum intensity projections were generated with Fiji-ImageJ and the number of foci per cell nuclei was quantified in at least 50 cells.

3.2.3. Molecular biology assays

3.2.3.1. RNA extraction and cDNA synthesis

For RNA isolation, the Trizol-containing reagent TriFAST was used according to the manufacturer's instructions. In short, cell pellets were resuspended in 500 µl of TriFAST and either prepared directly or stored at -80°C for later preparation. Samples were then mixed with 100 µl of chloroform, thoroughly vortexed and centrifuged at 12000 rpm and 4°C for 5 min. The upper aqueous phase was then transferred to a new cap and nucleic acids were precipitated by adding 250 µl of isopropanol followed by centrifugation at 12000 rpm and 4°C for 30 min. The pellet was washed once with 70% ethanol and shortly dried at 37°C before being resuspended in 20 µl RNase-free water. Samples were then subjected to DNaseI digestion for 30 min at 37°C to eliminate genomic DNA contamination (see digestion reaction below). The DNaseI enzyme was then heat-inactivated for 10 min at 75°C, and the concentration of the extracted RNA was measured using a Nanodrop spectrophotometer.

DNA digestion reaction

Reagent	Vol. (for 30 µl)
purified RNA	20 µl
DNaseI buffer (10x)	3 µl
DNaseI enzyme (1 U/µl)	0.5 µl
ddH_2O	6.5 µl

For the conversion of RNA to cDNA, the High-Capacity Reverse Transcription kit was used following the manufacturer's instructions. Depending on the downstream application (mRNA or miRNA conversion) different protocols and RNA inputs were used:

mRNA conversion

Reaction mix (for 20 µl)	Conditions
500 ng total RNA	1. 25°C, 10 min
0.4 µl dNTPs (100 mM)	2. 37°C, 2 h
0.6 µl Reverse transcriptase (50 U/µL)	3. 85°C, 5 min
2 µl RT buffer (10x)	4. 4°C, hold
2 µl Random hexamer primers (10x)	
up to 20 µl RNase-free H_2O	

miRNA conversion

Reaction mix (for 10 µl)	Conditions
200 ng total RNA	1. 16°C, 30 min
0.2 µl dNTPs (100 mM)	2. 45°C, 30 min
0.3 µl Reverse transcriptase (50 U/µL)	3. 85°C, 5 min
1 µl RT buffer (10x)	4. 4°C, hold
1 µl miRNA-specific RT probe (5x)	
up to 10 µl RNase-free H_2O	

3.2.3.2. Real-time semi-quantitative PCR (qPCR)

After converting RNA to cDNA, the cDNA was diluted 1:5 with ddH_2O and relative quantification of specific genes was done in a Bio-Rad qCycler by using TaqMan probes in TaqMan master mix or specific primer pairs in SYBR Green master mix. For the SYBR Green qPCRs, a melting curve program was run after the PCR reaction to evaluate whether the amplification of the desired target was specific, as shown by the presence of only one PCR product depicted by a single peak in the melting curve.

TaqMan qPCR reaction

Reagent	Vol. (for 15 µl)
cDNA (1:5 diluted)	3µl
iTaq universal TM supermix (2x)	7.5µl
Taqman probe (20x)	0.3µl
ddH2O	4.2µl

TaqMan qPCR cycling

Cycles	Conditions	Phase
1x	95°C, 5min	Initial denaturation
49x	95°C, 10sec	Denaturation
	60°C, 40sec	Annealing + extension
	Plate Read	Fluorescence measurement
1x	25°C, hold	End

SYBR Green qPCR reaction

Reagent	Vol. (for 15 µl)
cDNA (1:5 diluted)	3 µl
iTaq universal SG supermix (2x)	7.5 µl
Forward primer (10 µM)	0.3 µl
Reverse primer (10 µM)	0.3 µl
ddH_2O	3.9 µl

SYBR Green qPCR cycling

Cycles	Conditions	Phase
1x	95°C, 5 min	Initial denaturation
49x	95°C, 10 sec	Denaturation
	60°C, 40sec	Annealing + extension
	Plate Read	Fluorescence measurement
1x	65°C, 30 sec	Melting curve initiation
60x	65°C - 95°C, 5 sec	Melting curve
	+ 0.5°C/cycle	Temperature increments
	Plate Read	Fluorescence measurement
1x	25°C, hold	End

The results from the qPCR reaction were visualized with the Bio-Rad CFX Manager Software, which depicted the threshold cycle value (Ct) of every amplified sample. The ΔΔCt method was applied to quantify the expression of a target gene in a given condition, relative to the expression of a housekeeping gene under the same condition. Unless indicated otherwise in the figure legends, HPRT1 was used as a housekeeping gene for mRNA quantification and U6 snRNA was used as a housekeeping small RNA for miRNA quantification. Results were depicted either as relative expression or as fold change, calculated as follows:

$$\text{Relative Expression} = 2^{-\Delta Ct}$$

$$\Delta Ct = Ct_{\text{target gene}} - Ct_{\text{housekeeping gene}}$$

$$\text{Fold Change Expression} = 2^{-\Delta\Delta Ct}$$

$$\Delta\Delta Ct = \Delta Ct_{\text{condition}} - \Delta Ct_{\text{control}}$$

3.2.3.3. Protein extraction and quantification

For protein extraction, cell pellets were lysed in RIPA Buffer (20 mM Tris-HCl pH 7.5, 150 mM NaCl, 0.5% sodium deoxycholate, 1% Triton X-100, 0.1% SDS) supplemented with protease inhibitors (PMSF, Antipain, Benzamidin (each diluted 1:1000), Leupeptin, Aprotinin (each diluted 1:2000)) by incubation for 20 min on ice, and protein lysates were pre-cleared by centrifugation at 12000 rpm and 4°C for 5 min to eliminate the cell debris. Protein quantification was conducted by using the Pierce bicinchoninic acid (BCA) assay kit according to the manufacturer's instructions. This assay relies on a peptidic bond-mediated reduction of Cu^{2+} ions to Cu^{1+} ions, which then react with the BCA to form colored complexes whose absorbance (measured at 562nm) is proportional to the sample protein concentration. The concentration of a sample can then be estimated from its absorbance interpolated to the equation of a standard curve, obtained by reading the absorbance of a group of samples with linearly-increasing known protein concentrations. The concentration of the protein lysates was then generally adjusted to 1 µg/µl and lysates were denatured by incubation with SDS Buffer (12% glycerol, 60 mM Na_2EDTA pH 8, 0.6% SDS, 0.003% bromophenol blue) at 95℃ for 10min. For proteasome or autophagy inhibition, cells were cultured for 4 h in the presence of 20 µM MG132 or 200 nM Bafilomycin A1, respectively, washed once with PBS, and further harvested for protein extraction as specified above. For RNA digestion of total lysates, RNase A was added to the lysates to a final concentration of 200 µg/ml and lysates were incubated at 37°C for 30 min prior to their denaturation. Dephosphorylation of total lysates was conducted prior to their denaturation as follows:

Protein dephosphorylation reactions

Alkaline Phosphatase (AP)	Lambda Phosphatase (λP)
20 µl Lysate (1 µg/µl)	20 µl Lysate (1 µg/µl)
2.5 µl Fast AP buffer (10x)	2.5 µl PMP buffer (10x)
2.5 µl Fast AP (1 U/µl)	2.5 µl $MnCl_2$ (10 mM)
	1 µl λP (400 U/µl)
Incubation: 37°C, 30 min	Incubation: 30°C, 30 min

3.2.3.4. Western blotting (WB)

After denaturation, protein samples were loaded onto PAGE-SDS gels (20 µg of protein per lane) in order to separate them according to their molecular weight, while running at 80-120 V for approximately 2 h in Laemmli Running buffer (25 mM Tris, 192 mM glycine, 0.1 % SDS). Proteins were then wet-transferred to a nitrocellulose membrane at 80 V for 2 h in Transfer buffer (25 mM Tris-HCl pH 7.6, 192 mM glycine, 20% methanol, 0.03% SDS) and membranes were then blocked in 5% Milk powder diluted in 1x TBST (50 mM Tris-HCl pH 7.6, 150 mM NaCl, 0.05% Tween-20), before an overnight incubation at 4°C with the required primary antibodies diluted in blocking solution. After three washing steps with 1x TBST, membranes were incubated with suitable HRP-coupled secondary antibodies for 1 h at RT followed by three more washing steps in 1x TBST. Membranes were then developed with Pierce ECL Substrate kit following the manufacturer's instructions by membrane exposure to a chemoluminiscent film. Densitometry quantification of western blot bands was conducted with the LI-COR Image Studio Lite software.

3.2.3.5. Protein immunoprecipitation (IP)

For protein interaction studies, proteins were extracted on IP buffer (50 mM Tris-HCl pH 7.5, 1 mM EGTA, 1 mM EDTA, 270 mM Sucrose, 1% Triton X-100) supplemented with phosphatase inhibitors (10 mM Glycerophosphate, 50 mM Sodium Fluoride, 5 mM Sodium Pyrophosphate, 1 mM Sodium Vanadate) and protease inhibitors (as specified above). Protein lysates were pre-cleared by centrifugation at 12000 rpm and 4°C for 5 min, quantified using the Pierce BCA assay kit, and at least 500 µg of protein were incubated with 10 µl of magnetic beads at 4°C in a rotating wheel for 5 h or overnight. A portion of each whole cell lysate was retained as input control. Sigma ANTI-FLAG M2 magnetic beads were used for the IP of Flag-tagged proteins, Ni^{2+} Dynabeads for the IP of His-tagged proteins and Protein A/G Dynabeads for the IP of Ig-tagged proteins or endogenous proteins by pre-coupling the beads to the desired primary antibody. Pre-coupling was performed in 300 µl of IP buffer with the suitable antibodies diluted 1:50 at 4℃ for 2 h in a rotating wheel. After IP, beads were washed five times with IP-buffer and bound proteins were eluted from the beads by boiling in SDS buffer, followed by PAGE-SDS separation and WB as described above. For RNase treatment after IP, washed IP fractions were incubated in IP buffer containing 200 µg/ml RNase A at 37°C for 30 min and washed three more times with IP buffer before protein elution. For protein dephosphorylation after IP, washed IP fractions were incubated in IP buffer containing a phosphatase enzyme. The dephosohorylation reaction was prepared as specified above, but substituting the indicated lysate volume by IP buffer. After dephosphorylation, IP samples were washed three more times with IP buffer before protein elution.

3.2.3.6. UV-crosslinking RNA immunoprecipitation (RNA-IPs)

For RNA-IP, two fully confluent 10 cm dishes of HEK293T cells per condition were used 48 hpt with the required Ig- or Flag-constructs. After carefully washing the plates once with cold PBS, provided that cells remained adherent, open dishes were irradiated once with UV light at 300 mJ/cm^2 to crosslink nucleic acids to their protein binding partners. Cells were then harvested and resuspended in 500 µL RNA-IP buffer (20 mM Tris-HCl pH 7.4, 100 mM KCl, 5 mM $MgCl_2$, 0.2% NP-40) supplemented with 120 U/mL RNase inhibitor and protease inhibitors. Cell lysates were pre-cleared by centrifugation, quantified using the Pierce BCA assay kit, and 2 mg of protein per condition were incubated with 50 µl of suitable magnetic beads at 4°C in a rotating wheel overnight. A portion of each whole cell lysate was retained as input protein control (total protein) and input RNA control (total RNA). After washing the beads five times with RNA-IP buffer, 20% of the IP lysate was used for WB analysis (IP protein) together with the total protein samples, while 80% of the IP lysate was digested with 500 µg/ml Proteinase K for 30 min at 37°C, and used for RNA extraction followed by qPCR (IP RNA) together with the total RNA samples. For a given target, quantified IP RNA values were normalized to total RNA values to calculate the IP enrichment (see below), and the IP enrichment of each specific target mRNA was normalized to the unspecific IP enrichment of the housekeeping 18S rRNA, as follows:

$$\text{Specific IP enrichment}_{\text{target gene}} = \text{IP enrichment}_{\text{target gene}} / \text{IP enrichment}_{\text{housekeeping gene}}$$

$$\text{IP enrichment} = 2^{-\Delta\Delta Ct}$$

$$\Delta Ct = Ct_{\text{IP RNA}} - Ct_{\text{Total RNA}}$$

$$\Delta\Delta Ct = \Delta Ct_{\text{Condition}} - \Delta Ct_{\text{Control}}$$

3.2.3.7. mRNA stability assays

For the estimation of mRNA stability, mRNA decay rates were monitored upon transcriptional inhibition by culturing cells in 5 µg/ml of Actinomycin D, and taking samples for RNA extraction 1 h, 2 h, 4 h and 6 h after treatment initiation. Cells treated with DMSO were used as 0 h control. For a given mRNA target, the quantified expression of Actinomycin D-treated samples at different time points was normalized to the expression of the DMSO-treated control sample, and expressed as percentage to depict mRNA decay rate over time. The resultant mRNA-decay curves were adjusted by non-linear regression using GraphPad Prism7 in order to estimate the half-life ($t_{1/2}$) of each target mRNA as a measurement of its stability.

3.2.3.8. Luciferase reporter assays

For luciferase assays, cells were co-transfected with the required psiCHECK2 dual luciferase plasmid and the specified pRK5-Flag construct in a 1:4 ratio, and cells were harvested for further analysis 48 hpt. If miRNA overexpression or siRNA-mediated knockdown was required, miRNA/siRNA transfection was conducted 24 h before DNA transfection.

psiCHECK2 plasmids contained the desired 3'UTR sequence downstream of an ORF encoding for the Renilla Luciferase, while the Firefly Luciferase, expressed under the control of a different promoter and not subjected to any altered UTR regulation, was used as normalization control. To eliminate the possible 3'UTR-independent impact that each condition/construct could have on the psiCHECK2 vector backbone, a psiCHECK2 vector with no insert downstream of the Renilla sequence (Renilla-empty) was generated. Renilla and Firefly luminescence signals were measured with a luminometer connected to the Winglow Software by using the Dual Luciferase Reporter Assay kit following the manufacturer's instructions. In short, cells growing in 12- or 24-well plates were lysed in 50-100 µl of 1x Passive Lysis buffer and 10-20 µl of lysate were used to measure first the Firefly signal upon addition of 40 µl of LARII substrate, and next the Renilla signal upon addition of 40 µl of Stop&Glo substrate. To evaluate the effect of each condition or construct in the repression of a given 3'UTR, the Renilla-3'UTR/Firefly ratio was calculated and then normalized to the Renilla-empty/Firefly ratio calculated for the same condition. The resultant values were specified as normalized Relative Light Units (Norm. RLU).

The Repression Strength (ratio between given Norm. RLU values) was calculated as an additional parameter representing the degree of repression for every specific construct/condition. Repression Strength values higher than 1 were observed upon repression of a specific miRNA or 3'UTR, while values equal or below 1 implied that no repression was observed. When studying the effect of TRIM71 on miRNA activity (Results, Chapter I), the repression strength is directly proportional to the miRNA reporter signal. In this context, the repression strength was calculated as norm. RLU (Flag-TRIM71) / norm. RLU (Flag) and it represented a measurement of how strong did TRIM71 repress the activity of a miRNA, i.e. derepress the miRNA reporter. In contrast, when studying the effect of TRIM71 on the 3'UTR its mRNA targets (Results, Chapter II), the repression strength is inversely proportional to the 3'UTR reporter signal. In this case, the repression strength was calculated as norm. RLU (Flag) / norm. RLU (Flag-TRIM71) and it represented a measurement of how strong could TRIM71 repress the 3'UTR in question.

3.2.4. Biochemical assays

3.2.4.1. Vaccinia virus-mediated production of human TRIM71 Flag-NHL recombinant protein

Generation of recombinant Vaccinia virus:

CV1 primate kidney cells were grown in DMEM media supplemented with 10% FBS and 1% Pen/Strep antibiotic solution until 100% confluence was reached. Cells where then split 1:2 and grown overnight in order to have a freshly split confluent dish the following day. One confluent 10 cm dish was prepared for viral infection by washing cells once with PBS and adding 2.5 ml DMEM media without supplements, since the FBS promotes viral aggregation leading to a decreased infection efficiency. The wild type virus stock was thawed, vigorously vortex and sonicated for 1 min in order to disaggregate viral particles. The solution was then cleared by centrifugation for 5 min at 4500 rpm and RT, and CV1 cells were infected with 5 µl of the clear supernatant. After 2 h incubation at 37°C, the virus-containing media was aspirated and replaced by 4 ml DMEM supplemented with 10% FBS and 1% Pen/Strep antibiotic solution. Cells were then transfected by the calcium phosphate method as previously described, with a Vaccinia virus-expression pTKg vector containing a construct which encoded for the NHL domain of the human TRIM71 protein fused to a Flag-tag (Flag-NHL). The Flag-NHL construct had been excised from a previously-generated pRK5-Flag-NHL vector and ligated into the pTKg vector by HindIII/NotI-directed cloning. Within the pTKg-vector, the Flag-NHL construct was flanked by sequences of the viral Thymidinkinase (TK) protein in order to be incorporated into the genome of the wild-type virus by homologous recombination. Recombinant viruses were thus generated in transfected-infected CV1 cells, while wild type viruses continued to propagate within untransfected cells. CV1 cells were monitored for the following 24-48h until cells looked rounded, indication of an advanced-infection stage. Cells were then carefully washed in PBS, detached with a scraper and collected in PBS, followed by centrifugation for 5 min at 1500 rpm and RT. The cell pellet was resuspended in 500 µl of 10 mM Tris pH 9 and incubated for 30 min at RT to allow cell lysis, generating a new viral stock with a mixture of wild type and recombinant viruses.

Purification of recombinant Vaccinia virus:

Confluent CV1 cells growing in DMEM media supplemented with 10% FBS and 1% Pen/Strep antibiotic solution were washed once in PBS and pre-incubated for 3 h at 37°C with MPA media (DMEM media supplemented with 2.5% FBS, 0.25 mg/ml Xanthine solution (10 mg Xanthine/ml 0.1 N NaOH), 0.015 mg/ml Hypoxanthine solution (10 mg Xanthine/ml 0.1 N NaOH) and 0.025 mg/ml mycophenolic acid (MPA) solution (10 mg MPA/ml 0.1 N NaOH)). Since insertion of the Flag-NHL transgene into the viral genome occurs via homologous recombination within the viral TK gene, the resulting recombinant viruses are TK-deficient. Instead, they carry the transgene of interest together with the E. coli xanthine-guanine phosphoribosyltransferase (XGPR) as selection marker. XGPR is able to convert Xanthine into xanthinemonophosphate (XMP), which can be further processed to gunaninemonophosphate (GMP), essential for the virus survival. MPA inhibits the inosinemonophosphate dehydrogenase (IMPDH), an enzyme that is essential for guaninemonophosphate (GMP) biosynthesis. Thereby, recombinant vaccinia viruses were selected with MPA medium, in which wild type virus death is promoted, whereas recombinant virus survival is ensured by the presence of Xanthine and their XGPR expression. After a 3 h pre-incubation with MPA-media at 37°C, the media was aspirated and replaced by DMEM without

supplements. CV1 cells were then infected as described above with the newly produced mixed viral stock and incubated for 1 h at 37°C. Next, the infection media was replaced again with MPA media and cells were incubated for 24-48h until infection plaques were visible. Plaques were numbered, and a part of each plaque was taken with a pipette tip while looking the plaques under the microscope. Each tip was dipped into a tube properly labeled with the plaque number containing 100 µl of 10 mM Tris pH 9, and the tubes were stored at -20°C. Infected-cell plates were then fixed with 2% PFA/PBS for 20 min at RT, washed twice with 2% Glycine/PBS and permeabilized with 0.2% Triton X-100/PBS for 10 min at RT. Cells were then stained with Alkaline phosphatase (AP)-conjugated anti-Flag antibody for 1 h at RT under gentle shaking. After two PBS washing steps, the AP substrate solution (BCIP/NBT) was added and cells were monitored under the microscope until plaques positive for recombinant virus turned purple. The samples taken from the purple plaques were used for successive rounds of selection, whereas samples taken from negative/unstained plaques - infected with wild type virus - were discarded. For the following plaque selection rounds, the total 100 µl viral solution was used for infection. The purification of recombinant viruses ended after 4-5 selection rounds, when all plaques within a plate were positive/purple-stained. Last, in order to amplify the purified recombinant virus, one confluent 15 cm dish of CV1 cells was infected with the total volume (100 µl) of a positive plaque from the last selection round, and 24-48h after infection, when the cells looked rounded, they were harvested and lysed in 500 µl of 10 mM Tris pH 9 for 30 min at RT. The lysate (pure recombinant virus stock) was stored at -80°C until further use for the production of recombinant human Flag-NHL protein.

Production and purification of human TRIM71 Flag-NHL recombinant protein:

20x 15 cm dishes of confluent CV1 cells were infected for 1 h at 37°C with 25 µl of pure recombinant virus stock per plate as previously described. 48h post-infection, cells were harvested and lysed in RIPA buffer for 30 min on ice. The lysate was then cleared by centrifugation for 5 min at 14000 rpm and 4°C. After transferring the clear supernatant to a new tube, the concentration of the lysate was measured and adjusted to 5 mg/ml with RIPA buffer. The lysate was then incubated at 4°C in a rotating wheel overnight with 200 µl of M2 anti-FLAG magnetic beads for the IP of the Flag-NHL recombinant protein. Assuming a yield of 5 µg of Flag-NHL recombinant protein per dish, a total of 100 µg of Flag-NHL recombinant protein was estimated to be produced. Given that M2 anti-FLAG magnetic beads have a binding capacity of 0.6 mg protein per ml of beads, around 170 µl of beads would be needed to bind 100 µg of Flag-tagged protein. After IP, beads were washed 5x 10 min with 2 ml TBS buffer (50 mM Tris-HCl, pH 7.5; 150 mM NaCl), and The Flag-NHL protein was then eluted from the beads in its native conformation by adding an excess of 3x FLAG peptide. Two elution steps were performed subsequently with 500 µg/ml 3x FLAG peptide in 500 µl TBS. Each elution step was conducted by incubation for 30 min at 4°C in rotation. The two eluates were then mixed, and centrifuged for 30 min at 5000 rpm and RT through a 10 KDa size-exclusion centrifugal unit column to eliminate the excess of 3x FLAG peptide and to concentrate the protein solution. The concentration of Flag-NHL recombinant protein was then measured, and protein purity, integrity and identity were evaluated by running a PAGE-SDS gel followed by Coomassie Blue staining and WB detection with an anti-FLAG antibody.

3.2.4.2. Electrophoretic mobility shift assays (EMSA)

The capability of Myc-LIN28A and Flag-NHL recombinant proteins to directly bind pre-miRNAs was evaluated by EMSA, a technique to determine if a protein is able to bind a given nucleic acid molecule as well as to investigate if more than one protein is involved in such a binding, based on the gel migration retardation of a labeled nucleic acid upon protein(s) binding. Therefore, pre-let-7 and pre-miR-16 molecules were radioactively 5'-labeled with ^{32}P isotopes by incubation with ^{32}P-YATP and the phosphorylating enzyme T4 Poly-Nucleotide Kinase (PNK) for 30 min at 37°C (see labeling reaction below), followed by enzyme inactivation for 10 min at 65°C. ^{32}P-Labeled pre-miRNAs were then purified with ProbeQuant G-50 MicroColumns according to the manufacturer's instructions in order to eliminate the T4 PNK enzyme and the excess of ^{32}P-YATP, and radioactivity levels (cpm = counts per minute) of the purified samples were quantified using a liquid scintillation counter. A fixed amount of each ^{32}P-labeled pre-miRNA was incubated with increasing concentrations of Myc-LIN28A and/or Flag-NHL recombinant proteins in a range of 10-1000 nM, and samples were brought to the equilibrium for 30 min at 37°C in Binding buffer (10 mM MOPS pH 7.5, 50 mM KCl, 5 mM $MgCl_2$, 3 mM EDTA pH 8, 30 µg/ml heparin, 5% glycerol) supplemented freshly with 1 mM DTT and competitor yeast tRNA in a 1000-fold excess over the ^{32}P-pre-miRNA to prevent unspecific binding (see binding reaction below). Control samples containing only each of the ^{32}P-labeled pre-miRNAs were included to evaluate the migration of such pre-miRNAs in the absence of protein(s). Next, the total volume of each sample was directly loaded on a 10% native PAGE gel and run for 4 h at 4°C and 200 V. Gels were then dehydrated for 30-45 min at 80°C in a vacuum dryer and exposed to autoradiography films for the visualization of ^{32}P-Labeled pre-miRNAs-protein complexes, detected as up-shifted bands as compared to the bands observed in control samples. Densitometry quantification of up-shifted bands was conducted with the LI-COR Image Studio Lite software and binding-saturation curves were built and adjusted by non-linear regression using GraphPad Prism7 to estimate the equilibrium dissociation constant (K_D) of pre-miRNAs-protein complexes.

Labeling reaction

Reagent	Vol. (for 50 µl)
30 pmol pre-miRNA (10 µM)	3 µl
30 µCi ^{32}P-YATP (10 µCi/µl)	3 µl
T4 PNK (10 U/µl)	1 µl
PNK-A buffer (10x)	5 µl
H_20	38 µl

Binding reaction

Reagent	Vol. (for 30 µl)
60 fmol ^{32}P-pre-miRNA	1 µl
60 pmol yeast tRNA	0.15 µl
Recombinant protein	Variable
Binding buffer (+1 mM DTT)	up to 30 µl

3.2.4.3. Fluorescence polarization assays

The capability of TRIM71 to directly bind RNA through its NHL domain was evaluated by measuring changes in the polarization of 5'-Cy3-conjugated 13-mer ssRNAs (100 nM) upon binding with increasing concentrations of human TRIM71 Flag-NHL recombinant protein. Samples were brought to the equilibrium in 1x TBST buffer for 30 min at RT, and polarization was measured using a fluorescent plate reader equipped with polarizers. Of note, binding did not alter the fluorescent intensity of the ssRNAs (data not shown). The resultant binding-saturation curves were adjusted by non-linear regression using GraphPad Prism7 to estimate the equilibrium dissociation constant (K_D) of RNA-protein complexes.

3.2.5. Structural modeling of the human TRIM71 NHL domain

The protein sequences from zebrafish Trim71/Lin41 and human TRIM71 share an overall identity of 84% over the 390 amino acids covering the FLN and NHL domains, corresponding to a sequence similarity of 96% (data not shown). As the crystal structure of the zebrafish FLN-NHL domains bound to a 13-mer stem-loop RNA sequence has been recently determined[85], we were able to model the human TRIM71 NHL domain in complex with the 13-mer stem-loop RNA motif (sequence 5'-GUCUUGUGAAGGC-3') that we identified in CDKN1A 3'UTR, and we have termed TRIM71 responsive element (TRE). Structural modelling of human TRIM71 FLN-NHL protein domains (residues 479-868) was performed using Swiss-Model[143], based on the Trim71/Lin41 crystal structure 6FQ3 which was determined at 1.9 Å resolution[85]. The interaction between the human NHL domain and TRE has been modelled on the RNA of the 6FQ3 complex by single nucleotide exchange using Coot software[144].

3.2.6. Statistical data analysis

For the analysis of quantitative differences observed between two samples, statistical significance was calculated with a two-tailed unpaired Student's t-test (ns = non-significant; *P-value < 0.05; **P-value < 0.01; ***P-value < 0.005). Usually, such differences were evaluated comparing a given condition sample to the control sample. When that was not the case, the compared samples were linked in graphs with a line. For the analysis of quantitative differences observed between three or more samples, statistical significance was calculated by an Analysis Of Variance test (ANOVA), where the P-value summary indicated the significance of the overall variability among samples (*P-value < 0.05; **P-value < 0.01; *** P-value < 0.005). For the analysis of regression curves, namely binding-saturation curves and mRNA-decay curves, GraphPad Prism7 was used for non-linear adjustments and estimation of dissociation constants (K_D) and mRNA half-lives ($t_{1/2}$), respectively. Furthermore, GraphPad Prism7 was also used for Area Under Curve (AUC) measurements, and the differences between two samples' AUC values were analyzed by a two-tailed unpaired Student's t-test.

4. Results

4.1. Chapter I: TRIM71-mediated miRNA regulation

4.1.1. TRIM71 cooperates with LIN28 proteins in the repression of let-7 expression through the interaction with the terminal uridyltransferase TUT4

TRIM71 deficiency was found to induce major changes in the miRNA landscape of mESCs, showing a downregulation of ESC-specific miRNAs at expenses of an upregulation of differentiation-promoting miRNAs[113]. Some of the strongest upregulated miRNAs in TRIM71 knockout ESCs were members of the let-7 miRNA family, well-known as important differentiation inducers and tumor suppressors. Previous studies in our lab suggested that TRIM71 cooperates with LIN28A in the repression of pre-let-7 maturation. Specifically, both TRIM71 and LIN28A single knockout ESCs showed an upregulation of mature let-7 miRNA species – but not of pri- or pre-let-7 species –, whereas a double TRIM71-LIN28A knockout mESC line induced no additional let-7 upregulation compared to the single LIN28A knockout (unpublished data, see again Introduction Fig. 1.9). A different study had also linked TRIM71 to the regulation of let-7 expression through its interaction with the paralog protein LIN28B. However, such a mechanism involved TRIM71-mediated LIN28B ubiquitylation followed by its proteasomal degradation, leading to the upregulation of let-7 levels[140]. Although these findings seem contradictory to our previous studies, they are not necessarily mutually exclusive, since TRIM71 could either downregulate or upregulate let-7 expression depending on its binding to LIN28A or LIN28B, respectively. To validate the existence of such a mechanism, we first chose HEK293 cells as a system in which the two mechanisms could not compete, since these cells only express LIN28B, while they lack LIN28A expression. Furthermore, Lee *et al.* precisely used HEK293 cells to study TRIM71-mediated LIN28B ubiquitylation[140]. Therefore, we measured endogenous let-7 miRNA levels and LIN28B protein levels in HEK293 cells stably overexpressing GFP-TRIM71 and compared them with those in HEK293 cells overexpressing only GFP as a control. In contrast to the findings of Lee *et al.*, and in line with our previous observations in mESCs, TRIM71 overexpression in HEK293 cells resulted in let-7a and let-7g specific downregulation, whereas the levels of the housekeeping miR-16 remained unaltered (Fig. 4.1.1A). Furthermore, TRIM71-overexpressing HEK293 cells showed unaltered LIN28B protein levels compared with control HEK293 cells (Fig. 4.1.1B), arguing against TRIM71-mediated LIN28B proteasomal degradation. Of note, LIN28B mRNA levels were comparable between TRIM71-overexpressing and control HEK293 cells (Fig. 4.1.1A), discarding the possibility that an induced degradation of LIN28B in the presence of TRIM71 was compensated by an enhanced *LIN28B* expression. Altogether, our findings showed that TRIM71 specifically represses the expression of let-7 family members without impacting on LIN28B mRNA or protein levels.

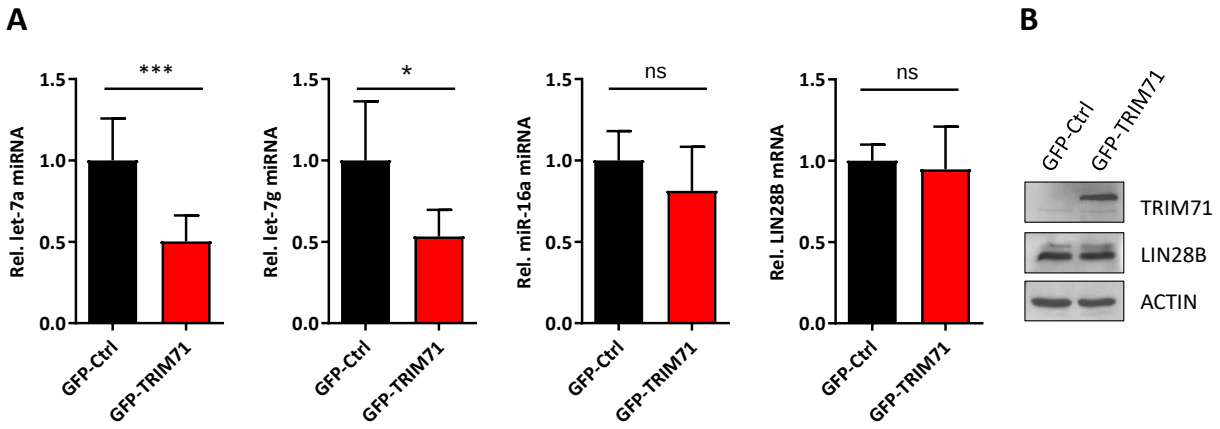

Figure 4.1.1. TRIM71 specifically represses the expression of let-7 miRNAs without affecting LIN28B mRNA or protein levels. A) qPCR measurements of let-7a miRNA levels (n=6), let-7g miRNA levels (n=6), miR-16 levels (n=6) and LIN28B mRNA levels (n=3) in control (GFP-Ctrl) and TRIM71-overexpressing (GFP-TRIM71) HEK293 cells. U6 and HPRT housekeeping genes were used for normalization of miRNA and mRNA levels, respectively. **B)** Representative immunoblot showing GFP-tagged TRIM71 and endogenous LIN28B protein levels in control and TRIM71-overexpressing HEK293 cells. All graphs represent Mean ± SD. Statistical significance was calculated with a two-tailed unpaired Student's t-test (ns = non-significant; *P-value < 0.05; ***P-value < 0.005).

Lee and co-workers mapped the interaction between TRIM71 and LIN28B to the 50 aa-stretch present in the C-terminus of LIN28B – absent in LIN28A – (Fig. 4.1.2A) and claimed that TRIM71 was thus unable to bind LIN28A[140]. Furthermore, they claimed that a TRIM71 ubiquitylation mutant, with an impaired E3 ligase activity due to point mutations in two catalytic cysteines within the RING domain (C12LC15A)[105,115,140], failed not only to ubiquitylate, but also to bind LIN28B. We therefore transiently overexpressed wild type TRIM71 and C12LC15A mutant in HEK293T cells and evaluated their ability to interact with both LIN28 proteins. Opposing the findings of Lee *et al.*, both TRIM71 and C12LC15A co-precipitated with endogenously expressed LIN28B (Fig. 4.1.2B), as well as with ectopically expressed LIN28A (Fig. 4.1.2C). These findings demonstrated that neither TRIM71 E3 ligase activity nor an intact RING domain are required for the establishment of such interactions, and argued against the aforementioned LIN28B-specific 50-aa stretch to be the motif mediating the interaction with TRIM71.

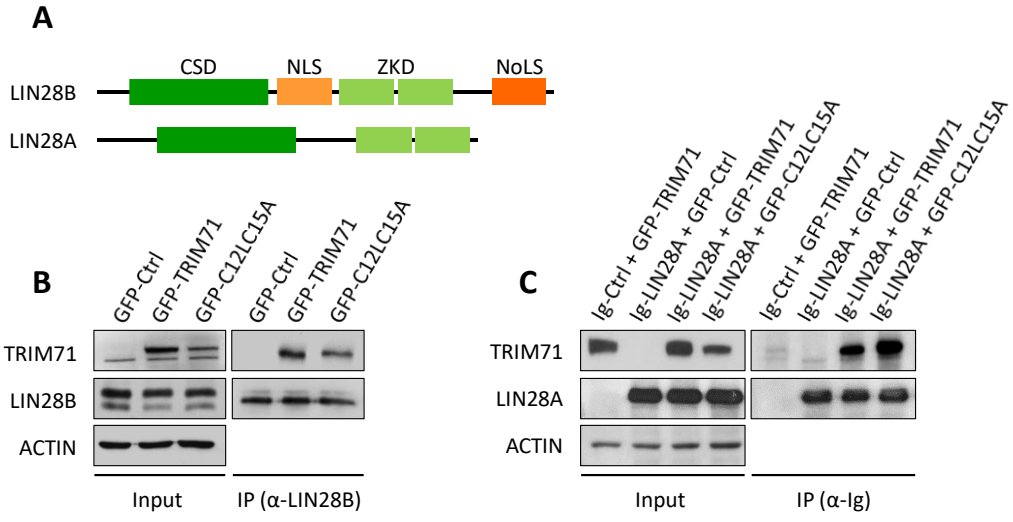

Figure 4.1.2. TRIM71 E3 ligase activity is dispensable for its interaction with LIN28 proteins. A) Schematic representation of LIN28 proteins domain organization. CSD = Cold Shock Domain; ZKD = Zinc Knuckle domain; NoLS = putative nucleolar localization sequence; NLS = Nuclear localization signal. **B)** Representative immunoblot showing GFP-tagged TRIM71 and C12LC15A co-precipitation with endogenous LIN28B in HEK293T cells. **C)** Representative immunoblot showing GFP-tagged TRIM71 and C12LC15A co-precipitation with Ig-tagged LIN28A overexpressed in HEK293T cells. Overexpression of an Ig-empty vector together with wild type TRIM71 (first lane) excluded an Ig-mediated TRIM71-LIN28A interaction. Of note, GFP alone was not found co-precipitated with neither LIN28A nor LIN28B (data not shown), also excluding a possible GFP-mediated interaction.

We next conducted LIN28 proteins IPs in HEK293T cells overexpressing several TRIM71 truncated constructs (Fig. 4.1.3A) and were able to map LIN28-TRIM71 interaction to the NHL domain of TRIM71 (Fig. 4.1.3B-C). In summary, our findings opposed those of Lee *et al* regarding the role of TRIM71 in the LIN28B/let-7 axis[140]. We found that TRIM71 overexpression in HEK293 cells resulted in the downregulation of let-7 miRNA species, that TRIM71 was able to interact with both LIN28A and LIN28B regardless TRIM71 E3 ligase activity, and that TRIM71 did not affect the stability of LIN28 proteins. We therefore proposed that TRIM71 cooperates with LIN28A and LIN28B in the repression of let-7 biogenesis.

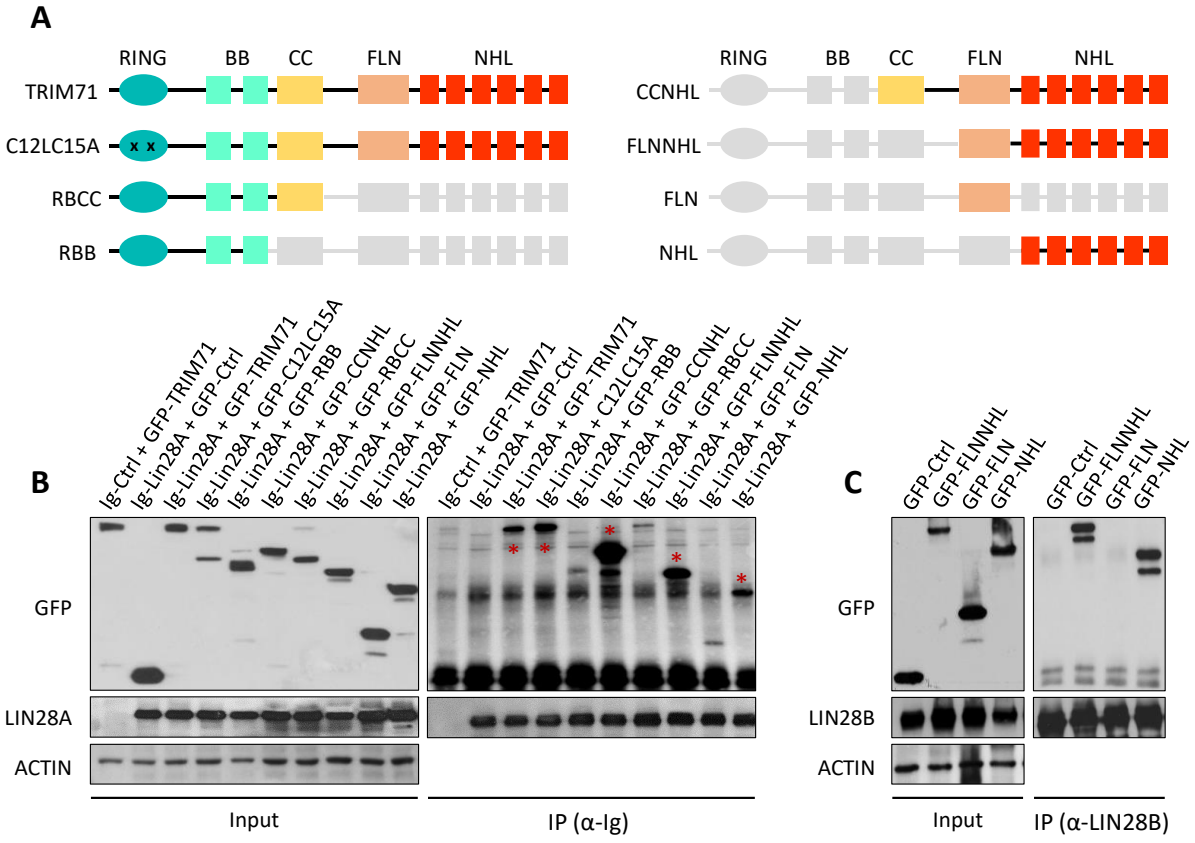

Figure 4.1.3. The NHL domain of TRIM71 is necessary and sufficient for its interaction with LIN28 proteins: A) Schematic representation of TRIM71 truncated constructs used in experiments depicted in B-C. Grey areas represent the deleted domains within each construct. **B)** Representative immunoblot showing the co-precipitation of different GFP-tagged TRIM71 constructs with Ig-tagged LIN28A overexpressed in HEK293T cells. Truncated TRIM71 constructs co-precipitated with Ig-LIN28A to at least the same extent as the wild type full length TRIM71 protein are marked in the IP fraction with a red asterisk (*). **C)** Representative immunoblot showing the co-precipitation of different GFP-tagged TRIM71 constructs with endogenous LIN28B in HEK293T cells.

Affinity regulation has a major impact on the fate of protein-RNA complexes. Binding of other proteins or post-translational modifications (PTMs) can strongly affect the affinity of a RNA-binding protein (RBP) for its target RNA[145,146]. The binding of TRIM71 to LIN28 proteins could enhance their affinity for pre-let-7 miRNAs binding, thereby promoting a more efficient downstream pre-let-7 degradation. In order to test this hypothesis, we conducted electrophoretic mobility shift assays (EMSA) with purified components.

To evaluate whether the presence of TRIM71 enhanced the binding affinity of the LIN28A-pre-let-7 complex, non-saturating levels of LIN28A were required. Therefore, we first estimated the dissociation constant (K_D) of the Protein-RNA complex (PR) formed between LIN28A protein and pre-let-7 miRNA, which represents the concentration of LIN28A that binds half of the present pre-let-7 molecules at the equilibrium. To this end, increasing concentrations of LIN28A protein were incubated with a fixed amount of radioactively labelled ^{32}P-pre-let-7a. ^{32}P-pre-miR-16a was used as a negative control, since we have shown that TRIM71 does not affect miR-16a expression levels (see again Fig. 4.1.1A). Accordingly, LIN28A formed a complex with pre-let-7a but not with pre-miR16a (Fig. 4.1.4A). The K_D estimated for the LIN28A-pre-let-7a complex was 55,2 nM (Fig. 4.1.4B). Next, a second EMSA was performed with the same ^{32}P-pre-miRNAs concentrations as before, a fixed LIN28A concentration of 50 nM and increasing concentrations of human TRIM71 recombinant Flag-NHL protein. Again, LIN28A bound pre-let-7a but not pre-miR16, whereas the Flag-NHL domain alone did not bind either of these pre-miRNAs (Fig. 4.1.4C-D). Furthermore, Flag-NHL did not increase the binding between LIN28A and pre-let-7 at any of the tested concentrations, but strikingly, it neither upshifted the LIN28A-pre-let7 complex, indicating that Flag-NHL did not bind the LIN28-pre-let7 complex under these conditions (Fig. 4.1.4C-D). The fact that the NHL domain is sufficient for the interaction with LIN28 proteins within cells (see again Fig. 4.1.3), but not in a biochemical assay with purified components (Fig. 4.1.4C-D), suggests the participation of other cellular components in the formation or stabilization of such an interaction. Therefore, whether TRIM71 indirectly enhances the affinity of LIN28 proteins for let-7 miRNAs remains undetermined.

LIN28 proteins are known to trigger pre-let-7 degradation through the recruitment of the terminal uridyltransferase enzymes TUT4 and TUT7[147]. Based on our cooperation hypothesis, it is reasonable to assume that TRIM71 may join this complex to assist let-7 repression. We therefore evaluated the ability of TRIM71 to interact with TUT4, and whether such an interaction was dependent on the presence of LIN28 proteins. Our results showed that TUT4 co-precipitated with TRIM71 in control HEK293T cells, which lack LIN28A, as well as in LIN28B knockdown HEK293T cells (Fig. 4.1.5A), indicating that both LIN28 proteins are dispensable for the interaction between TRIM71 and TUT4. However, TRIM71 could require TUT4 in order to interact with LIN28 proteins, since our EMSAs suggested that the interaction between TRIM71 and LIN28A is facilitated by other cellular components.

Therefore, we hypothesized that TUT4 stabilized or mediated the interaction between TRIM71 and LIN28 proteins. The stabilization of such an interaction may require the formation of a tri-molecular complex in which each protein is able to interact with the other two. In this context, and considering that TRIM71 interacts with LIN28 proteins via its NHL domain, TRIM71 may then employ a different domain to bind TUT4. On the contrary, if TUT4 mediates the interaction between TRIM71 and LIN28 acting as a bridge between these two proteins, the interaction with TUT4 is expected to be mediated by TRIM71 NHL domain.

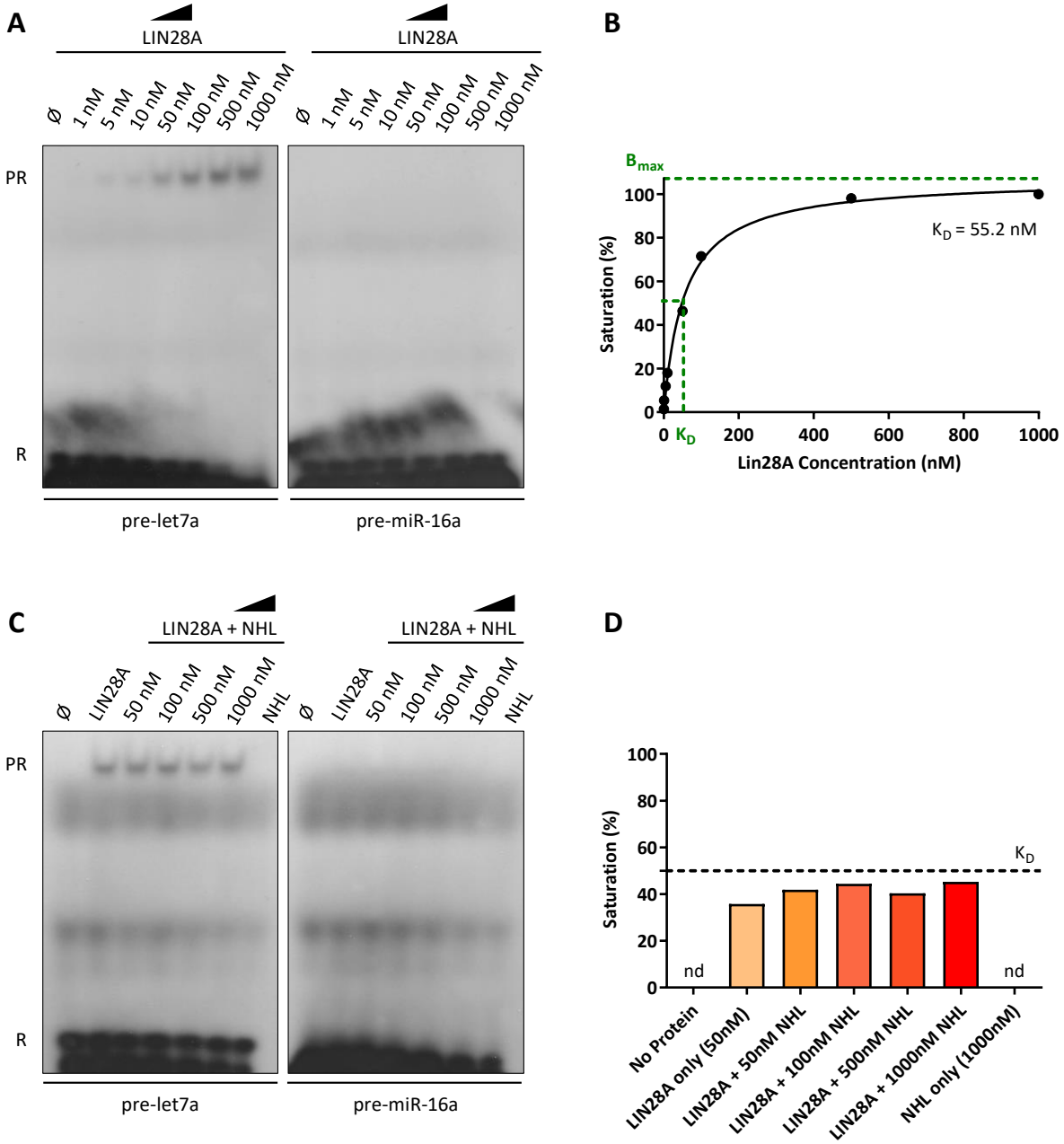

Figure 4.1.4. The interaction between TRIM71 and LIN28A is facilitated by other cellular components. A) EMSA performed with increasing concentrations of recombinant myc-tagged LIN28A protein and fixed amounts of ^{32}P-labelled pre-let-7a or pre-miNA-16a (R)**. B)** LIN28A binding-saturation curve derived from the Protein-RNA complexes (PR) band intensities from A, representing the binding between LIN28A and pre-let-7. The dissociation constant (K_D) was estimated from the graph equation $Y = (B_{max} * X) / (K_D + X)$. **C)** EMSA performed with 50 nM of myc-tagged LIN28A and fixed amounts of ^{32}P-labelled pre-let-7a or pre-miR-16a in the presence of increasing concentrations of recombinant Flag-tagged TRIM71 NHL protein (NHL). The capability of the NHL domain alone to bind pre-miRNAs was also tested (last lane) by using 1000 nM of NHL protein. **D)** Quantification of the LIN28A saturation levels reached in the absence and presence of increasing concentrations of NHL, calculated based on the PR band intensities of C. The dash line at 50% saturation levels (K_D threshold) represents the approximated maximal saturation that can be reached for the used LIN28A concentration (50 mM), according to experiments depicted in A-B. Ø = No Protein.

Therefore, we next overexpressed different truncated TRIM71 constructs and evaluated their interaction ability with TUT4. Paralleling TRIM71-LIN28 interaction, the NHL domain of TRIM71 was necessary and sufficient for the interaction with TUT4 (Fig. 4.1.5B), suggesting that either TUT4 mediates the interaction between TRIM71 and LIN28, or that LIN28 and TUT4 bind TRIM71 independently, and therefore compete for such interaction. We next evaluated the capability of TRIM71 to bind LIN28B upon TUT4 knockdown. Such an interaction should be diminished in case of being mediated through TUT4, and enhanced in case of a competition between TUT4 and LIN28B for TRIM71 binding. Confirming the role of the TUT4 as a "bridge protein", the binding between TRIM71 and LIN28B was abrogated upon TUT4 knockdown (Fig. 4.1.5C). Importantly, the interaction of TRIM71 with both TUT4 and LIN28B was RNA-independent (Fig. 4.1.5D), demonstrating the formation of a stable protein complex between these three proteins. Last, the ubiquitylation mutant C12LC15A, which we have shown to be able to bind both LIN28 proteins (see again Fig. 4.1.3), was also co-precipitated with TUT4 (Fig. 4.1.5E). Collectively, all these data strongly support the formation of a TRIM71/TUT4/LIN28 complex, which seems to mediate the degradation of pre-let-7 miRNA more efficiently than the TRIM71-lacking complex.

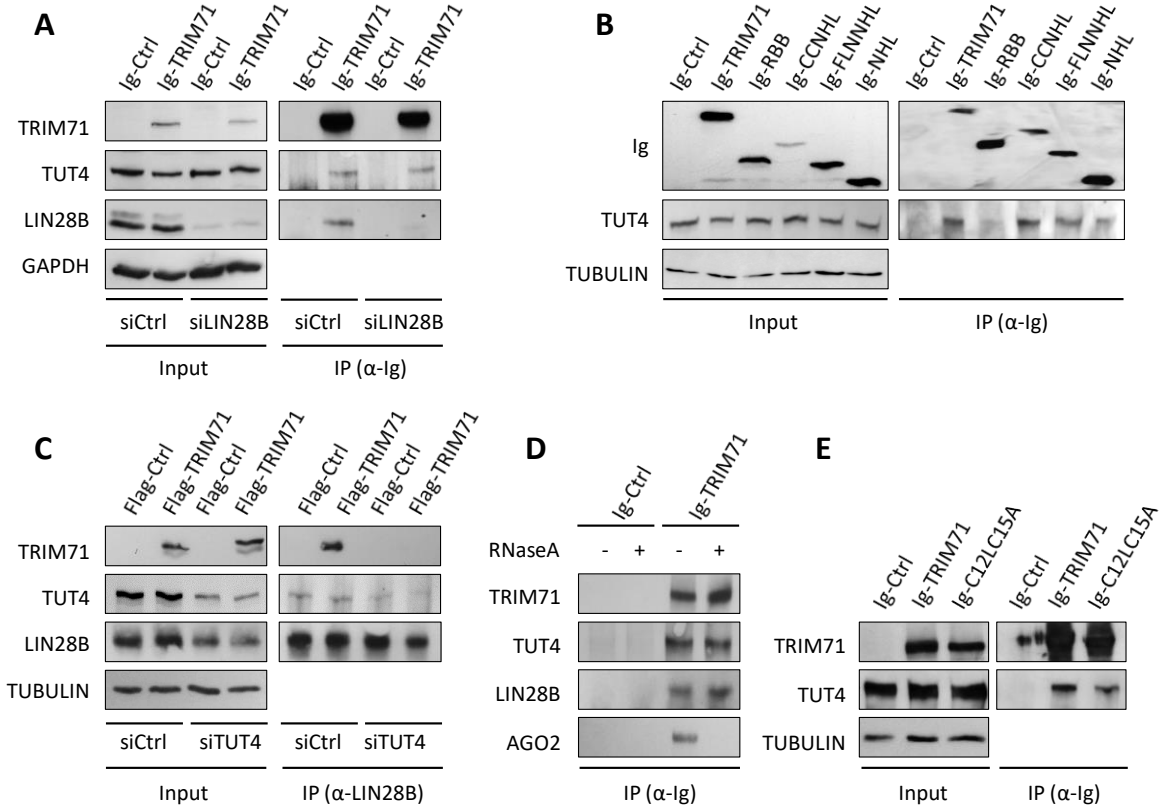

Figure 4.1.5. TUT4 mediates the interaction between TRIM71 and LIN28. **A)** Representative immunoblot showing the co-precipitation of TUT4 with TRIM71 in the absence of LIN28A (siCtrl) and the absence of both LIN28 proteins upon LIN28B knockdown (siLIN28B) in HEK293T cells. **B)** Representative immunoblot showing the co-precipitation of TUT4 with different TRIM71 truncated proteins in HEK293T cells. **C)** Representative immunoblot showing the co-precipitation of TRIM71 with endogenous LIN28B in HEK293T cells, in the presence of TUT4 (siCtrl) or upon TUT4 knockdown (siTUT4). **D)** Representative immunoblot showing the interaction between TRIM71 and TUT4 or LIN28B upon RNase treatment (total Lysate not shown). AGO2 was used as a control of RNA-dependent interaction. **E)** Representative immunoblot showing the co-precipitation of TUT4 with full length wild type TRIM71 and ubiquitylation mutant C12LC15A overexpressed in HEK293T cells.

After having characterized the interaction of TRIM71 with LIN28 proteins, we focused on their putative common role in the regulation of the expression of let-7 miRNAs. In order to confirm that TRIM71 and LIN28 proteins cooperate for the regulation of let-7 expression, we evaluated TRIM71-mediated let-7 downregulation in the absence of LIN28 proteins in mESCs, in which this cooperation was initially proposed. mESCs express LIN28A endogenously, but not LIN28B (Fig. 4.1.6A). We therefore overexpressed TRIM71 in wild type and LIN28A knockout mESCs, and measured let-7a miRNA levels. Overexpression of TRIM71 reduced let-7a miRNA levels significantly in wild type mESCs but not in LIN28A knockout mESCs (Figure 4.1.6B). The levels of overexpressed TRIM71 in wild type mESCs were comparable to those in LIN28A knockout mESCs (Fig. 4.1.6C), excluding the possibility that the observed differences in let-7a regulation derived from different TRIM71 transfection efficiencies or even differential TRIM71 regulation upon LIN28A knockout. These results clearly show that TRIM71-mediated downregulation of let-7 miRNA in mESCs depends on the presence of LIN28A, thereby confirming a cooperation between TRIM71 and LIN28A in the repression of let-7 biogenesis.

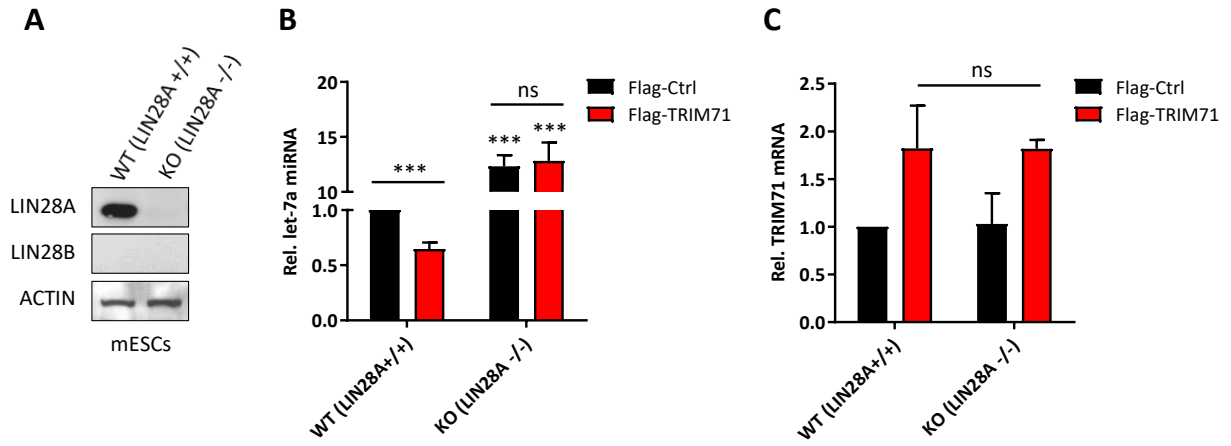

Figure 4.1.6. TRIM71 depends on LIN28A for the repression of let-7 expression in mESCs. A) Representative immunoblot showing endogenous Lin28A and Lin28B levels in wild type (WT, Lin28A+/+) and LIN28A knockout (KO, Lin28A -/-) mESCs. **B)** qPCR measurements of let-7a miRNA levels in WT and Lin28A KO mESCs overexpressing Flag or Flag-TRIM71 (n=5). **C)** qPCR measurements of TRIM71 mRNA levels in WT and Lin28A KO mESCs overexpressing Flag or Flag-TRIM71 (n=3). U6 and HPRT1 housekeeping genes were used for normalization of miRNAs and mRNAs, respectively. All graphs represent Mean ± SEM. Statistical significance was calculated with a two-tailed unpaired Student's t-test (ns = non-significant; ***P-value < 0.005).

An important aspect yet to clarify with respect to the TRIM71/TUT4/LIN28/pre-let-7 axis concerns the involvement of the RING domain in TRIM71-mediated let-7 downregulation. We have shown that the ubiquitylation mutant C12LC15A interacts with TUT4 and LIN28 proteins to a similar extent as the wild type TRIM71. However, if TRIM71 depended on its E3 ligase function to affect pre-let-7 maturation, the mutant C12LC15A would fail to regulate let-7 expression despite being able to join the TUT4/LIN28/pre-let-7 complex. We therefore evaluated the capability of wild type TRIM71 and mutant C12LC15A to regulate let-7 expression and let-7 activity in several cell lines with different expression of LIN28 proteins: mESCs, expressing only LIN28A, HEK293T cells, expressing only LIN28B, the mouse embryonic fibroblast cell line NIH3T3, lacking both LIN28 proteins, and the human malignant T cell line Jurkat E6.1, lacking both LIN28 proteins as well (Fig. 4.1.7A).

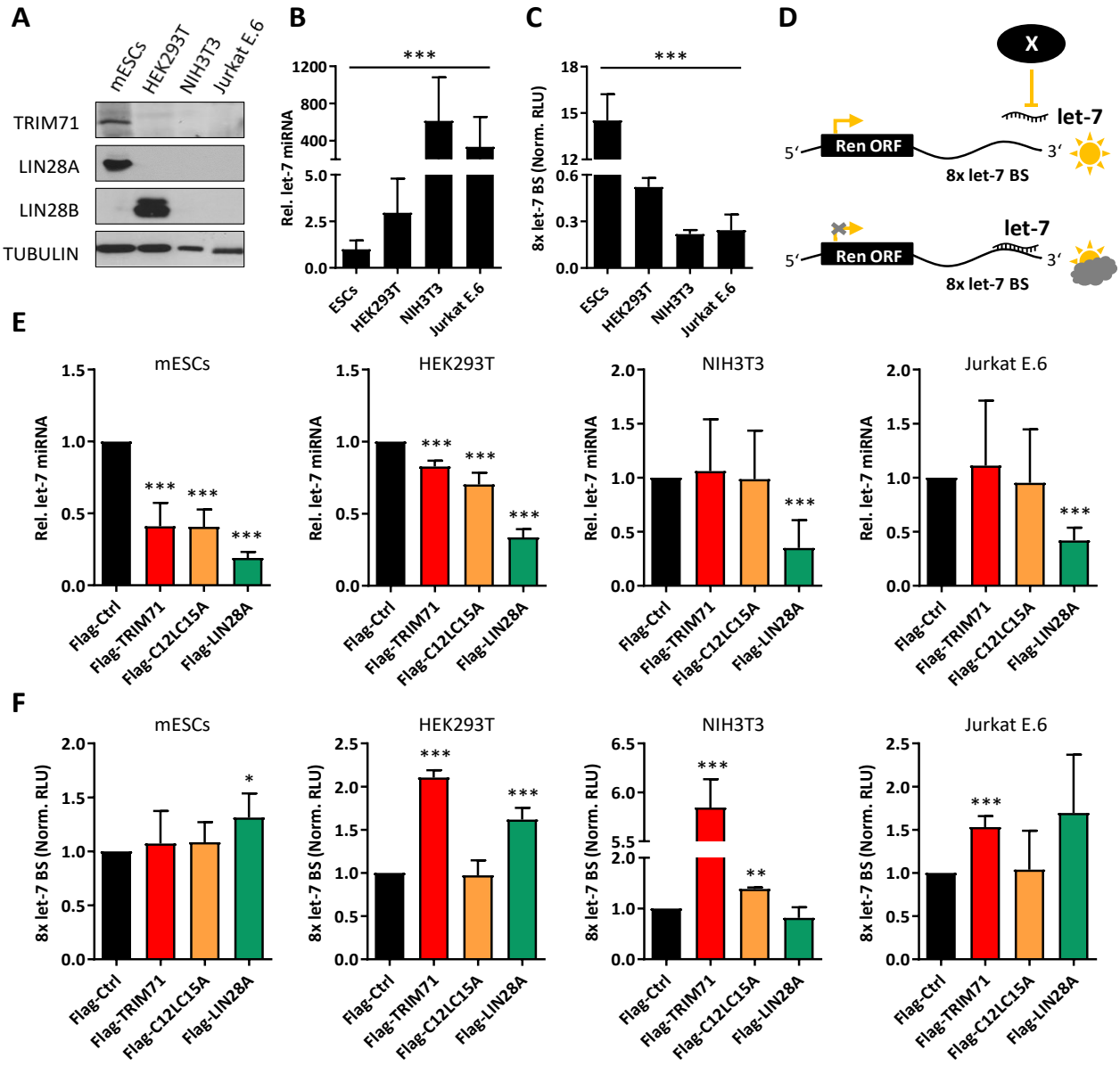

Figure 4.1.7. TRIM71 E3 ligase activity is dispensable for the regulation of let-7 expression, but required for the regulation of let-7 activity. A) Representative immunoblot showing the levels of endogenously expressed TRIM71 and LIN28 proteins in the indicated cell lines, used for experiments depicted in B-F. **B)** qPCR measurements of mature let-7a miRNA levels in several cell lines with different LIN28 proteins occurrence (n=3-6). **C)** Luciferase-miRNA reporter assays (depicted in D) showing let-7 activity in several cell lines with different LIN28 proteins occurrence (n=3). **D)** Schematic representation of a luciferase-miRNA reporter assay. Repression of let-7 activity results in the derepression of the Renilla luciferase reporter (up), whereas let-7 annealing to its 8x binding sites (BS) present in the 3'UTR downstream of the Renilla open reading frame (ORF), results in the repression of the reporter. Thus, miRNA activity and reporter activity are inversely correlated. **E)** qPCR measurements of mature let-7a miRNA levels in the indicated cell lines upon overexpression of Flag-empty/Flag-TRIM71/Flag-C12LC15A/Flag-LIN28A (n=3-8). **F)** Luciferase-miRNA reporter assays showing let-7 activity in the indicated cell lines upon overexpression of Flag-empty/Flag-TRIM71/Flag-C12LC15T/Flag-LIN28A (n=3-8). Norm. RLU = Normalized Relative Light Units. All graphs represent Mean ± SD. For B and C, statistical significance was calculated by one-way ANOVA, showing significant differences in let-7 expression (B) and activity (C) among all cell lines tested (***P-value summary < 0.005). For E and F, statistical significance was calculated with a two-tailed unpaired Student's t-test (*P-value < 0.05; **P-value < 0.01; ***P-value < 0.005).

The differences in LIN28 protein levels in the used cell lines inversely correlated with let-7 expression levels (Fig. 4.1.7B) and thereby also with overall let-7 miRNA activity, as shown by luciferase-miRNA reporter assays (Fig. 4.1.7C-D). The measurements of mature let-7 expression levels in these cell lines following overexpression of wild type TRIM71, ubiquitylation mutant C12LC15T or LIN28A allowed us to make several valuable observations (Fig. 4.1.7E). First, TRIM71-mediated let-7 downregulation was only possible in cell lines containing either of the LIN28 proteins (ESCs and HEK293T), whereas let-7 levels were unaltered upon TRIM71 overexpression in LIN28-lacking cells (NIH3T3 and Jurkat E6.1). These results confirmed again, by a different approach, that TRIM71 depends on LIN28 proteins to downregulate let-7 miRNAs. Second, LIN28A overexpression, which was used as a control for successful let-7 downregulation, repressed let-7 expression more efficiently than TRIM71. These results are in line with previous studies in our lab comparing let-7 mature levels in TRIM71 knockout and LIN28A knockout ESCs (unpublished data, see again Introduction Fig. 1.9). These data suggested that LIN28 proteins have a major role for triggering pre-let-7 degradation, whereas TRIM71 seems to be rather involved in fine-tuning or optimization of such a process. Third, both TRIM71 and C12LC15A could downregulate let-7 expression to the same extent, proving that the E3 ligase activity of TRIM71 is not required for the fulfillment of such a function. Fourth, the capability of TRIM71 to downregulate let-7 expression was higher in mESCs than in HEK293T cells, suggesting that Lin28A may be more efficient in the repression of let-7 expression than Lin28B. This hypothesis is supported by the fact that let-7 expression and activity levels are lower in mESCs, expressing LIN28A, as compared to HEK293T cells, expressing LIN28B (Fig. 4.1.7B-C). Last, the results concerning the regulation of let-7 activity upon TRIM71, C12LC15A and LIN28A overexpression in the different cell lines (Fig. 4.1.7F) did not represent the corresponding measurements of let-7 miRNA levels under the same conditions, and will be extensively discussed in the following section.

Altogether, our results so far have shown that TRIM71 indirectly interacts with LIN28 proteins via TUT4 binding through its NHL domain, and cooperates in the repression of pre-let-7 maturation without relying on its E3 ligase function.

4.1.2. TRIM71 regulates let-7 activity via a TUT4/LIN28-independent mechanism

When we compared let-7 activity with let-7 expression measurements in ESCs, HEK293T, NIH3T3 and Jurkat E.6 cell lines, we observed some important incongruences (Fig. 4.1.7E-F). First, whereas the strongest TRIM71-mediated repression of let-7a expression was observed in mESCs, the activity of let-7 was unaltered upon TRIM71 or C12LC15A overexpression in these cells. Second, whereas TRIM71-mediated regulation of let-7 expression was independent from its E3 ligase function, let-7 activity regulation seemed to be ubiquitylation-dependent, since only wild type TRIM71 – but not C12LC15A mutant – could repress let-7 activity (shown as a derepression of the miRNA-reporter in luciferase assays) in HEK293T, NIH3T3 and Jurkat E6.1 cells. Last, whereas TRIM71 did not regulate let-7 expression in LIN28-deficient cell lines (NIH3T3 and Jurkat E.6), let-7 activity was significantly repressed by wild type TRIM71 in those cells. Such a differential regulation of let-7 activity by TRIM71 and C12LC15A, occurring both in the presence and absence of LIN28 proteins, could be explained by a TRIM71-mediated TUT4/LIN28-independent regulation of the miRNA activity.

In light of these results, we hypothesized that TRIM71 employs two distinct mechanisms for the regulation of let-7 expression and let-7 activity. Supporting this hypothesis, impairing the TUT4/LIN28-dependent mechanism by either LIN28B knockdown or TUT4 knockdown had no effect on TRIM71-mediated let-7 activity regulation (Fig. 4.1.8A-C). A regulation of miRNA activity independently from expression regulation can only occur at the mature miRNA state, whereas the TUT4/LIN28-mediated mechanism targets pre-let7 species, thereby exerting an expression-dependent activity regulation. Accordingly, overexpression of LIN28A was only able to regulate the activity of endogenously expressed let-7 or overexpressed pre-let7, but not of overexpressed mature let-7 miRNA. However, TRIM71 was indeed able to regulate the activity of overexpressed mature let-7 (Fig. 4.1.8A and D), demonstrating that TRIM71-mediated miRNA activity regulation occurs downstream of TUT4/LIN28 functions.

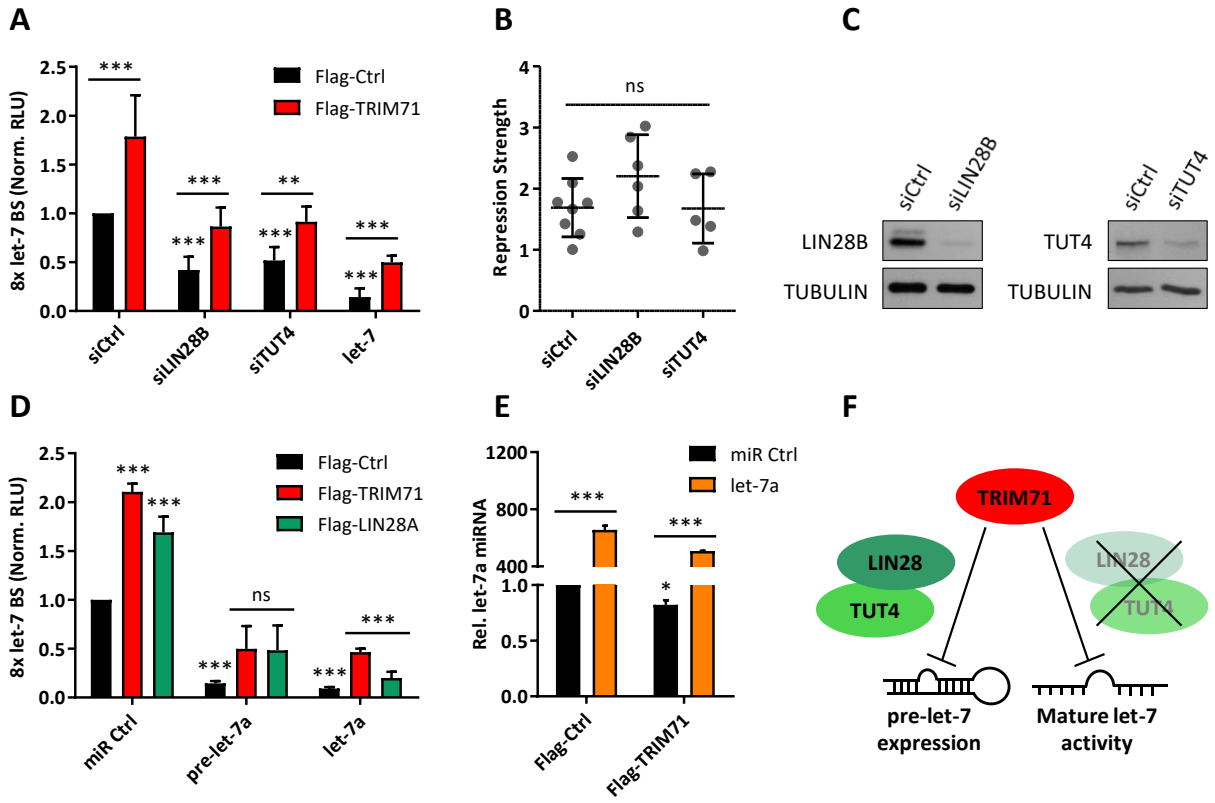

Figure 4.1.8. TRIM71-mediated let-7 activity regulation is TUT4/LIN28-independent and is therefore decoupled from pre-let-7 expression regulation. A) Luciferase-miRNA reporter assay upon TRIM71 overexpression in HEK293T cells after LIN28B or TUT4 knockdown. Ectopic let-7 miRNA expression was used as a control for efficient let-7 reporter repression (n=4-7). **B)** TRIM71-mediated let-7 activity repression strength, calculated from values in A, as the ratio between norm. RLU Flag-TRIM71 and norm. RLU Flag-Ctrl values. **C)** Representative immunoblots showing levels of LIN28B and TUT4 upon specific LIN28 knockdown (siLIN28B) and TUT4 knockdown (siTUT4), respectively. Of note, a proof of efficient LIN28B and TUT4 knockdowns was already shown in A by the enhanced repression of the let-7 reporter, result of an upregulation of endogenous let-7 levels under such conditions. **D)** Luciferase-miRNA reporter assay upon TRIM71 or LIN28A overexpression after ectopic expression of pre-let-7 and mature let-7 miRNA mimics, as compared to the overexpression of a miRNA control (miR Ctrl), representing the regulation of endogenously expressed let-7 (n=3-9). **E)** qPCR measurements of endogenous let-7a miRNA levels (miR Ctrl) and overexpressed let-7 miRNA levels (let-7 mimic) after Flag-Ctrl or Flag-TRIM71 overexpression (n=3-4). **F)** Schematic representation of TRIM71-mediated pre-let-7 expression regulation and mature let-7 activity regulation in a LIN28/TUT4-dependent and -independent manner, respectively. Norm. RLU = Normalized Relative Light Units. All graphs represent Mean ± SD. Statistical significance was calculated with a two-tailed unpaired Student's t-test (ns = non-significant; *P-value < 0.05; **P-value < 0.01; ***P-value < 0.005).

Supporting a decoupling of the TRIM71-mediated let-7 activity regulation from the TRIM71/TUT4/LIN28-mediated pre-let-7 expression regulation, TRIM71 was less efficient than LIN28A in the downregulation of let-7 expression (see again Fig. 4.1.7E), but more efficient in the repression of let-7 activity (Fig. 4.1.8D, miR Ctrl condition). Furthermore, quantification of let-7 levels following its ectopic expression in control and TRIM71-overexpressing cells shows that let-7 levels remained remarkably high (more than 400-fold) in the presence of TRIM71 (Fig. 4.1.8E). These results indicate that TRIM71 does not rely on mature let-7 degradation to achieve activity repression and thereby proves activity regulation to be expression-independent. Collectively, these data show that TRIM71 is able to regulate let-7 expression and activity via two independent mechanisms: for the former mechanism, TRIM71 relies on its interaction with the TUT4/LIN28/pre-let-7 complex to repress the maturation of pre-let-7 species, thereby downregulating let-7 expression; in the latter mechanism, TRIM71 relies on its E3 ligase function to repress the activity of the mature let-7 miRNA in a TUT4/LIN28-independent manner (Fig. 4.1.8F).

4.1.3. TRIM71-mediated miRNA activity regulation depends on AGO2 binding

Mature miRNAs require assistance by the RNA-induced silencing complex (RISC) to exert their activity and induce mRNA target repression[34]. Argonaute (AGO) proteins – commonly and well-characterized AGO2 – are the major effectors of the RISC, since they bind the miRNA, identify the guide miRNA strand, and find the complementary mRNA partner to repress its translation and commonly induce its degradation[36]. The interaction of TRIM71 with AGO proteins is long known, well-characterized and conserved among species[86]. However, the functional outcome of such interaction has been controversially discussed and remains poorly understood. To test whether TRIM71-mediated let-7 activity regulation was linked to AGO2 function, we repeated the let-7 reporter assay in AGO2 knockout HEK293T cells (Fig. 4.1.9A). Indeed, TRIM71-mediated repression of let-7 activity was impaired in AGO2 knockout HEK293T cells (Fig. 4.1.9B), being the repression strength of TRIM71 significantly diminished in the absence of AGO2 (Fig. 4.1.9C). These results suggested an AGO2 dependency for the fulfilment of such a function. However, it is reasonable to argue that the repression of the let-7 reporter was impaired due to a global miRNA-mediated silencing dysfunction in AGO2 knockout cells. Nevertheless, the overexpression of let-7 miRNA continued to induce efficient repression of *bona fide* let-7 targets in the absence of AGO2, as shown by decreased HMGA2 mRNA levels (Fig. 4.1.9D). These results indicated that other AGO proteins take over miRNA-mediated silencing in AGO2 knockout HEK293T cells and thereby proved our miRNA reporter assay to be perfectly functional in these cells.

Consistent with an AGO2 dependency of this mechanism, the ubiquitylation mutant C12LC15A, which failed to repress let-7 activity in our previous experiments (see again Fig. 4.1.7F), did not co-precipitate with AGO2 (Fig. 4.1.9E). An intact RING domain was not sufficient for TRIM71-AGO2 binding, since the deletion of the whole FLNNHL domain (RBCC construct) or even only the last NHL repeat (ΔNHL6 construct) also abrogated TRIM71-AGO2 interaction (Fig. 4.1.9E-F). Consistently, all constructs which failed to interact with AGO2 showed an impaired regulation of let-7 activity (Fig. 4.1.9G).

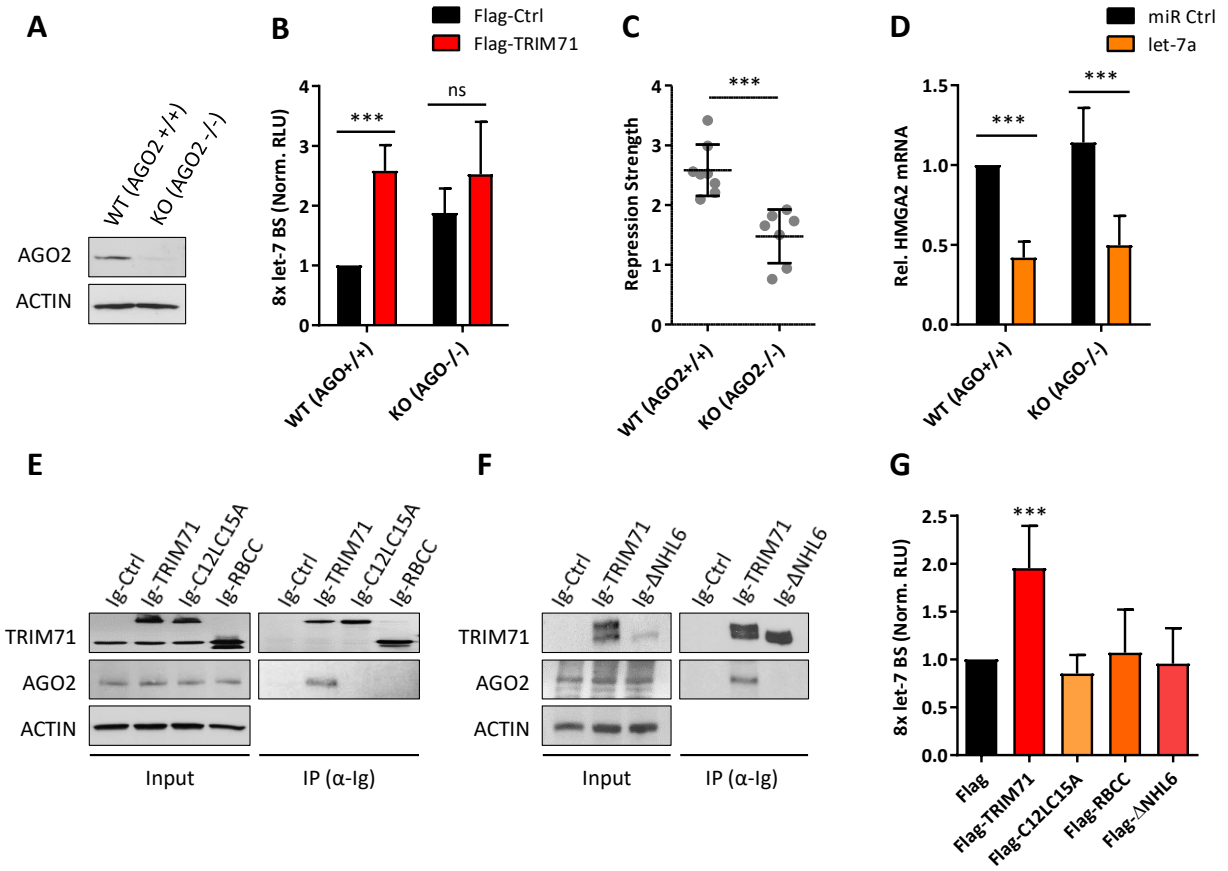

Fig. 4.1.9. TRIM71-mediated let-7 activity regulation depends on AGO2 binding, and requires not only a functional RING domain, but also an intact NHL domain. A) Representative immunoblot showing AGO2 protein levels in wild type (WT, AGO2 +/+) and AGO2 knockout (KO, AGO2 -/-) HEK293T cells. **B)** luciferase-miRNA reporter assay showing TRIM71-mediated let-7 activity regulation in WT and AGO2 KO HEK293T cells (n=7-8). **C)** TRIM71-mediated let-7 activity repression strength in WT and AGO2 KO HEK293T cells, calculated from data depicted in B as the ratio between norm. RLU Flag-TRIM71 and norm. RLU Flag-Ctrl values. **D)** qPCR quantification of the *bona fide* let-7 target HMGA2 upon miR Ctrl or let-7 overexpression in WT and AGO2 KO HEK293T cells (n=4). **E)** Representative immunoblot showing the co-precipitation ability of AGO2 with Ig-TRIM71, Ig-C12LC15A and Ig-RBCC constructs in HEK293T cells. **F)** Representative immunoblot showing the co-precipitation ability of AGO2 with Ig-TRIM71 and Ig-ΔNHL6 constructs in HEK293T cells**. G)** Luciferase-miRNA reporter assay for the indicated TRIM71 constructs with distinct AGO2 binding ability used in E-F (n=3-9). Norm. RLU = Normalized Relative Light Units. All graphs represent Mean ± SD. Statistical significance was calculated with a two-tailed unpaired Student's t-test (ns = non-significant; ***P-value < 0.005).

Given that the ability of different TRIM71 constructs to repress let-7 activity correlated with their AGO2-binding capacity, we hypothesized that the functional outcome of the TRIM71-AGO2 interaction is the inhibition of let-7 activity. This hypothesis was in essence already formulated by a previous study, which postulated that TRIM71-mediated let-7 activity repression resulted from a global miRNA activity inhibition as a consequence of TRIM71-mediated AGO2 ubiquitylation and proteasomal degradation[105]. However, we did not observe changes in AGO2 protein stability upon TRIM71 overexpression in HEK293T cells (Fig. 4.1.10A-B). Consistently, reporter assays for other miRNAs showed that TRIM71 overexpression does not result in a global miRNA activity repression. Specifically, TRIM71 repressed the activity of let-7a, let-7g and that of the pro-differentiation brain-specific miR-128a, whereas the activity of other miRNAs such as

miR-16a or miR-19a was not affected upon TRIM71 overexpression (Fig. 4.1.10C). These results clearly showed that TRIM71 specifically represses the activity of a subset of differentiation-promoting miRNAs, without neither inducing AGO2 degradation nor generally impairing miRNA-mediated silencing.

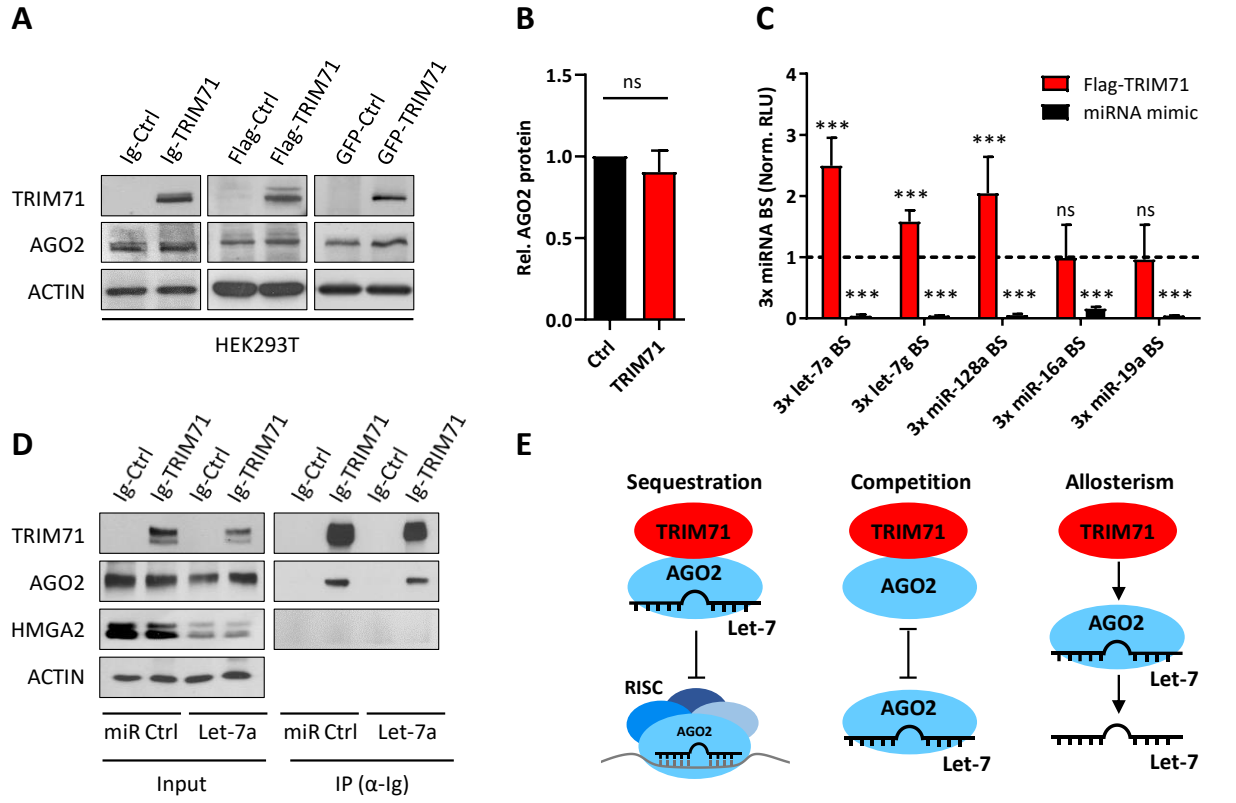

Figure 4.1.10. TRIM71 specifically represses the activity of several differentiation-promoting miRNAs, without neither affecting AGO2 stability nor global miRNA activity. A) Representative immunoblots showing AGO2 protein levels in control and TRIM71-overexpressing HEK293T cells. Different tags (Ig, Flag, GFP) were used to eliminate the possibility of a tag-specific-mediated inhibition of the TRIM71 E3 ligase function. **B)** AGO2 band densitometry quantification relative to ACTIN bands of the blots depicted in A (and other blots replicates of A), where "Ctrl" accounts for Ig-Ctrl, Flag-Ctrl and GFP-Ctrl, whereas "TRIM71" accounts for Ig-TRIM71, Flag-TRIM71 and GFP-TRIM71 (n=7). **C)** Luciferase-miRNA reporter assays for several miRNAs upon TRIM71 overexpression in HEK293T cells. The dashed-line represents the repression of the indicated miRNA upon Flag-empty overexpression. Overexpression of the indicated mimic miRNAs proved that the respective luciferase reporters properly responded to miRNA regulation. **D)** Representative immunoblot showing AGO2 co-precipitation with Ig-TRIM71 upon miR Ctrl or let-7a miRNA mimic overexpression. **E)** Hypothetic models proposed for TRIM71-mediated AGO2-dependent let-7 activity inhibition (discussed in the main text). Norm. RLU = Normalized Relative Light Units. All graphs represent Mean ± SD. Statistical significance was calculated with a two-tailed unpaired Student's t test (ns = non-significant; ***P-value < 0.005).

TRIM71-mediated miRNA activity repression could be based on a AGO2-miRNA complex sequestration from the RISC complex, implying that TRIM71 preferentially binds AGO2 when AGO2 is already bound to specific miRNAs (Fig. 4.1.10E, left panel). Alternatively, TRIM71-mediated miRNA activity repression could be based on a competition with such specific miRNAs to bind AGO2, implying that TRIM71 sequesters AGO2 away from those miRNAs (Fig. 4.1.10E, middle panel). Last, TRIM71 could regulate AGO-miRNA binding by an allosteric-dependent mechanism, decreasing the affinity of AGO2 for specific miRNAs upon binding (Fig. 4.1.10E, right panel).

Given that the TRIM71-AGO2 interaction is known to be RNA-dependent[105,115] (see again Fig. 4.1.5D), a sequestration mechanism seems more likely than a competition one. In case of AGO2-let7 sequestration, TRIM71 binding to AGO2 would be enhanced by let-7 overexpression, whereas in case of a competition between TRIM71 and let-7 miRNAs for AGO2 binding, TRIM71 binding to AGO2 would be decreased by let-7 overexpression. However, the levels of AGO2 co-precipitated with TRIM71 were not affected upon let-7 overexpression (Fig. 4.1.10D), excluding both, sequestration and competition mechanisms. Therefore, it is more likely that TRIM71 interaction with AGO2 alters AGO2 affinity for specific miRNA families, decreasing AGO2 binding to miRNAs like let-7 or miR-128 and maybe even increasing AGO2 binding to other miRNAs yet to be identified. Furthermore, given the RNA-dependent interaction between TRIM71 and AGO2, such an allosteric regulation occurs likely in active RISCs.

4.1.4. Phosphorylation of TRIM71 does not affect its role as a let-7 regulator

We have shown that TRIM71 is able to regulate let-7 expression and activity via TUT4/LIN28-dependent and AGO2-dependent mechanisms, respectively. The ubiquitylation mutant C12LC15A failed to bind AGO2 and to regulate let-7 activity, whereas the regulation of let-7 expression via TUT4/LIN28 binding was preserved in this mutant. Upon overexpression of wild type TRIM71 and mutant C12LC15A in HEK293T cells, it came to our attention that they show distinct banding patterns in WB. Wild type TRIM71, able to perform both, the TUT4/LIN28-dependent and the AGO2-dependent mechanism, consists of two bands, while the ubiquitylation mutant C12LC15A, able to perform only the TUT4/LIN28-dependent mechanism, consist of only one band (Fig. 4.1.11A, HEK293T cells). We therefore reasoned that the upper TRIM71 band, only present in wild type TRIM71, may be responsible for the AGO2-dependent mechanism, while the lower band, present in both TRIM71 and C12LC15A, might be responsible for the TUT4/LIN28-dependent mechanism. In order to test this hypothesis, we further investigated the nature of TRIM71 upper band.

It is very unlikely that the upper TRIM71 band derives from alternative splicing, since we overexpressed the ORF of TRIM71, lacking introns and UTRs, cloned from a cDNA library. The overexpression of TRIM71 with different tags in HEK293T cells excluded that the upper band resulted from tag-specific modifications (Fig. 4.1.11A). Discarding also overexpression artefacts, endogenously expressed TRIM71 consisted of two bands in the embryonic carcinoma (EC) cell lines NCCIT and TCam-2, and both bands were downregulated upon TRIM71 knockdown (Fig. 4.1.11A).

The ubiquitylation mutant C12LC15A lacks two catalytic cysteines required for the E3 ligase function. Cysteines can establish disulfide bonds, and such covalent interactions can be partially maintained even in the denaturing conditions in which WB are performed, altering the migration of the protein. We therefore incubated lysates in 5% β-mercaptoethanol to provide a highly reducing environment which ensures the disruption of all disulfide bonds prior to immunoblotting. However, TRIM71 upper band was still present after this treatment (Fig. 4.1.11B). Since TRIM71 is a RNA-binding protein, we next tested whether the upper band resulted from migration retardation due to protein-RNA interactions. Nevertheless, the upper TRIM71 band was still present after RNase treatment (Fig. 4.1.11.C).

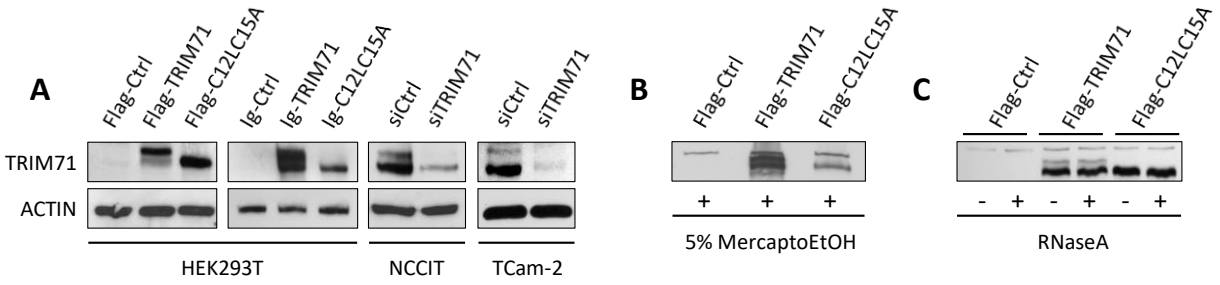

Figure 4.1.11. The upper TRIM71 band is not an overexpression artefact, and does neither result from C12/C15-mediated structural alterations nor RNA interactions. A) Representative immunoblot showing the banding pattern of full length wild type TRIM71 and ubiquitylation mutant C12LC15A upon overexpression of Flag-tagged and Ig-tagged constructs in HEK293T cells, and representative immunoblots showing a double band for endogenously expressed TRIM71 in the embryonic carcinoma cell lines NCCIT and TCam-2 (siCtrl), and the downregulation of both bands for each cell line upon TRIM71 knockdown (siTRIM71). **B)** Representative immunoblot showing the banding pattern of Flag-tagged TRIM71 and C12LC15A overexpressed in HEK293T cells after 5% β-mercaptoethanol treatment of total lysates to promote full protein denaturation. **C)** Representative **i**mmunoblot showing the banding pattern of Flag-tagged TRIM71 and C12LC15A overexpressed in HEK293T cells after RNase treatment of total lysates to promote dissociation of protein-RNA interactions.

Having excluded the possibility that the upper TRIM71 band resulted from overexpression artefacts, C12/C15-mediated structural alterations or RNA interactions, we hypothesized that the upper TRIM71 band resulted from its post-translational modification (PTM). Ubiquitylation would be the most obvious PTM that could be present in wild type TRIM71 and absent in the mutant C12LC15A, as a result of self-ubiquitylation.

To test this hypothesis, we overexpressed wild type TRIM71 or C12LC15A in HEK293T cells together with a His-Ubiquitin construct, and pulled down the whole ubiquitylated proteome with anti-His Ni^{2+} magnetic beads. Strikingly, both wild type TRIM71 and mutant C12LC15A were found pulled down among the ubiquitylated proteins in HEK293T cells (Fig. 4.1.12A). However, TRIM71 contains a histidine-rich stretch within its RING domain which might have been recognized by the Ni^{2+} beads used for the isolation of His-ubiquitylated proteins.

Therefore, we repeated the experiment, this time with HA-Ubiquitin instead, and immunoprecipitated the whole ubiquitylated proteome with an anti-HA antibody. Again, both wild type TRIM71 and mutant C12LC15A could be found pulled down among the ubiquitylated proteins in HEK293T cells (Fig. 4.1.12B). Furthermore, the precipitated TRIM71 and C12LC15A constructs were recognized by an anti-Ubiquitin (UBI) antibody, suggesting that both overexpressed proteins seem to be ubiquitylated by other proteins within the cell (Fig. 4.1.12B). Consistent with these results, both TRIM71 and C12LC15A were accumulated upon MG132-mediated proteasomal inhibition, as compared to their levels in HEK293T cells treated with DMSO as a control (Fig. 4.1.12C).

Altogether, these data demonstrated that, although ubiquitylation followed by proteasomal degradation affects the turnover of overexpressed TRIM71 and C12LC15A proteins in HEK293T cells, the upper TRIM71 band does not result from self-ubiquitylation.

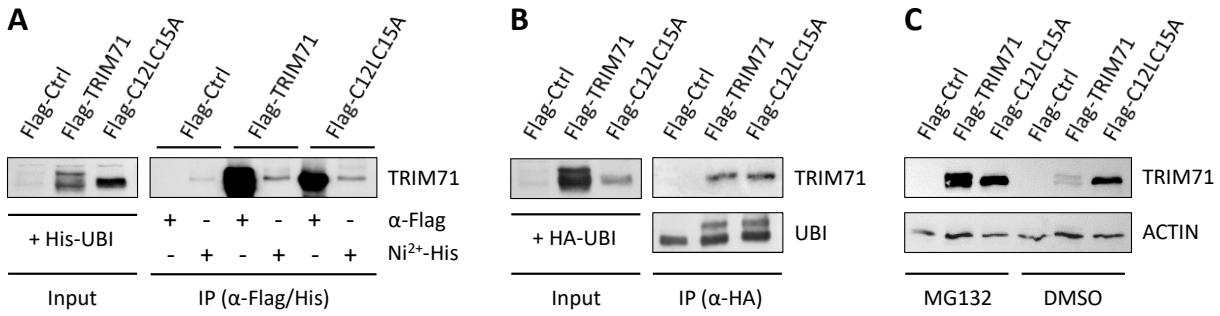

Figure 4.1.12. The upper TRIM71 band is not self-ubiquitylated TRIM71. A) Representative immunoblot showing Flag-tagged TRIM71 and C12LC15A overexpressed in HEK293T cells to be pulled down within the His-ubiquitylated proteome. A parallel anti-Flag IP of TRIM71 and C12LC15A was used as a control. **B)** Representative immunoblot showing Flag-tagged TRIM71 and C12LC15A overexpressed in HEK293T cells to be pulled down within the HA-ubiquitylated proteome. Detection with anti-UBI antibody was used as an extra control to confirm ubiquitylation of these proteins. **C)** Representative immunoblot showing the levels of Flag-tagged TRIM71 and C12LC15A in total lysates of HEK293T cells treated with 25μM of the proteasome inhibitor MG132 or with DMSO as a control.

One of the most common PTMs is phosphorylation. In order to test whether the upper band was phosphorylated TRIM71 (p-TRIM71), we overexpressed wild type TRIM71 and mutant C12LC15A in HEK293T cells and treated whole protein lysates with alkaline phosphatase (AP) prior to their denaturation. AP treatment successfully led to the dephosphorylation of typically phosphorylated proteins such as ERK1/2 (p-ERK1/2) or AKT (p-AKT), without affecting total ERK1/2 or AKT protein levels, and also led to the partial disappearance of the TRIM71 upper band (Fig. 4.1.13A). Similar results were observed upon dephosphorylation of whole protein lysates using lambda phosphatase (λP) (Fig. 4.1.13B), confirming the nature of the upper TRIM71 band as p-TRIM71.

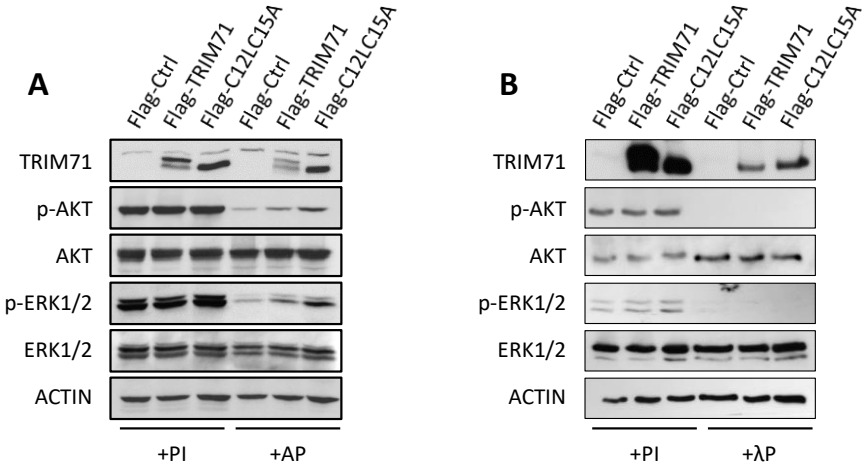

Figure 4.1.13. The upper TRIM71 band is phosphorylated TRIM71 (p-TRIM71). A) Representative immunoblot showing the partial disappearance of the upper TRIM71 band upon alkaline phosphatase (AP) treatment. **B)** Representative immunoblot showing the total disappearance of the upper TRIM71 band upon lambda phosphatase (λP) treatment. Phosphatase inhibitors (PI) were added to the control lysates. P-ERK/total ERK and p-AKT/total AKT were used as controls for the dephosphorylation treatment in each case.

In order to narrow down the location of TRIM71 phosphorylation site(s), we overexpressed several truncated TRIM71 proteins and observed which of them showed a double banding pattern. An RBCC_WT construct, lacking the FLN and NHL domains, showed two bands, whereas mutating the two RING domain catalytic cysteines within this construct (RBCC_C12LC15A) resulted in the disappearance of the upper band, resembling the banding pattern of the full length wild type TRIM71 and C12LC15A mutant, respectively (Fig. 4.1.14A). These results confirmed that TRIM71 phosphorylation(s) occurred within the RBCC region, being the FLN and NHL domains dispensable for TRIM71 phosphorylation. However, an intact RING domain was not sufficient for TRIM71 phosphorylation to occur, since the deletion of the CC (RBB construct) resulted in the disappearance of the upper band (Fig. 4.1.14A). This implied, either that the phosphorylation site(s) lie within the CC region, or that the CC region is required for the phosphorylation to occur somewhere else within the RBB region.

To test these hypothesis, we located all possible phosphorylation sites (serines, threonines or tyrosines) within the CC region, and mutated them to evaluate the appearance of the TRIM71 upper band. Two phosphorylation sites were located within the CC region of TRIM71 (Fig. 4.1.14B), each of them with several aa susceptible of phosphorylation, but close enough to each other to be mutated at once. However, mutation of each *phosphosite* (SY/AF mutation of phosphosite I and STS/AAA mutation of phosphosite II) did not lead to the disappearance or diminishment of the upper band (Fig. 4.1.14C), demonstrating that TRIM71 upper band does not result from phosphorylation(s) within the CC region, and confirming that the CC is required for the phosphorylation(s) to occur somewhere within the RBB region.

The RBB full region contained too many possible phosphosites for individual mutation. We therefore overexpressed the RBCC construct in HEK293T cells and purified upper and lower bands separately for mass spectrometry analysis (MS), in order to find differential phosphosites between the two bands (MS data not shown). A phosphorylation in Ser26/Ser27 was found to be present in the upper band while absent in the lower band. Mutation of these two serines to valines (SS/VV mutant) resulted in a significant reduction of TRIM71 upper band (p-TRIM71) relative to the total amount of overexpressed TRIM71 (total TRIM71), but not in its complete disappearance (Fig. 4.1.14D-E), suggesting that other phosphosites may account for the total migration shift observed for the TRIM71 upper band.

The RING domain sequence contains a total of 14 serines susceptible to be phosphorylated, many of which cluster close to each other (Fig. 4.1.14F). We therefore hypothesized that overall phosphorylation within this region may be responsible for the electrophoretic mobility of this protein species relative to the unphosphorylated one. We then introduced a silent mutation within the RING domain that generated a new and unique SacII restriction site downstream of all 14 serines (Fig. 4.1.14F), and were able to exchange the first stretch of the protein by an artificial sequence in which all 14 serines present within the RING domain had been mutated to valines (14xS/V mutant). The mutation of all serines within the RING domain indeed resulted in the total disappearance of the TRIM71 upper band (Fig. 4.1.14G).

Our results collectively showed that, in a mechanism requiring the two catalytic cysteines C12 and C15 within the RING domain and the presence of the CC region, TRIM71 is phosphorylated in several serines within the RING domain, including Ser26/Ser27. These collective phosphorylations grant p-TRIM71 with a different electrophoretic mobility relative to its unphosphorylated form.

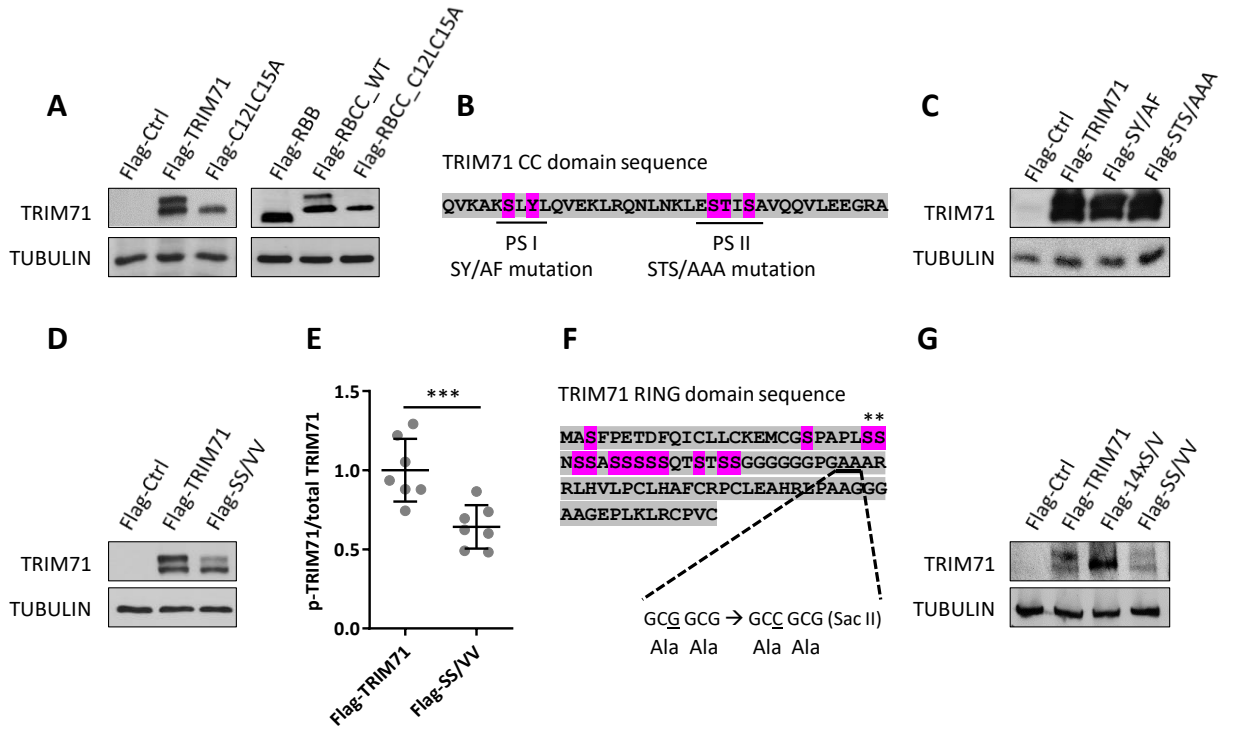

Figure 4.1.14. The phosphorylation of several serines within the RING domain of TRIM71 (including Ser26/Ser27) depends on the presence of the two RING domain catalytic cysteines (C12 and C15) and the CC region. A) Representative immunoblot showing the banding pattern of several Flag-tagged TRIM71 constructs overexpressed in HEK293T cells. **B)** Sequence of the TRIM71 Coiled-Coil (CC) region, highlighting in purple the aa mutated in phosphosites I (PS I) and II (PS II). **C)** Representative immunoblot showing the banding pattern of CC mutants SY/AF (PS I) and STS/AAA (PS II). **D)** Representative immunoblot showing the banding pattern of the SS/VV mutant overexpressed in HEK293T cells compared to the wild type TRIM71 banding pattern. SS = Ser26/Ser27 identified to be phosphorylated in TRIM71 upper band by MS. **E)** Densitometry quantification of the upper TRIM71 band intensity (p-TRIM71) relative to the total overexpressed TRIM71 or SS/VV constructs (total TRIM71) in several blots replicates of D (n=7). Graph represents Mean ± SD. Statistical significance was calculated with a two-tailed unpaired Student's t-test (***P-value < 0.005). **F)** Sequence of the TRIM71 RING domain, highlighting in purple all serines present (14), as well as the location and DNA sequence encoding for the region where the silent mutation (G/C underlined), generating a new and unique SacII restriction site was incorporated. **G)** Representative immunoblot showing the banding pattern of the SS/VV and 14xS/V mutants compared to the wild type TRIM71 banding pattern.

After we had found the upper TRIM71 band to be p-TRIM71, and having generated mutants that could partially or totally abrogate TRIM71 phosphorylation within the RING domain, we investigated whether p-TRIM71 was required for the AGO2-dependent regulation of let-7 activity, as previously hypothesized. To this end, we first evaluated the requirement of TRIM71 phosphorylation for AGO2 interaction. Opposing our hypothesis, both phospho-mutants, SS/VV and 14xS/V, were found co-precipitated with AGO2 (Fig. 4.1.15A). Furthermore, the co-precipitation of AGO2 with wild type TRIM71 was preserved even when the IP fraction was subjected to λP-mediated dephosphorylation (Fig. 4.1.15B), indicating that p-TRIM71 does not mediate the interaction with AGO2. Consistent with these results, both phospho-mutants, SS/VV and 14xS/V, were able to repress the activity of let-7 miRNA (Fig. 4.1.15C), demonstrating that p-TRIM71 is not required for the AGO2-dependent let-7 activity regulation.

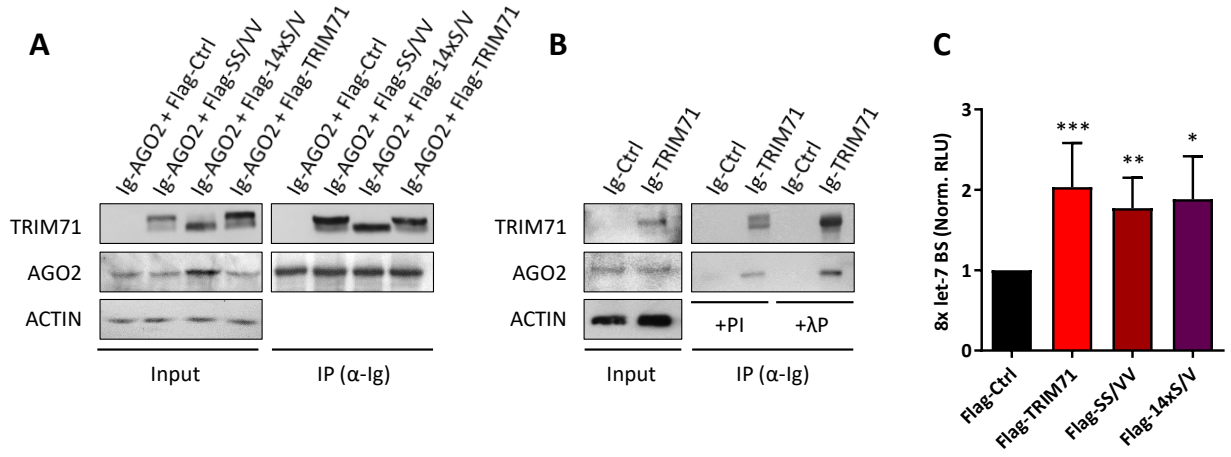

Figure 4.1.15. TRIM71 phosphorylation is dispensable for the fulfilment of the TRIM71-mediated AGO2-dependent let-7 activity repression. A) Representative immunoblot showing the TRIM71 phospho-mutants SS/VV and 14xS/V co-precipitated with Ig-tagged AGO2 overexpressed in HEK293T cells. **B)** Representative immunoblot showing the co-precipitation of endogenous AGO2 with Ig-tagged TRIM71 after PI or λP treatment of the IP fraction. PI = phosphatase inhibitors, preserving phosphorylated proteins. λP = Lambda phosphatase, mediating protein dephosphorylation. **C)** Luciferase-miRNA reporter assay showing the capability of TRIM71 phospho-mutants SS/VV and 14xS/V to repress let-7 activity in HEK293T cells (n=4-8). Norm. RLU = Normalized Relative Light Units. Graph represents Mean ± SD. Statistical significance was calculated with a two-tailed unpaired Student's t-test (*P-value < 0.05; **P-value < 0.01; ***P-value < 0.005).

Altogether, we found TRIM71 to be phosphorylated in several serines within the RING domain, including Ser26/Ser27, resulting in the appearance of a TRIM71 upper band. The phosphorylation depends on the presence of the CC region, and the two RING domain catalytic cysteines C12 and C15. However, we have shown that p-TRIM71 is not involved in the AGO2-dependent regulation of let7-activity. Therefore, our hypothesis of the upper TRIM71 band being responsible for the AGO2-dependent mechanism, and the lower TRIM71 band being responsible for the TUT4/LIN28-dependent let-7 expression regulation had to be discarded at this point. Nevertheless, p-TRIM71 could be involved in other TRIM71-mediated functions which may be of physio-pathological relevance.

In this chapter, we have proven that TRIM71 is able to regulate both, miRNA expression and miRNA activity, via two independent mechanisms. TRIM71-mediated miRNA regulation can, in turn, regulate mRNA expression. However, TRIM71 itself can directly regulate the expression of mRNAs by recognition of regulatory elements within their UTRs, inducing their translational inhibition and/or triggering mRNA degradation[115,126]. A well-known TRIM71 mRNA target is CDKN1A mRNA, encoding for the cell cycle inhibitor and tumor suppressor p21. TRIM71 was shown to repress CDKN1A 3'UTR in mESCs and EC cells[41].

To test whether phosphorylation of TRIM71 influences its ability to act as an mRNA repressor, we conducted luciferase-3'UTR reporter assays upon wild type TRIM71, ubiquitylation mutant C12LC15A, and phospho-mutants SS/VV and 14xS/V overexpression in HEK293T cells. In this case, our luciferase reporter was under the control of the full length human CDKN1A 3'UTR. Therefore, a TRIM71-mediated CDKN1A 3'UTR repression should induce the repression of the luciferase reporter (Fig. 4.1.16A), in contrast to our previous luciferase-miRNA reporter assays, where TRIM71-mediated miRNA repression induced a

derepression of the luciferase reporter (see again Fig. 4.1.7D). Our results showed that TRIM71 significantly repressed the 3'UTR of CDKN1A in our luciferase-3'UTR reporter assays (Fig. 4.1.16B). The ubiquitylation mutant C12LC15A, unable to be phosphorylated within the RING domain, significantly repressed the CDKN1A 3'UTR as well (Fig. 4.1.16B), although to a lesser extent when compared to the wild type TRIM71 construct, as shown by the repression strength of each construct (Fig. 4.1.16C). Interestingly, the SS/VV phospho-mutant repressed the CDKN1A 3'UTR to a similar extent as the ubiquitylation mutant C12LC15A (Fig. 4.1.16B-C). However, the 14xS/V phospho-mutant did not yield any significant repression of the CDKN1A 3'UTR, but given that the unphosphorylated C12LC15A construct was, to some extent, able to repress the 3'UTR of CDKN1A, the lack of this function in the 14xS/V phospho-mutant cannot be attributed to its unphosphorylated status (Fig. 4.1.16B-C).

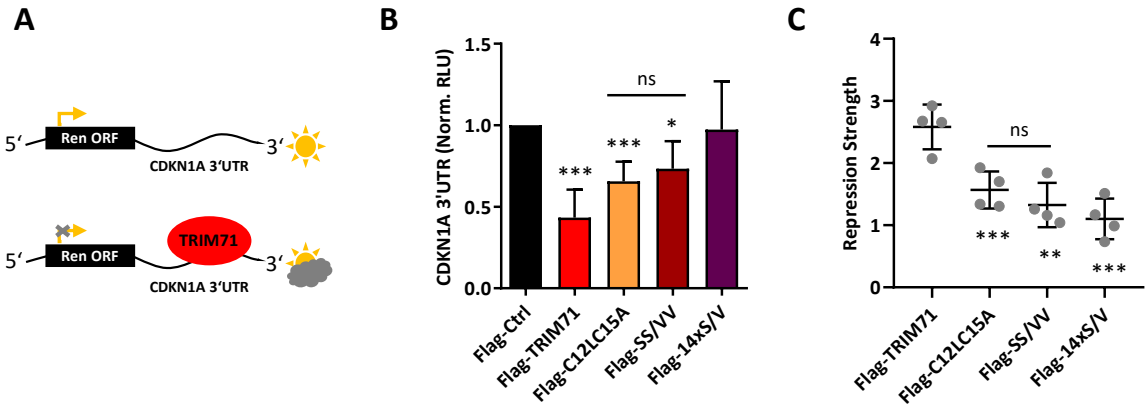

Figure 4.1.16. Phosphorylation of TRIM71 may be involved in fine-tuning/optimization of its mRNA repression function. A) Schematic representation of a luciferase-3'UTR reporter assay. TRIM71-mediated 3'UTR repression results in the repression of the Renilla (Ren) Luciferase reporter. **B)** Luciferase-3'UTR reporter assay showing the repression of the full length human CDKN1A 3'UTR reporter mediated by the indicated TRIM71 constructs (n=4). **C)** Repression strength of the indicated TRIM71 constructs for the repression of the human CDKN1A 3'UTR, calculated from data depicted in B, as the ratio between Norm. RLU Flag-Ctrl and Norm. RLU Flag-TRIM71-Construct-X values. Norm. RLU = Normalized Relative Light Units. All graphs represent mean ± SD. Statistical significance was calculated with an unpaired two-tailed Student's t-test (ns = non-significant; *P-value < 0.05; **P-value < 0.01; ***P-value < 0.005).

Collectively, these data suggested that the E3 ligase function of TRIM71 is required for its phosphorylation to occur, and that such phosphorylated status, although not entirely required for its mRNA repression role, seems to serve TRIM71 for the optimization or fine-tuning of such a role, in order to reach maximal target repression. Further aspects of TRIM71-mediated mRNA regulation will be thoroughly described in the following chapter.

4.2. Chapter II: TRIM71-mediated mRNA regulation

4.2.1. TRIM71 downregulates the expression of the cell cycle inhibitor and tumor suppressor CDKN1A/p21, and promotes proliferation in HEK293 and HepG2 cancer cells.

TRIM71 is a stem cell-specific factor whose expression is restricted to early developmental stages. Thereby, TRIM71 expression is mostly absent in healthy adults, with exception of its expression in brain stem cells, spermatogonia, and to a lesser extent, in skin stem cells[105,106,148]. However, the expression of TRIM71 is reactivated upon oncogenic transformation in some instances, being presumably confined to cancer stem cells (CSCs), and correlated with advanced stages and poor prognosis in several human cancers[107,108]. Therefore, TRIM71 is considered to act as an oncogene or tumor promoter, although an independent study reported its role as a tumor suppressor in non-small cell lung cancer (NSCLC)[141].

In order to have a broad idea in which cancer types could TRIM71 play an oncogenic role, we first used the R2 platform for genomics analysis and visualization (http://r2.amc.nl/), which provides an interface to high throughput data derived from RNA sequencing. We interrogated several cancer datasets for TRIM71 expression and found TRIM71 to be upregulated in several tumor types compared to their paired normal/healthy tissue samples (Fig. 4.2.1A). TRIM71 upregulation in hepatocellular carcinoma (HCC), acute myeloid leukaemia (AML) and high-risk neuroblastoma, was consistently observed in several datasets, while TRIM71 upregulation in colorectal cancer was only observed for the specified dataset, being unaltered in others (data not shown). Furthermore, TRIM71 upregulation in kidney cancer or brain cancer was specific for the subtypes Wilms carcinoma and paediatric ependymoma, respectively. As a second source, we used the GEPIA server (http://gepia.cancer-pku.cn/), which provides information about the expression of a gene of interest across different TGCA cancer datasets. Again, we found TRIM71 to be upregulated in several cancer types (Fig. 4.2.1B), including hepatocellular carcinoma (LIHC), acute myeloid leukemia (AML) and colorectal cancer (READ), as already shown by the R2 database, as well as in skin melanoma (SKCM), ovarian carcinoma (OV), uterus carcinoma (UCS) and testicular germ cell tumors (TGCT).

These data collectively showed an upregulation of TRIM71 in several human cancers, revealing a possible oncogenic contribution of TRIM71 expression to the pathogenesis. Interestingly, TRIM71 upregulation in the aforementioned cancer types was observed, not only in the specific tissues where TRIM71 expression occurs naturally (skin, brain and gonads), but also in tissues where TRIM71 is normally absent in a healthy adult (liver, immune system).

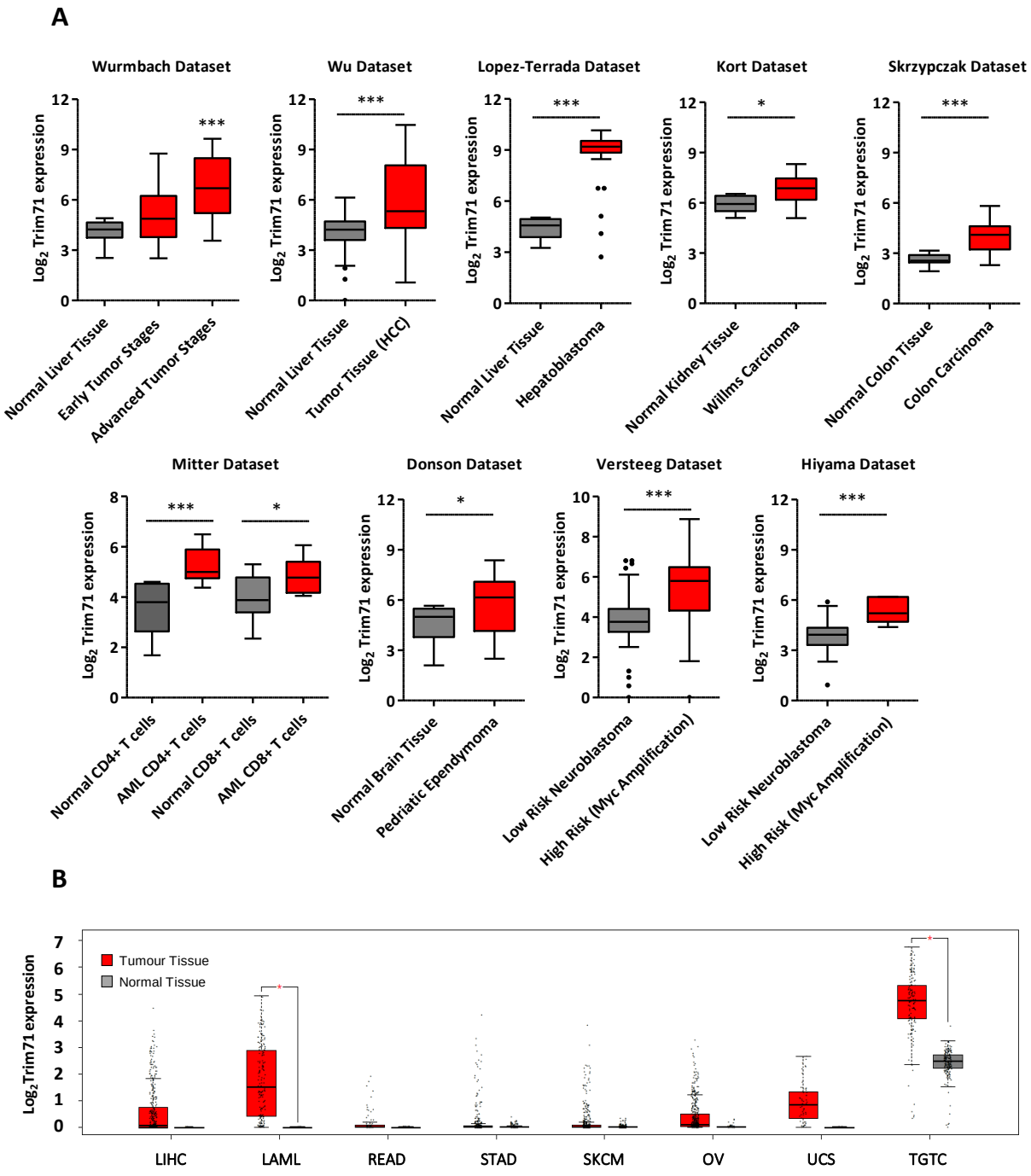

Figure 4.2.1. TRIM71 is upregulated in several human cancers. A) Upregulation of TRIM71 is various human cancers according to data from the R2 Genomics Analysis and Visualization Platform (http://r2.amc.nl). The name/ID of the dataset employed to produce each graph is indicated on top of the respective graph. Graphs are depicted as Tukey Box-Plots. Statistical significance was calculated with an unpaired two-tailed Student's t-test (*P-value < 0.05; ***P-value < 0.005). **B)** Upregulation of TRIM71 in various human cancers according to the GEPIA Server (http://gepia.cancer-pku.cn/). LIHC = Liver hepatocellular carcinoma (also commonly abbreviated as HCC). LAML = Acute Myeloid Leukemia. READ = Rectum adenocarcinoma. STAD = Stomach adenocarcinoma. SKCM = Skin Cutaneous Melanoma. OV = Ovarian Serous Cystadenocarcinoma. UCS = Uterine Carcinosarcoma. TGCT = Testicular Germ Cell Tumors (cancer names according to GEPIA's nomenclature). Of note, the GEPIA server does not provide the raw data used to depict the graphs, but instead builds the graphs with their statistics by itself. (Fig. adapted from[149]).

To confirm to some extent these *in silico*-obtained data, we measured TRIM71 mRNA levels in different representative cancer cell lines, and compared them with its expression in mESCs as TRIM71 natural expression niche. Because the expression of typically-used housekeeping genes may vary among different cell lines, we first converted the same RNA amount for each cell line to cDNA and measured the variability of the qPCR Threshold Cycle values (Ct) of several housekeeping genes (Fig. 4.2.2A). HPRT1 was the housekeeping gene showing less fluctuations among the different cell lines tested, and was therefore used for normalization. In line with the information obtained from the R2 and GEPIA servers, a high TRIM71 expression was detected in HepG2 (hepatocellular carcinoma cell line), NCCIT (testicular germ cell tumor cell line), and SKNBE (neuroblastoma cell line), whereas other evaluated cancer cell lines such as A546 (lung cancer cell line), LCNAP and PC3 (prostate cancer cell lines) or MCF7 (breast cancer cell line) showed low or undetectable TRIM71 expression (Fig. 4.2.2B). Depicting TRIM71 Ct values in the different cell lines tested showed that the choice of HPRT1 as housekeeping gene had been adequate, since TRIM71 expression values after HPRT1 normalization (Fig. 4.2.2B) nicely represented the changes in TRIM71 Ct values observed among the different cancer cell lines (Fig. 4.2.2C).

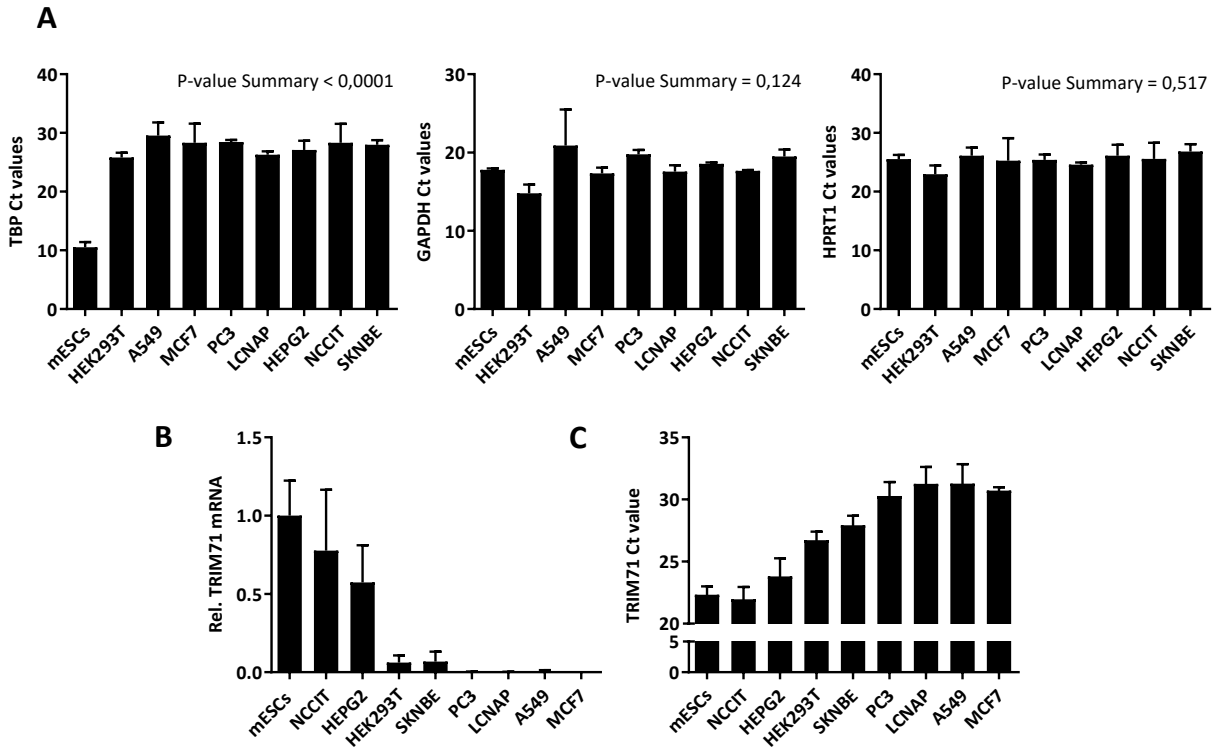

Figure 4.2.2. Comparison of TRIM71 expression in several human cancer cell lines. A) Measurements of three typically used housekeeping genes Ct values by qPCR and calculation of data variability among the samples with a one-way ANOVA test. **B)** Relative TRIM71 mRNA expression quantified by qPCR in different cancer cell lines using HPRT1 as housekeeping gene for normalization. **C)** TRIM71 Ct values measured by qPCR in different cancer cell lines. All graphs represent mean ± SD. mESCs = mouse embryonic stem cells (natural niche of TRIM71 healthy expression); HEK293T = Kidney cancer; A459 = Lung cancer; MCF7 = Breast cancer; PC3 and LCNAP = Prostate cancer; HepG2 = Liver cancer (hepatocellular carcinoma); NCCIT = Testicular germ cell tumors (non-seminoma subtype); SKNBE = Neuroblastoma. Cell lines in B and C are depicted in decreasing order of TRIM71 expression.

Given the lack of TRIM71 expression in the normal liver tissue, we considered the activation of TRIM71 expression in HCC an interesting phenomenon and decided to continue investigating the implications of TRIM71 in this pathogenesis. Consistent with its observed upregulation in HCC patients, TRIM71 was shown to promote proliferation *in vitro* of several HCC cell lines as well as liver cancer progression *in vivo* in mouse xenograft models[107]. The authors of that work proposed that TRIM71 controls tumorigenesis though its E3 ligase role via AGO2 protein destabilization, a mechanism that was postulated in an earlier work[105]. However, later studies were not able to confirm the existence of such a mechanism[41,106,113,115]. Accordingly, we did not observe changes in AGO2 protein stability following TRIM71 alteration in various cell lines, including TRIM71 overexpression in HEK293T cells (Fig. 4.2.3A), TRIM71 knockdown in the TGCT cell lines NCCIT (Fig. 4.2.3B) and TCam-2 (Fig. 4.2.3C), TRIM71 knockdown in the HCC cell line HepG2 (Fig. 4.2.3D), and TRIM71 knockout in mESCs (Fig. 4.2.3E).

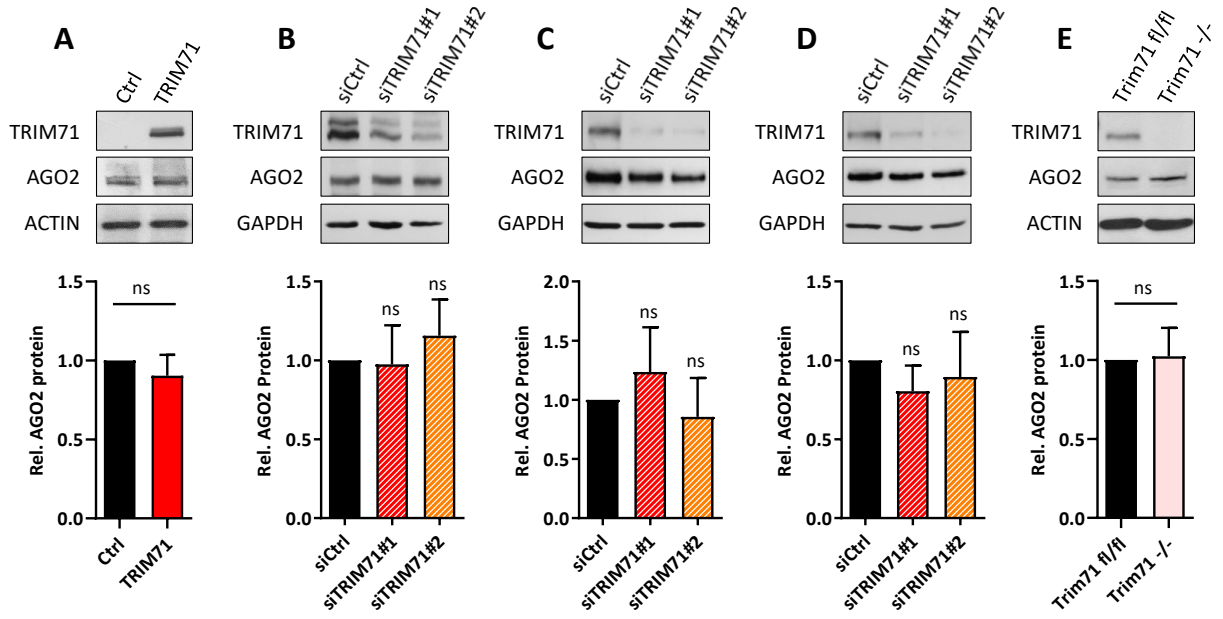

Figure 4.2.3. TRIM71 does not regulate AGO2 protein stability. Representative immunoblots showing AGO2 protein levels (up) and AGO2 band densitometry quantification (down) in **A)** TRIM71-overexpressing HEK293T cells (already shown in chapter I), **B)** TRIM71 knockdown NCCIT cells, **C)** TRIM71 knockdown TCam-2 cells, **D)** TRIM71 knockdown HepG2 cells and **C)** Trim71 knockout mESCs. For TRIM71 overexpression, several tags (Ig-tag, Flag-tag and GFP-tag) were used to exclude possible inhibitory effects of the tag in TRIM71 E3 ligase activity. For TRIM71 knockdown, two different siRNAs were used to exclude possible off-target effects that may somehow impact AGO2 stability. All graphs represent Mean ± SD. Quantifications were done for several replicates of the representative blots depicted above each respective graph (n=3-4). Statistical significance was calculated with a two-tailed unpaired Student's t-test (ns = non-significant). (Fig. adapted from[149]).

In a previous work, TRIM71 was shown to repress the expression of the mRNA encoding the cell cycle inhibitor and tumor suppressor CDKN1A/p21 in mESCs and EC cells[41]. Interestingly, according to the R2 database, the increased TRIM71 expression observed in patients with advanced HCC stages (Fig. 4.2.4A) negatively correlates with CDKN1A expression – while positively correlates with AGO2 expression – in HCC patient samples (Fig. 4.2.4B-C).

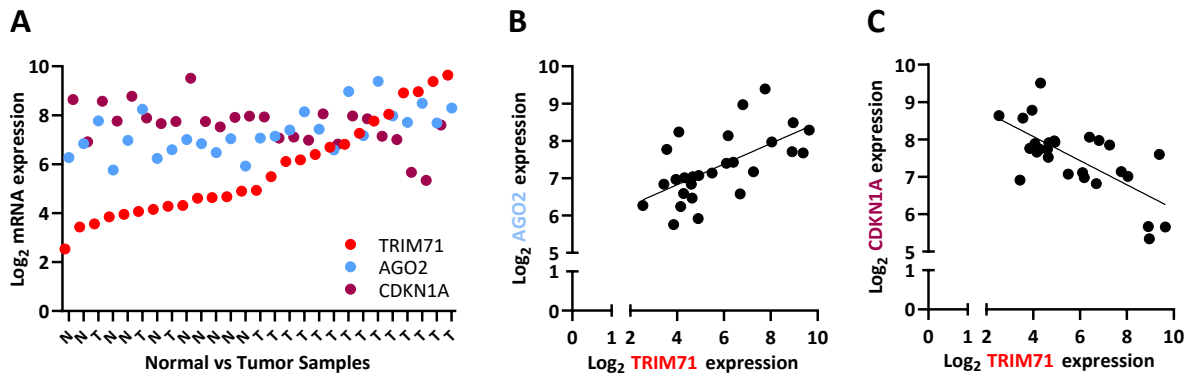

Figure 4.2.4. TRIM71 mRNA expression correlation with CDKN1A and AGO2 in HCC patients. A) mRNA expression of TRIM71, AGO2 and CDKN1A in samples from control patients (Normal tissue) and advanced-stage HCC patients (Tumor) depicted in increasing order of TRIM71 expression (n=27). **B)** Positive correlation between TRIM71 and AGO2 mRNA expression in samples from A (Pearson correlation coefficient r = +0,62; P-value = 0,0006). **B)** Negative correlation between TRIM71 and CDKN1A mRNA expression in samples from A (Pearson correlation coefficient r = -0,69; P-value = 0,0034). (Source: R2 Genomics Analysis and Visualization Platform (http://r2.amc.nl), Wurmbach Dataset). (Fig. adapted from[149]).

In order to confirm this correlation and its involvement in HCC progression, we knocked down TRIM71 with two different siRNAs in HepG2 cells and measured CDKN1A mRNA levels, as well as the levels of its encoded protein, better known as p21. Efficient TRIM71 knockdown (Fig. 4.2.5A) resulted in CDKN1A mRNA and p21 protein significant increase (Fig. 4.2.5B-C). A low expression of CDKN1A/p21 is required in actively proliferating cells, while the upregulation of CDKN1A/p21 prolongs the G1 and G2 cell cycle phases resulting in a slower proliferation rate, and ultimately promotes cell cycle arrest upon induction of terminal differentiation[150]. To evaluate whether the observed TRIM71-mediated CDKN1A/p21 regulation had an impact on cell proliferation, we conducted *in vitro* proliferation assays in TRIM71 knockdown HepG2 cells. We therefore stained cells with the proliferation dye eFluor670 and monitored the loss of fluorescence intensity upon every cell division by FACS every 24 h for 4 days.

TRIM71 knockdown in HepG2 cells resulted in a decreased proliferation, as shown by a slower fluorescence loss (Fig. 4.2.5D), corresponding to a decreased number of cell divisions at the end of the experiment, as compared to control HepG2 cells (Fig. 4.2.5E-F). The differences observed in the number of cell divisions may appear mild, but should not be underestimated: control HepG2 cells divided 5,2 times in 4 days, being their average cell cycle duration of around 18,5 h; TRIM71 knockdown cells divided around 3,8 times (siTRIM71#1) and 4,2 times (siTRIM71#2) in the same period, which means that their cell cycle lasted 25,3 h and 22,5 h, respectively (Fig. 4.2.5G). A delay of 6,8h (siTRIM71#1) and 4,1h (siTRIM71#2) in a cell cycle of normally 18,5h (siCtrl) entails a 37,17% (siTRIM71#1) and 22,27% (siTRIM71#2) reduction of proliferation.

Conversely, stable overexpression of GFP-TRIM71 in HEK293 cells (Fig. 4.2.6A), naturally expressing low TRIM71 levels (see again Fig. 4.2.2B), resulted in decreased CDKN1A mRNA levels and p21 protein levels (Fig. 4.2.6B-C), and an enhanced proliferation (up to a 15%) as compared to GFP-overexpressing control HEK293 cells (Fig. 4.2.6D-G). Such TRIM71-induced changes in cell proliferation rates may have severe consequences during developmental and oncogenic processes.

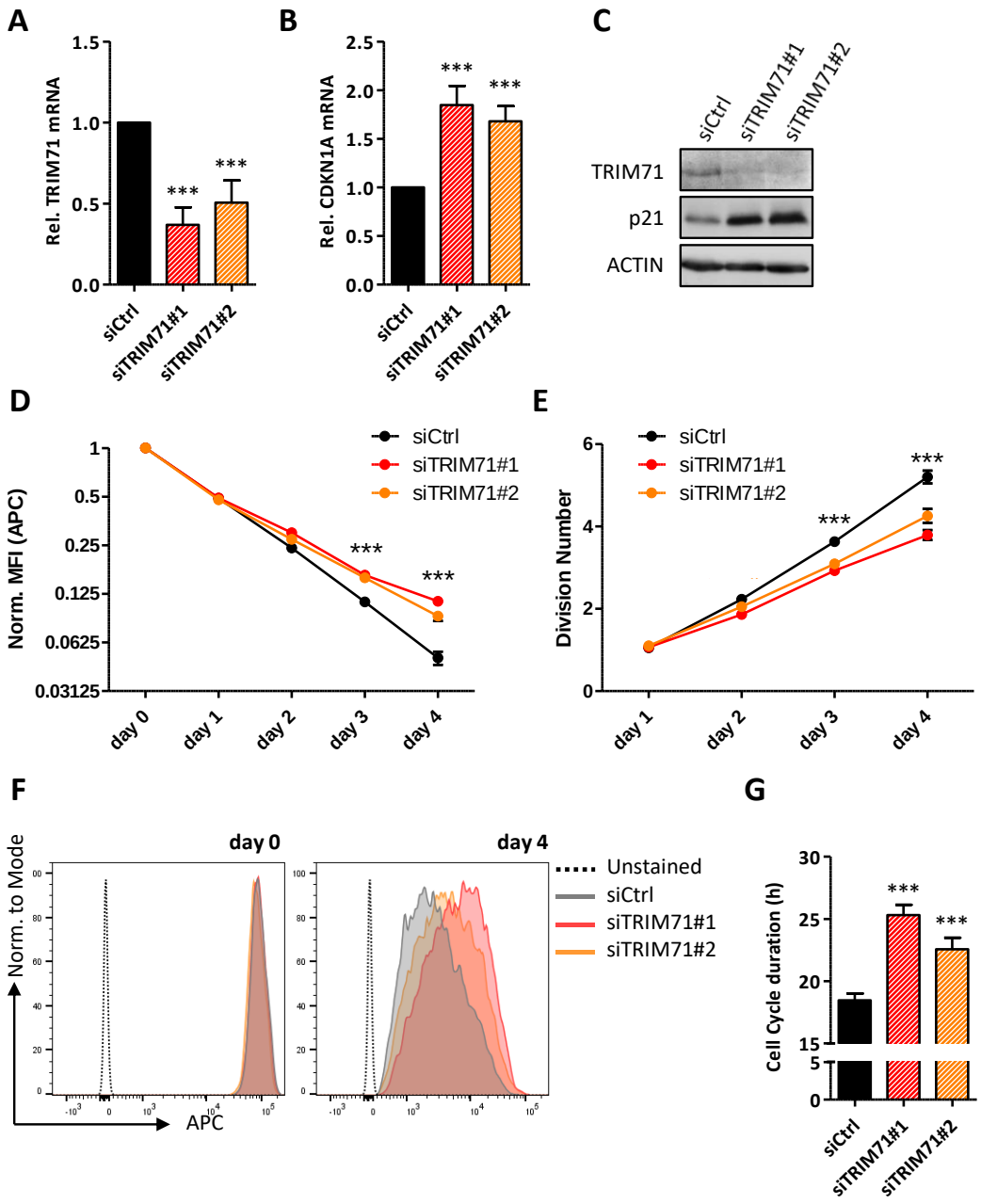

Figure 4.2.5. TRIM71 regulates CDKN1A/p21 and controls proliferation of HepG2 cells. A) TRIM71 and **B)** CDKN1A mRNA levels measured by qPCR in control (siCtrl) and TRIM71 knockdown (siTRIM71#1 and #2) HepG2 cells 72 hpt. HPRT1 housekeeping gene was use for normalization (n=6). **C)** Representative immunoblot showing TRIM71 and p21 protein levels in HepG2 cells upon TRIM71 knockdown, corresponding to mRNA levels from A and B. **D)** Progressive loss of fluorescence intensity overtime of the dye eFluor670 as a result of cell proliferation in control and TRIM71 knockdown HepG2 cells. MFI = Median Fluorescence Intensity of APC (eFluo670). **E)** Number of cell divisions undergone overtime by Control and TRIM71 knockdown HepG2 cells, calculated as Log_2 (MFI_{day0} - $MFI_{unstained}$) / (MFI_{dayX} - $MFI_{unstained}$). **F)** Overlap of APC (eFluo670) histograms of control and TRIM71 knockdown HepG2 cell populations, showing comparable staining for the different populations at the beginning of the proliferation assay (left panel: day 0, 24 hpt), and the retardation of TRIM71 knockdown histograms as result of a diminished proliferation at the end of the experiment (right panel: day 4, 120 hpt). **G)** Average cell cycle duration in hours (h) calculated for control and TRIM71 knockdown HepG2 cells from the number of cell divisions at the end of the proliferation assay (day 4). D-G show the results of one representative experiment out of four, each of them including three technical replicates. Graphs represent Mean ± SD. Statistical significance was calculated with a two-tailed unpaired Student's t-test (***P-value<0.005). (Fig. adapted from[149]).

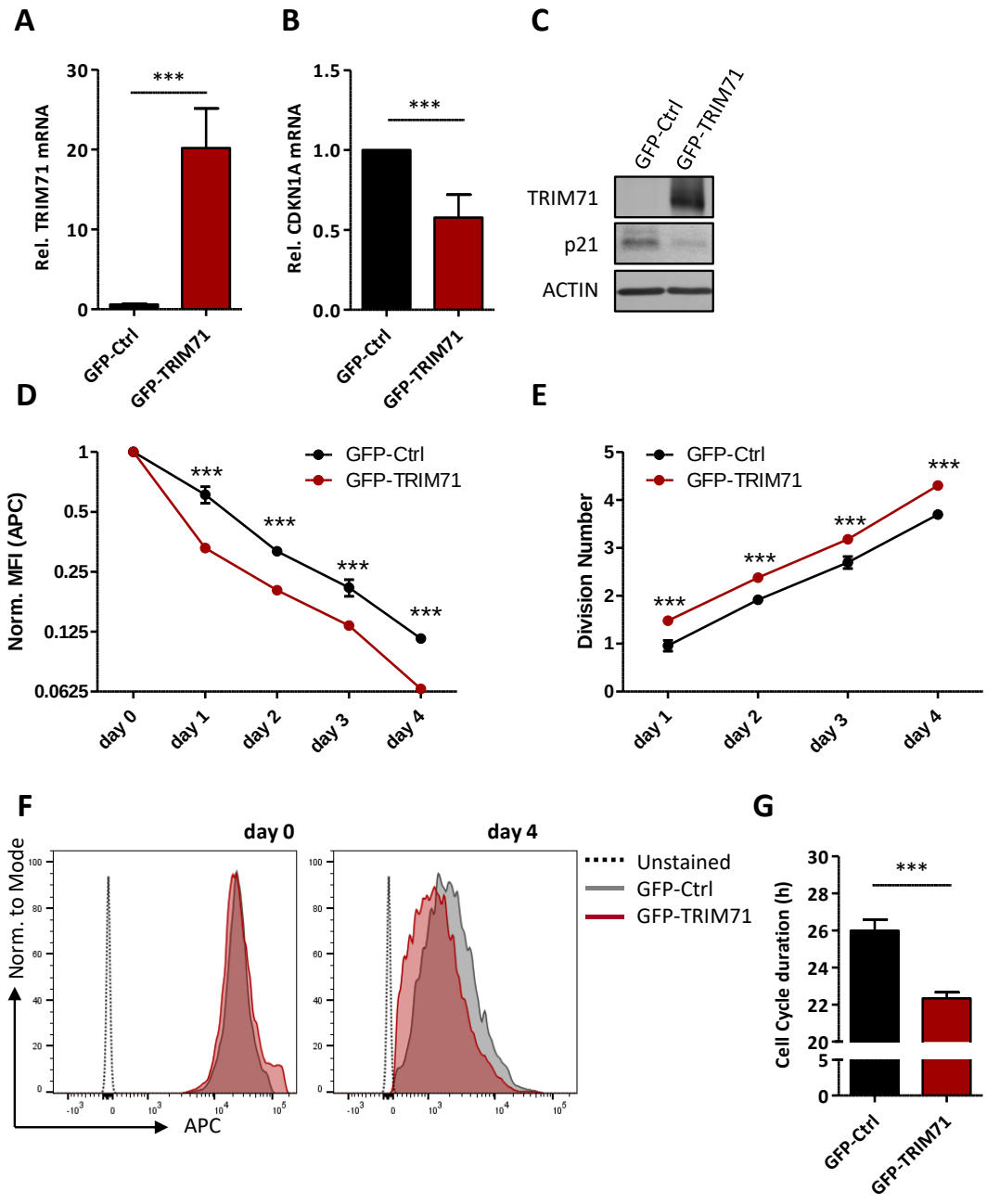

Figure 4.2.6. TRIM71 regulates CDKN1A/p21 and controls proliferation of HEK293 cells. A) TRIM71 and **B)** CDKN1A mRNA levels measured by qPCR in control (GFP) and TRIM71-overexpressing (GFP-TRIM71) stable HEK293 cells. HPRT1 housekeeping gene was use for normalization (n=4). **C)** Representative immunoblot showing TRIM71 and p21 protein levels in HEK293 cells upon stable TRIM71 overexpression, corresponding to mRNA levels from A-B. **D)** Progressive loss of fluorescence intensity overtime of the dye eFluor670 as a result of cell proliferation in control and TRIM71-overexpressing HEK293 cells. MFI = Median Fluorescence Intensity of APC (eFluo670). **E)** Number of cell divisions undergone overtime by control and TRIM71-overexpressing HEK293 cells, calculated as specified in Fig. 4.2.5E. **F)** Overlap of APC (eFluo670) histograms of control and TRIM71 overexpressing HEK293 cell populations, showing comparable staining for the different populations at the beginning of the proliferation assay (left panel: day 0), and the advanced GFP-TRIM71 histogram as result of an enhanced proliferation at the end of the experiment (right panel: day 4). **G)** Average cell cycle duration in hours (h) calculated for control and TRIM71-overexpressing HEK293 cells from the number of cell divisions at the end of the proliferation assay (day 4). D-G show the results of one representative experiment out of three, each of them including three technical replicates. Graphs represent Mean ± SD. Statistical significance was calculated with a two-tailed unpaired Student's t-test (*P-value < 0.05; **P-value < 0.01; ***P-value < 0.005). (Fig. adapted from[149]).

4.2.2. TRIM71 directly and specifically interacts with the 3'UTR of CDKN1A mRNA, and represses its expression post-transcriptionally via mRNA degradation

TRIM71-mediated CDKN1A regulation was first reported in ES and EC cells[41]. Our results show such a regulation to occur both, upon TRIM71 knockdown in HepG2 cells and upon ectopic TRIM71 expression in HEK293 cells, resulting in decreased or enhanced cell proliferation, respectively. Any alteration in the control of cell cycle progression driven by TRIM71 may be of patho-physiological relevance during developmental disorders and oncogenic transformation. This prompted us to continue investigating in detail the molecular mechanisms underlying TRIM71-mediated CDKN1A regulation.

The regulation of CDKN1A/p21 exerted by TRIM71 in HepG2 and HEK293 cells was observable already at mRNA levels, indicating that TRIM71 affects CDKN1A mRNA expression either transcriptionally – indirectly – or post-transcriptionally – via its mRNA repression role –, leading to altered p21 protein levels as a consequence. However, since TRIM71 is not only an mRNA repressor, but also an E3 ligase, we next investigated whether the changes observed in p21 protein levels could partially result from post-translational protein destabilization via TRIM71-mediated ubiquitylation.

Ubiquitylated proteins can be degraded by either the proteasome or the autophagy machinery. Therefore, HEK293 cells stably overexpressing GFP or GFP-TRIM71 were treated with either MG132 for proteasomal inhibition or Bafilomycin A1 for autophagy inhibition, and the levels of p21 were measured to evaluate its accumulation in the presence or absence of TRIM71. MG132 treatment resulted in a dramatic p21 accumulation compared to the DMSO control treatment, indicating that in these cells, p21 is mostly subjected to proteasomal degradation (Fig. 4.2.7A). However, despite the MG132 treatment, p21 levels remained downregulated in TRIM71-overexpressing HEK293 cells relative to GFP-Ctrl cells, as shown by the quantified p21 protein ratios (Fig. 4.2.7B).

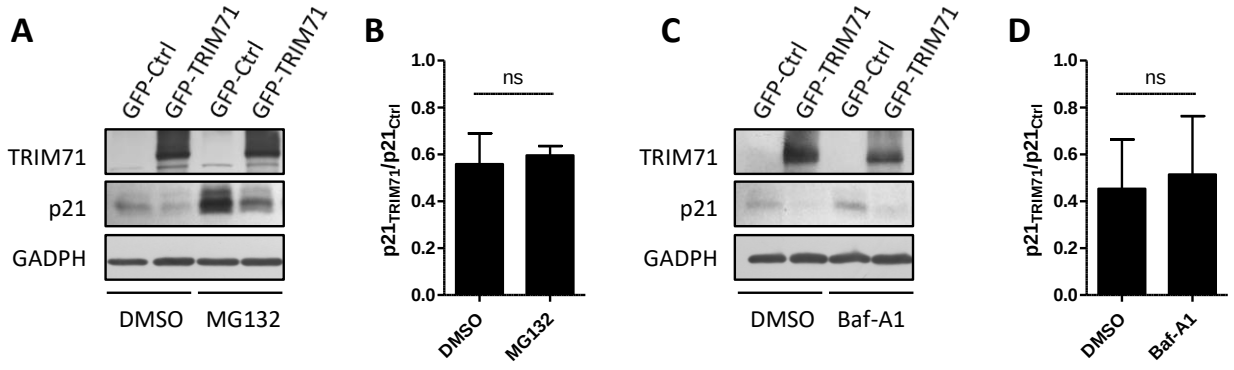

Figure 4.2.7. TRIM71 does not regulate p21 post-translationally via its E3 ligase function. A) Representative immunoblot of whole cell lysates from HEK293 cells stably overexpressing GFP-Ctrl or GFP-TRIM71, showing the expression of p21 upon treatment with DMSO as a control, or with 25 μM of the proteasome inhibitor MG132. **B)** Quantification of TRIM71-mediated p21 repression, depicted as the ratio between p21 amounts in GFP-TRIM71 and GFP-Ctrl HEK293 cells. For each condition, the p21 band densitometry was quantified and normalized to that of the respective GAPDH band, used as loading control. **C)** Representative immunoblot of whole cell lysates from HEK293 cells stably overexpressing GFP-Ctrl or GFP-TRIM71, showing the expression of p21 upon treatment with DMSO as a control, or with 200 nM of the autophagy inhibitor Bafilomycin A1. **D)** Quantification of TRIM71-mediated p21 repression, depicted as specified in B. Graphs represent Mean ± SD (n=3). Statistical significance was calculated with a two-tailed unpaired Student's t-test (ns = non-significant).

A mild p21 accumulation was observed upon Bafilomycin A1 treatment, revealing a moderate autophagic contribution to the regulation of p21 turnover (Fig. 4.2.7C). However, similar to what we had observed for the MG132 treatment, the downregulation of p21 exerted by TRIM71 was not relieved upon Bafilomycin A1 treatment (Fig. 4.2.7D). Collectively, these results showed a TRIM71-independent regulation of p21 protein stability via proteasomal and autophagic mechanisms, thereby proving that TRIM71 does not regulate p21 post-translationally via its E3 ligase function.

We next investigated whether TRIM71 could regulate CDKN1A mRNA post-transcriptionally. Five different transcript variants have been described for the human CDKN1A gene (NCBI ID: 1026), all of which share most of the coding sequence (CDS) and 3'UTR but differ in their 5'UTR. We then cloned the CDS and the full length 3'UTR separately into two different luciferase reporter plasmids, and evaluated whether TRIM71 repressed their expression in HEK293T cells. Transient TRIM71 overexpression led to reduced endogenous CDKN1A mRNA levels (Fig. 4.2.8A), as well as reduced luciferase activity of the full length CDKN1A 3'UTR reporter (as already shown in Chapter I), whereas no changes were observed for the CDS reporter (Fig 4.2.8B-C). These results demonstrated that TRIM71 post-transcriptionally regulates CDKN1A mRNA expression via 3'UTR recognition followed by mRNA degradation.

We then further investigated whether TRIM71 could physically interact with CDKN1A mRNA. To this end, we overexpressed either TRIM71, a TRIM71 mutant lacking the last NHL repeat (ΔNHL6), which was found to phenocopy the total loss of TRIM71 expression during murine development[110], or the pro-differentiation TRIM-NHL protein TRIM32[94] in HEK293T cells (Fig. 4.2.8D), and conducted RNA-IPs.

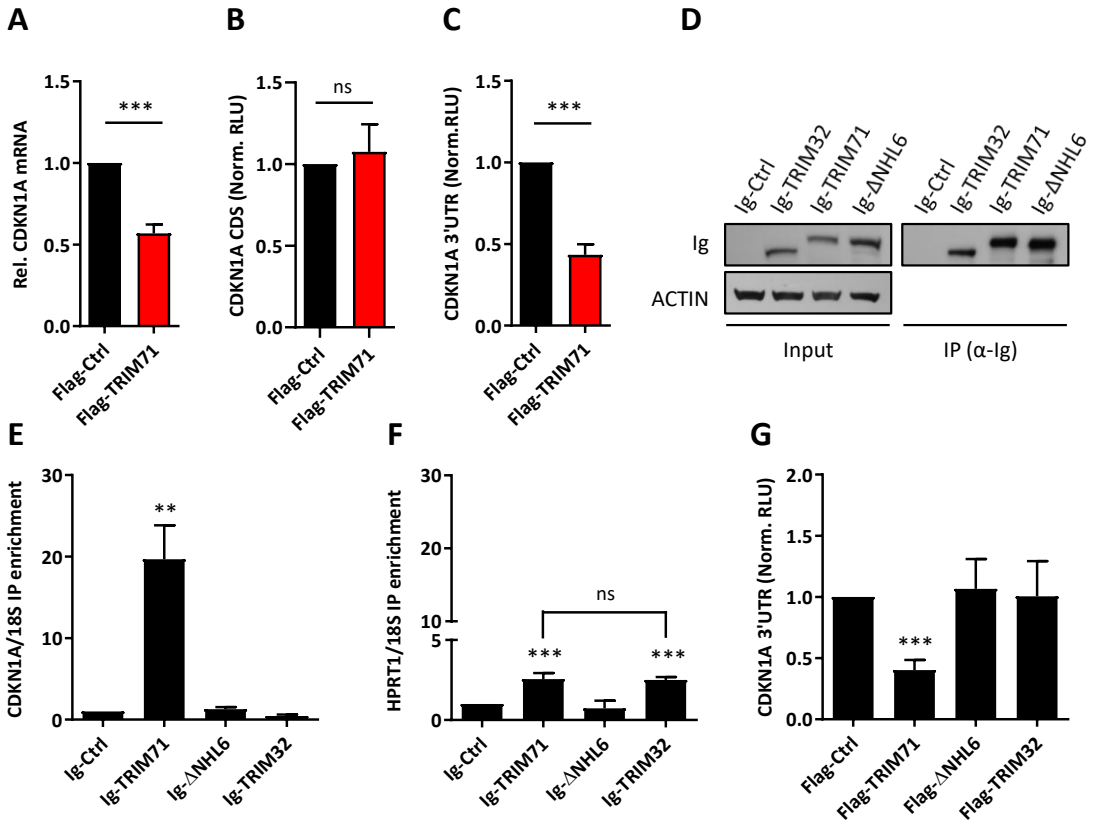

Figure 4.2.8. TRIM71 physically and specifically interacts with CDKN1A mRNA, and represses its expression through the recognition of its 3'UTR. A) CDKN1A mRNA levels measured by qPCR in HEK293T cells transiently transfected with Flag or Flag-TRIM71. (n=5). HPRT1 housekeeping gene was used for normalization. **B)** Repression of a luciferase reporter under the control of the human CDKN1A CDS in HEK293T cells transiently transfected with Flag or Flag-TRIM71 (n=7). **C)** Repression of a luciferase reporter under the control of the full length human CDKN1A 3'UTR in HEK293T cells transiently transfected with Flag or Flag-TRIM71 (n=7). **D)** Representative immunoblot showing levels of Ig-Ctrl/Ig-TRIM32/Ig-TRIM71/Ig-ΔNHL6 overexpression in total lysates (input) and pull down fractions (IP) after RNA-IPs. **E)** CDKN1A mRNA IP enrichment and **F)** HPRT1 mRNA IP enrichment after RNA-IPs in HEK293T cells transiently transfected with Ig-Ctrl/Ig-TRIM32/Ig-TRIM71/Ig-ΔNHL6 (n=4). Quantifications of specific mRNAs were performed by qPCR and IP enrichment was calculated as $2^{-((IP_{target}-IP_{ref})-(INPUT_{target}-INPUT_{ref}))}$, where 18S rRNA was used as a reference (ref) for normalization. **G)** Repression of the full length CDKN1A 3'UTR luciferase reporter in HEK293T cells transiently transfected with Ig-Ctrl/Ig-TRIM32/Ig-TRIM71/Ig-ΔNHL6 (n=3-4). Norm. RLU = Normalized Relative Light Units. All graphs represent Mean ± SEM. Statistical significance was calculated with a two-tailed unpaired Student's t-test (ns = non-significant; *P-value < 0.05; **P-value < 0.01; ***P-value < 0.005). (Fig. adapted from[149]).

TRIM71 pull down fractions showed a specific CDKN1A mRNA IP enrichment of 20-fold over the control pull down fraction (Ig-Ctrl), after normalization to the unspecific IP enrichment of the 18S rRNA (Fig. 4.2.8E). A mild (2-fold) HPRT1 IP enrichment was observed for both TRIM71 and TRIM32 pull down fractions (Fig. 4.2.8F), indicating that both TRIM-NHL proteins have a similar ability to unspecifically bind RNA, and thereby highlighting the target specificity of TRIM71 for CDKN1A mRNA. Interestingly, the deletion of the last NHL repeat totally abrogated mRNA binding (Fig. 4.2.8E-F). Consistent with the CDKN1A mRNA binding ability of the different constructs, only TRIM71 – but neither TRIM32 nor ΔNHL6 – was able to repress the 3'UTR of CDKN1A (Fig. 4.2.8G). The differences observed in 3'UTR repression were not attributable to different transfection efficiencies, since WB analysis showed that all constructs were expressed in similar levels[149] (data not shown). Altogether, our findings showed that TRIM71 is able to physically and specifically interact with CDKN1A mRNA, and that this interaction – and consequently CDKN1A 3'UTR repression – relies on an intact NHL domain.

Agreeing with these results, a previous study showed that TRIM71-mediated Cdkn1a repression in mESCs occurred via 3'UTR recognition[41]. Such repression was proposed to be assisted by miRNAs, since TRIM71 repressed a 59-bp fragment of the mouse Cdkn1a 3'UTR containing a binding site for the ES-specific miR-302[41]. Nevertheless, *in silico* prediction of conserved miRNA-binding sites (http://www.targetscan.org/) showed that the human CDKN1A 3'UTR lacks a site for miR-302 binding (Fig. 4.2.9). This prompted us to identify the responsive element(s) for TRIM71 in the human CDKN1A 3'UTR. To this end, we cloned the 3'UTR of CDKN1A in three consecutive 500-bp fragments (F1, F2 and F3, marked under the human CDKN1A 3'UTR in Fig. 4.2.9) and evaluated their repression by TRIM71, as compared to the repression of the full length (FL) 3'UTR. TRIM71 overexpression resulted in a significant repression of all three fragments, implying that several recognition sites for TRIM71 are present along the whole CDKN1A 3'UTR (Fig. 4.2.10A). However, F2 was more strongly repressed than F1 and F3 (Fig. 4.2.10B). Thus, we next cloned four new reporters by performing 100-bp serial deletions from the F2 3'end (F2_0-400, F2_0-300, F2_0-200 and F2_0-100), and compared their repression by TRIM71 to that of the full F2 (now called F2_0-500). TRIM71 significantly repressed the F2_0-400, F2_0-300, and F2_0-200 reporters, but not the F2_0-100 reporter (Fig. 4.2.10C), indicating that a responsive element for TRIM71 was located between 100-200 bp within the F2 fragment. Last, we cloned a reporter containing only the F2_100-200 region and confirmed its TRIM71-mediated repression (Fig. 4.2.10D).

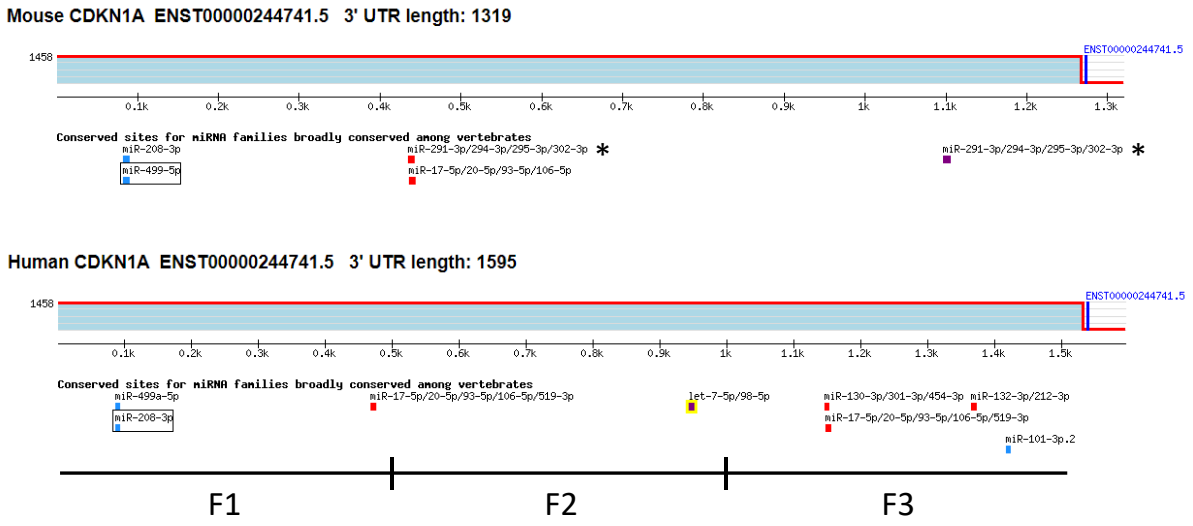

Figure 4.2.9. *In silico* prediction of conserved miRNA-binding sites in mouse and human CDKN1A 3'UTRs. Note that the two binding sites for miR-302 present in the mouse 3'UTR (up), marked with an asterisk (*), are absent in the human 3'UTR (down). Prediction was obtained from TargetScan (http://www.targetscan.org/). The human CDKN1A 3'UTR was cloned in three consecutive 500-bp independent fragments, marked as F1, F2 and F3 on the bottom of the figure. (Fig. adapted from[149]).

A recent study has identified the *C. elegans* LIN-41 (CeLIN41) responsive element (LRE) to be an RNA structural motif consisting of a stem-loop with specific nucleotides in conserved positions[85] (Fig. 4.2.11A). We therefore used the F2_100-200 sequence for *in silico* RNA secondary structure prediction and identified a candidate stem-loop structure in this region (Fig. 4.2.11B-C), which we termed as TRIM71 responsive element (TRE). We next cloned several F2_100-200 reporters containing distinct mutations within the TRE, and evaluated their repression by TRIM71 (Fig. 4.2.11D). Deletion of the TRE from F2_100-200 (M#1 ΔTRE) or mutations reported to disrupt the LRE structure[85] (M#3 G/C and M#4 A/C) completely abrogated TRIM71-mediated repression of the F2_100-200 reporter, whereas a predicted permissive mutation[85] (M#2 G/A) did not affect TRIM71-mediated F2_100-200 reporter repression (Fig. 4.2.11D).

The NHL domain of TRIM71 orthologue proteins Brat (*D. melanogaster*) and CeLIN41 are known mediate direct RNA interaction[83,84,126], and later Kumari *et al.,* proved the direct interaction of the FLN-NHL domains of CeLIN41 and *D. rerio* Lin41 (DrLIN41) with their reported LRE[85]. The FLN-NHL domains from zebrafish and human have a sequence similarity of 96%, with an 84% shared identity (data not shown). There are not even single aa inserts or gaps found in the alignment of these two domain sequences, indicating the importance of this protein over a large species diversity. Based on these similarities, we were able to model the human TRIM71 FLN-NHL domains structure alone (Fig. 4.2.12A) and in complex with the TRE identified in the CDKN1A 3'UTR F2_100-200 fragment (Fig. 4.2.12B-C). Importantly, all 14 residues identified in DrLIN41 NHL domain to interact with the LRE[85] are identical in the human TRIM71 protein. The β-propeller structure of the NHL domain forms a positively charged binding pocket, in which several residues (R608, R625, R655, K672, R720, R751, R796 and R814) are predicted to form electrostatic interactions with the negatively charged phosphate groups of the 3-mer RNA loop (I-III) and the succeeding A (+1) nucleotide of the first U-A stem pair (Fig. 4.2.12B-C).

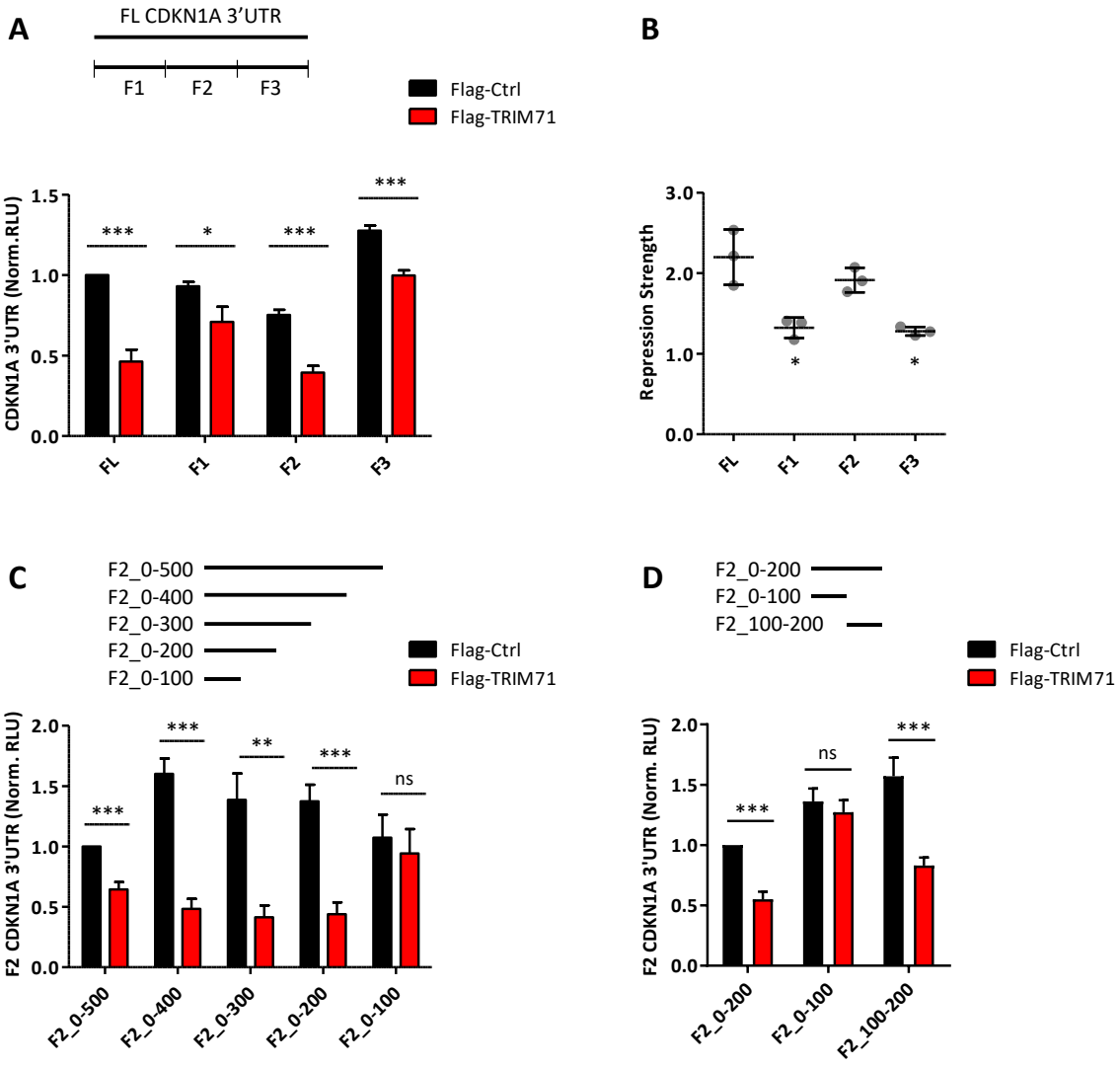

Figure 4.2.10. TRIM71 recognizes several responsive elements along the human CDKN1A 3'UTR. A) Repression of a luciferase reporter under the control of different CDKN1A 3'UTR fragments (depicted above the graph) in HEK293T cells transiently transfected with Flag or Flag-TRIM71. (n=3). FL = full length CDKN1A 3'UTR (1536 bp). F1 = Fragment 1 (507 bp), spanning from 1-507 bp within the FL 3'UTR. F2 = Fragment 2 (510 bp), spanning from 508-1017 bp within the FL 3'UTR. F3 = Fragment 3 (519 bp), spanning from 1018-1536 bp within the FL 3'UTR. **B)** TRIM71-mediated repression strength for the different CDKN1A 3'UTR fragments used in A, calculated from data depicted in A, as the ratio between Norm. RLU Flag-Ctrl and Norm. RLU Flag-TRIM71 values. **C)** Repression of a luciferase reporter under the control of different CDKN1A 3'UTR F2 fragments (depicted above the graph) in HEK293T cells transiently transfected with Flag or Flag-TRIM71 (n=4). F2_0-500 (510 bp) = F2 used A-B. F2_0-400 (401 bp), resulting from a 109 bp deletion from the 3' end of F2_0-500. F2_0-300 (292 bp), resulting from a 218 bp deletion from the 3' end of F2_0-500. F2_0-200 (214 bp), resulting from a 296 bp deletion from the 3' end of F2_0-500. F2_0-100 (106 bp), resulting from a 405 bp deletion from the 3' end of F2_0-500. **D)** Repression of a luciferase reporter under the control of different CDKN1A 3'UTR F2 fragments (depicted above the graph), namely F2_0-200, F2_0-100 (used in C) and F2_100-200 (n=4-5). Norm. RLU = Normalized Relative Light Units. All graphs represent Mean ± SD. Statistical significance was calculated with a two-tailed unpaired Student's t-test (ns = non-significant; *P-value < 0.05; **P-value < 0.005; ***P-value < 0.005). (Fig. adapted from[149]).

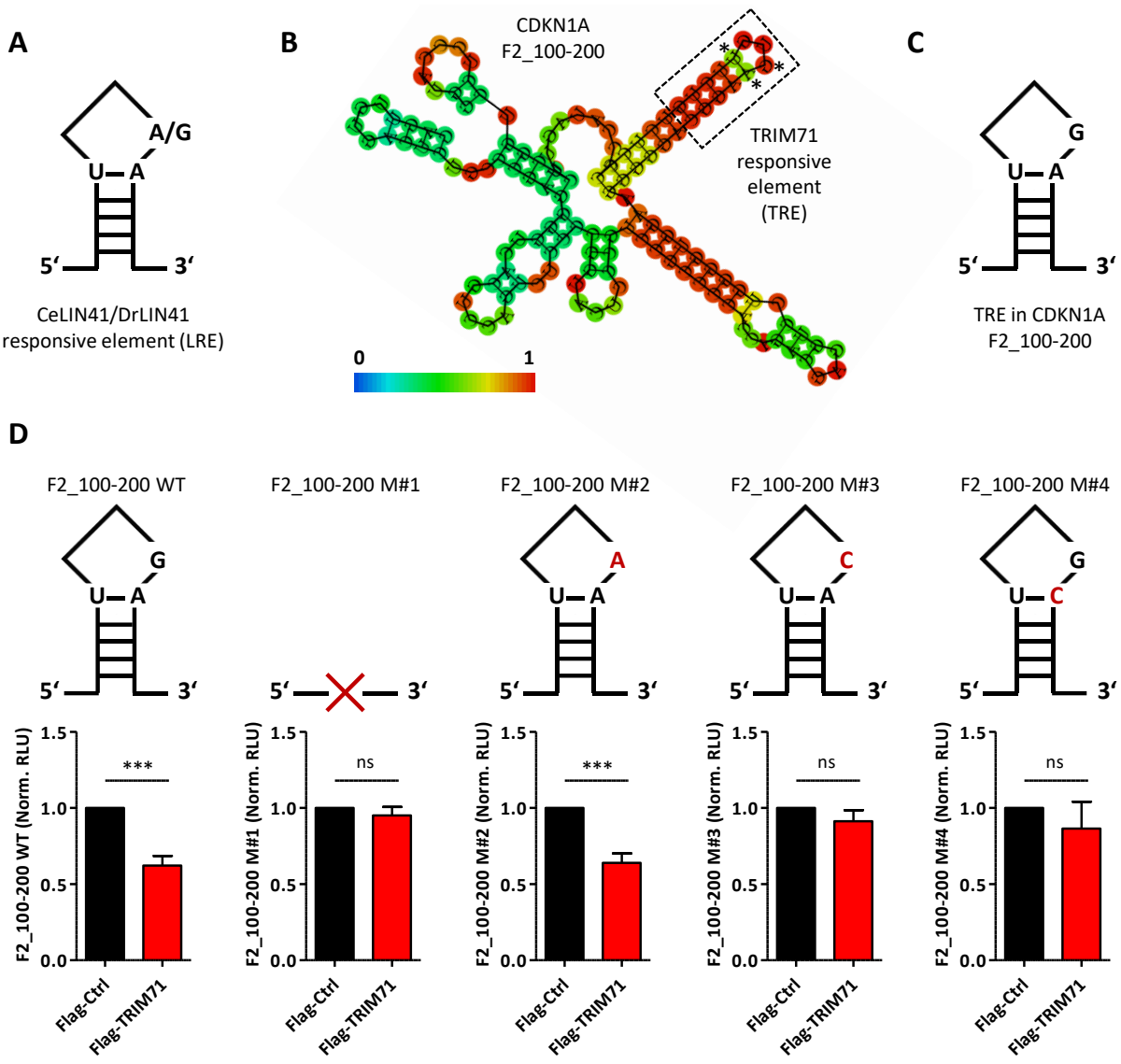

Figure 4.2.11. The TRIM71 responsive element (TRE) is a stem-3base-loop RNA motif located in the CDKN1A 3'UTR. A) Schematic representation of CeLIN41/DrLIN41 responsive element (LRE) identified in a previous study[85], consisting of a 13-mer stem-3base-loop RNA structure with specific nucleotides in conserved positions, namely A/G in loop position III, U in stem position -1 respective to the loop and A in stem position +1 respective to the loop, according to previous nomenclature[85]. **B)** *In silico* prediction of the secondary structure for the RNA sequence of the CDKN1A 3'UTR fragment F2_100-200 using RNAfold (http://rna.tbi.univie.ac.at/cgi-bin/RNAWebSuite/RNAfold.cgi) identified a LRE-like motif (TRE). TRE is enclosed by the dashed-line-box, in which the nucleotides in positions III, -1 and +1 have been marked with an asterisk (*). The color bar represents nucleotide position probability. **C)** Schematic representation of the TRE identified in B. **D)** TRIM71-mediated repression of several F2_100-200 reporters containing TRE mutations, as depicted in red by schematic drawings on top of each graph. Mutant 1 (M#1) = 13-mer TRE deleted; Mutant 2 (M#2) = permissive G/A mutation; Mutant 3 (M#3) = disruptive G/C mutation; Mutant 4 (M#4) = disruptive A/C mutation. Norm. RLU = Normalized Relative Light Units. All graphs represent Mean ± SEM (n=3). Statistical significance was calculated with a two-tailed unpaired Student's t-test (ns = non-significant; ***P-value < 0.005). (Fig. adapted from[149]).

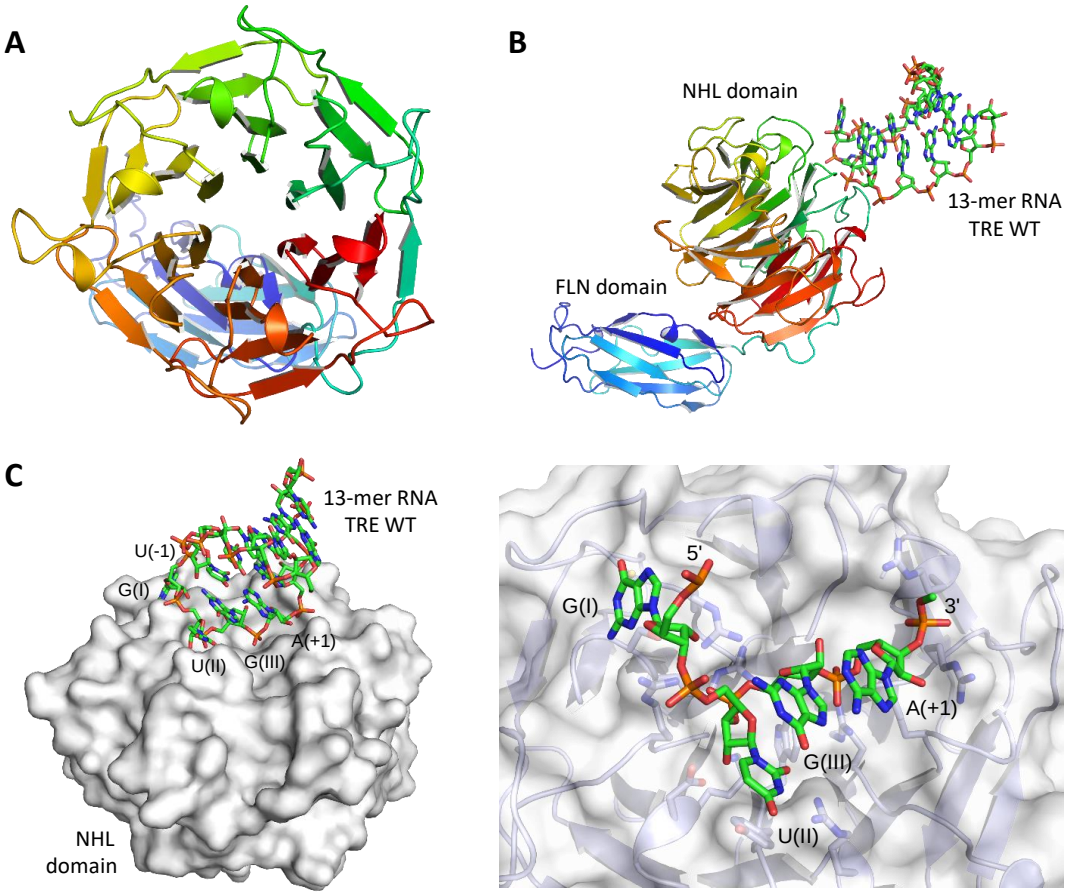

Figure 4.2.12. Structural modeling of the human TRIM71 FLN-NHL domains in complex with the TRE identified in CDKN1A 3'UTR. A) Top view of the model for the human TRIM71 NHL domain with the FLN domain underneeth. **B)** Side view of the model for the human TRIM71 FLN-NHL domains in complex with the 13-mer stem-3base-loop RNA motif identified as TRIM71 responsive element (TRE). The models in A and B are shown in cartoon representation. **C)** Side (left) and top (right) views for the model of the human TRIM71 NHL domain in complex with the TRE. The NHL protein is shown as surface display and the RNA in stick representation. Direct contacts of the protein are mediated to the three nucleotides of the loop region G(I), U (II) and G(III), and the succeeding stem nucleotide A(+1). A positively charged binding pocket accommodates the phosphate backbone groups of the loop region. Structural modeling was performed for residues 479-868 using Swiss-Model (https://swissmodel.expasy.org) based on the LIN41 crystal structure 6FQ3 which was previously determined at 1.9 Å resolution[85]. (Fig. adapted from[149]).

Based on the similarities between the human TRIM71 NHL domain structure and that of CeLIN41 and DrLIN41 NHL domains, as well as on the conservation of the interacting nucleotides in LRE and TRE, we predicted that the human TRIM71 NHL domain could directly interact with the TRE identified in the CDKN1A 3'UTR F2_100-200 fragment. Furthermore, according to our structural modeling, the FLN domain does not seem to play a role in the predicted interaction. We therefore aimed at confirming the direct interaction between the human TRIM71 NHL domain and the TRE by biochemical assays with purified components. To this end, we purified the human Flag-tagged TRIM71 NHL domain (without including the FLN domain) via recombinant vaccinia virus-driven protein production in CV1 cells (Fig. 4.2.13A), and evaluated its binding ability to 5'Cy3-labelled 13-mer ssRNAs (TRE WT and TRE M#3 (Fig. 4.2.13B)) via

fluorescence polarization assays. The human Flag-TRIM71-NHL recombinant protein robustly bound the TRE WT RNA, but not the TRE M#3 (Fig. 4.2.13C-D), consistent with our previous luciferase assays showing that TRIM71-mediated repression was abrogated by the G/C (III) mutation (M#3). The binding constant for the interaction between the Flag-TRIM71-NHL recombinant protein and the TRE WT RNA stem-loop U(-1)-G(I)-U(II)-G(III)-A(+1) (K_D: 0.925 µM) was similar to the affinity previously determined for the interaction between CeLIN41 and the LRE stem loop U(-1)-C(I)-C(II)-A(III)-A(+1) (K_D: 1.322 µM)[85].

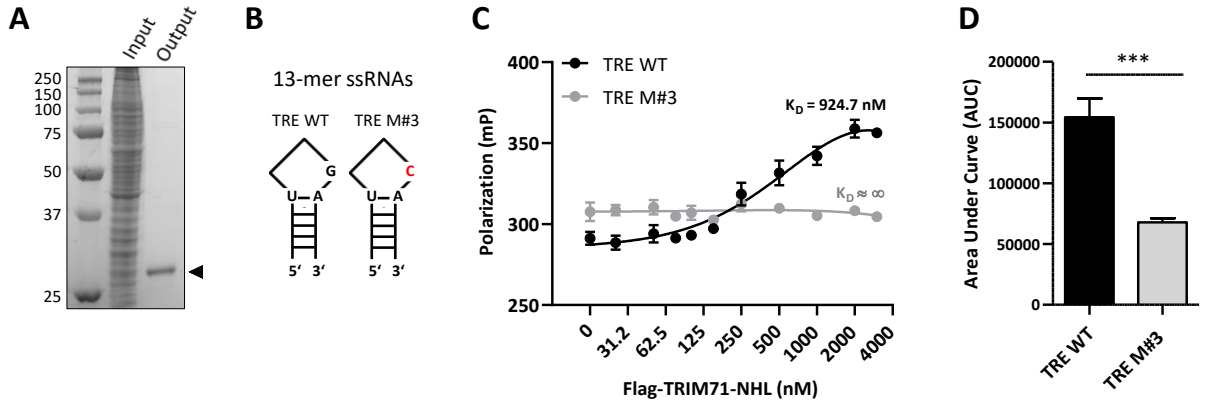

Figure 4.2.13. TRIM71 directly interacts via its NHL domain with the TRE identified in CDKN1A 3'UTR. A) Coomassie staining of a 12% PAGE-SDS gel loaded with the whole cell lysate (input) and the α-Flag IP fraction (output) of CV1 cells expressing human Flag-TRIM71-NHL recombinant protein (33 kDa). **B)** Schematic representation of the 5'-Cy3-labelled 13-mer ssRNAs used for experiments depicted in C-D. **C)** Fluorescence polarization assay showing the binding-saturation curves and equilibrium dissociation constants (K_D) for the interaction between purified human Flag-TRIM71-NHL recombinant protein and two synthetized 13-mer ssRNAs (depicted in B), namely TRE WT and TRE M#3 (n=3). mP = units of millipolarization. **C)** Area under the curve (AUC) calculated for the binding-saturation curves depicted in B, measured for each individual fluorescence polarization assay. All graphs represent Mean ± SEM (n=3). Statistical significance was calculated with a two-tailed unpaired Student's t-test (***P-value < 0.005). (Fig. adapted from[149]).

Altogether, our findings showed that TRIM71 is able to physically and specifically interact with CDKN1A mRNA to mediate its repression via 3'UTR recognition followed by mRNA degradation. We furthermore have identified a TRIM71 responsive element (TRE) within a specific region of the human CDKN1A 3'UTR, consisting of a stem-3base-loop RNA motif, and have demonstrated that the TRIM71 NHL domain is sufficient to mediate a direct interaction with that TRE.

4.2.3. TRIM71-mediated CDKN1A mRNA repression correlates with P-body localization

To investigate the involvement of other TRIM71 domains in its mRNA repression function, we performed full length CDKN1A 3'UTR reporter assays upon overexpression of several TRIM71 truncated constructs in HEK293T cells (Fig. 4.2.14A-B). The ubiquitylation mutant C12LC15A significantly repressed the CDKN1A 3'UTR reporter, although, as we had previously shown (see again Fig. 4.1.16C, Chapter I), this mutant has a diminished repression strength as compared to the wild type full length TRIM71 (Fig. 4.2.14C). As expected, due to the lack of the NHL domain, the RBB construct failed to repress the 3'UTR of CDKN1A, whereas the CCNHL construct retained its repression ability. Interestingly, deletion of the CC region from that construct (FLNNHL) totally abrogated TRIM71-mediated CDKN1A 3'UTR repression, demonstrating

that the NHL domain is required, but not sufficient to achieve mRNA repression, since the CC region seems to be required as well. Indeed, deletion of the CC region from a full length construct (TRIM71ΔCC) also resulted in the abrogation of TRIM71-mediated 3'UTR repression (Fig. 4.2.14C).

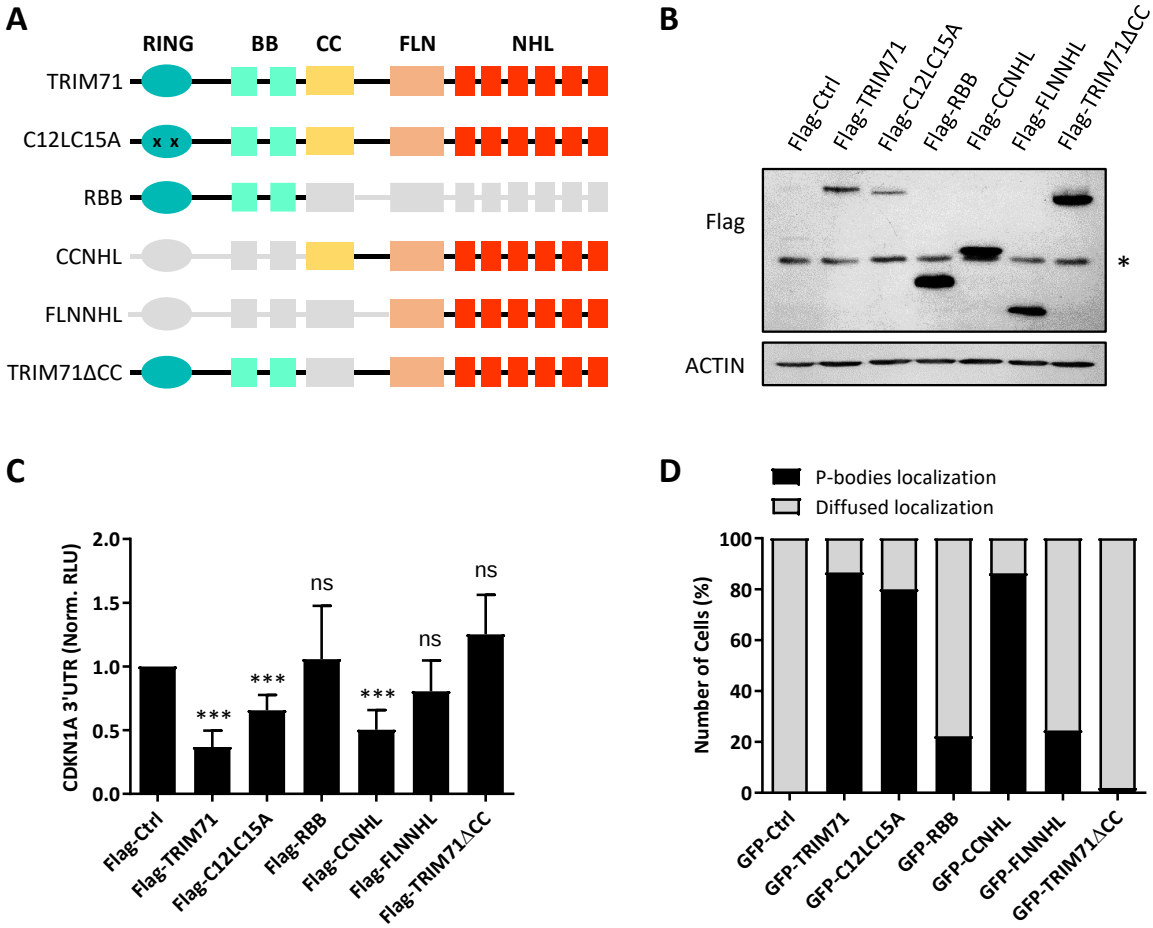

E

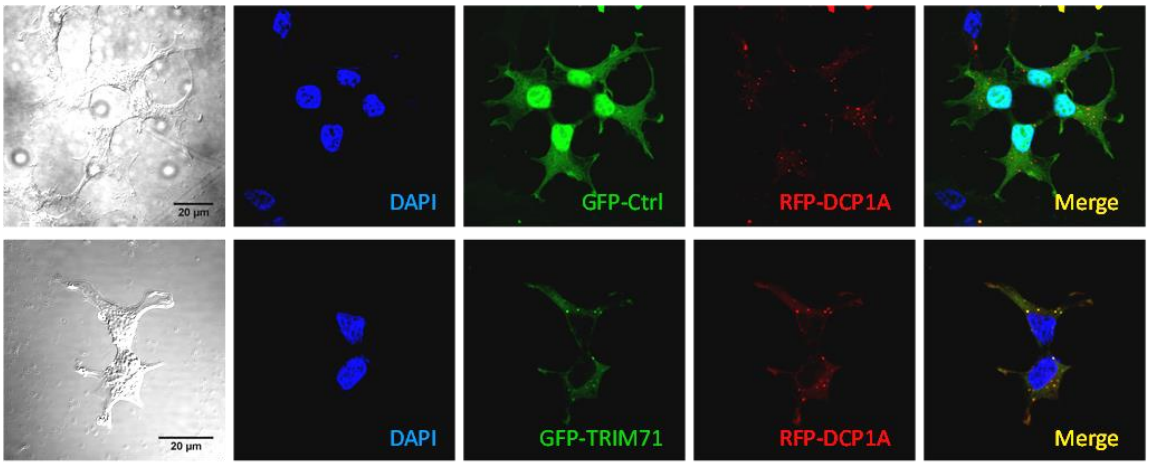

Figure continues...

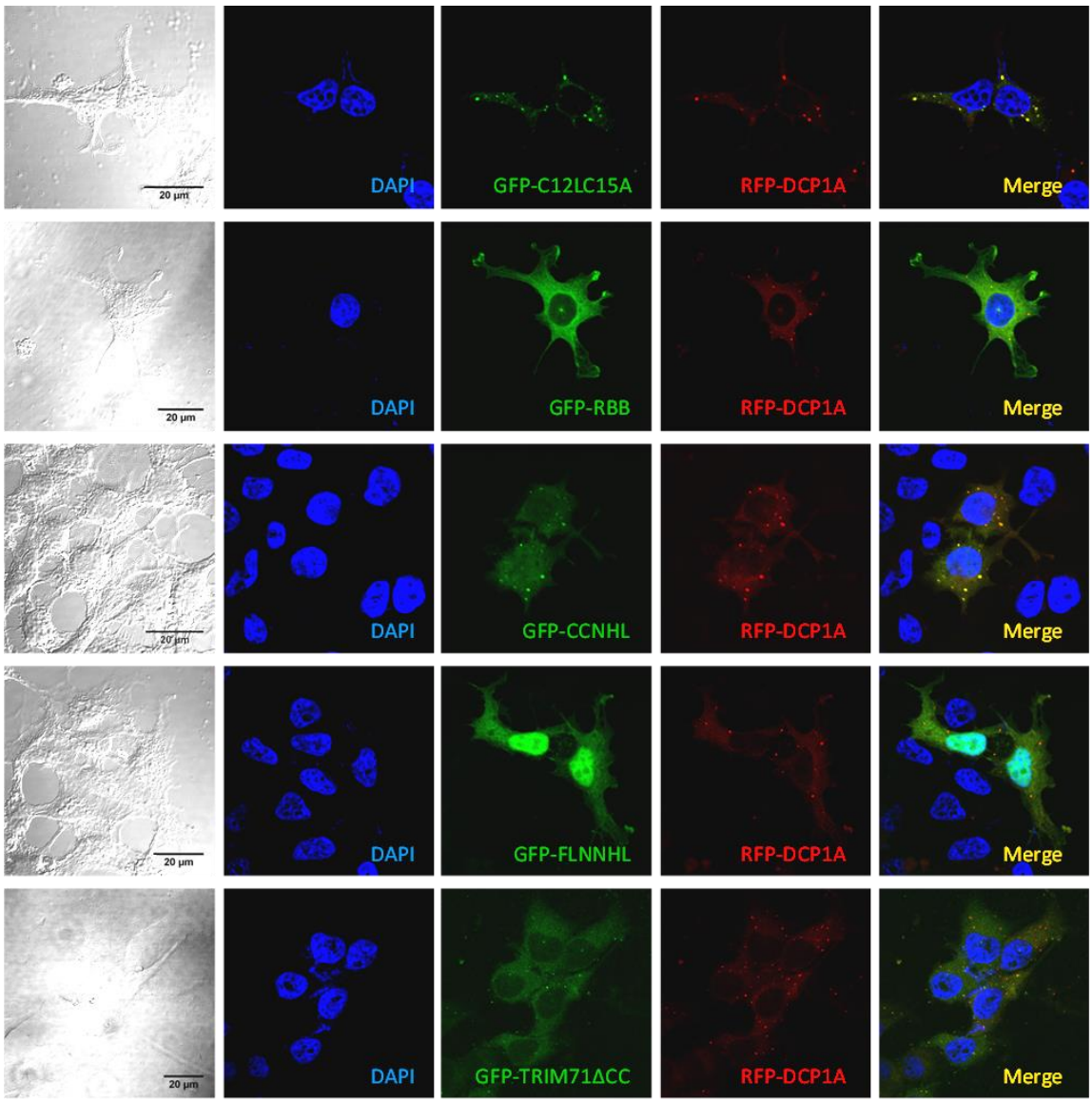

Figure 4.2.14. TRIM71-mediated CDKN1A 3'UTR repression correlates with P-body localization. A) Schematic representation of several TRIM71 truncated constructs used in B-E. Grey areas depict the deleted domains within each construct. **B)** Representative immunoblot showing the expression levels of each TRIM71 construct used for the experiment depicted in C. The asterisk (*) marks an unknown protein of approximately 50 kDa which is unspecifically recognized by the α-Flag antibody. **C)** Repression of the full length CDKN1A 3'UTR luciferase reporter in HEK293T cells transiently transfected with the indicated Flag-tagged TRIM71 constructs, depicted in A, and whose expression levels are shown in B. Norm. RLU = Normalized Relative Light Units. Graph represent Mean ± SD (n=4-7). Statistical significance was calculated with a two-tailed unpaired Student's t-test (ns = non-significant; ***P-value < 0.005. **D)** Percentage of HEK293T cells in which the specified GFP-tagged TRIM71 truncated constructs co-localized with the RFP-tagged specific P-body marker DCP1A, or diffussed through the cell cytoplasm. A total of 50 cells per condition were observed under a confocal microscope for GFP-RFP co-localization. **E)** Representative microscopy images showing the co-localization of the specified GFP-tagged TRIM71 constructs (green) and the RFP-tagged specific P-body marker DCP1A (red) in HEK293T cells. (Fig. adapted from[149]).

Several studies before had shown that truncated versions of TRIM71 were unable to properly locate to P-bodies[41,105]. We therefore investigated whether the constructs that we had used in our reporter assays were localized within P-body structures. To this end, we overexpressed the corresponding GFP-tagged TRIM71 truncated constructs, together with the RFP-tagged specific P-body marker DCP1A[132], and evaluated their co-localization by confocal scanning laser microscopy (Fig. 4.2.14D-E). Interestingly, only the constructs containing the CC region (TRIM71, C12LC15A and CCNHL) were able to form aggregates which co-localized with DCP1A, while the constructs lacking the CC region (RBB, FLNNHL and TRIM71ΔCC), which failed to repress the full length CDKN1A 3'UTR reporter, were unable to localize to P-bodies, instead being evenly distributed through the cell cytoplasm, and in some cases even entering the nuclei (Fig. 4.2.14D-E).

Altogether, these experiments uncovered a correlation between the CDKN1A 3'UTR repression ability of the different constructs and their proper localization within P-bodies. Such a correlation suggested that the role of TRIM71 as an mRNA repressor is developed in P-bodies, organelles well known to host many proteins involved in various RNA surveillance mechanisms[132].

4.2.4. TRIM71-mediated CDKN1A mRNA repression is AGO2- and miRNA-independent

P-bodies are RNA surveillance organelles hosting several RNA degradation pathways[132], such as miRNA-mediated mRNA silencing[133]. In mESCs, TRIM71-mediated Cdkn1a 3'UTR repression was assisted by miR-302[41]. However, the human CDKN1A 3'UTR lacked binding sites for miR-302 and no conserved miRNA binding sites were predicted in the region spanning the F2_100-200 fragment (see again Fig. 4.2.9), in which we had identified a TRE. Furthermore, TRIM71 was found to repress several mRNA targets without assistance of neither AGO2 nor miRNAs, even when such targets were also under the control of the miRNA pathway[115]. This prompted us to investigate whether TRIM71 could also repress the human CDKN1A 3'UTR independently from the miRNA machinery.

We therefore interfered with the miRNA pathway in HEK293 cells stably overexpressing GFP-Ctrl or GFP-TRIM71, by impairing either miRNA synthesis/expression via DGCR8 knockdown, or miRNA activity via AGO2 knockdown. Neither DGCR8 knockdown nor AGO2 knockdown abrogated or relieved TRIM71-induced CDKN1A/p21 downregulation – in fact, such an effect was even mildly enhanced upon AGO2 knockdown – (Fig. 4.2.15A-B), suggesting that TRIM71 can regulate CDKN1A without relying on miRNA assistance. In order to confirm these results, we used AGO2 knockout cells (Fig. 4.2.15C). Strikingly, overexpression of let-7 miRNA in AGO2 knockout HEK293T cells resulted in the repression of its *bona fide* target HMGA2 (Fig. 4.2.15D), demonstrating that these cells were still able to conduct miRNA-mediated silencing and suggesting that other Argonaute proteins may take over this role upon AGO2 depletion. Thus, this cell line was not suitable to prove miRNA independency of TRIM71-mediated mRNA target repression. However, AGO2 independency could be confirmed, since TRIM71 was able to repress CDKN1A 3'UTR in AGO2 knockout HEK293T cells to a similar extent as in wild type cells (Fig. 4.2.15E-F).

In order to confirm whether TRIM71-mediated CDKN1A 3'UTR repression occurred in a miRNA-independent manner, we used Dgcr8 knockout mESCs (Fig. 4.2.15G), which are unable to produce mature functional miRNAs[41] (Fig. 4.2.15H). Despite the absence of miRNAs, TRIM71 repressed CDKN1A 3'UTR in Dgcr8 knockout mESCs to the same extent as in wild type mESCs (Fig. 4.2.15I-J), demonstrating that TRIM71-mediated CDKN1A regulation does not require miRNA assistance.

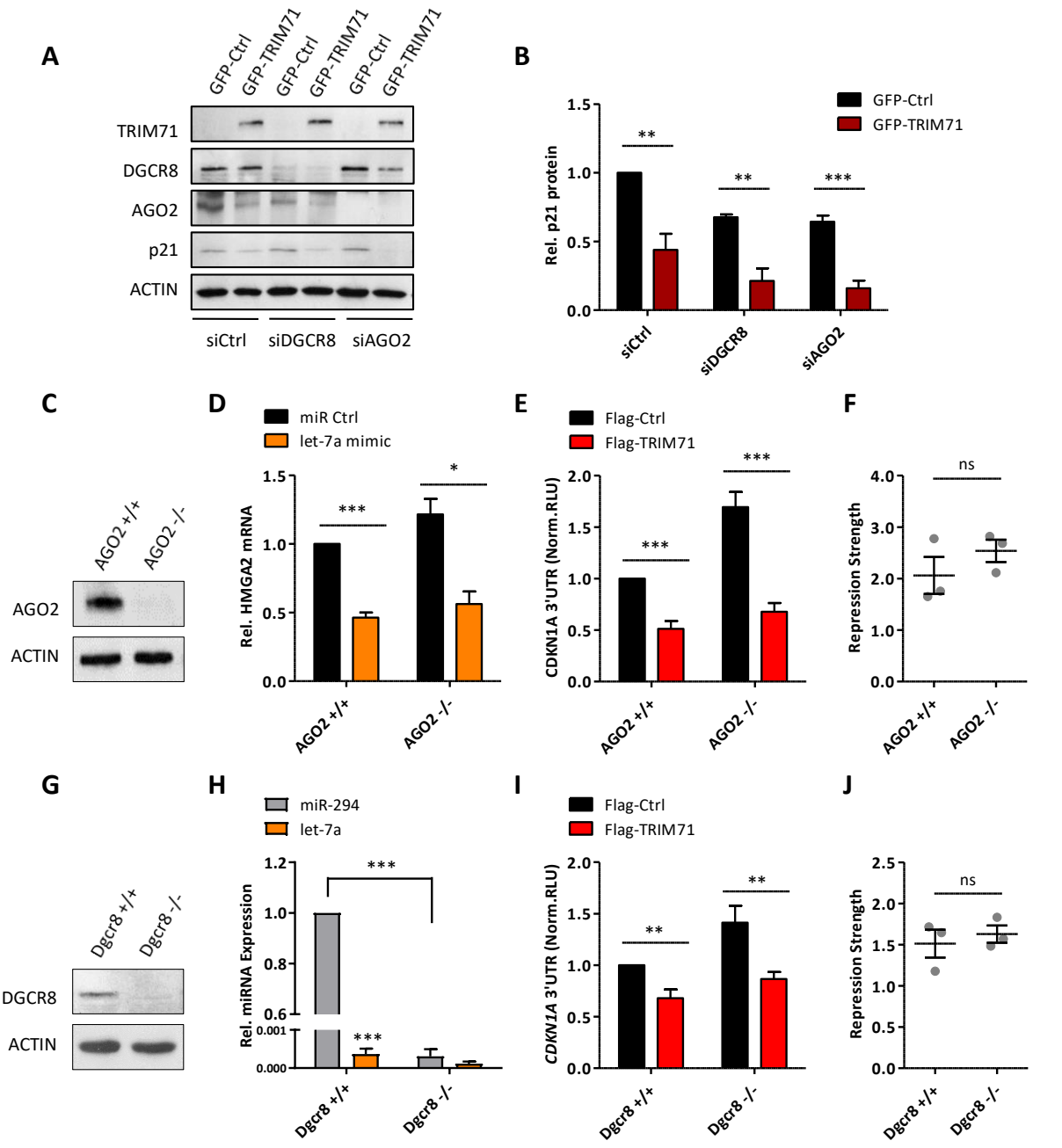

Figure 4.2.15. TRIM71-mediated CDKN1A repression is AGO2- and miRNA-independent. A) Representative immunoblot showing p21 protein levels in HEK293 cells stably overexpressing GFP or GFP-TRIM71 upon DGCR8 or AGO2 knockdown. **B)** Quantification of p21 band densitometry relative to ACTIN bands from several blots replicates of A (n=3). **C)** Representative immunoblot showing AGO2 protein levels in wild type (WT, AGO2 +/+) and AGO2 knockout (KO, AGO2 -/-) HEK293T cells. **D)** qPCR measurements of the *bona fide* let-7 mRNA target HMGA2 upon miRCtrl or let-7a miRNA mimic overexpression in WT and AGO2 KO HEK293T cells (n=3). **E)** Repression of the full length CDKN1A 3'UTR luciferase reporter in WT and AGO2 KO HEK293T cells transiently transfected with Flag or Flag-TRIM71 (n=3). **F)** Repression Strength of TRIM71-mediated CDKN1A repression, calculated from data depicted in E. **G)** Representative immunoblot showing DGCR8 protein levels in wild type (WT, Dgcr8+/+) or Dgcr8 knockout (KO, Dgcr8-/-) mESCs. **H)** qPCR measurements of the stem cell-specific miR-294 and the differentiation-promoting miRNA let-7a in WT and Dgcr8 KO mESCs (n=3). **I)** Repression of the full length CDKN1A 3'UTR luciferase reporter in WT and Dgcr8 KO mESCs transiently transfected with Flag or Flag-TRIM71 (n=3). **J)** Repression Strength of TRIM71-mediated CDKN1A repression, calculated from data depicted in I. All graphs represent Mean ± SEM. Statistical significance was calculated with a two-tailed unpaired Student's t-test (ns = non-significant; *P-value < 0.05; **P-value < 0.01; ***P-value < 0.005). (Fig. adapted from[149]).

Conversely, Trim71 knockdown in mESCs (Fig. 4.2.16A) resulted in upregulated endogenous Cdkn1a mRNA levels (Fig. 4.2.16B) and a significant derepression of the CDKN1A 3'UTR reporter in both, wild type (Fig. 4.2.16C) and Dgcr8 knockout (Fig. 4.2.16D) mESCs.

The fact that the upregulation of endogenous Cdkn1a levels upon Trim71 knockdown was non-significant, whereas the activity of the CDKN1A 3'UTR reporter was significantly affected under the same conditions, may be explained by previous findings which showed that TRIM71-mediated translational inhibition was a preferred mechanism over mRNA degradation in mESCs[115].

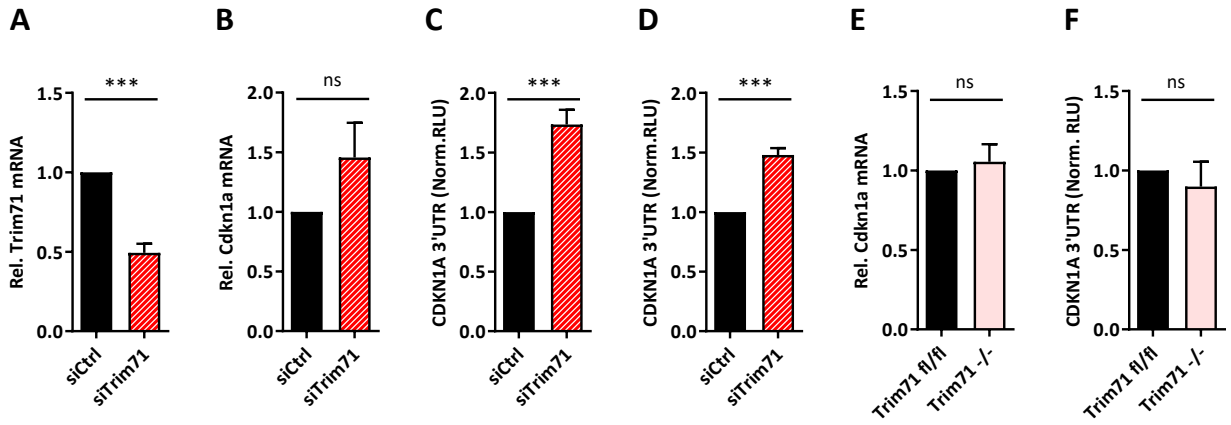

Figure 4.2.16. Trim71 knockdown in mESCs results in Cdkn1a derepression, but Trim71 knockout mESCs do not show any regulation of Cdkn1a. A) qPCR measurements of Trim71 mRNA (n=4) and **B)** Cdkn1a mRNA (n=4) in wild type (WT, siCtrl) and Trim71 knockdown (KD, siTrim71) mESCs. Hprt housekeeping gene was used for normalization. **C)** Derepression of the full length CDKN1A 3'UTR luciferase reporter upon Trim71 KD in wild type (Dgcr8+/+) and **D)** Dgcr8 knockout (Dgcr8-/-) mESCs (n=3-4). **E)** qPCR measurements of Cdkn1a mRNA in wild type (WT, Trim71 fl/fl) and Trim71 knockout (KO, Trim71 -/-) mESCs (n=6). **C)** Luciferase reporter assay with the full length CDKN1A 3'UTR reporter in WT and Trim71 KO mESCs (n=4). Norm. RLU = Normalized Relative Light Units. All graphs represent Mean ± SEM. Statistical significance was calculated with a two-tailed unpaired Student's t-test (ns = non-significant; ***P-value < 0.005). (Fig. adapted from[149]).

Strikingly, Trim71 knockout mESCs did not show neither changes in endogenous Cdkn1a mRNA expression (Fig. 4.2.16E) nor in CDKN1A 3'UTR reporter activity (Fig. 4.2.16F) as compared to wild type mESCs. Accordingly, whereas proliferation of Trim71 knockdown mESCs was indeed affected, as shown by an 11.5% decrease in proliferation derived from a 1.5 h-delay in their cell cycle (Fig. 4.2.17A-D), Trim71 knockout mESCs did not show proliferation defects when compared to wild type mESCs (Fig. 4.2.17E-H).

The results observed in Trim71 knockdown mESCs suggested that TRIM71 is able to regulate CDKN1A and to control proliferation also in mESCs, as we had already shown for HEK293 and HepG2 cells. However, Trim71 knockout mESCs must have undergone a clonal adaptation involving a compensation of Cdkn1a levels to maintain their proliferation rate. These findings are in line with previous experiments conducted in these Trim71-deficient mESCs, showing that, although these cells were primed towards differentiation, their stemness in steady-state was maintained despite the absence of TRIM71[113].

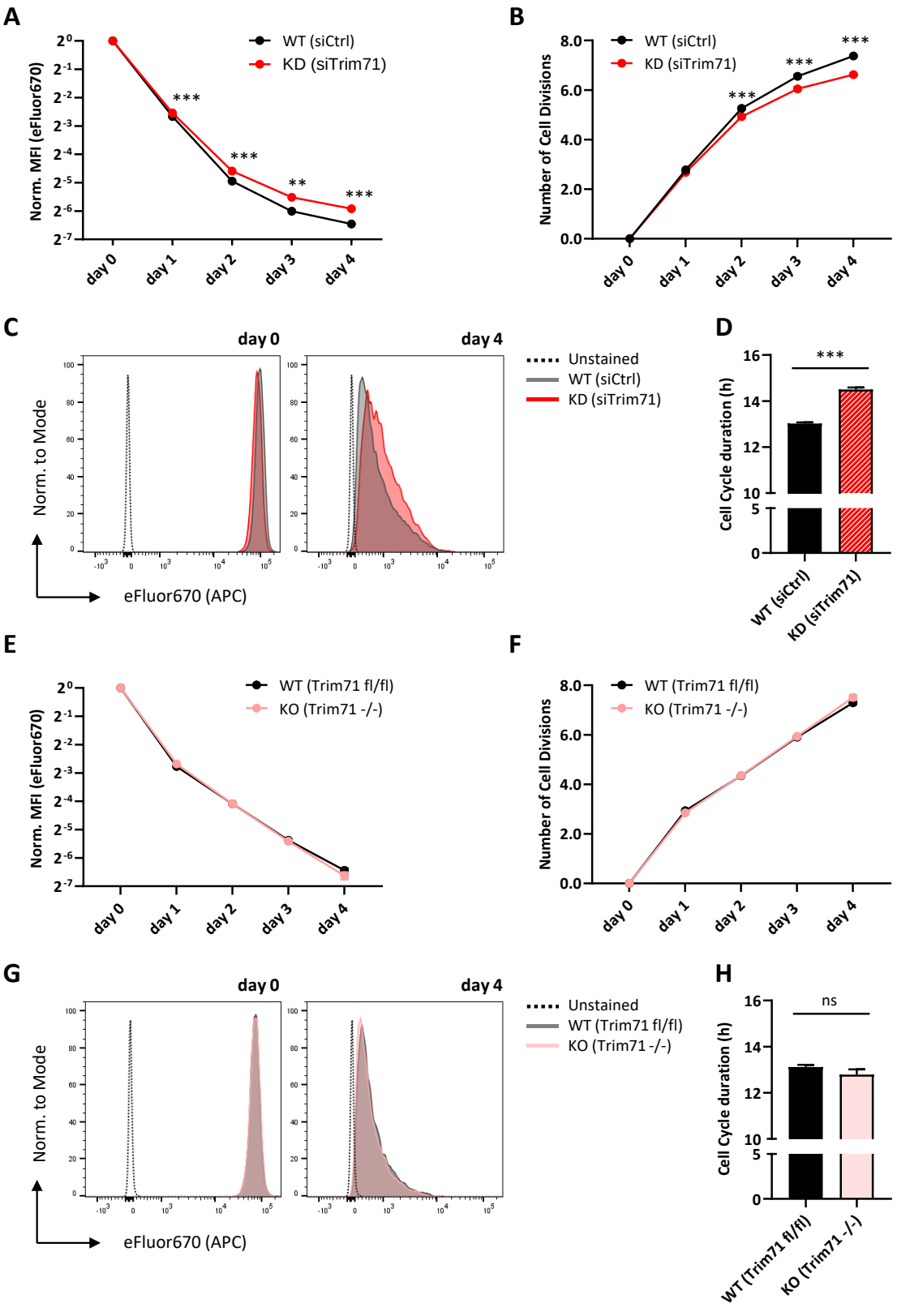
A
Norm. MFI (eFluor670)
WT (siCtrl)
KD (siTrim71)
day 0
day 1
day 2
day 3
day 4
B
Number of Cell Divisions
C
day 0
day 4
Norm. to Mode
eFluor670 (APC)
Unstained
WT (siCtrl)
KD (siTrim71)
D
Cell Cycle duration (h)
WT (siCtrl)
KD (siTrim71)
E
WT (Trim71 fl/fl)
KO (Trim71 -/-)
F
G
H
ns

Figure 4.2.17. Trim71 knockdown in mESCs results in a decresed proliferation, but Trim71 knockout mESCs do not show any proliferation defect. A) Progressive loss of fluorescence intensity over time of the dye eFluor670 upon proliferation of WT (siCtrl) and TRIM71 KD (siTrim71) mESCs. MFI = Median Fluorescence Intensity of APC (eFluor670). **B)** Number of cell divisions undergone overtime by WT and Trim71 KD mESCs, calculated as previously specified in Fig. 4.2.5. **C)** Overlap of APC (eFluor670) histograms of WT and Trim71 KD mESC populations, showing comparable staining for the different populations at the beginning of the proliferation assay (left panel: day 0, 24 hpt) and the retardation of Trim71 KD mES cells histogram as result of a diminished proliferation at the end of the experiment (right panel: day 4, 120 hpt). **D)** Average cell cycle duration (h) calculated from the number of cell divisions at day 4. **E)** Progressive loss of fluorescence intensity over time of the proliferation dye eFluor670 upon proliferation of WT (Trim71 fl/fl) and Trim71 KO (Trim71-/-) mES cells. MFI = Median Fluorescence Intensity of APC (eFluor670). **B)** Number of cell divisions undergone overtime by WT and Trim71 KO mESCs, calculated as previously specified in Fig. 4.2.5. **C)** Overlap of APC (eFluor670) histograms of WT and Trim71 KO mES cells populations showing comparable staining for the different populations at the beginning (left panel: day 0) and at the end of the proliferation assay (right panel: day 4). **D)** Average cell cycle duration (h) calculated from the number of cell divisions at day 4. A-H show the results of one representative experiment in each case, including three technical replicates. All graphs represent Mean ± SD. Statistical significance was calculated with a two-tailed unpaired Student's t-test (ns = non-significant; **P-value < 0.01; ***P-value < 0.005).

Leaving aside the differences observed between Trim71 knockdown and knockout mESCs concerning the regulation of Cdkn1a mRNA, our experiments collectively demonstrated, by using several knockdown and knockout mouse and human cell lines, that TRIM71-mediated CDKN1A 3'UTR repression can occur in an AGO2- and a miRNA-independent manner.

4.2.5. TRIM71-mediated CDKN1A mRNA repression is achieved via Nonsense-Mediated Decay (NMD)

Since TRIM71-mediated CDKN1A mRNA repression was not assisted by the miRNA pathway, we next investigated which other pathways operating within P-bodies may assist TRIM71 in mRNA silencing. To this end, we knocked down the expression of several proteins which are known to be localized in P-bodies and had been linked to mRNA degradation processes, and evaluated TRIM71-mediated CDKN1A 3'UTR repression under such conditions.

We included the knockdown of AGO2 and DGCR8 again as a control; the knockdown of the RNA-binding protein PUM2, known to be a TRIM71 binding partner and to share some mRNA targets with TRIM71[115]; the knockdown of the TUT4 enzyme, responsible for targeting specific miRNAs and mRNAs for degradation via uridylation[147,151], and which we have identified as a new TRIM71 binding partner in the previous chapter; and the knockdowns of UPF1 and SMG1, two major effectors of the Nonsense-Mediated Decay (NMD) pathway[152] (Fig. 4.2.18).

In line with our previous experiments, AGO2 and DGCR8 knockdowns did not affect TRIM71 ability to repress CDKN1A 3'UTR in HEK293T cells. Similarly, the knockdowns of PUM2 or TUT4 did not impair TRIM71-mediated CDKN1A 3'UTR repression. Of note, a previous study revealed that PUM motifs were not enriched in TRIM71 mRNA targets and that PUM knockdown did not have an impact on TRIM71-mediated mRNA silencing[115], as we just confirmed. Interestingly, impairment of NMD by either UPF1 or SMG1 knockdown significantly decreased TRIM71-mediated CDKN1A 3'UTR repression (Fig. 4.2.18).

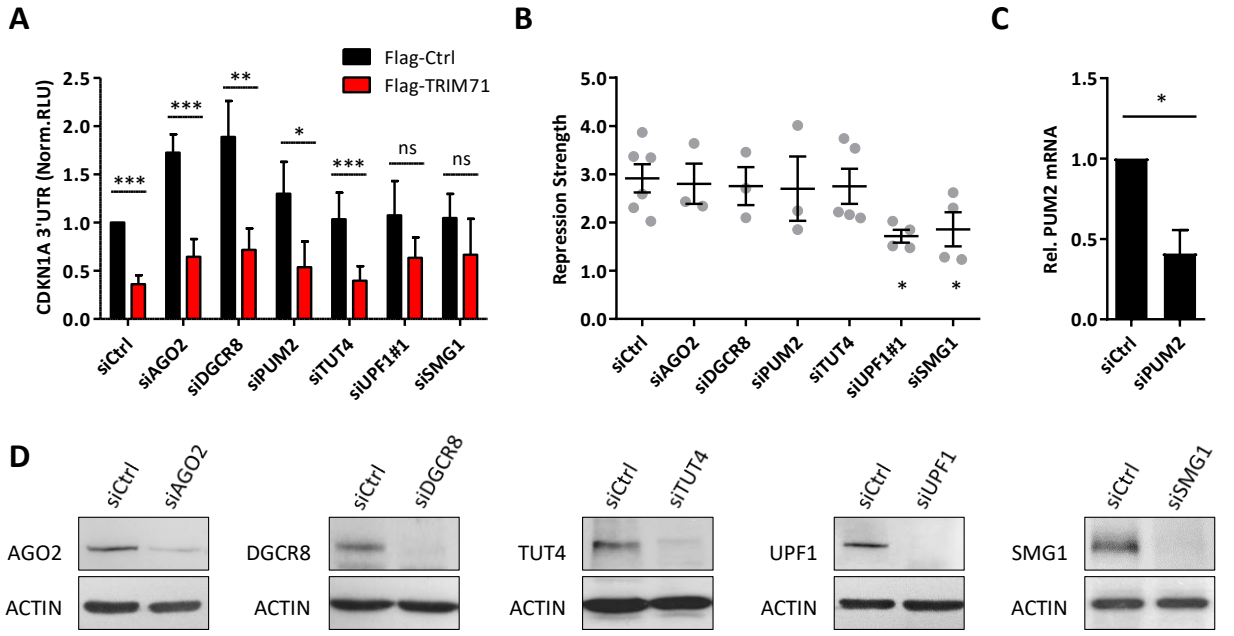

Figure 4.2.18. TRIM71-mediated CDKN1A repression is relieved upon knockdown of the NMD components UPF1 and SMG1. A) Repression of the full length CDKN1A 3'UTR luciferase reporter in HEK293T cells transiently transfected with Flag or Flag-TRIM71 upon knockdown of the indicated proteins (n=3-6). **B)** Repression strength of TRIM71-mediated CDKN1A repression upon knockdown of the indicated proteins, calculated from data depicted in A, as the ratio between Norm. RLU Flag-Ctrl and Norm. RLU Flag-TRIM71 values. **C)** qPCR measurements of PUM2 mRNA levels as knockdown control for the experiment depicted in A-B. Of note, PUM2 protein was undetectable in WB analysis (data not shown). **D)** Representative immunoblots for the indicated proteins as knockdown controls for the experiment depicted in A-B. Norm. RLU = Normalized Relative Light Units. All graphs represent Mean ± SEM. Statistical significance was calculated with a two-tailed unpaired Student's t-test (ns = non-significant; *P-value < 0.05; **P-value < 0.01; ***P-value < 0.005). (Fig. adapted from[149]).

NMD is an RNA surveillance pathway for the degradation of transcripts containing a premature termination codon (PTC)[57,153]. In the last years, it has become evident that NMD can also mediate the degradation of functional transcripts lacking PTCs, although how the NMD machinery recognizes such transcripts remain largely elusive[55,56]. Further understanding of such "non-canonical" NMD functions would require the identification of RBPs enabling the recruitment and/or activation of the NMD machinery for specific mRNA targets. Given that TRIM71-mediated CDKN1A repression was impaired upon UPF1 and SMG1 knockdowns, we hypothesized that TRIM71 may be one of these proteins. Our results showed that UPF1 and SMG1 were co-precipitated with overexpressed TRIM71 in HEK293T cells (Fig. 4.2.19A). UPF1 was also co-precipitated with endogenous TRIM71 in HepG2 cells (Fig. 4.2.19B). Interestingly, our TRIM71 mutant ΔNHL6, which had fail to bind RNA, could neither bind UPF1 (Fig. 4.2.19C), suggesting such an interaction to be RNA-dependent. Indeed, TRIM71 interactions with UPF1 and SMG1 were disrupted after RNase treatment (Fig. 4.2.19D), indicating that TRIM71, UPF1 and SMG1 may be bound to common mRNA targets, and supporting a cooperation between TRIM71 and these NMD components to achieve specific target degradation. Furthermore, the TRIM71-UPF1 interaction did not depend on TRIM71 E3 ligase activity, since UPF1 was also found co-precipitated with the ubiquitylation mutant C12LC15A in HEK293T cells (Fig. 4.2.19E) and in mESCs (Fig. 4.2.19F).

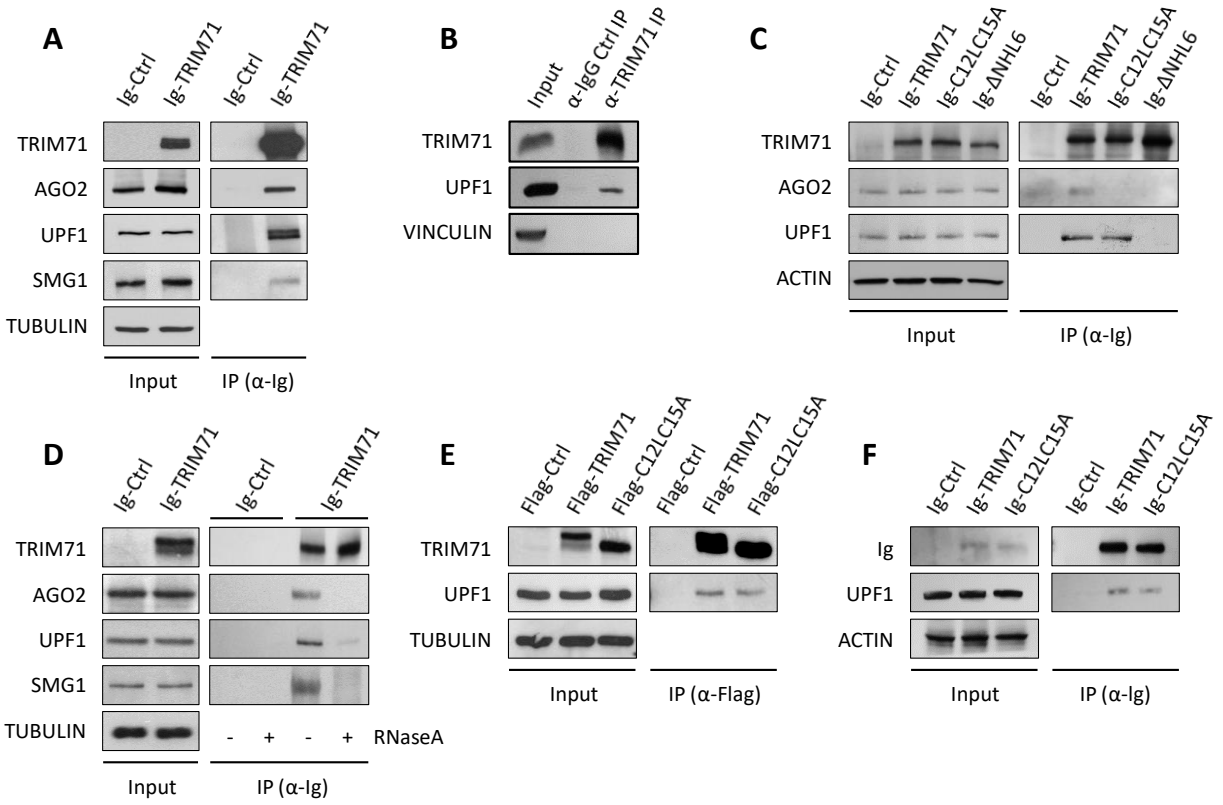

Figure 4.2.19. TRIM71 interacts with the NMD components UPF1 and SMG1 via common RNA targets: A) Representative immunoblot showing the co-precipitation of UPF1 and SMG1 with TRIM71 overexpressed in HEK293T cells. **B)** Representative immunoblot showing the co-precipitation of UPF1 with endogenous TRIM71 in HepG2 cells. **C)** Representative immunoblot showing UPF1 co-precipitation ability with Ig-Ctrl/Ig-TRIM71/Ig-C12LC15A/Ig-ΔNHL6 in HEK293T cells. **D)** Representative immunoblot showing the co-precipitation of UPF1 and SMG1 with TRIM71 overexpressed in HEK293T cells upon RNase A treatment. **E)** Representative immunoblot showing UPF1 co-precipitation with wild type TRIM71 and ubiquitylation mutant C12LC15A overexpressed in HEK293T cells and **F)** mESCs. AGO2 was used as positive control for a RNA-dependent TRIM71 binding partner. (Fig. adapted from[149]).

After SMG1 and UPF1 have initiated NMD, mRNA target degradation can be assisted by the recruitment of the SMG6 endonuclease, which cleaves the mRNA in the vicinity of the PTC, and the recruitment of the SMG5-SMG7 dimer, which trigger deadenylation and decapping followed by exonucleolytic cleavage[154,155]. To evaluate whether CDKN1A degradation occurs indeed via NMD, and not via other UPF1-mediated downstream decay mechanisms[73,74], we evaluated TRIM71-mediated CDKN1A 3'UTR repression upon SMG6 and SMG7 knockdowns in HEK293T cells. Our results showed that SMG7 knockdown, but not SMG6 knockdown, relieved TRIM71-mediated CDKN1A 3'UTR repression (Fig. 4.2.20A-C). Furthermore, SMG7 was found co-precipitated with TRIM71 overexpressed in HEK293T cells (Fig. 4.2.20D), and conversely, endogenous TRIM71, together with UPF1 and SMG1, were found co-precipitated with endogenous SMG7 in HepG2 cells (Fig. 4.2.20E).

Degradation of PTC-containing transcripts by canonical NMD occurs in the pioneer round of translation, when transcripts are bound by the cap-binding complex formed by CBP80 and CBP20[156,157]. In contrast, functional/PTC-lacking transcripts in steady-state translation are bound by the cap-binding protein eIF4E[156,157], and thereby non-canonical NMD can also occur in eIF4E-bound mRNAs[158]. Interestingly, the

RNase-sensitive co-precipitation of eIF4E with endogenous SMG7 was enhanced upon overexpression of TRIM71 in HEK293T cells (Fig. 4.2.20F), indicating that TRIM71 increases the binding of SMG7 to functional transcripts which are under steady-state translation. Since SMG7 is recruited to the mRNA target only after NMD has been activated[159], these results suggested that TRIM71 enables NMD activation on specific eIF4E-bound mRNAs. Activation of NMD is achieved by SMG1-mediated UPF1 phosphorylation, and results in the phospho-dependent recruitment of SMG7[159]. Our results showed that SMG7 binds phospho-UPF1 (p-UPF1) in a RNA-independent manner, as previously described[159], whereas SMG7 interaction with TRIM71 was RNase-sensitive (Fig. 4.2.20F), in line the previously demonstrated RNA-dependent interactions of TRIM71 with SMG1 and UPF1 (see again Fig. 4.2.19D). These results strengthened the hypothesis that TRIM71 and the NMD machinery bind to common mRNA targets, and are therefore found within the same messenger ribonucleoparticle (mRNP) complex, supporting a cooperation between TRIM71 and NMD for specific target degradation.

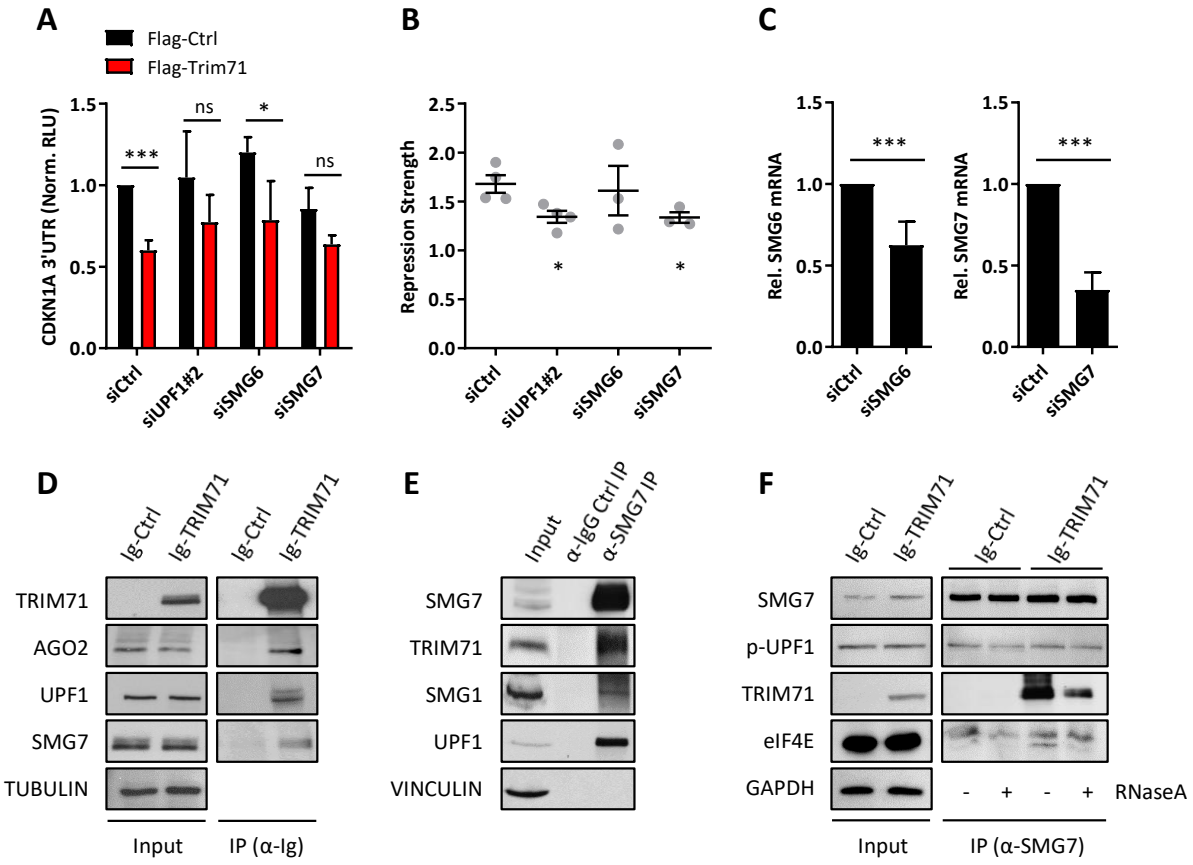

Figure 4.2.20. TRIM71 interacts with the NMD component SMG7 via common RNA targets which are under steady-state translation. A) Repression of the full length CDKN1A 3'UTR luciferase reporter in HEK293T cells transiently transfected with Flag or Flag-TRIM71 upon knockdown of the indicated NMD factors (n=3-4). **B)** Repression strength of TRIM71-mediated CDKN1A repression, calculated from data depicted in A, as the ratio between Norm. RLU Flag-Ctrl and Norm. RLU Flag-TRIM71 values. **C)** qPCR measurements of SMG6 and SMG7 mRNA levels as knockdown controls for the experiment depicted in A-B. **D)** Representative immunoblot showing UPF1 and SMG7 co-precipitation with TRIM71 overexpressed in HEK293T cells. AGO2 was used as a positive control for a TRIM71 binding partner. **E)** Immunoblot showing the co-precipitation of endogenous TRIM71, SMG1 and UPF1 with endogenous SMG7 in HepG2 cells. **F)** Immunoblot showing the co-precipitation of phospho-UPF1 (Ser 1127), TRIM71 and eIF4E with endogenous SMG7 upon RNase treatment in HEK293T cells. Norm. RLU = Normalized Relative Light Units. All graphs represent Mean ± SEM. Statistical significance was calculated with a two-tailed unpaired Student's t-test (ns = non-significant; *P-value < 0.05; ***P-value < 0.005). (Fig. adapted from[149]).

Altogether, our data suggested that TRIM71-mediated CDKN1A 3'UTR repression resulted from SMG1/UPF1/SMG7-mediated decay. To confirm these results, we next measured endogenous CDKN1A mRNA levels upon NMD components knockdown in HEK293T cells. In line with the previous luciferase assays, CDKN1A mRNA was upregulated upon UPF1, SMG1 and SMG7 knockdowns, but not SMG6 knockdown (Fig. 4.2.21A), whereas the mRNA of ATF3, a known NMD target which contains a PTC resulting from alternative splicing[160], was upregulated upon UPF1, SMG1, SMG6 and SMG7 knockdowns (Fig. 4.2.21B). Importantly, TRIM71 expression was not altered upon NMD components knockdown (Fig. 4.2.21C) while NMD components cross-regulated each other (Fig. 4.2.21D-F), as it was previously described[161]. These results, on one hand supported the notion that TRIM71 is not involved in canonical NMD functions, and on the other hand, excluded that the NMD-induced CDKN1A mRNA regulation occurred indirectly through a downstream TRIM71 regulation.

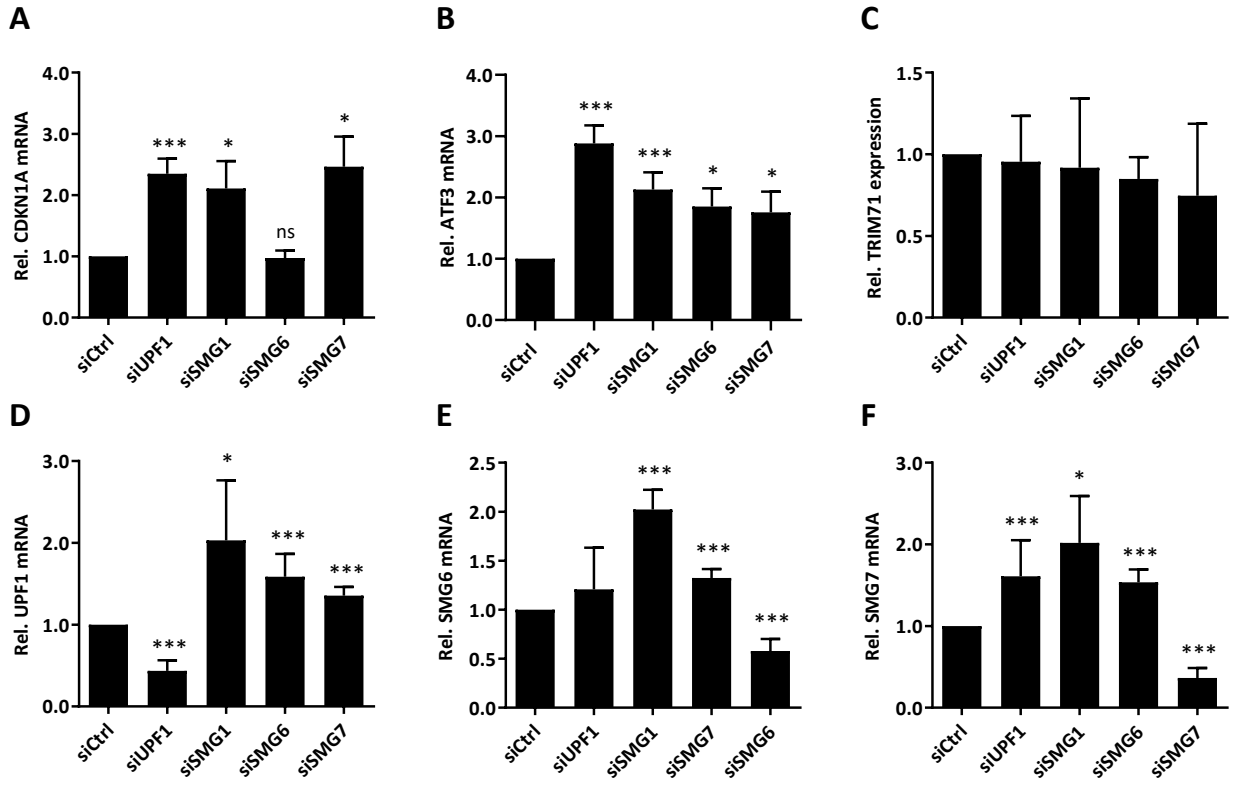

Figure 4.2.21. Knockdown of NMD components results in endogenous CDKN1A mRNA upregulation. A) qPCR measurements of CDKN1A, **B)** ATF3, **C)** TRIM71, **D)** UPF1, **E)** SMG6 and **F)** SMG7 endogenous mRNA levels upon NMD components knockdown in HEK293T cells. HPRT1 housekeeping gene was used for normalization. All graphs represent Mean ± SD (n=3-5). Statistical significance was calculated with a two-tailed unpaired Student's t-test (ns = non-significant; *P-value < 0.05; ***P-value < 0.005). (Fig. adapted from[149]).

Although TRIM71 and NMD factors are post-transcriptional mRNA regulators, a transcriptional contribution could account for the observed CDKN1A mRNA upregulation. In fact, TRIM71 has been shown to destabilize p53 protein in mESCs undergoing differentiation[117], and p53 is a well-known CDKN1A/p21 transcriptional activator. Furthermore, p53 is stabilized and activated (phosphorylated) upon DNA damage, and NMD components are involved in DNA damage response[162–165].

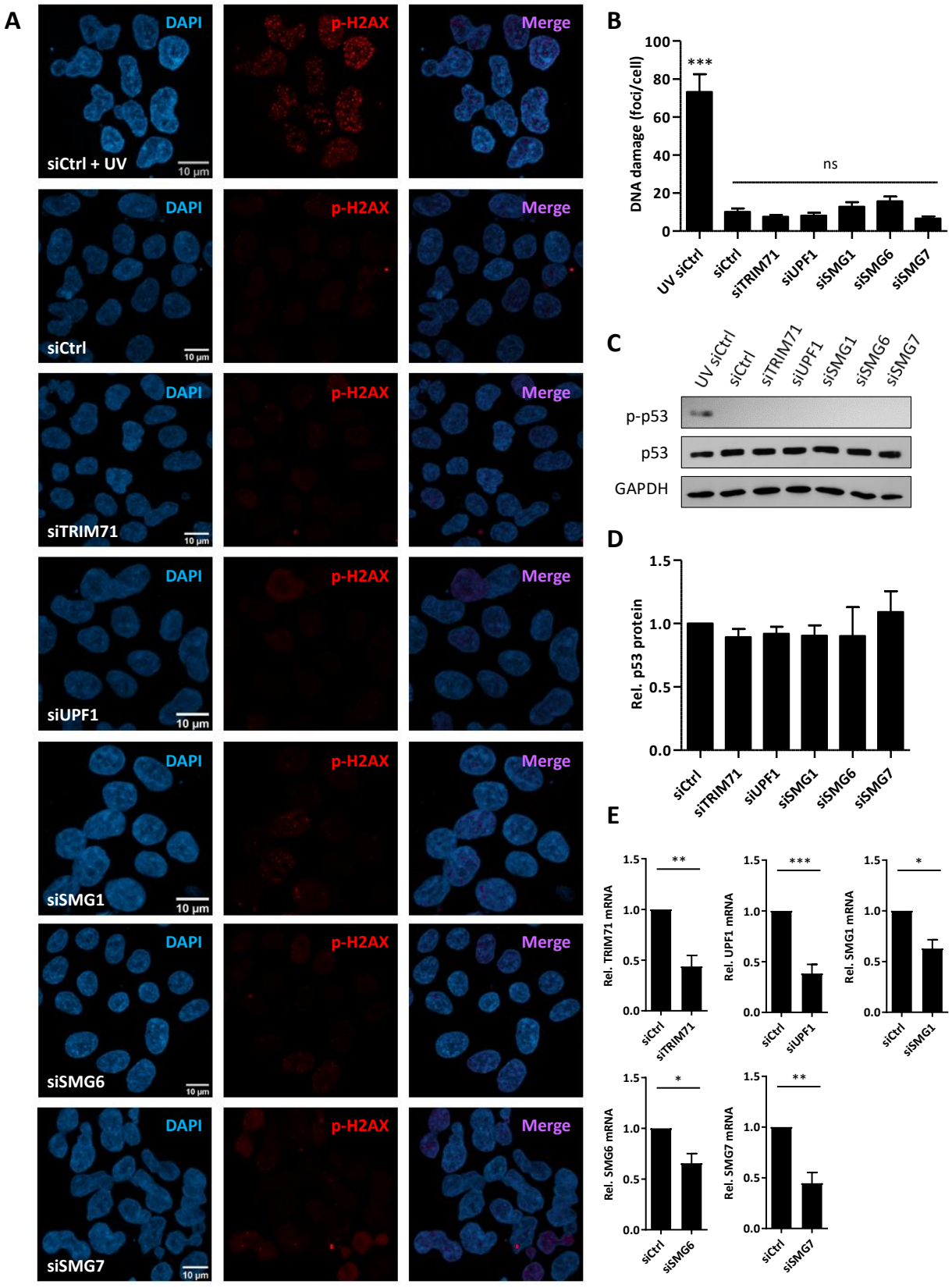
A
DAPI
p-H2AX
Merge
siCtrl + UV
siCtrl
siTRIM71
siUPF1
siSMG1
siSMG6
siSMG7
10 µm
B
DNA damage (foci/cell)
***
ns
UV siCtrl
siCtrl
siTRIM71
siUPF1
siSMG1
siSMG6
siSMG7
C
p-p53
p53
GAPDH
D
Rel. p53 protein
E
Rel. TRIM71 mRNA
Rel. UPF1 mRNA
Rel. SMG1 mRNA
Rel. SMG6 mRNA
Rel. SMG7 mRNA

Figure 4.2.22. CDKN1A mRNA upregulation upon NMD impairment does not result from p53-dependent transcriptional activation. A) Confocal microscopy maximal intensity projection images (stacked) showing phospho-H2AX (Ser139) staining in HEK293T cells upon TRIM71 and NMD components knockdowns. A control sample was UV-irradiated with 100 J/cm^2 to induce DNA damage i.e. high H2AX phosphorylation levels. **B)** Quantification of phospho-H2AX staining (foci per cell) as a measure for DNA damage in at least 50 cells per condition. Graph represents Mean ± SEM. **C)** Representative immunoblot showing levels of p53 and phospho-p53 (Ser15) in samples used for A-B. **D)** Quantification of p53 band densitometry in several blot replicates of C (n=4). **E)** qPCR quantification of the indicated mRNAs to control the knockdown levels of TRIM71 and NMD components for experiments depicted in A-D (n=3). Graphs in D and E represent Mean ± SD. Statistical significance was calculated with a two-tailed unpaired Student's t-test (ns = non-significant; *P-value < 0.05; **P-value < 0.01; ***P-value < 0.005).(Fig. adapted from[149]).

In order to exclude that the upregulation of CDKN1A mRNA resulted from a p53-mediated transcriptional activation upon knockdown of TRIM71 and/or NMD components, we investigated DNA damage levels via phospho-H2AX (Ser139) IF staining and p53/phospho-p53 (Ser15) levels via WB analysis in HEK293T cells under such conditions (Fig. 4.2.22). As a positive control for DNA damage and p53 activation, HEK293T cells transfected with a control siRNA (siCtrl) were UV-irradiated and harvested 3 h after UV irradiation for further analysis, together with the non-irradiated samples. Neither DNA damage levels (Fig. 4.2.22A-B) nor total p53 levels (Fig. 4.2.22C-D) were altered upon knockdown of TRIM71 or NMD components, as compared to non-irradiated siCtrl cells. Furthermore, phospho-p53 was undetected under these conditions, being only upregulated upon exposure to UV irradiation (Fig. 4.2.22C). These findings excluded the possibility that CDKN1A mRNA upregulation resulted from p53-dependent transcriptional activation under our experimental conditions.

Our luciferase reporter assays showed that TRIM71 relied on NMD factors for the repression of CDKN1A 3'UTR (see again Fig. 4.2.18A-B and Fig. 4.2.20A-B), and conversely, the measurements of endogenous CDKN1A mRNA levels showed that NMD impairment led to CDKN1A upregulation (see again 4.2.21A). We next aimed at investigating whether NMD-induced CDKN1A mRNA regulation was TRIM71-dependent and asked whether ablation of TRIM71 in NMD knockdown cells could rescue the observed CDKN1A upregulation. Since HEK293T cells express very low amounts of TRIM71, ablation of TRIM71 in these cells could be easily achieved by siRNA-mediated silencing. We therefore compared CDKN1A mRNA upregulation upon impairment of NMD in the presence and absence of TRIM71, by knocking down NMD components alone or simultaneously knocking down NMD components and TRIM71, respectively. Indeed, CDKN1A mRNA upregulation upon impairment of NMD was only observed in the presence of endogenous TRIM71 (+TRIM71), whereas the knockdown of NMD components in the absence of TRIM71 (-TRIM71) had no effect on CDKN1A mRNA levels (Fig. 4.2.23A-C), demonstrating that the SMG1/UPF1/SMG7-mediated decay of CDKN1A mRNA was TRIM71-dependent.

These data, together with the previous luciferase assays and protein interaction studies, confirmed that TRIM71 and NMD cooperate in an interdependent manner to regulate CDKN1A mRNA, and prompted us to investigate whether other known NMD targets and TRIM71 targets were also regulated by the here-reported TRIM71/NMD axis. Interestingly, the known TRIM71 targets E2F7, HOXA5 and MYB[115], as well as FOXJ1[113] (not shown), were also upregulated upon UPF1 knockdown in the presence of TRIM71 but not in its absence, while the canonical NMD targets ATF3 and GADD45A, as well as TBL2 and GADD45B (not shown) [72,160,166,167], were all derepressed upon UPF1 knockdown regardless the presence of TRIM71 (Fig. 4.2.23D).

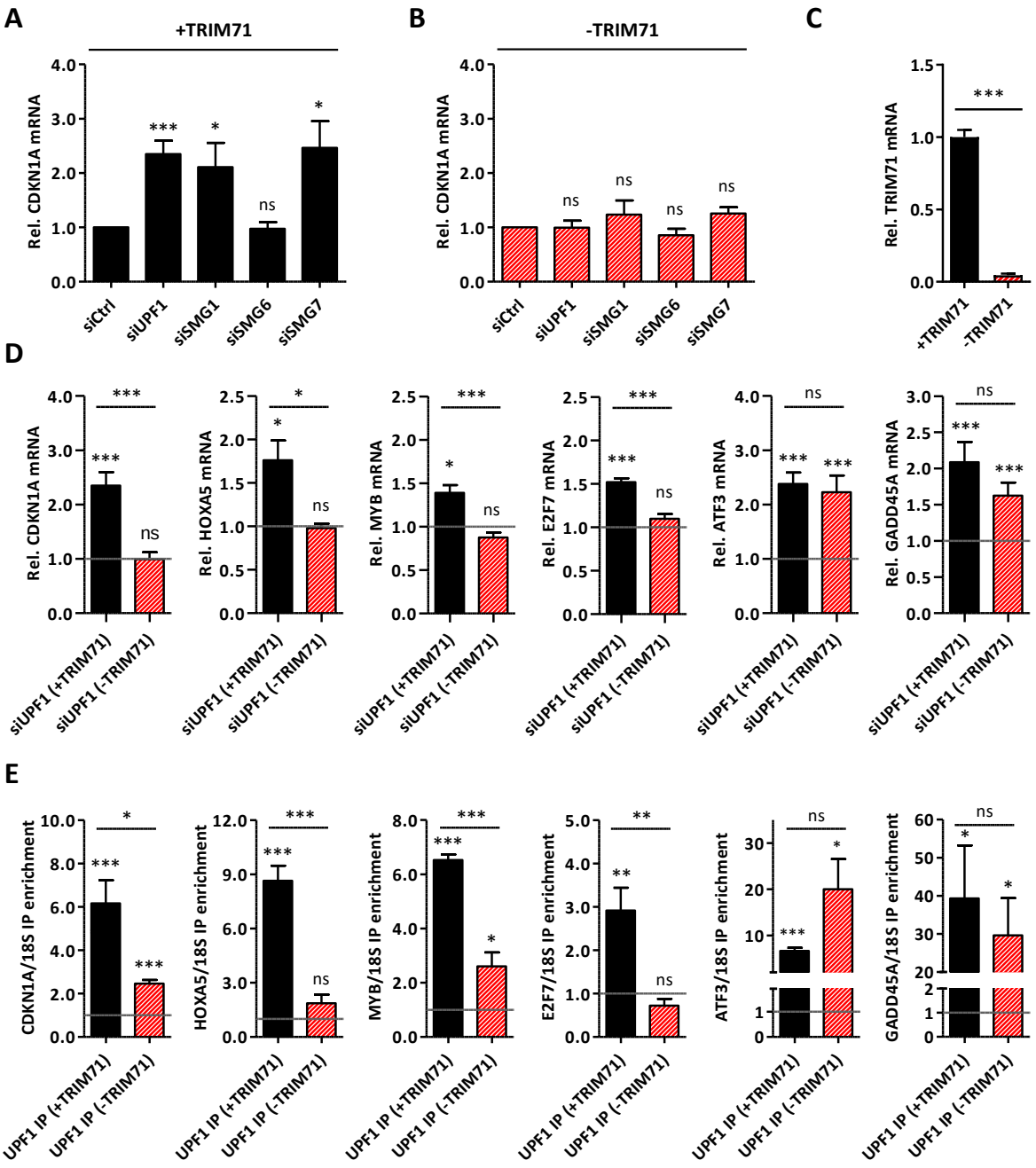

Figure 4.2.23. NMD-induced degradation of several functional mRNA targets is TRIM71-dependent. A) qPCR quantification of endogenous CDKN1A mRNA levels upon knockdown of NMD components in the presence of TRIM71 (+TRIM71) (n=4) or **B)** its absence (-TRIM71) (n=4), achieved by TRIM71 knockdown in HEK293T cells, which endogenously express low TRIM71 levels. **C)** qPCR quantification of TRIM71 levels corresponding to presence (+) and absence (-) of TRIM71 from A-E (n=3). **D)** qPCR quantification of several mRNA targets upon UPF1 knockdown (siUPF1) in HEK293T cells in the presence (+) and absence (-) of TRIM71 (n=3-6). HPRT1 housekeeping gene was used for normalization. **E)** Specific IP enrichment of several mRNA targets after RNA-IP with Flag-UPF1 (UPF1 IP) overexpressed in HEK293T cells in the presence (+) and absence (-) of TRIM71. IP enrichment was calculated as $2^{-((IP_{target}-IP_{ref})-(INPUT_{target}-INPUT_{ref}))}$, where 18S rRNA was used as a reference (ref) for normalization (n=3-4). Data in D-E represent the fold change expression (D) or fold change specific IP enrichment (E) over the control condition (siCtrl in D and Flag-Ctrl IP in E), represented as the grey line depicted in each respective graph at y=1. All graphs represent Mean ± SEM. Statistical significance was calculated with a two-tailed unpaired Student's t-test (ns = non-significant; *P-value < 0.05; **P-value < 0.01; ***P-value < 0.005). (Fig. adapted from[149]).

To evaluate whether the UPF1-mediated regulation of all those targets was achieved directly via mRNA decay, we conducted RNA-IPs in order to confirm the direct binding of UPF1 to those mRNA targets. Consistently, CDKN1A, E2F7, HOXA5 and MYB mRNAs were found co-precipitated with UPF1 overexpressed in HEK293T cells only in the presence of TRIM71, while UPF1 interaction with those mRNAs was diminished or abrogated upon TRIM71 depletion (Fig. 4.2.23E). The specific interaction of UPF1 with its canonical targets ATF3 and GADD45A was observed both, in the presence and absence of TRIM71 (Fig. 4.2.23E), as well as the unspecific interaction of UPF1 with the housekeeping HPRT1 mRNA[149] (not shown).

Of note, all included NMD targets are known to be regulated by canonical (i.e. EJC-dependent) NMD because of the existence of a PTC generated by alternative splicing (ATF3, TBL2 and GADD45A), or because of the presence of an EJC downstream of the normal stop codon, due to the existence of an intron within the 3'UTR (GADD45B)[72,160,166,167]. Thus, our results clearly showed that TRIM71 enabled the degradation of specific PTC-lacking mRNAs by NMD, while it was seemingly dispensable for the degradation of canonical NMD targets.

We next investigated whether the regulation of CDKN1A in HepG2 cells, where we had first identified TRIM71 to regulate CDKN1A mRNA and to control proliferation, was also mediated by the TRIM71/NMD axis. Interestingly, the R2 Genomic Analysis and Visualization Platform showed UPF1 and TRIM71 expression to be positively correlated in samples from patients with advanced HCC stages, being therefore the expression of UPF1 and CDKN1A negatively correlated (Fig. 4.2.24A-C). This data supported a role for the regulation of CDKN1A by the TRIM71/NMD axis in the pathogenesis of HCC.

Knockdown of UPF1 or TRIM71 in HepG2 cells led to p21 protein upregulation (Fig. 4.2.24D) and CDKN1A mRNA upregulation (Fig. 4.2.24E). Both UPF1 and TRIM71 knockdowns relieved CDKN1A 3'UTR repression (Fig. 4.2.24F), confirming that CDKN1A regulation occurred via 3'UTR recognition and mRNA degradation in HepG2 cells as well. Excluding any transcriptional contribution to this regulation, CDKN1A pre-mRNA levels were found unaltered upon both, UPF1 and TRIM71 knockdowns (Fig. 4.2.24G).

To further confirm a post-transcriptional regulation via mRNA decay, HepG2 cells were treated with Actinomycin D for transcriptional inhibition and the CDKN1A mRNA decay was monitored over time. The stability of CDKN1A mRNA was increased in UPF1 and TRIM71 knockdown HepG2 cells as compared to siCtrl cells (Fig. 4.2.25). HOXA5 and MYB mRNAs were also stabilized under the same conditions, while only UPF1 knockdown, but not TRIM71 knockdown, enhanced the stability of the canonical NMD target ATF3 (Fig. 4.2.25). These results were consistent with the changes in endogenous mRNA levels observed for these targets upon UPF1 and TRIM71 knockdown in HepG2 cells (Fig. 4.2.24H-K). Altogether, we were able to recapitulate our findings concerning CDKN1A mRNA degradation via the TRIM71/NMD axis also in HepG2 cells, and these results were consistent with human transcriptomic data collected from advanced-stage HCC patients, suggesting that the novel RNA surveillance mechanism identified by our work may contribute to the HCC pathogenesis.

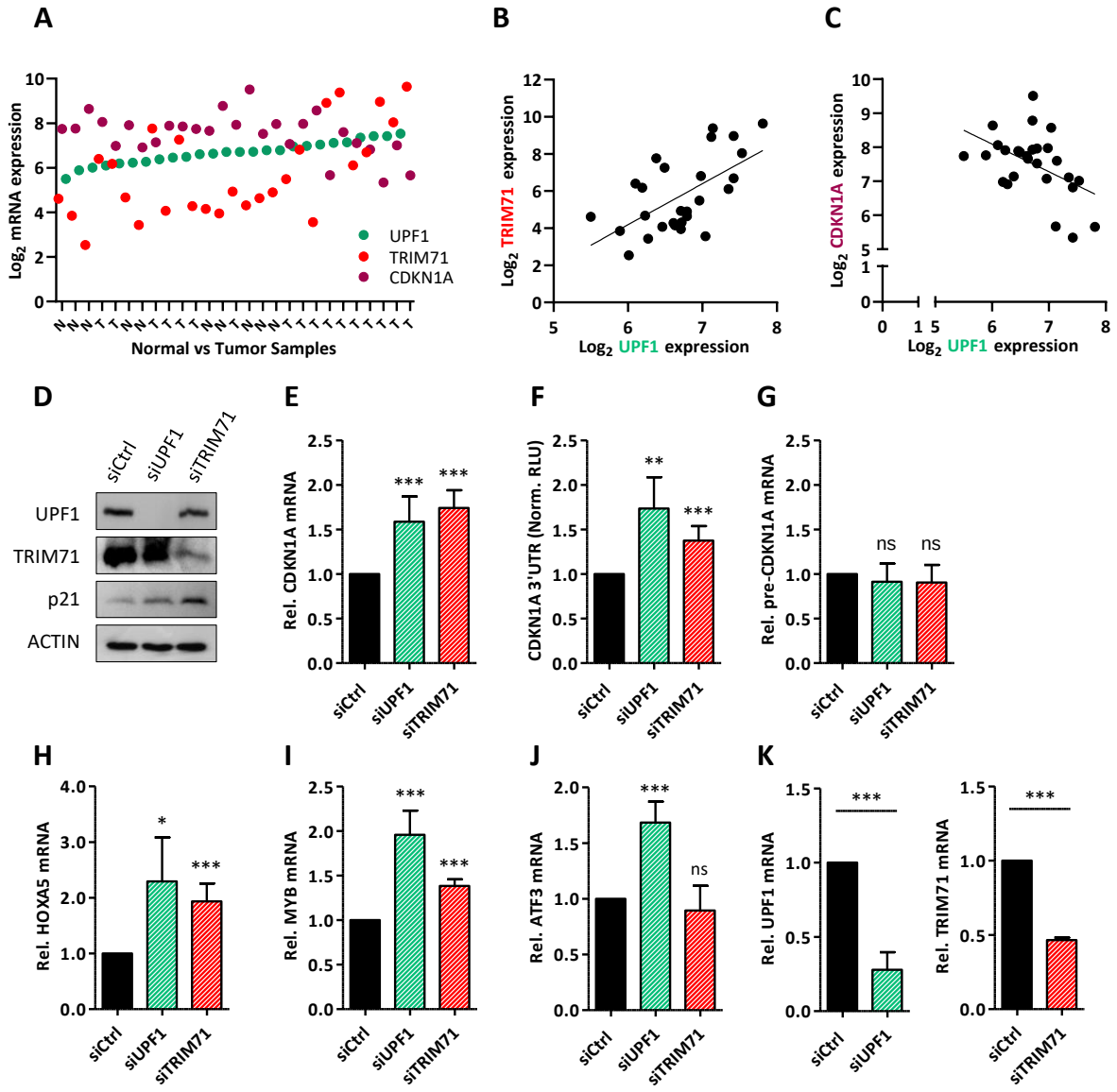

Figure 4.2.24. CDKN1A mRNA is post-transcriptionally regulated by TRIM71 and UPF1 in HepG2 cells: A) mRNA expression of UPF1, TRIM71 and CDKN1A in samples from control patients (Normal tissue) and advanced-stage HCC patients (Tumor), depicted in increasing order of UPF1 expression (n=27). **B)** Positive correlation between UPF1 and TRIM71 mRNA expression in samples from A (Pearson correlation coefficient r = +0,6; P-value = 0,0009). **C)** Negative correlation between UPF1 and CDKN1A mRNA expression in samples from A (Pearson correlation coefficient r = -0,48; P-value = 0,0122). For A-C, source: R2 Genomics Analysis and Visualization Platform (http://r2.amc.nl), Wurmbach Dataset. **D)** Immunoblot showing the upregulation p21 protein levels upon knockdown of UPF1 and TRIM71 in HepG2 cells. **E)** qPCR measurements of endogenous CDKN1A mRNA levels upon knockdown of UPF1 and TRIM71 in HepG2 cells (n=5-8). **F)** Repression of the full length CDKN1A 3'UTR luciferase reporter upon knockdown of UPF1 and TRIM71 in HepG2 cells (n=3-4). **G)** qPCR measurements of endogenous CDKN1A pre-mRNA levels upon knockdown of UPF1 and TRIM71 in HepG2 cells (n=3-6). **H)** qPCR measurements of HOXA5 mRNA levels **I)** MYB mRNA levels and **J)** ATF3 mRNA levels upon knockdown of UPF1 and TRIM71 in HepG2 cells (n=3-6). **K)** qPCR measurements of UPF1 and TRIM71 mRNA levels as knockdown controls for experiments depicted in E-J, and for the upcomming Fig. 4.2.25 (n=4). Norm. RLU = Normalized Relative Light Units. All graphs represent Mean ± SD. Statistical significance was calculated with a two-tailed unpaired Student's t-test (ns = non-significant; *P-value < 0.05; **P-value < 0.01; ***P-value < 0.005). (Fig. adapted from[149]).

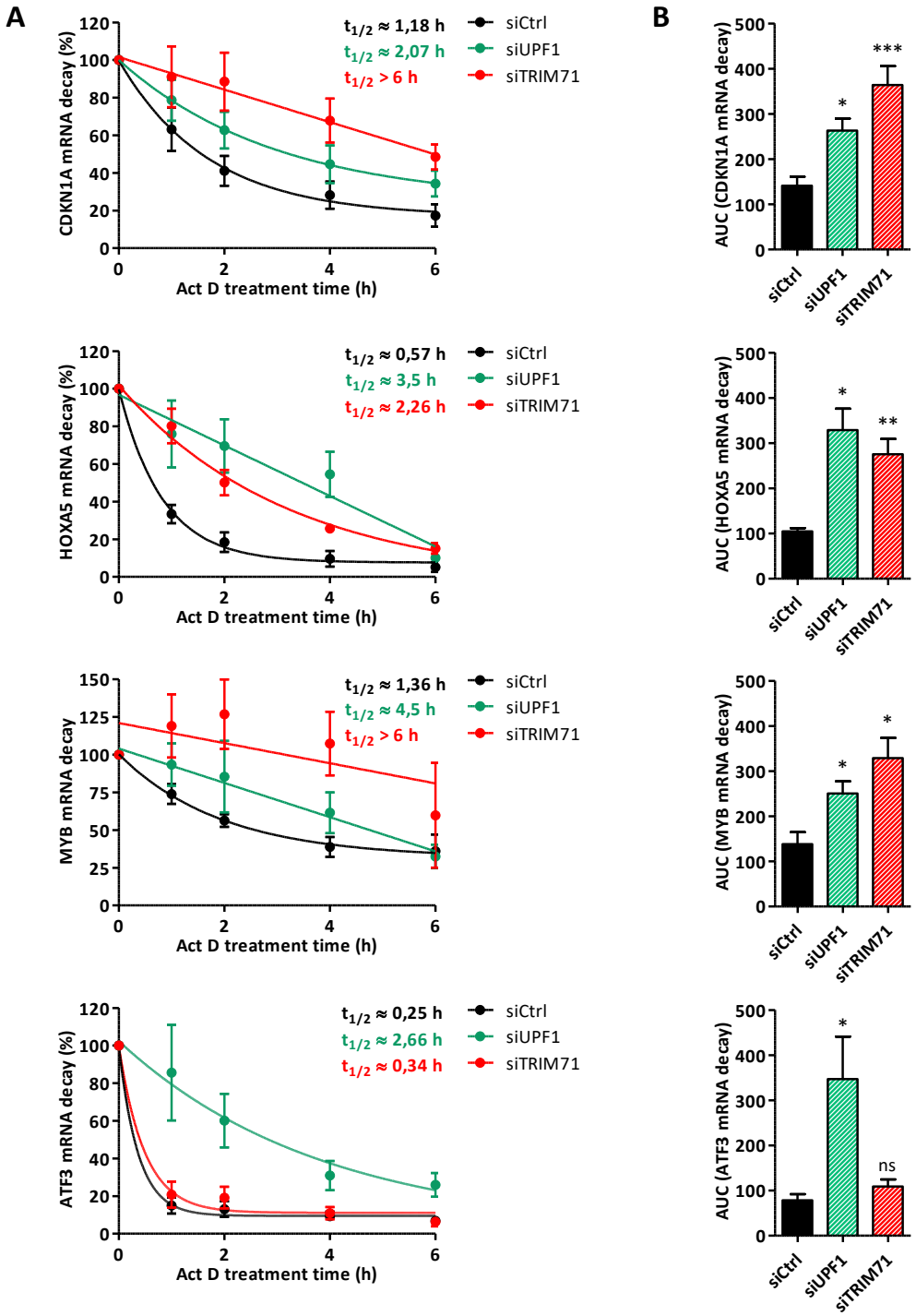

Figure 4.2.25. UPF1 knockdown in HepG2 cells enhances the stability of known TRIM71 mRNA targets. A) mRNA decay curves of the indicated targets in control (siCtrl), UPF1 knockdown (siUPF1) and TRIM71 knockdown (siTRIM71) HepG2 cells, 1h, 2h, 4h and 6h after transcriptional inhibition with 5 µg/ml of Actinomycin D. mRNA decay is depicted as percentage (%), relative to the initial amount of mRNA quantified in the DMSO control (used as time point 0h). Decay curves were adjusted by non-linear regression with GraphPad Prism7 to calculate the mRNA half-life for each target ($t_{1/2}$) as a measurement of mRNA stability. **B)** Area under curve measurements (AUC, units = % mRNA*h) of the individual decay curves whose average curves are depicted in A, calculated with GraphPad Prism7. Graphs represent Mean ± SEM (n=3-4). Statistical significance was calculated with a two-tailed unpaired Student's t-test (ns = non-significant; *P-value < 0.05; **P-value < 0.01; ***P-value < 0.005).(Fig. adapted from[149]).

4.2.6. The 3'UTR length plays a key role in target regulation via the TRIM71/NMD axis

Canonical/EJC-dependent NMD occurs in PTC-containing transcripts, while non-canonical/EJC-independent NMD, also referred as *fail-safe* NMD, has been typically observed in transcripts with long 3'UTRs[55,65,168,169]. All the TRIM71 mRNA targets which we have shown to be regulated by NMD/UPF1-dependent mechanisms had a long 3'UTR (>750 bp), suggesting that 3'UTR length played a key role in the TRIM71/NMD axis reported by our work. Interestingly, a previous study identified CDKN1A as a target of NMD in P19 cells[71], which of note, are known to express TRIM71[41,148]. The regulation of CDKN1A by NMD was attributed to an upstream open reading frame (uORF) present in one of the transcript variants encoding for CDKN1A[71,170].

There are five described CDKN1A transcript variants (TVs), all of which share the main coding sequence and 3'UTR but differ in their 5'UTR (Fig. 4.2.26A). CDKN1A TV1, TV2, TV4, and TV5, all encode for same p21 isoform, whereas TV3 encodes for a longer isoform, containing 34 extra aa in the N-terminus due to the presence of an uORF. uORFs are NMD-inducing features because they can lead to the appearance of a PTC upon alternative frame-reading. However, the reading frame of TV3 is unaltered because its uORF is in-frame with the main coding sequence, and thereby this transcript variant does not contain a PTC.

Furthermore, specific amplification of CDKN1A TV3 showed that this transcript variant is barely expressed in HEK293T and HepG2 cells, as compared to the significantly higher expression of CDKN1A TV1-5, which was amplified with primers recognizing all five TVs (Fig. 4.2.26A-B). It is reasonable to argue that TV3 is precisely expressed in such low levels due to its efficient degradation via NMD. However, TV3 was not upregulated upon UPF1 knockdown in HEK293T cells, while the upregulation of TV1-5 in UPF1 knockdown cells (Fig. 4.2.26C) perfectly corresponded to the CDKN1A mRNA upregulation observed in our previous experiments, in which CDKN1A was amplified with a TaqMan probe. These results demonstrated that the TRIM71/NMD-induced CDKN1A regulation reported by our work was not triggered by the uORF present in TV3, and supported the long 3'UTR of CDKN1A to be its NMD-inducing feature.

Indeed, our previous luciferase experiments have shown a TRIM71/NMD-dependent repression of the full length CDKN1A 3'UTR reporter (see again Fig. 4.2.18A-B, Fig. 4.2.20A-B and Fig. 4.2.24F). However, we have also shown a TRIM71-dependent repression of the TRE-containing F2_100-200 short fragment (see again 4.2.11D). But whether such a regulation was achieved also via NMD, or instead via other TRIM71-mediated repression mechanisms, remained to be investigated.

Therefore, we next evaluated whether the F2_100-200 reporter was derepressed upon knockdown of NMD components. The full length (FL) CDKN1A 3'UTR luciferase reporter was indeed significantly derepressed by siUPF1, siSMG1 and siSMG7 – but not siSMG6 – (Fig. 4.2.26D), as predicted from the previously observed upregulation of endogenous CDKN1A mRNA levels under the same conditions (see again Fig. 4.2.21A). However, NMD impairment did not have an effect on the regulation of the F2_100-200 reporter (Fig. 4.2.26D), confirming that 3'UTR length plays a key role for target degradation via the TRIM71/NMD axis. These results are in line with the notion that NMD is actively inhibited in short 3'UTRs[171,172], as it will be later discussed.

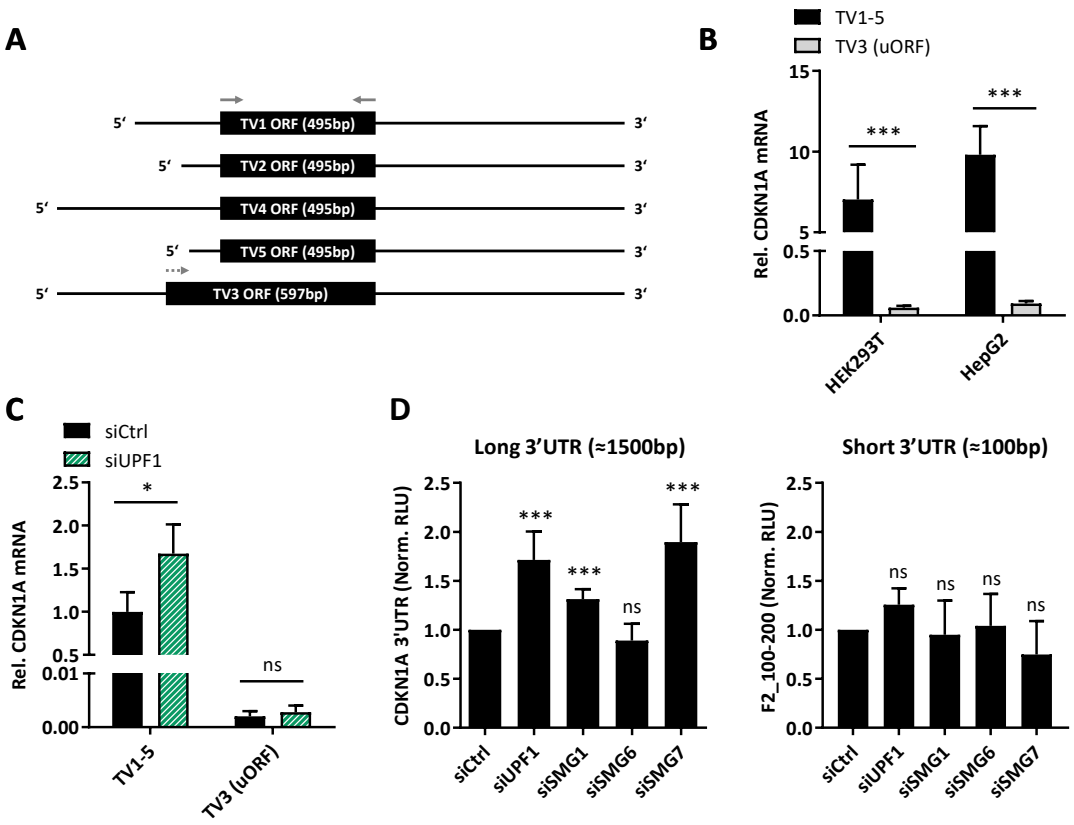

Figure 4.2.26. A long 3'UTR is the NMD-inducing feature of CDKN1A mRNA. A) Schematic representation of all transcript variants (TVs) described for the human CDKN1A gene (NCBI gene ID: 1026). Grey arrows represent the primers used for the specific amplification of TV3 versus unspecific amplification of all TVs (TV1-5), used in experiments depicted in B-C. Common forward and reverse primers (continuous-line arrows) were used for the simultaneous amplification of all TVs mRNAs (TV1-5), whereas the use of a different forward primer (dashed-line arrow) enabled the specific amplification of TV3 mRNA. **B)** qPCR measurements of endogenous CDKN1A TV3 mRNA levels and CDKN1A TV1-5 mRNAs levels in HEK293T and HepG2 cells (n=3). **C)** qPCR measurements of endogenous CDKN1A TV3 mRNA levels and CDKN1A TV1-5 mRNAs levels in HEK293T cells upon UPF1 knockdown (n=3-4). **D)** Luciferase reporter assays with the full length (FL) CDKN1A 3'UTR reporter ("long 3'UTR" reporter) and the wild type F2_100-200 reporter ("short 3'UTR" reporter) in HepG2 cells, upon knockdown of the indicated NMD components (n=3-4). For qPCRs, HPRT1 was used for normalization. Norm. RLU = Normalized Relative Light Units. All graphs represent Mean ± SD. Statistical significance was calculated with a two-tailed unpaired Student's t-test (ns = non-significant; *P-value < 0.05; *** P-value < 0.005).

Importantly, these results also highlighted that TRIM71-mediated target repression can be achieved by mechanisms that do not involve the NMD pathway. Indeed, we found that several other known TRIM71 mRNA targets[113,115] were not upregulated – some of them were even downregulated – upon UPF1 knockdown in HEK293T cells (Fig. 4.2.27A). How TRIM71 selects a given repression mechanism for each of its targets is enigmatic and remains to be investigated. In this context, comprehensive transcriptomic studies are required to expand and better characterize targets that are specifically regulated by the TRIM71/NMD axis in contrast to "TRIM71-only" targets and "NMD-only" targets (Fig. 4.2.27B). Such studies will broaden the knowledge about the principles underlying the fulfilment of this novel stem cell- and cancer-specific RNA surveillance mechanism.

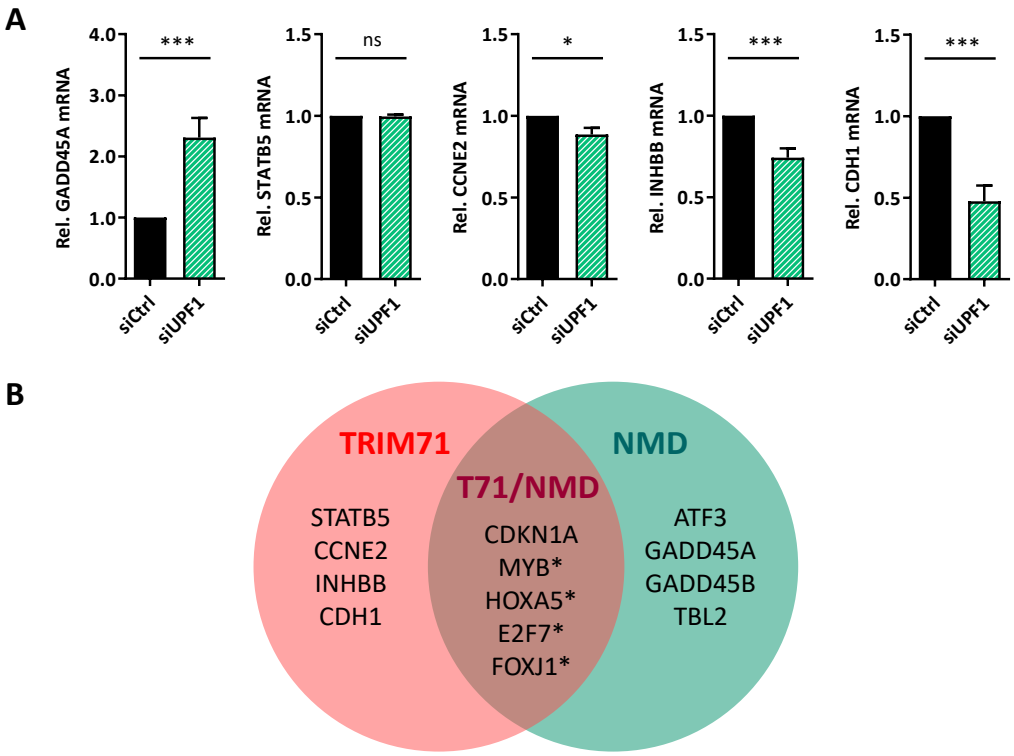

Figure 4.2.27. TRIM71 can regulate mRNA targets by NMD-dependent and NMD-independent mechanisms. A) qPCR measurements of the canonical NMD target GADD45A and the known TRIM71 mRNA targets STATB5, CCNE2, INHBB and CDH1[113,115] upon UPF1 knockdown (siUPF1) in HEK293T cells (n=3-4). HPRT1 housekeeping gene was used for normalization. All graphs represent Mean ± SD. Statistical significance was calculated with a two-tailed unpaired Student's t-test (ns = non-significant; *P-value < 0.05; *** P-value < 0.005). **B)** Venn Diagram showing the regulation of all mRNA targets used in the present study by either TRIM71-only (from results depicted in A), NMD-only, or by the TRIM71/NMD axis identified by our work. *These targets were regulated by a TRIM71/UPF1-dependent mechanism. (Fig. adapted from[149]).

4.2.7. The regulation of CDKN1A mRNA by the TRIM71/NMD axis is impaired in human Congenital Hydrocephalus

Hydrocephalus results from an accumulation of cerebrospinal fluid (CSF) within the brain, causing an increased pressure inside the skull[173]. Hydrocephalus can be acquired throughout life due to several causes including meningitis, brain tumors, traumatic brain injury, intraventricular hemorrhage, and subarachnoid hemorrhage, but is more often arising from developmental defects – thereby termed Congenital Hydrocephalus (CH) – such as neural tube closure defects[173]. CH is the most common brain malformation, affecting 1 one of every 1000 newborns[174], and yet CH pathogenesis is poorly understood and had been attributed to failed CSF homeostasis, being treated by lifelong surgical CSF shunting with substantial morbidity[111,175]. However, a recent study in a cohort of CH patients identified mutations in four genes involved in neural tube development and neural stem cell fate regulation – TRIM71 being one of them –, implicating that the disease may arise from impaired neurogenesis, rather than from active CSF accumulation[111]. Specifically, two recurrent mutations were identified in the TRIM71 gene – R608H and R796H – and both of them located at homologous positions in different NHL repeats within highly-conserved **R**PQGV motifs[111].

Crystallization of the NHL domain of homolog proteins Brat (*D. melanogaster*) and LIN-41 (*C.elegans*)[83–85] revealed that residues R608 and R796 are involved in RNA binding, and therefore the mutations R608H and R796H observed in CH patients are predicted to disrupt the RNA binding ability of the human TRIM71 protein[111]. In order to confirm this, we cloned the TRIM71 CH mutants R608H and R796H and evaluated their ability to bind and repress the CDKN1A mRNA via RNA-IPs and luciferase experiments in HEK293T cells, respectively. Similar to what we had previously observed in our ΔNHL6 mutant, both CH mutants showed RNA binding defects, as depicted by a significantly lower CDKN1A mRNA IP enrichment compared to that of the wild type TRIM71 (Fig. 4.2.28A). Accordingly, both CH mutants failed to repress the 3'UTR of CDKN1A (Fig. 4.2.28B), and their interaction with UPF1 and SMG1 correlated to their RNA binding capacity and was thereby dramatically diminished (Fig. 4.2.28C). Tethering the R796H mutant to the CDKN1A 3'UTR via the λN-BoxB system[176] was sufficient to restore its repression ability (Fig. 4.2.28D-F), demonstrating that the mutation exclusively impairs mRNA binding, but does not affect the triggering of downstream mRNA repression mechanisms.

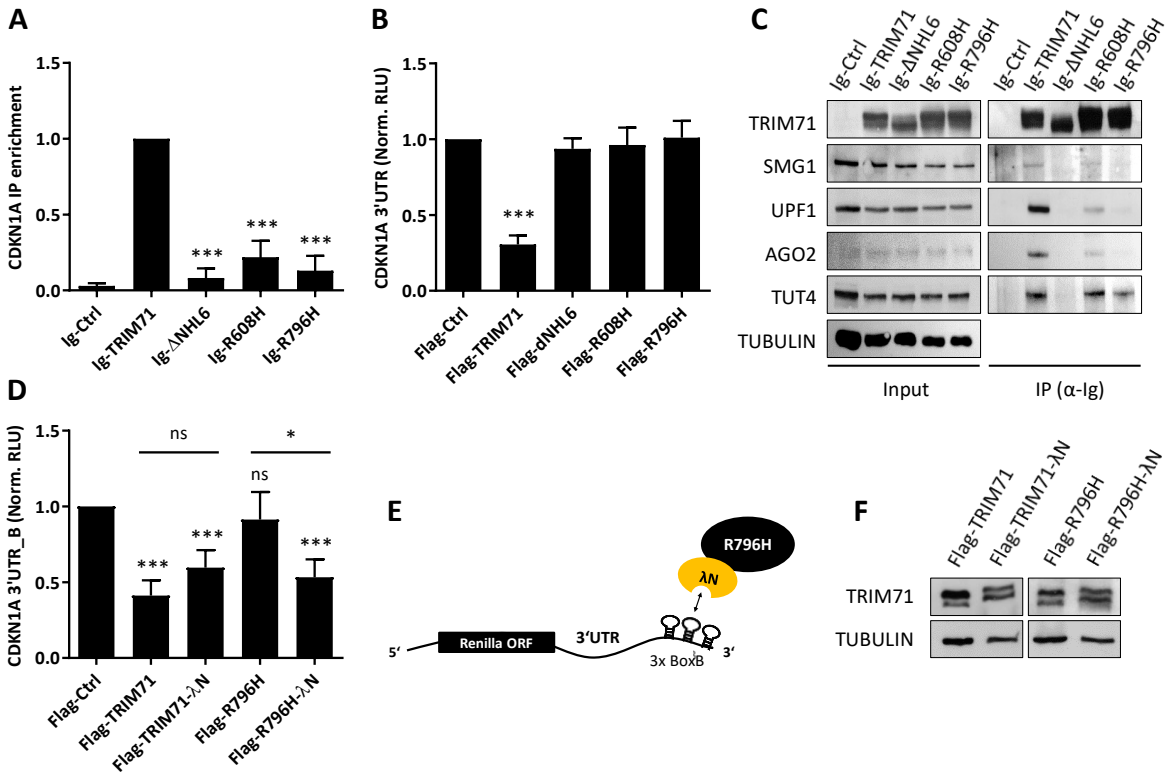

Figure 4.2.28. The TRIM71/NMD-dependent CDKN1A mRNA repression is abrogated in CH mutants due to an impaired mRNA binding ability. A) IP enrichment of CDKN1A mRNA after RNA-IP in HEK293T cells transiently transfected with Ig-Ctrl/Ig-TRIM71/Ig-ΔNHL6/Ig-R608H/Ig-R796H (n=3-4). **B)** Repression of the full length CDKN1A 3'UTR luciferase reporter in HEK293T cells transiently transfected with Ig-Ctrl/Ig-TRIM71/Ig-ΔNHL6/Ig-R608H/Ig-R796H (n=5). **C)** Representative immunoblot showing the co-precipitation of several RNA-dependent (SMG1, UPF1 and AGO2) and RNA-independent (TUT4) TRIM71 binding partners with Ig-Ctrl/Ig-TRIM71/Ig-ΔNHL6/Ig-R608H/Ig-R796H in HEK293T cells. **D)** Repression of the CDKN1A 3'UTR-3xBoxB luciferase reporter (CDKN1A 3'UTR_B) in HEK293T cells transiently transfected with Ig-Ctrl/Ig-TRIM71/Ig-TRIM71-λN/Ig-R796H/Ig-R796H-λN. **E)** Schematic representation of the λN-BoxB tethering system used in D. The fusion of the λN peptide to the C-terminus of wild type TRIM71 and mutant R796H forces their interaction with the CDKN1A 3'UTR-3xBoxB reporter mRNA. **F)** Representative immunoblot showing the expression levels of Flag-TRIM71/Flag-TRIM71-λN/Flag-R796H/Flag-R796H-λN corresponding to the experiment depicted in D. All graphs represent Mean ± SD. Statistical significance was calculated with a two-tailed unpaired Student's t-test (ns = non-significant; *P-value < 0.05; *** P-value < 0.005).

These results suggested that TRIM71-induced brain developmental defects in CH pathogenesis derive from its function as an mRNA regulator. In order to evaluate whether the impairment of TRIM71-mediated mRNA repression affected the proliferation-differentiation balance during early developmental stages, Dr. Kahle (Yale School of Medicine) kindly provided us with mESCs derived from a Trim71 R595H (analogous to human R608H) mutant mouse. We then investigated the effects of TRIM71 deficiency or the R595H mutation in the proliferation of mESCs upon induction of their differentiation into neural stem cells (NSCs). Differentiation of mESCs (OCT4+, SOX1-) into NSCs (OCT4-, SOX1+) can be achieved after 4 days in culture with N2B27 differentiation media[177].

Therefore, we first cultured wild type mESCs in N2B27 media for 4 days and measured daily changes in the protein levels of TRIM71, OCT4 and SOX1 in the course of neural differentiation. Indeed, OCT4 protein levels were progressively downregulated upon differentiation, being undetectable 4 days after N2B27 culture, whereas SOX1 levels increased in the course of differentiation. TRIM71 protein levels were also decreased upon N2B27-induced neural differentiation, but its expression was still detectable in NSCs after 4 days in N2B27 culture (Fig. 4.2.29A).

Because CDKN1A/p21 is known to increase upon neural differentiation[32], we next cultured wild type, Trim71 knockout, and Trim71 mutant R595H mESCs in N2B27 media for 4 days, and measured p21 protein levels increase as well as proliferation levels in the course of differentiation. Interestingly, a premature p21 upregulation was observed in Trim71 knockout and Trim71 mutant R595H mESCs as compared to their respective wild type parental mESCs (Fig. 4.2.29B). In wild type mESCs, p21 protein was detectable after 4 days in N2B27 culture, whereas in Trim71 knockout and Trim71 mutant R595H mESCs, p21 was already detectable after 2 days in N2B27 culture and was further upregulated after 4 days. Consistent with these results, Trim71 knockout and Trim71 mutant R595H mESCs showed a decreased proliferation in the course of differentiation as compared to their wild type counterparts (Fig. 4.2.29C-F). Although proliferation defects of Trim71 knockout and Trim71 mutant R595H mESCs seemed in principle mild, with "only" one more cell division event for both wild type mESC lines, such an effect could have dramatic consequences for the development of the CNS. Given the exponential rate of cell proliferation, translating these results to an *in vivo* context would mean that wild type mice could have up to 2-fold more NSCs than Trim71 knockout or Trim71 mutant R595H mice. The numbers of NSCs present in the developing brain certainly have an impact on the upcoming neurogenesis stages[178,179]. Given that TRIM71 expression was still observed in NSCs after 4 days in N2B27 culture, it would be interesting to evaluate whether TRIM71 plays a further role during later neurogenesis stages.

Importantly, p21 upregulation dynamics and proliferation defects of Trim71 knockout and Trim71 mutant R595H mESCs were very similar – as also the results for both wild type cell lines were highly comparable – suggesting that TRIM71-mediated mRNA repression mechanisms are responsible for such effects, and implying that the RNA-binding ability of TRIM71 plays a major role in the control of the proliferation-differentiation balance during neural development.

Altogether, our results showed that TRIM71 mutations associated with human CH disrupt TRIM71-mediated mRNA regulatory mechanisms due to an impaired mRNA binding. CH mutations thereby result in reduced proliferation levels during neural differentiation due to – at least in part – a premature upregulation of CDKN1A/p21.

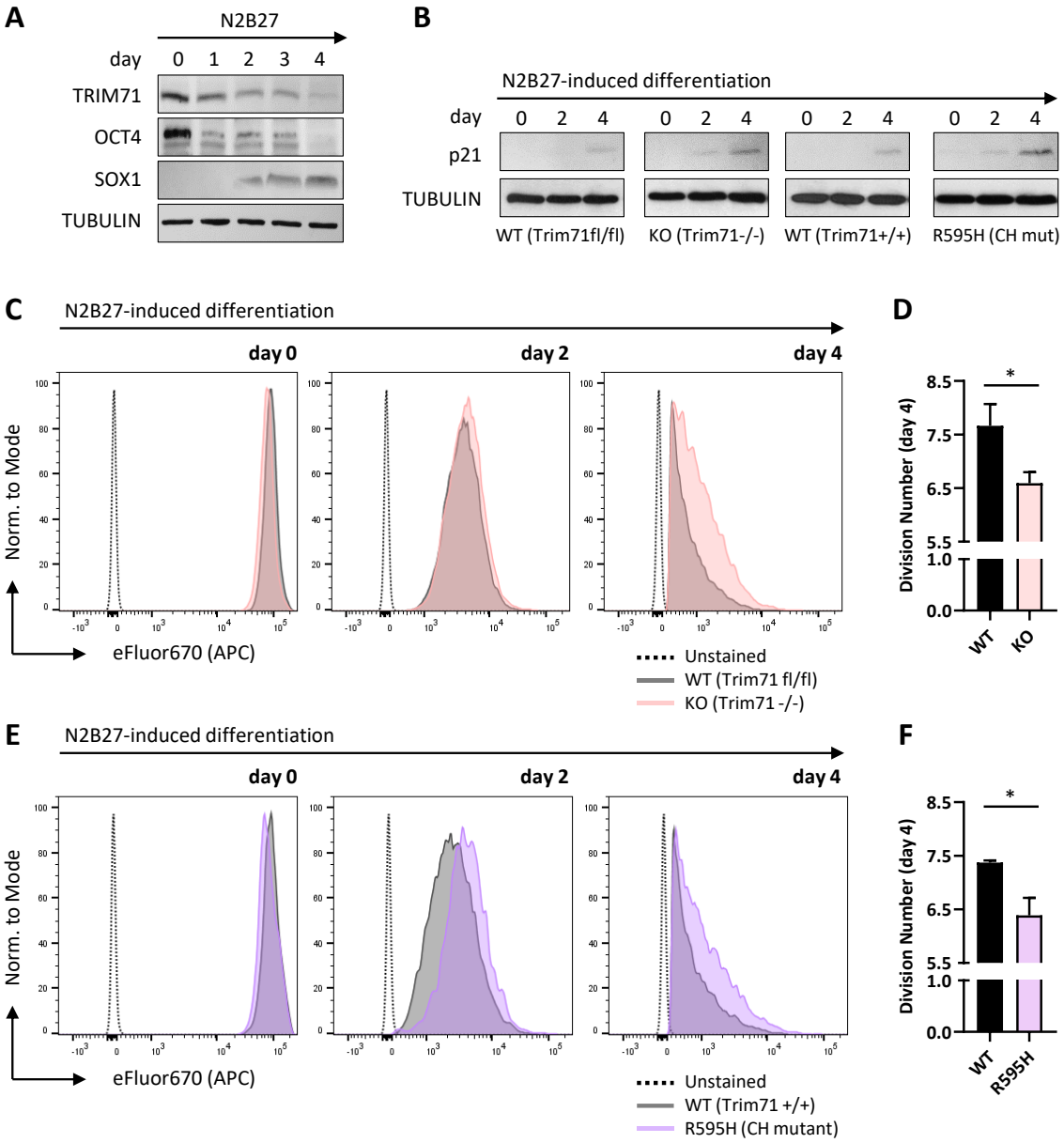

Figure 4.2.29. Trim71 knockout and CH mutant R595H mESCs show increased CDKN1A/p21 levels and reduced proliferation in the course of N2B27-induced differentiation. A) Immunoblot showing the downregulation of TRIM71 and OCT4, and the upregulation of the NSC-specific marker SOX1 in the course of differentiation, 0-4 days after wild type (WT) mESCs culture in N2B27 media. **B)** Immunoblot showing the upregulation of CDKN1A/p21 protein levels in WT (Trim71 fl/fl), KO (Trim71 -/-), WT (Trim71 +/+) and R595H (CH mutant) mESCs upon their N2B27-induced differentiation into NSCs. **C)** Overlap of APC (eFluor670) representative histograms of WT (Trim71 fl/fl) and Trim71 KO mESC populations, showing comparable staining for the different populations at the beginning of the proliferation assay (day 0), and the retardation of Trim71 KO mESCs histogram as result of a diminished proliferation in the course of of N2B27-induced differentiation (day 2 and day 4). **D)** Number of cell divisions undergone by WT (Trim71 fl/fl) and Trim71 KO mESCs differentiated into NSCs after 4 days in culture with N2B27 (n=3). **E)** Overlap of APC (eFluor670) representative histograms of WT (Trim71 +/+) and R595H mESC populations, showing comparable staining for the different populations at the beginning of the proliferation assay (day 0), and the retardation of R595H mESCs histogram as result of a diminished proliferation in the course of N2B27-induced differentiation (day 2 and day 4). **F)** Number of cell divisions undergone by WT (Trim71 +/+) and R595H mESCs differentiated into NSCs after 4 days in culture with N2B27 (n=3). All graphs represent Mean ± SD. Statistical significance was calculated with a two-tailed unpaired Student's t-test (*P-value < 0.05).

5. Discussion

5.1. TRIM71-mediated miRNA regulation

TRIM proteins of different species have been linked to the regulation of miRNA expression and activity in various manners[86]. In the present work, we investigated TRIM71-mediated miRNA regulatory mechanisms specifically focusing on the regulation of the pro-differentiation and tumor suppressor miRNA let-7, which is known to play important roles in developmental and oncogenic processes[180]. Aiming at investigating TRIM71-mediated regulation of both, miRNA synthesis and miRNA activity, we were able to clarify the controversial role of TRIM71 in the LIN28/let-7 axis, and have provided novel data concerning the functional outcome of the interaction between TRIM71 and AGO2.

5.1.1. TRIM71 downregulates let-7 miRNA expression by enhancing the TUT4/LIN28-mediated degradation of pre-let-7 miRNAs

Previous studies in our lab showed that TRIM71-deficient mESCs have an altered miRNA landscape, with upregulated pro-differentiation and tissue-specific miRNAs and downregulated ESC-specific miRNAs[113]. Let-7 family members were some of the strongest upregulated miRNAs in TRIM71-deficient mESCs[113], and such an upregulation seemed to be achieved by TRIM71 in cooperation with the let-7 repressor LIN28A, since a double TRIM71-LIN28A knockout mESC line did not show any additional let-7 upregulation to that observed in single LIN28A knockout mESCs (unpublished data). Previous studies revealed controversial functions of TRIM71 in the regulation of let-7 expression: on one hand, and in line with our observations in mESCs, TRIM71 was proposed to cooperate with LIN28A in the repression of let-7 expression in HEK293T cells[105]. On the other hand, TRIM71 was claimed to indirectly upregulate let-7 expression in HEK293T cells, NIH3T3 fibroblasts and NCI-H1299 lung cancer cells via ubiquitylation and proteasomal degradation of the paralog protein LIN28B[140,141]. In light of all these findings, we aimed at clarifying the role of TRIM71 in the regulation of let-7 expression and its interaction with LIN28A and LIN28B proteins.

Stable overexpression of TRIM71 in HEK293 cells resulted in the downregulation of let-7a and let-7g mature miRNAs, but did neither affect the expression of the housekeeping miR-16 nor decreased LIN28B protein stability. Previous studies in our lab showed that TRIM71-deficient mESCs, as well as LIN28A-deficient mESCs, upregulate mature let-7a/g but not pri- or pre-let-7a/g molecules (unpublished data), suggesting that, like LIN28A, TRIM71 inhibits let-7 expression by blocking its maturation at the last stage of let-7 biogenesis (processing of pre-let-7 to mature let-7). Because both LIN28 proteins bind pre-let-7 molecules to block their maturation and promote their degradation via recruitment of TUT4/TUT7-

uridylating activities[48,147,181], we investigated the ability of TRIM71 to interact with LIN28 proteins. TRIM71 bound both LIN28A and LIN28B proteins in HEK293T cells in a RNA-independent and E3 ligase function-independent manner via its NHL domain. However, our EMSA studies showed that TRIM71 NHL domain could neither interact with LIN28A directly, nor with the pre-let-7 miRNA, whereas LIN28A directly bound the pre-let-7 miRNA but not the housekeeping pre-miR-16. Collectively, these data supported a TRIM71-mediated regulation of pre-let7 – but not of pre-miR-16 – via LIN28 binding, but revealed the requirement of a third party to mediate the interaction between TRIM71 and the LIN28/pre-let-7 complex. We discovered that the uridylating-enzyme TUT4 was meeting these requirements. TRIM71 bound TUT4 via its NHL domain also in a RNA-independent and E3 ligase function-independent manner, and the interaction between TRIM71 and LIN28B was disrupted upon TUT4 knockdown in HEK293T cells. Our results revealed the formation of a TRIM71/TUT4/LIN28/pre-let-7 complex which seems to be more efficient than the TRIM71-lacking complex in the downregulation of let-7 expression. It would be interesting to elucidate whether such a mechanism also applies to the closely-related uridylating enzyme TUT7.

Interestingly, another TRIM protein was found to mediate a similar mechanism: TRIM25 was found to enhance the TUT4/LIN28-mediated pre-let-7 degradation[182]. Specifically, TRIM25, which lacks a NHL domain, was found to directly interact via its CC region with the LIN28A/pre-let-7 complex and to enhance TUT4-mediated pre-let-7 uridylation. The role of TRIM25 as an E3 ligase in this context was not investigated, and the exact mechanism of uridylation enhancement remains to be elucidated, since a direct interaction between TRIM25 and TUT4 was not demonstrated[182]. Nevertheless, such a mechanism revealed the existence of miRNA-specific cofactors that stimulate TUT4-mediated uridylation[182]. We therefore propose that TRIM71 may also enhance pre-let-7 degradation by stimulating TUT4-mediated uridylation (Fig. 5.1, left panel). In order to confirm this, future studies should investigate the uridylation levels of pre-let-7 in the presence and absence of TRIM71.

Furthermore, our results showed that the NHL domain of TRIM71 was not able to directly interact with the pre-let-7 miRNA. Accordingly, a previous study investigated the repertory of pre-miRNA-binding proteins within mESCs, and identified TRIM71 as one of them for its binding to pre-miR-1 and pre-miR-29a, but not pre-let-7 species[129]. These findings, together with our results, indicate that the interaction of TRIM71 with the pre-let-7 is only indirectly bridged by the TUT4/LIN28 complex, and therefore TUT4 and LIN28, but not TRIM71, are responsible for the pre-miRNA target specificity. Thus, it is reasonable to assume that TRIM71 may be able to enhance the degradation of other pre-miRNAs reported to be regulated by the TUT4/LIN28 axis. Indeed, TRIM71-deficient mESCs showed an upregulation of miR-9 and miR-200 species[113], both of which are pro-differentiation[183] and tumor suppressor miRNAs[184] whose precursors are downregulated via TUT4/LIN28-mediated degradation[147,183].

Altogether, we have confirmed that TRIM71 is a repressor of let-7 expression and have characterized the controversial interactions of TRIM71 with both LIN28 proteins. We furthermore found that these interactions are mediated by the TUT4 enzyme, uncovering a new TRIM71 binding partner which is also connected to miRNA biogenesis and at the same time strengthening our hypothesis of TRIM71 cooperation with LIN28 proteins for the downregulation of let-7 expression.

5.1.2. TRIM71 represses let-7 miRNA expression and activity via two independent mechanisms

The cooperation of TRIM71 and LIN28 proteins in the repression of let-7 expression was first confirmed in mESCs, which express endogenous LIN28A, but not LIN28B. Overexpression of TRIM71 in wild type mESCs resulted in mature let-7 downregulation, but had no effect on mature let-7 levels in LIN28A knockout mESCs. Furthermore, overexpression of TRIM71 in HEK293T cells, which express LIN28B, but not LIN28A, resulted in a moderate but significant downregulation of mature let-7 levels, but had no effect on mature let-7 levels in mouse NIH3T3 and human Jurkat E6.1 cells, which lack the expression of both LIN28 proteins. Consistent with the E3 ligase function-independent interaction of TRIM71 with TUT4/LIN28, overexpression of the TRIM71 ubiquitylation mutant C12LC15A led to a downregulation of let-7 expression – similar to that induced by the wild type TRIM71 – in mESCs and HEK293T cells, but had no effect on let-7 levels in neither NIH3T3 nor Jurkat E6.1 cells. Collectively, these data demonstrated that TRIM71-mediated let-7 expression regulation is LIN28-dependent.

Whereas the LIN28A/TUT4-mediated pre-let-7 regulation occurs in the cytoplasm, LIN28B-mediated regulation of let-7 miRNAs can additionally occur in a TUT4-independent manner inside the nucleus, where LIN28B is known to bind pri- and pre-let-7 molecules preventing their further processing and cytoplasmic export[50]. However, LIN28B localization is not exclusively nuclear, and its cytoplasmic uridylation-dependent pathway is known to actively participate in blockade of let-7 biogenesis[147,185]. Given the cytoplasmic localization of TRIM71[41,105], the efficiency of TRIM71-mediated let-7 regulation in LIN28B-expressing cells is limited by the cytoplasmic amount of LIN28B, and may vary among cell types. This may explain why TRIM71-mediated let-7 downregulation was more efficient in mESCs than in HEK293T, expressing LIN28A or LIN28B, respectively.

Our luciferase miRNA reporter assays revealed the existence of a TRIM71-mediated LIN28/TUT4-independent regulation of let-7 activity. In contrast to what we had observed for let-7 expression regulation, let-7 activity regulation was only mediated by wild type TRIM71 – but not by the ubiquitylation mutant C12LC15A – and was also observed in LIN28-lacking NIH3T3 and Jurkat E6.1 cells. Furthermore, TRIM71-mediated let-7 activity regulation was not impaired upon LIN28B or TUT4 knockdown in HEK293T cells and did not rely on let-7 degradation. The *D. melanogaster* orthologue protein Mei-26 had also been reported as a miRNA repressor but in such a case Mei-P26 decreased global miRNA expression levels[119]. However, the *C. elegans* orthologue protein NHL-2 and mammalian TRIM32 were also found to affect miRNA activity downstream of miRNA biogenesis – i.e. without influencing miRNA expression levels –[94,96]. Consistently, TRIM71-mediated let-7 activity regulation was not only observed for endogenously expressed let-7, but also upon overexpression of an already matured let-7 miRNA mimic molecule, bypassing the LIN28/TUT4-dependent regulation which operates at the pre-let-7 stage. Collectively, our data demonstrated that TRIM71 is able to mediate two distinct let-7 regulatory mechanisms, and while the regulation of let-7 expression was mediated via the LIN28/TUT4-induced pre-let-7 degradation, the regulation of let-7 activity operated at the mature miRNA stage and was LIN28/TUT4-independent.

A substantial regulation of miRNA expression levels is expected to impact on the overall miRNA activity, leading to altered levels of its mRNA targets. TRIM71 overexpression induced quite a strong let-7 downregulation in mESCs, but the activity of let-7 was unaltered in these cells as shown by unaltered levels of the let-7 reporter. This may be explained by the presence of ESC-specific mechanisms known to

counteract the activity of differentiation-promoting miRNAs such let-7[42,186]. Accordingly, although let-7 family members were significantly upregulated in Trim71-deficient mESCs, let-7 targets were not significantly altered in these cells[113], demonstrating that, regardless of the levels of let-7, this miRNA remains mostly inactive during pluripotent stages. Such mechanisms may also be responsible for the co-existence of primed neural differentiation programs and yet intact stemness of Trim71-deficient mESCs[113].

5.1.3. TRIM71 regulates specific miRNA activity via AGO2 binding

In an earlier study, Rybak *et al* claimed that TRIM71 is an inhibitor of miRNA-mediated silencing, a function that was presumably achieved via AGO2 protein ubiquitylation and proteasomal degradation, followed by a consequent reduction of overall miRNA activity[105]. Consistent with these findings, wild type TRIM71 – but not ubiquitylation mutant – repressed let-7 activity in wild type HEK293T cells, and such a repression was abrogated in AGO2 knockout HEK293T cells, confirming that TRIM71-mediated let-7 activity repression depends on AGO2. Importantly, such an effect was not due to a global impairment of the miRNA pathway in AGO2 knockout cells, since overexpression of let-7 resulted in successful repression of its *bona fide* mRNA target HMGA2.

Furthermore, deletion of the whole TRIM71 NHL domain (RBCC) or only the last NHL repeat (ΔNHL6) abrogated AGO2 interaction, and let-7 activity regulation was consistently impaired for both RBCC and ΔNHL6 mutants. These results are in line with previous findings showing that TRIM71 interacts with AGO2 via its NHL domain[41,115], in contrast to the results of Rybak *et al.*, who claimed that this interaction was mediated by the TRIM71 CC region[105]. Drosophila orthologues Brat and Mei-P26, as well as the putative Drosophila TRIM71 Wech/Dappled, were all found to interact with AGO1 via their NHL domain, but in neither case such an interaction resulted in reduced AGO1 protein stability[119]. Similarly, although our results show that TRIM71-dependent let-7 activity regulation depends on TRIM71 intrinsic E3 ligase activity and AGO2 interaction, we and others[41,106,113,115] have not observed TRIM71-mediated changes in AGO2 stability. Consistently, we did neither observe an overall reduction of miRNA activity mediated by TRIM71, but rather a specific activity repression of pro-differentiation miRNAs such as let-7a, let-7g and the brain-specific miRNA-128, whereas the activity of other miRNAs such as miR-16 or miR-19 was unaltered upon TRIM71 overexpression in HEK293T cells. Interestingly, *C. elegans* NHL-2 and mammalian TRIM32 were also found to affect the activity of specific miRNAs – but not overall miRNA activity –, without altering miRNA expression levels and without affecting AGO2 protein stability[94,96]. Specifically, both NHL-2 and TRIM32 were found to enhance the activity of let-7 miRNAs and to promote differentiation[94,96].

Although TRIM71- and TRIM32-mediated miRNA activity regulation result in opposite functional outcomes regarding the control of the proliferation-differentiation balance, the mechanisms employed by these proteins to regulate miRNA activity seem to be highly similar: both proteins interact with AGO2 via their NHL domain, and affect the activity of a specific miRNA subset without altering AGO2 protein stability[94]. Interestingly, a later study showed that both TRIM32 and TRIM71 mediated AGO2 ubiquitylation without leading to their degradation[115], indicating that ubiquitylation-dependent events regulate AGO2 function without affecting its stability, and explaining why the TRIM71 ubiquitylation mutant C12LC15A was not able to repress let-7 activity in our reporter assays.

Other post-translational modifications (PTMs) have been shown to alter AGO2 function[187]. For instance, phosphorylation of AGO2 resulted in specific miRNA activity inhibition. Specifically, AGO2 phosphorylation resulted in let-7a miRNA dissociation from the RISC complex and a consequent relieve of the repression of let-7 targets[188]. We therefore propose a similar mechanism for TRIM71-mediated miRNA activity repression, in which TRIM71 interaction with AGO2 results in AGO2 ubiquitylation and consequent allosteric inhibition of AGO2 binding to specific miRNAs, being such miRNAs released from the RISC complex (Fig. 5.1, right panel). Given that TRIM71 is a mRNA-binding protein and that TRIM71-AGO2 interaction is RNA-dependent, we propose such a mechanism to operate in active RISCs, a hypothesis that is supported by the interaction of TRIM71 with other RISC components, such as DICER[105]. For instance, it is possible that TRIM71 binds to specific mRNA targets that are then "scanned" by the RISC, bringing AGO2 and TRIM71 in close proximity and leading to TRIM71-mediated ubiquitylation of AGO2, and consequent miRNA and mRNA release from the RISC. In this context, the binding of TRIM71 to such mRNAs would enhance their stability. Therefore, transcriptomic studies combined with RIP-sequencing would be the best approach to elucidate if and which mRNAs are stabilized or destabilized upon TRIM71 binding.

How such a mechanism only affects a specific subset of miRNAs remains to be investigated. A pure speculative but exciting explanation would be that TRIM71 is able to interact with specific miRNA-binding sites within the 3'UTRs of mRNAs. A RNA stem-loop structural motif has been recently identified as the *C. elegans* and *D. rerio* LIN41 binding site[85], and has been validated by the present work to be the human TRIM71 responsive element (TRE). It is possible that the binding site sequences for specific miRNAs subsets fold into TRE-similar structures, or into other architectures yet to be identified which could also be recognized by TRIM71. To start validating such a hypothesis, it would be interesting to evaluate whether TRIM71 interacts with let-7 or miRNA-128 mRNA targets, and whether mutation of miRNA-binding sites in those targets abrogate TRIM71 binding. Furthermore, such targets should then be upregulated in the presence of TRIM71. If that would be the case, and since TRIM71 is a well-known mRNA repressor, it would be required to further investigate which mechanisms govern the distinct fates – degradation or enhanced stability – of TRIM71-bound mRNAs.

5.1.4. Phosphorylation of TRIM71 and its functional relevance

Our results have shown that TRIM71 is phosphorylated in Ser26/Ser27 and predicted other phosphorylation events to occur within the RING domain. Indeed, a recent publication has reported the PKA-mediated phosphorylation of TRIM71 in Ser3[189], although whether PKA is also responsible for Ser26/27 phosphorylation remains to be investigated. Furthermore, it would be interesting to see if mutating all three Ser3/Ser26/Ser27 completely abrogates the appearance of the TRIM71 upper band or whether other phosphorylation events within the RING domain remain to be identified.

Phosphorylation of TRIM71 was found to have important implications in tumor growth and tumor immune evasion[189]. Specifically, TRIM71 was found to be upregulated in breast cancer cells where it mediated ubiquitylation of several components of the peptide-loading complex (PLC), leading to their degradation and thereby decreasing MHC-I-dependent tumor-antigen presentation. In the same context, TRIM71-mediated ubiquitylation of Rb and p53 proteins promoted proliferation and prevented apoptosis of cancer

cells. Interestingly, phosphorylation of TRIM71 in Ser3 seemed to decrease its E3 ligase function, since only hypophosphorylated TRIM71 was found associated with the ubiquitin-proteasome machinery[189].

Our results showed that the ubiquitylation mutant C12LC15A cannot be phosphorylated within the RING domain. Phosphorylation of TRIM71 was not required for the regulation of let-7 expression via the TUT4/LIN28-dependent mechanism, since such a regulation was not impaired in the C12LC15A mutant. Similarly, although the regulation of let-7 activity mediated by TRIM71 via an AGO2-dependent mechanism was indeed impaired for the C12LC15A mutant, let-7 activity regulation was not impaired for the phospho-mutants SS/VV and 14xS/V, and p-TRIM71 was not involved in AGO2 binding. These results indicated that TRIM71 RING phosphorylation does not play a role in the TRIM71-mediated miRNA regulatory mechanisms reported by our work. Interestingly, both the C12LC15A and SS/VV mutants showed a mild reduction of the repression of the CDKN1A 3'UTR, indicating that ubiquitylation-dependent events may be involved in the fine-tuning of TRIM71 function as a mRNA repressor and/or that phosphorylated TRIM71 may be more efficient in such a function, as it is less efficient as an E3 ligase[189]. Together, these findings suggested that phosphorylation of TRIM71 may control the switch between its E3 ligase and mRNA repression functions. The implications of phosphorylation and other PTMs in TRIM71 function are just now beginning to emerge and remain to be further investigated.

5.1.5. Graphical Summary

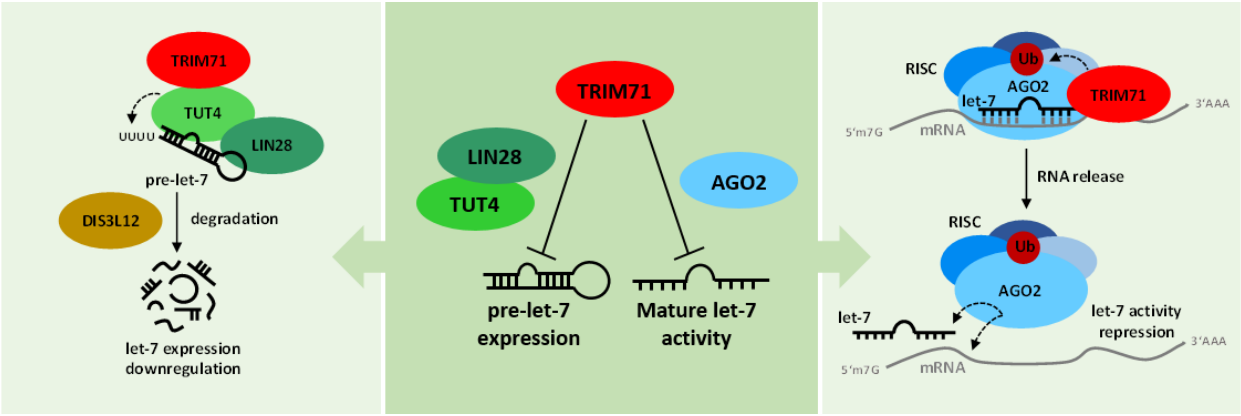

Figure 5.1. Mechanisms of TRIM71-mediated let-7 miRNA regulation. Our findings (middle panel) reveal two distinct mechanisms by which TRIM71 inhibits miRNA expression and activity independently. On one hand, TRIM71 downregulates the expression of let-7 miRNAs by targeting the pre-let-7 molecule for degradation via a TUT4/LIN28-dependent mechanism. Our working model for this mechanism (left panel) depicts the interaction of TRIM71 with TUT4, which in turn bridges to the LIN28/pre-let-7 complex. The interaction of TRIM71 with the TUT4/LIN28/pre-let-7 complex is mediated by TRIM71 NHL domain in a RNA-independent manner. TRIM71-mediated let-7 expression downregulation does not rely on its E3 ligase function. We propose that TRIM71 binding enhances the TUT4-mediated uridylation of the pre-let-7 miRNAs. On the other hand, TRIM71 represses the activity of the mature let-7 miRNA via an AGO2-dependent mechanism. Our working model for this mechanism (right panel) depicts the interaction of TRIM71 with AGO2, presumably occurring within the active RISC. Such an interaction is mediated by TRIM71 NHL domain in a RNA-dependent manner and does not affect AGO2 protein stability nor global miRNA activity. However, TRIM71-mediated let-7 activity repression is indeed dependent on its E3 ligase function. We therefore propose that TRIM71-mediated ubiquitylation of AGO2 results in the allosteric inhibition of AGO2-RNA binding, inducing the release of the miRNA and mRNA from the RISC. TRIM71-mediated let-7 activity repression thereby occurs without inducing changes in the miRNA expression levels.

5.2. TRIM71-mediated mRNA regulation

TRIM71 belongs to the TRIM-NHL protein family. Its structural domain organization enables TRIM71 function, on one hand, as an E3 ligase via its RING domain, and on the other hand, as an mRNA repressor via its NHL domain. Although TRIM71 has been reported to repress a significant number of mRNA targets[41,53,113,115], the exact mechanisms for target recognition and repression remain largely elusive. In this chapter, we have investigated the molecular requirements for TRIM71-mediated mRNA recognition and repression using CDKN1A/p21 mRNA as a model target, since this cell cycle inhibitor and tumor suppressor is known to play important roles in development and cancer[32,190,191].

5.2.1. TRIM71 represses the expression of CDKN1A/p21 via 3'UTR recognition followed by mRNA degradation, and promotes cancer cell proliferation

Genomic analysis and visualization platforms such as R2 and GEPIA showed the pathological upregulation of TRIM71 in several cancer types, including hepatocellular carcinoma (HCC/LIHC), acute myeloid leukemia (AML), testicular germ cell tumors (TGCT) and neuroblastoma. Our experiments confirmed a high TRIM71 expression in HepG2 (HCC), NCCIT (TGCT) and SKNBE2 (neuroblastoma) cancer cell lines. A previous study showed that 50% of HCC patients have an upregulated TRIM71 expression which is correlated with advanced tumor stages, earlier tumour recurrence and poor prognosis[107]. The same study postulated that TRIM71 controlled the proliferation of several HCC cell lines via AGO1/2 protein destabilization[107]. However, as mentioned before, these findings could not be reproduced in later studies[41,106,113,115]. Similarly, we did not observe TRIM71-dependent changes in the stability of AGO2 in any of the cell lines tested, which included not only HepG2 cells, but also HEK293T, NCCIT, TCam-2 and mESCs. Furthermore, key components of the miRNA pathway, such as DROSHA, DGCR8, AGO1, and AGO2, are frequently upregulated in HCC[192], and AGO2 has been found to promote HCC progression, tumor vascularization[193] and metastasis[194]. In line with those findings, we showed TRIM71 and AGO2 expression to be positively correlated in HCC patient samples. We found, however, a negative correlation between TRIM71 and CDKN1A expression in samples from advanced-stage HCC patients. Our results furthermore proved that TRIM71 regulated CDKN1A mRNA and controlled proliferation in HEK293 and HepG2 cancer cells, in line with earlier findings in mESCs and EC cells[41].

Previous studies in *C. elegans* showed that CeLIN41-mediated mRNA silencing was achieved via either 3'UTR recognition followed by mRNA degradation or via 5'UTR recognition followed by translational inhibition[126]. We found that overexpression of TRIM71 in HEK293T cells resulted in the repression of a full length CDKN1A 3'UTR reporter – but not of a CDKN1A CDS reporter –, and conversely, knockdown of TRIM71 in HepG2 cells relieved the repression of the CDKN1A 3'UTR reporter. These results correlated with changes in the levels of endogenous CDKN1A mRNA mediated by TRIM71 in those cells, indicating that the regulation of CDKN1A is achieved via 3'UTR recognition and mRNA degradation. However, we cannot exclude a simultaneous regulation through 5'UTR binding. Given that five different transcript variants encode for the human CDKN1A mRNA and that all of them differ in their 5'UTR, reporter assays for all different 5'UTRs should be conducted to evaluate whether translational inhibition occurs, and for which of those transcript variants. In this regard, it would be interesting to investigate the expression pattern of the different CDKN1A transcript variants in development and cancer.

5.2.2. TRIM71 directly interacts with a structural RNA motif present in the 3'UTR of CDKN1A mRNA via its NHL domain

TRIM71 has been described as a mRNA[128] and miRNA[129] binding protein, and many protein interactions mediated by TRIM71 are indeed RNA-dependent[105,115]. Via specific RNA binding, TRIM71 lies in close proximity to other RBPs which might assist its mRNA repressive role. The NHL domain of orthologue proteins Brat (*D. melanogaster*), CeLIN41 and DrLIN41 has a β-propeller WD40-like structure – a domain present in other RNA binding proteins[84,128,130] – and mediates direct interaction to RNA[83,85,126]. A human TRIM71 mutant lacking the full NHL domain failed to repress its mRNA targets unless tethered to the mRNA[115], suggesting that the NHL domain of the human TRIM71 protein is also responsible for physical RNA binding. Our RNA-IPs showed that TRIM71, but not the closely-related TRIM-NHL protein TRIM32, was able to physically and specifically interact with the CDKN1A mRNA, while merely deleting TRIM71 last NHL repeat (ΔNHL6 mutant) completely abrogated mRNA binding. Consistently, only TRIM71, but neither TRIM32 nor ΔNHL6, was able to repress the CDKN1A 3'UTR reporter.

We identified several TRIM71 responsive elements along the whole CDKN1A 3'UTR and accurately located and characterized one of these elements (TRE), based on its structural similarity to the previously reported CeLIN41 responsive element (LRE)[85]. Via fluorescent polarization assays with purified components, we have demonstrated for the first time a direct interaction between the human TRIM71 protein and its target mRNA, and provided a computational model of the human NHL native structure in complex with the TRE. We proved that the NHL domain is sufficient for RNA binding, in contrast to other studies which had used the FLN-NHL domains of CeLIN41 and DrLIN41 in similar assays[85,126]. A short CDKN1A 3'UTR fragment (F2_100-200) containing the TRE was significantly repressed by TRIM71, and mutations found to disrupt the LRE structure[85] abrogated the repression of the F2_100-200 reporter and the direct binding to the TRE. A recent study showed that TRIM71 targets usually contain several TRIM71 responsive elements along their 3'UTR – consistent with our observations in CDKN1A 3'UTR –, and the number of those binding sites was correlated with the corresponding mRNA abundance, with non-significant degradation observed for targets with a single binding site[131]. Nevertheless, the same study showed a moderate TRIM71-mediated repression of a luciferase reporter containing a single binding site, as we have shown for F2_100-200, suggesting that one binding site might be sufficient for TRIM71-mediated translational inhibition whereas two or more binding sites may be required for TRIM71 to trigger mRNA degradation[131]. Collectively, our results showed that an intact NHL domain is required and sufficient for direct RNA interaction and thereby essential for mRNA target repression.

Interestingly, a mouse TRIM71 mutant model merely lacking the last NHL repeat – equivalent to our human ΔNHL6 mutant – was embryonically lethal and showed neural tube closure defects, phenocopying the total loss of TRIM71 in murine development[110]. In *C. elegans,* most of the mutations causing CeLIN41 loss of function also affected the NHL domain[99]. Furthermore, two recurrent TRIM71 mutations located in the NHL domain (R608H and R796H) have been recently identified in a cohort of congenital hydrocephalus (CH) patients[111], uncovering for the first time a role of TRIM71 in a human developmental disease. We and others[131] have proved that such mutations disrupt RNA binding. Our findings, together with the aforementioned studies, link the RNA-binding ability of TRIM71 to its essential functions during development and highlight the importance of studying TRIM71-mediated mRNA repression mechanisms.

5.2.3. TRIM71-mediated CDKN1A mRNA repression correlates with its P-body localization ability and occurs independently of the miRNA pathway

Our results have revealed a correlation between the 3'UTR repression ability of different TRIM71 constructs and their proper localization within P-bodies. Interestingly, only the TRIM71 constructs containing the CC region were able to properly co-localize with the P-body marker DCP1A and to induce significant CDKN1A 3'UTR repression. In line with our findings, previous studies showed that deletion of the TRIM domain (ΔRBCC) abrogated P-body localization[105] while deletion of the RING domain alone did not[41]. The RING domain was previously shown to be dispensable for mRNA repression[115], decoupling the E3 ligase activity of TRIM71 from this function. Accordingly, our experiments show that a RING mutant lacking ubiquitylation capability (C12LC15A) was properly localized in P-bodies and was able to mediate CDKN1A 3'UTR significant repression, while a construct consisting only of the RING domain and the two B-boxes (RBB) failed to repress the 3'UTR of CDKN1A and was not co-localized with DCP1A.

Furthermore, a previous study showed that the NHL domain of TRIM71 was necessary but not sufficient for P-body localization[41]. Consistently, our FLNNHL construct failed to localize to P-bodies and to repress CDKN1A 3'UTR, while a CCNHL construct, consisting of CC, FLN and NHL domains, resulted in efficient 3'UTR repression and was the minimal motif for P-body localization in our assays. Interestingly, the CC-FLN domains were found to be sufficient for mRNA repression when tethered to the RNA[115], demonstrating that the NHL domain is only responsible for RNA binding, whereas downstream repression mechanisms are triggered by the CC-FLN domains after binding has occurred. How exactly the FLN domain participates in mRNA repression remains to be further investigated. Altogether, our results showed that TRIM71-mediated mRNA repression depended on P-body localization and thereby is likely to occur in P-bodies. Furthermore, our data revealed that the CC region is essential for mRNA repression because it enables TRIM71 proper localization within these RNA surveillance organelles.

One of the best-characterized RNA surveillance pathways occurring in P-bodies is the miRNA-mediated mRNA silencing pathway. The murine TRIM71 protein was reported to cooperate with the ES-specific miR-302 to repress the mouse Cdkn1a 3'UTR[41]. Simultaneous miR-302 and TRIM71 knockdown resulted in additional Cdkn1a upregulation as compared to individual knockdowns, showing that such a "cooperation" involves a shared function between miR-302 and TRIM71 in repressing the target, but not proving an interdependence between them to fulfil such a function. Our results showed that TRIM71 repressed the human CDKN1A 3'UTR, which lacks the miR-302 binding site described in the mouse 3'UTR. Indeed, we had found TRIM71 to repress a short CDKN1A 3'UTR fragment (F2_100-200) in which no conserved miRNA-binding sites were predicted. Furthermore, using AGO2 and DGCR8 knockdown and knockout mouse and human cells, we clearly proved that TRIM71-mediated CDKN1A 3'UTR repression relies on factors other than AGO2 and miRNAs, similar to what was previously reported for several other TRIM71 targets[115]. Our results from the previous chapter supported a role for TRIM71 in the regulation of miRNA biogenesis and miRNA function, specifically repressing miRNA expression and activity, but we and others[115] have clearly shown that TRIM71 can efficiently repress its mRNA targets – including CDKN1A – in a AGO2- and a miRNA-independent manner.

5.2.4. TRIM71 triggers specific mRNA target degradation by Nonsense-Mediated Decay (NMD)

NMD is well known for its role as a quality control pathway in the degradation of premature termination codon (PTC)-containing transcripts, but in the recent years it has become evident that NMD functions extend beyond mere quality control, since NMD regulates ~10% of the normal transcriptome[57,195]. Transcripts harboring PTCs are targeted to NMD via the Exon Junction Complex (EJC) model[152] (canonical pathway), but the EJC-independent regulation of PTC-lacking transcripts by NMD (non-canonical pathway) remains poorly understood and often occurs in mRNAs with long 3'UTRs[64–66]. Our results showed that TRIM71-mediated repression of the CDKN1A 3'UTR – which of note, is 1500-bp long – was compromised upon NMD impairment via SMG1, UPF1 and SMG7 individual knockdowns in HEK293T cells. Consistently, endogenous CDKN1A mRNA levels were upregulated under the same conditions, suggesting that TRIM71 triggers CDKN1A mRNA degradation by NMD. We showed the co-precipitation of such NMD factors with ectopically-expressed TRIM71 in HEK293T cells and with endogenously-expressed TRIM71 in HepG2 cells. TRIM71 ubiquitylation mutant C12LC15A, which properly located to P-bodies and significantly repressed CDKN1A 3'UTR, was also found co-precipitated with UPF1 in HEK293T and mESCs. In contrast, the TRIM71 embryonic lethal mutant ΔNHL6, which neither bound CDKN1A mRNA nor repressed its 3'UTR, was not able to interact with UPF1. We demonstrated the interactions between TRIM71 and NMD components to be RNase-sensitive, suggesting that such interactions are mediated by common mRNA targets, and are thereby likely established within messenger ribonucleoprotein (mRNP) complexes.

Although CDKN1A/p21 is a well-known p53 target, our results confirmed that the TRIM71/NMD-induced regulation of CDKN1A mRNA was not indirectly mediated by p53-dependent transcriptional activation in HEK293T cells. Furthermore, TRIM71 or UPF1 knockdowns in HepG2 cells also resulted in an upregulation of CDKN1A mRNA, but did not alter CDKN1A pre-mRNA levels, excluding any p53-independent transcriptional contribution. We have confirmed that the TRIM71/NMD axis directly regulates CDKN1A mRNA post-transcriptionally, via 3'UTR recognition followed by mRNA degradation in HepG2 cells as well, since knockdown of TRIM71 or UPF1 relieved CDKN1A 3'UTR reporter activity and increased CDKN1A mRNA stability after transcriptional inhibition with Actinomycin D.

Importantly, the upregulation of endogenous CDKN1A mRNA levels upon NMD impairment was only observed in the presence of TRIM71, whereas depletion of TRIM71 impaired the regulation of CDKN1A by NMD. These results proved that TRIM71 is required for the NMD machinery to recognize CDKN1A mRNA. Indeed, we found CDKN1A mRNA co-precipitated with UPF1 in the presence of TRIM71, but such an interaction was significantly diminished upon TRIM71 depletion in HEK293T cells, demonstrating that TRIM71 enables the recruitment of the NMD machinery to the CDKN1A mRNA. Similarly, other known TRIM71 mRNA targets – all of which have a 3'UTR longer than 750 bp – were also bound and regulated by UPF1 in a TRIM71-dependent manner. In contrast, several known EJC-dependent NMD targets – all of which contain a PTC or an intron within the 3'UTR[72,160,166,167] – were bound and regulated by UPF1 in a TRIM71-independent manner. Accordingly, TRIM71 overexpression resulted in an increased SMG7 binding to eIF4E-bound mRNAs, demonstrating that TRIM71 enabled the activation of NMD for the degradation of transcripts which are under steady-state translation. These results collectively indicated that our work has uncovered a rather general mechanism – although not unique – by which TRIM71 achieve target degradation, and at the same time revealed the first RNA surveillance mechanism that enables the degradation of functional, PTC-lacking transcripts by NMD.

Importantly, our results strongly suggested that 3'UTR length plays a key role in target regulation via the TRIM71/NMD axis, since NMD impairment relieved the repression of the full length CDKN1A 3'UTR reporter but not of the short F2_100-200 reporter. The "faux 3'UTR model" described in *S. cerevisiae* postulates that the presence of either a PTC or a long 3'UTR, both result in an aberrant translation termination which triggers NMD, due to a failed interaction between the poly-A-binding protein PABP and the release factor eRF3, which is bound to the terminating ribosome[168]. A competition between PABP and UPF1 for binding to eRF3 has been reported[171]. Therefore, in short 3'UTRs, the PABP-eRF3 interaction actively inhibits NMD and promotes a normal translation termination[65,171,172,196]. Indeed, tethering PABP to an mRNA shortly downstream of a PTC inhibited its degradation by NMD[196] and conversely, extending the distance between the normal stop codon and the 3'end in a functional transcript resulted in its degradation by NMD[65].

The aberrant translation termination in transcripts with PTCs or long 3'UTRs thereby results in the recruitment of UPF1 and SMG1 together with the release factors eRF1 and eRF3 – the so-called surveillance complex (SURF)[197]. Following SURF recruitment, the EJC is known to mediate the activation of NMD in transcripts with PTCs. In the case of transcripts with long 3'UTRs, other factors present within the mRNP complex – until now unknown – must exert a EJC-like role to form a DECID-like complex that triggers NMD activation. Our work identified TRIM71 as one of these factors, which operates in a target-specific and cell-specific manner (Fig. 5.2). However, how TRIM71 mechanistically enables the NMD machinery recruitment and/or activation for the degradation of specific targets remains still unclear.

Since the interactions between TRIM71 and NMD components are RNA-dependent, such a recruitment/activation may involve allosteric-dependent interactions which are stabilized upon RNA binding. Thereby, those interactions would be favored within the mRNP complex, where they are functionally relevant. Allosteric-dependent interactions have been already described for other RBPs within mRNPs[198,199]. An interesting example is the preferential binding of the eIF4G/eIF4E complex to the bent conformation of the Poly-A-bound-PABP[200,201]. Such an interaction regulates translation in a mechanism that is able to discriminate between the mRNA-bound PABPs and the free-cytosolic PABPs[201]. As an alternative hypothesis, TRIM71 could indirectly promote the recruitment and/or activation of the NMD machinery by antagonizing NMD inhibitory molecules present in the mRNP. The fate of a given mRNA may ultimately be determined by the overall competition between NMD stimulators (e.g. EJC, TRIM71) and NMD inhibitors (e.g. PABP) present within the mRNP complex[171]. Such a competition may explain why some TRIM71 targets, as well as many long-3'UTR-containing transcripts, are indeed not regulated by NMD, since counteractive NMD inhibitory signals are most likely target-specific. In this regard, further scientific effort should be devoted to the identification of other NMD regulators that, like TRIM71, are present within mRNP complexes.

Last, since TRIM71 and NMD regulate common targets in an interdependent manner, they are likely involved in the regulation of common physiological and pathological processes. Indeed, NMD has been described to participate in several processes where TRIM71 is known to be involved[97,113]: (1) NMD promotes proliferation and prevents differentiation of several cell types[69] – including TRIM71-expressing cells such as P19 cells, mESCs, NSCs, and muscle progenitor cells[71,74]. In those cells, the downregulation of NMD activity was required for the initiation of differentiation. (2) Dysregulation of NMD has been associated with several cancer types[202], including neuroblastoma[58]. (3) NMD plays a role in maintaining

cell viability by suppressing apoptosis-promoting factors[203]. Indeed, caspases trigger apoptosis in part by cleaving UPF1 leading to the downregulation of NMD[204]. (4) Several studies highlight a role of NMD in neurogenesis and the proper development of the CNS[205–208]. For instance, UPF1 knockdown was sufficient to initiate neuronal differentiation in P19 cells - where TRIM71 is also present – result of an upregulation of several cell cycle inhibitors, including CDKN1A/p21[71]. A later study showed that the downregulation of UPF1 is required for neural differentiation *in vivo* and is mediated by miR-128, a brain-specific miRNA which is upregulated during neural differentiation[72]. Interestingly, previous studies in our lab reported a significant upregulation of miR-128 in Trim71-deficient mESCs[113] and our results from chapter I showed that TRIM71 is able to inhibit miR-128 activity. We have shown that knockdown of NMD components does not affect endogenous TRIM71 expression, but weather TRIM71 alteration affects NMD components expression – via miR-128 regulation – remains to be investigated. Given the parallelisms in physiological and pathological processes where TRIM71 and NMD are involved, further scientific effort should be devoted to the identification of other targets regulated by the TRIM71/NMD axis during development and cancer.

5.2.5. TRIM71 mutations associated with human congenital hydrocephalus (CH) disrupt several TRIM71-mediated RNA regulatory mechanisms

CH is a brain developmental disease with high incidence, difficult treatment and high morbidity[173,174]. A recent study has identified recurrent TRIM71 mutations associated with human CH – R608H and R796H – which were predicted to disrupt RNA binding[111]. Our results showed that both R608H and R796H mutants have an impaired mRNA binding ability, as was also recently confirmed in a parallel study[131]. Consequently, R608H and R796H mutants failed to interact with CDKN1A mRNA and to repress its 3'UTR. Accordingly, R608H and R796H mutants had a decreased ability to interact with NMD components. Tethering the R796H mutant to the CDKN1A 3'UTR restored the repression ability of this mutant. Of note, this experiment demonstrated that TRIM71 does not require an allosteric-dependent conformation upon RNA binding to trigger downstream repression. This fact needs to be taken into account given the aforementioned hypothesis concerning allosteric-dependent protein interactions between TRIM71 and NMD components, since it implies that only NMD components may be allosterically activated upon RNA binding to interact with TRIM71, and not *vice versa*.

Furthermore, our results showed that Trim71 knockout and R595H mutant mESCs have a decreased proliferation in the course of neural differentiation, as compared to their parental wild type mESCs. These defects may be explained by a premature upregulation of CDKN1A/p21 protein observed in Trim71 knockout and R595H mutant mESCs. Proliferation rates as well as CDKN1A/p21 protein levels were highly similar in Trim71 knockout and R595H mutant mESCs, suggesting that the R595H mutation may be able to phenocopy the total loss of TRIM71, at least at such an early developmental stage. However, it is important to highlight that TRIM71 was found dispensable for mESCs stemness maintenance[113]. Specifically, stem cell markers such as SOX2, OCT4 and NANOG were unaltered upon TRIM71 knockdown[41] or knockout[113] in mESCs, indicating that stemness was preserved even in the absence of TRIM71. TRIM71-deficient mESCs were however primed towards differentiation[113]. These findings collectively implied that TRIM71 is essential in development to prevent premature differentiation rather than to maintain

pluripotency, and suggested that the cells in which TRIM71 plays its most essential role are likely not ESCs, but rather specific progenitor cells such as NSCs/NPCs. Thus, the pathological upregulation of TRIM71 in cancer cells may promote proliferation by assisting their de-differentiation. Supporting this hypothesis, TRIM71 was used in exchange of MYC to reprogram differentiated cells into iPSCs[53].

Given that CH mutants have an impaired mRNA binding ability, whole networks of deregulated TRIM71 mRNA targets could contribute to the CH pathogenesis. Nevertheless, p21 is known to play crucial roles during neurogenesis in both the developing and the adult brain[32], and given the preliminary results of our work showing a defective CDKN1A/p21 regulation in CH mutants, it would be of great interest to investigate whether the TRIM71/NMD-dependent regulation of CDKN1A mRNA contributes to the pathogenesis of this developmental disease. Furthermore, the impaired mRNA binding ability of CH mutants also affected the RNA-dependent interaction of TRIM71 with AGO2, whereas its RNA-independent interaction with TUT4 was preserved in both CH mutants. Therefore, CH mutants likely have an impaired miRNA activity regulation, and it would be thus interesting to investigate whether the dysregulation of miRNAs such as let-7 or the brain-specific miR-128 contribute to the CH pathogenesis.

5.2.6. Graphical Summary

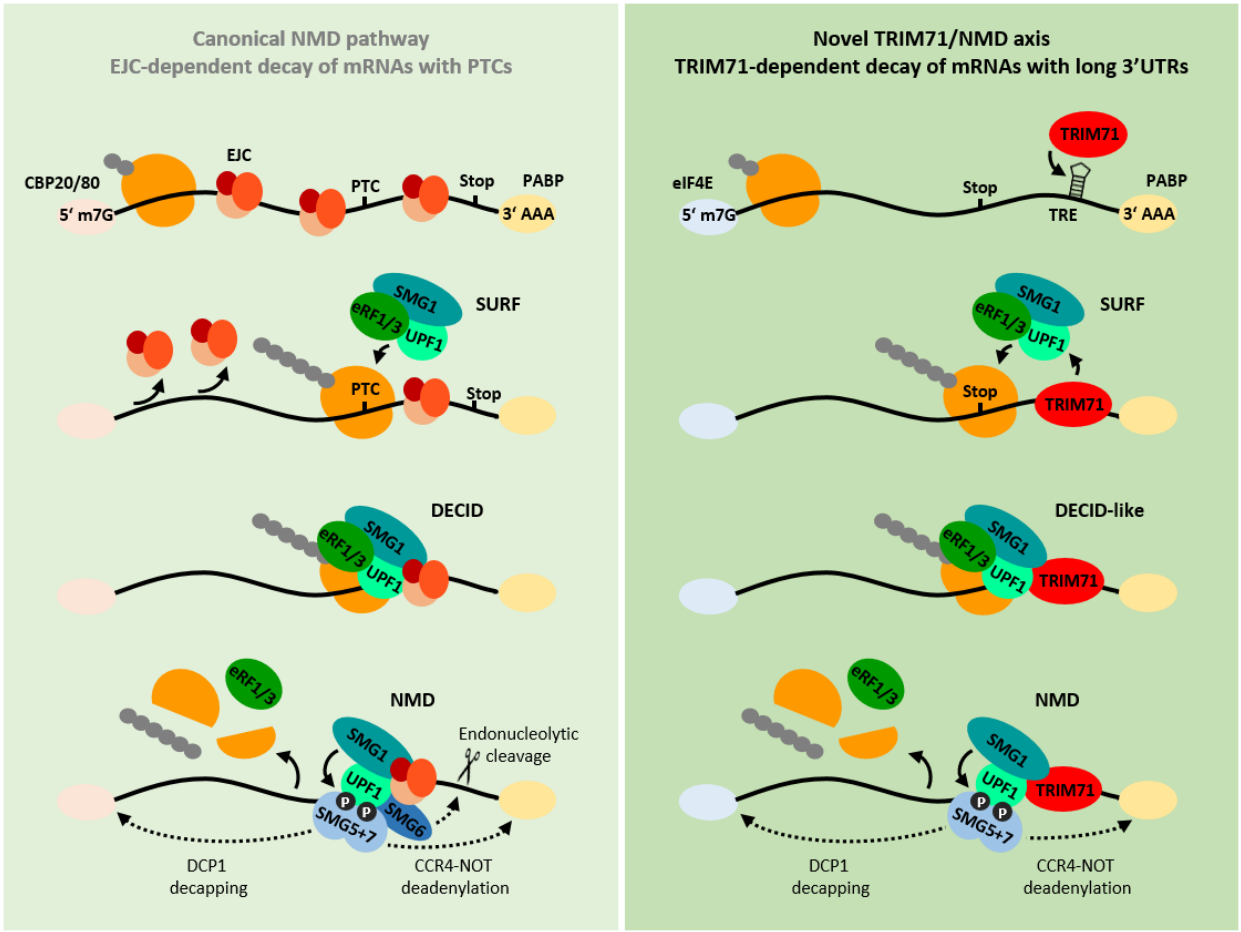

Figure 5.2. TRIM71 triggers NMD of specific mRNAs with long 3'UTRs. Canonical NMD (left panel) mediates the degradation of PTC-containing transcripts in the pioneer round of translation. The recognition of these transcripts is enabled by an EJC located downstream of the terminating ribosome, and results in the recruitment of the surveillance complex (SURF), which subsequently interacts with EJC components to form the decay-inducing complex (DECID). Such interactions activate the kinase activity of SMG1, which in turn phosphorylates UPF1. Phosphorylated UPF1 recruits the endonuclease SMG6, which cleaves the target mRNA in the vicinity of the PTC, and the SMG5-SMG7 dimer, which promote CCR4-NOT-mediated deadenylation and DCP1-mediated decapping[57]**.** Our work identified TRIM71 as a factor enabling the recognition of functional, long 3'UTR-containing transcripts by the NMD machinery (right panel). Specifically, TRIM71 binds to an RNA stem-3base-loop structural motif (TRIM71 responsive element, TRE) present in its specific mRNA targets, which are under steady-state translation, and enables the activation of SMG1/UPF1/SMG7-mediated decay for their degradation.

6. Summary

A dysregulation in the tight control of cell proliferation and differentiation severely affects developmental processes, and can lead to oncogenic transformation in the adult organism. The stem cell-specific protein TRIM71 is essential for embryonic development and has been associated with tumorigenesis in several cancer types. TRIM71 belongs to a highly-conserved family of TRIM-NHL proteins, whose structural domain organization enables their role as post-transcriptional regulators via mRNA binding, and as post-translational regulators via protein ubiquitylation. These distinct molecular functions assist TRIM71 in its role promoting proliferation and preventing premature differentiation of stem and progenitor cells, as well as cancer cells. However, a better characterization of TRIM71 molecular functions is mandatory in order to understand its essential functions in development, and eventually to design novel stem cell-/cancer-specific therapeutic strategies targeting TRIM71.

TRIM71 is known to interact with various proteins involved in the miRNA pathway, and previous studies in our lab showed that TRIM71-deficient mESCs had an altered miRNome. In the first chapter of this thesis, we have investigated the molecular mechanisms underlying TRIM71 participation in miRNA regulation. Our work has revealed that TRIM71 is able to regulate miRNA expression and miRNA activity via two independent mechanisms. Specifically, we showed that TRIM71 represses the expression of the pro-differentiation and tumor suppressor miRNA let-7 by enhancing the TUT4/LIN28-mediated degradation of its precursor miRNA pre-let-7. Our results showed that TRIM71-mediated let-7 expression regulation is entirely depending on LIN28 proteins function and does not require the TRIM71 intrinsic E3 ligase activity. To fulfill this function, TRIM71 directly interacts via its NHL domain with the uridylating enzyme TUT4, which in turn bridges TRIM71 interaction to the LIN28/pre-let-7 complex. An enhanced TUT4/LIN28-mediated degradation of pre-let-7 species may be achieved by an increased uridylation potential of TUT4 upon TRIM71 binding. Via this mechanism, TRIM71 may affect the expression of several other miRNAs regulated by the TUT4/LIN28 axis. Additionally, we showed that TRIM71 is able to regulate the activity of pro-differentiation miRNAs such as let-7 and the brain-specific miR-128, in a mechanism that depends on AGO2 binding. In contrast to the TUT4/LIN28-dependent mechanism, the AGO2-dependent mechanism affects the activity of mature miRNAs without altering miRNA expression, and requires TRIM71 E3 ligase activity, suggesting that ubiquitylation of AGO2, while not affecting its stability, may alter its binding affinity for specific miRNAs. Interestingly, the TRIM71 E3 ligase activity was also involved in reaching a TRIM71 phosphorylated status, but our data indicated that phosphorylation of TRIM71 is not involved in the TRIM71-mediated miRNA regulatory mechanisms reported by our work. The ability of TRIM71 to repress miRNA activity may be impaired in human congenital hydrocephalus (CH), since mutations R608H and R796H present in TRIM71 NHL domain have been associated with this brain developmental disease, and our results showed that such mutations abrogate the interaction between TRIM71 and AGO2.

Furthermore, TRIM71 is known to act as an mRNA repressor, but the mechanisms of mRNA target recognition and degradation remain largely elusive. The second chapter of this thesis describes the mechanistic unraveling of TRIM71-mediated recognition and repression of the CDKN1A mRNA, which encodes for the cell cycle inhibitor and tumor suppressor p21. A negative correlation between TRIM71 and CDKN1A expression has been observed in patients with advanced hepatocellular carcinoma (HCC),

and we have shown that TRIM71 represses CDKN1A/p21 expression and controls proliferation of HepG2 HCC cells. Our work has revealed that CDKN1A specific recognition involves the direct interaction of TRIM71 NHL domain with a structural RNA stem-3base-loop motif present in the 3'UTR of CDKN1A. Besides characterizing in detail the molecular requirements for specific mRNA binding, we also elucidated the domains required for subsequent mRNA repression and for the proper subcellular localization of TRIM71 within P-bodies, revealing an essential role for TRIM71 CC region in these matters. We have shown that TRIM71-mediated CDKN1A regulation is AGO2- and miRNA-independent. Instead, the Nonsense-Mediated Decay (NMD) factors SMG1, UPF1 and SMG7 assist TRIM71-mediated degradation of CDKN1A mRNA, among other targets. NMD is well known as a quality control pathway for the degradation of transcripts containing premature termination codons (PTCs), marked by the presence of an Exon Junction Complex (EJC) downstream of the terminating ribosome. However, NMD is also known to mediate the degradation of functional transcripts lacking PTCs (non-canonical NMD), although how such transcripts are recognized by the NMD machinery remains unknown. TRIM71 was absolutely required for the NMD machinery to recognize several mRNA targets, including CDKN1A, while the degradation of PTC-containing canonical NMD targets was TRIM71-independent. These findings not only identified SMG1, UPF1 and SMG7 as new TRIM71 binding partners participating in TRIM71-mediated mRNA repression, but also uncovered a role for TRIM71 in non-canonical NMD. The NMD field has long demanded the identification of EJC-like factors enabling the recruitment and/or activation of NMD for the degradation of functional, PTC-lacking transcripts. Our work has identified TRIM71 as one of these factors, which operates in a target-specific and a cell-specific manner, revealing the existence of a novel RNA surveillance mechanism which we have termed the TRIM71/NMD axis. Our results furthermore showed that 3'UTR length plays a key role in target repression via the TRIM71/NMD axis. Last, we have proved that the CH mutants R608H and R796H have an impaired mRNA binding ability, and thereby an impaired TRIM71/NMD axis. Indeed, TRIM71-deficient mESCs and TRIM71 CH mutant R595H mESCs showed a premature p21 upregulation accompanied by proliferation defects in the course of neural differentiation. Thus, the regulation of CDKN1A via the TRIM71/NMD axis, not only may play a fundamental role in tumorigenic processes such as HCC, but also in developmental diseases such as CH.

Altogether, our work has uncovered several novel mechanisms of TRIM71-mediated miRNA and mRNA regulation, and underscores the requirement of high-throughput sequencing studies for the identification of new targets of patho-physiological relevance regulated by either of these RNA surveillance pathways. Furthermore, our work will stimulate future studies to precisely elucidate the *in vivo* implications of the TRIM71-dependent dysregulation of let-7, miR-128 and CDKN1A/p21 in developmental and oncogenic processes.

Reference List

1. Can, A. (2008). A concise review on the classification and nomenclature of stem cells. *Turk J Haematol.* **25**(2):57-9

2. Blum, B. & Benvenisty, N. (2008). The Tumorigenicity of Human Embryonic Stem Cells. *Advances in cancer research* **100**, 133–158

3. Swijnenburg, R.-J. *et al.* (2008). Immunosuppressive therapy mitigates immunological rejection of human embryonic stem cell xenografts. *Proc. Natl. Acad. Sci. U. S. A.* **105**, 12991–6

4. Takahashi, K. & Yamanaka, S. (2006). Induction of Pluripotent Stem Cells from Mouse Embryonic and Adult Fibroblast Cultures by Defined Factors. *Cell* **126**, 663–676

5. Yu, J. *et al.* (2007). Induced Pluripotent Stem Cell Lines Derived from Human Somatic Cells. *Science* **318**, 1917–1920

6. Amabile, G. & Meissner, A. (2009). Induced pluripotent stem cells: current progress and potential for regenerative medicine. *Trends Mol. Med.* **15**, 59–68

7. Inoue, H. *et al.* (2014). iPS cells: a game changer for future medicine. *EMBO J.* **33**, 409–417

8. Friedmann-Morvinski, D. & Verma, I. M. (2014). Dedifferentiation and reprogramming: origins of cancer stem cells. *EMBO Rep.* **15**, 244–53

9. Wong, D. J., Segal, E. & Chang, H. Y. (2008). Stemness, cancer, and cancer stem cells. *Cell Cycle* **7**(23):3622-4

10. Batlle, E. & Clevers, H. (2017). Cancer stem cells revisited. *Nat. Med.* **23**, 1124–1134

11. Gaspar-Maia, A. *et al.* (2011). Open chromatin in pluripotency and reprogramming. *Nat. Rev. Mol. Cell Biol.* **12**, 36–47

12. Kraushaar, D. C. & Zhao, K. (2013). The epigenomics of embryonic stem cell differentiation. *Int. J. Biol. Sci.* **9**, 1134–44

13. Loh, Y.-H. *et al.* (2007). Jmjd1a and Jmjd2c histone H3 Lys 9 demethylases regulate self-renewal in embryonic stem cells. *Genes Dev.* **21**, 2545–2557

14. Feldman, N. *et al.* (2006). G9a-mediated irreversible epigenetic inactivation of Oct-3/4 during early embryogenesis. *Nat. Cell Biol.* **8**, 188–194

15. Papp, B. & Plath, K. (2013). Epigenetics of reprogramming to induced pluripotency. *Cell* **152**, 1324–43

16. Hu, C. *et al.* (2016). Energy Metabolism Plays a Critical Role in Stem Cell Maintenance and Differentiation. *Int. J. Mol. Sci.* **17**, 253

17. Gu, W. *et al.* (2016). Glycolytic Metabolism Plays a Functional Role in Regulating Human Pluripotent Stem Cell State. *Cell Stem Cell* **19**, 476–490

18. Cho, Y. M. *et al.* (2006). Dynamic changes in mitochondrial biogenesis and antioxidant enzymes during the spontaneous differentiation of human embryonic stem cells. *Biochem. Biophys. Res. Commun.* **348**, 1472–1478

19. Mukherjee, A., Kenny, H. A. & Lengyel, E. (2017). Unsaturated Fatty Acids Maintain Cancer Cell Stemness. *Cell Stem Cell* **20**, 291–292

20. Li, J. *et al.* (2017). Lipid Desaturation Is a Metabolic Marker and Therapeutic Target of Ovarian Cancer Stem Cells. *Cell Stem Cell* **20**, 303-314.e5

21. Fathi, A. *et al.* (2014). Quantitative proteomics analysis highlights the role of redox hemostasis and energy metabolism in human embryonic stem cell differentiation to neural cells. *J. Proteomics* **101**, 1–16

22. Vermeulen, K., Van Bockstaele, D. R. & Berneman, Z. N. (2003). The cell cycle: a review of regulation, deregulation and therapeutic targets in cancer. *Cell Prolif.* **36**, 131–149

23. Budirahardja, Y. & Gonczy, P. (2009). Coupling the cell cycle to development. *Development* **136**, 2861–2872

24. Sandhu, C. & Slingerland, J. (2000). Deregulation of the cell cycle in cancer. *Cancer Detect. Prev.* **24**, 107–18

25. Bonda, D. J. *et al.* (2010). Pathological implications of cell cycle re-entry in Alzheimer disease. *Expert Rev. Mol. Med.* **12**, e19

26. Li, V. C., Ballabeni, A. & Kirschner, M. W. (2012). Gap1 phase length and mouse embryonic stem cell self-renewal. *Proc. Natl. Acad. Sci. U. S. A.* **109**, 12550–5

27. Ruijtenberg, S. & van den Heuvel, S. (2016). Coordinating cell proliferation and differentiation: Antagonism between cell cycle regulators and cell type-specific gene expression. *Cell Cycle* **15**, 196–212

28. Van den Heuvel, S. & Dyson, N. J. (2008). Conserved functions of the pRB and E2F families. *Nat. Rev. Mol. Cell Biol.* **9**, 713–724

29. Sherr, C. J. & Roberts, J. M. (1999). CDK inhibitors: positive and negative regulators of G1-phase progression. *Genes Dev.* **13**, 1501–12

30. Suvorova, I. I., Katolikova, N. V. & Pospelov, V. A. (2012). New Insights into Cell Cycle Regulation and DNA Damage Response in Embryonic Stem Cells. *Int. Rev. Cell Mol. Biol.* **299**, 161–198

31. Buttitta, L. A. & Edgar, B. A. (2007). Mechanisms controlling cell cycle exit upon terminal differentiation. *Curr. Opin. Cell Biol.* **19**, 697–704

32. Cheffer, A., Tárnok, A. & Ulrich, H. (2013). Cell cycle regulation during neurogenesis in the embryonic and adult brain. *Stem Cell Rev. Reports* **9**, 794–805

33. Carnero, A. (2002). Targeting the cell cycle for cancer therapy. *Br. J. Cancer* **87**, 129–133

34. Ha, M. & Kim, V. N. (2014). Regulation of microRNA biogenesis. *Nat. Rev. Mol. Cell Biol.* **15**, 509–524

35. Mayr, F. & Heinemann, U. (2013). Mechanisms of Lin28-Mediated miRNA and mRNA Regulation—A Structural and Functional Perspective. *Int. J. Mol. Sci.* **14**, 16532–16553

36. Hutvagner, G. & Simard, M. J. (2008). Argonaute proteins: key players in RNA silencing. *Nat. Rev. Mol. Cell Biol.* **9**, 22–32

37. Broughton, J. P. *et al.* (2016). Pairing beyond the Seed Supports MicroRNA Targeting Specificity In Brief. *Mol. Cell* **64**, 320–333

38. Stadler, B. *et al.* (2010). Characterization of microRNAs Involved in Embryonic Stem Cell States. *Stem Cells Dev.* **19**, 935–950

39. Gruber, A. J. *et al.* (2014). Embryonic stem cell-specific microRNAs contribute to pluripotency by inhibiting regulators of multiple differentiation pathways. *Nucleic Acids Res.* **42**, 9313–9326

40. Wang, Y. *et al.* (2013). miR-294/miR-302 promotes proliferation, suppresses G1-S restriction point, and inhibits ESC differentiation through separable mechanisms. *Cell Rep.* **4**, 99–109

41. Chang, H.-M. *et al.* (2012). Trim71 cooperates with microRNAs to repress Cdkn1a expression and promote embryonic stem cell proliferation. *Nat. Commun.* **3**, 923

42. Wang, Y. *et al.* (2008). Embryonic stem cell–specific microRNAs regulate the G1-S transition and promote rapid proliferation. *Nat. Genet.* **40**, 1478–1483

43. Melton, C., Judson, R. L. & Blelloch, R. (2010). Opposing microRNA families regulate self-renewal in mouse embryonic stem cells. *Nature* **463**, 621–626

44. Kanellopoulou, C. *et al.* (2005). Dicer-deficient mouse embryonic stem cells are defective in differentiation and centromeric silencing. *Genes Dev.* **19**, 489–501

45. Wang, Y. *et al.* (2007). DGCR8 is essential for microRNA biogenesis and silencing of embryonic stem cell self-renewal. *Nat. Genet.* **39**, 380–385

46. Marson, A. *et al.* (2008). Connecting microRNA genes to the core transcriptional regulatory circuitry of embryonic stem cells. *Cell* **134**, 521–33

47. Nam, Y. *et al.* (2011). Molecular basis for interaction of let-7 microRNAs with Lin28. *Cell* **147**, 1080–91

48. Heo, I. J *et al.* (2008). Lin28 Mediates the Terminal Uridylation of let-7 Precursor MicroRNA. *Mol. Cell* **32**, 276–284

49. David, R. (2013). DIS3L2, the final player in let-7 degradation. *Nat. Rev. Mol. Cell Biol.* **14**, 328–328

50. Piskounova, E. *et al.* (2011). Lin28A and Lin28B inhibit let-7 microRNA biogenesis by distinct mechanisms. *Cell* **147**, 1066–79

51. Chang, T.-C. *et al.* (2008). Widespread microRNA repression by Myc contributes to tumorigenesis. *Nat. Genet.* **40**, 43–50

52. Chang, T.-C. *et al.* (2009). Lin-28B transactivation is necessary for Myc-mediated let-7 repression and proliferation. *Proc. Natl. Acad. Sci.* **106**, 3384–3389

53. Worringer, K. A. *et al.* (2014). The let-7/LIN-41 pathway regulates reprogramming to human induced pluripotent stem cells by controlling expression of prodifferentiation genes. *Cell Stem Cell* **14**, 40–52

54. Losson, R. & Lacroute, F. (1979). Interference of nonsense mutations with eukaryotic messenger RNA stability. *Proc Natl Acad Sci USA*. **76**(10):5134-7

55. He, F. & Jacobson, A (2015). Nonsense-Mediated mRNA Decay: Degradation of Defective Transcripts Is Only Part of the Story. *Annu Rev Genet.* **49**:339-66.

56. Lykke-Andersen, S. & Jensen, T. H. (2015). Nonsense-mediated mRNA decay: an intricate machinery that shapes transcriptomes. *Nat. Rev. Mol. Cell Biol.* **16**, 665–677

57. Hug, N., Longman, D. & Cáceres, J. F. (2016). Mechanism and regulation of the nonsense-mediated decay pathway. *Nucleic Acids Res.* **44**, 1483–95

58. Nickless, A., Bailis, J. M. & You, Z. (2017). Control of gene expression through the nonsense-mediated RNA decay pathway. *Cell Biosci.* **7**, 26

59. Kervestin, S. & Jacobson, A. (2012). NMD: a multifaceted response to premature translational termination. *Nat. Rev. Mol. Cell Biol.* **13**, 700–12

60. Le Hir, H. *et al.* (2000). The spliceosome deposits multiple proteins 20-24 nucleotides upstream of mRNA exon-exon junctions. *EMBO J.* **19**(24):6860-9

61. Le Hir, H. *et al.* (2001). The exon-exon junction complex provides a binding platform for factors involved in mRNA export and nonsense-mediated mRNA decay. *EMBO J.* **20**(17):4987-97

62. Lewis, B. P., Green, R. E. & Brenner, S. E. (2003). Evidence for the widespread coupling of alternative splicing and nonsense-mediated mRNA decay in humans. *Proc. Natl. Acad. Sci.* **100**, 189–192

63. Wittmann, J., Hol, E. M. & Jack, H.-M. (2006). hUPF2 Silencing Identifies Physiologic Substrates of Mammalian Nonsense-Mediated mRNA Decay. *Mol. Cell. Biol.* **26**, 1272–1287

64. Bühler, M. *et al.* (2006). EJC-independent degradation of nonsense immunoglobulin-μ mRNA depends on 3' UTR length. *Nat. Struct. Mol. Biol.* **13**, 462–464

65. Eberle, A. B. *et al.* (2008). Posttranscriptional Gene Regulation by Spatial Rearrangement of the 3' Untranslated Region. *PLoS Biol.* **6**(4):e92

66. Hogg, J. R. & Goff, S. P. (2010). Upf1 Senses 3'UTR Length to Potentiate mRNA Decay. *Cell* **143**, 379–389

67. Toma, K. G. *et al.* (2015). Identification of elements in human long 3' UTRs that inhibit nonsense-mediated decay. *RNA* **21**, 887–897

68. Vicente-Crespo, M. & Palacios, I. M. (2010). Nonsense-mediated mRNA decay and development: shoot the messenger to survive? *Biochem. Soc. Trans.* **38**, 1500–1505

69. Han, X. *et al.* (2018). Nonsense-mediated mRNA decay: a 'nonsense' pathway makes sense in stem cell biology. *Nucleic Acids Res.* **46**, 1038–1051

70. Lou, C.-H. *et al.* (2016). Nonsense-Mediated RNA Decay Influences Human Embryonic Stem Cell Fate. *Stem cell reports* **6**, 844–857

71. Lou, C. H. *et al.* (2014). Posttranscriptional Control of the Stem Cell and Neurogenic Programs by the Nonsense-Mediated RNA Decay Pathway. *Cell Rep.* **6**, 748–764

72. Bruno, I. G. *et al.* (2011). Identification of a microRNA that activates gene expression by repressing nonsense-mediated RNA decay. *Mol. Cell* **42**, 500–10

73. Park, E. & Maquat, L. E. (2013). Staufen-mediated mRNA decay. *Wiley Interdiscip Rev RNA.* **4**(4):423-35

74. Gong, C. *et al.* (2009). SMD and NMD are competitive pathways that contribute to myogenesis: effects on PAX3 and myogenin mRNAs. *Genes Dev.* **23**, 54–66

75. Cho, H. *et al.* (2012). Staufen1-Mediated mRNA Decay Functions in Adipogenesis. *Mol. Cell* **46**, 495–506

76. Weischenfeldt, J. *et al.* (2008). NMD is essential for hematopoietic stem and progenitor cells and for eliminating by-products of programmed DNA rearrangements. *Genes Dev.* **22**, 1381–1396

77. Wong, J. J.-L. *et al.* (2013). Orchestrated Intron Retention Regulates Normal Granulocyte Differentiation. *Cell* **154**, 583–595

78. MacDonald, C. C. & Grozdanov, P. N. (2017). Nonsense in the testis: multiple roles for nonsense-mediated decay revealed in male reproduction. *Biol. Reprod.* **96**, 939

79. Reddy, B. A., Etkin, L. D. & Freemont, P. S. (1992). A novel zinc finger coiled-coil domain in a family of nuclear proteins. *Trends Biochem. Sci.* **17**, 344–345

80. Joazeiro, C. & Weissman, M. (2000). RING finger proteins: mediators of ubiquitin ligase activity. *Cell* **102**, 549–52

81. Grigorian, G. & Keating, A. (2008). Structural specificity in coiled-coil interactions. *Curr. Opin. Struct. Biol.* **18**, 477–483

82. Slack, F. J. & Ruvkun, G. (1998). A novel repeat domain that is often associated with RING finger and B-box motifs. *Trends Biochem. Sci.* **23**, 474–475

83. Loedige, I. *et al.* (2014). The NHL domain of BRAT is an RNA-binding domain that directly contacts the hunchback mRNA for regulation. *Genes Dev.* **28**, 749–764

84. Loedige, I. *et al.* (2015). The Crystal Structure of the NHL Domain in Complex with RNA Reveals the Molecular Basis of Drosophila Brain-Tumor-Mediated Gene Regulation. *Cell Rep.* **13**, 1206–1220

85. Kumari, P. *et al.* (2018). Evolutionary plasticity of the NHL domain underlies distinct solutions to RNA recognition. *Nat. Commun.* **9**, 1549

86. Wulczyn, F. G. *et al.* (2010). MiRNAs need a trim: Regulation of miRNA activity by trim-NHL proteins. *Adv. Exp. Med. Biol.* **700**, 85–105

87. Balastik, M. *et al.* (2008). Deficiency in ubiquitin ligase TRIM2 causes accumulation of neurofilament light chain and neurodegeneration. *Proc. Natl. Acad. Sci. USA.* **105**, 12016–21

88. Labonté, D. *et al.* (2013). TRIM3 regulates the motility of the kinesin motor protein KIF21B. *PLoS One* **8**, e75603

89. Liu, Y. *et al.* (2014). TRIM3, a tumor suppressor linked to regulation of p21Waf1/Cip1. *Oncogene* **33**, 308–315

90. Boulay, J.-L. *et al.* (2009). Loss of heterozygosity of TRIM3 in malignant gliomas. *BMC Cancer* **9**, 71

91. Arama, E. *et al.* (2000). Mutations in the β-propeller domain of the Drosophila brain tumor (brat) protein induce neoplasm in the larval brain. *Oncogene* **19**, 3706–3716

92. Page, S. L. *et al.* (2000). Genetic studies of mei-P26 reveal a link between the processes that control germ cell proliferation in both sexes and those that control meiotic exchange in Drosophila. *Genetics* **155**, 1757–72

93. Kudryashova, E. *et al.* (2005). Trim32 is a Ubiquitin Ligase Mutated in Limb Girdle Muscular Dystrophy Type 2H that Binds to Skeletal Muscle Myosin and Ubiquitinates Actin. *J. Mol. Biol.* **354**, 413–424

94. Schwamborn, J. C., Berezikov, E. & Knoblich, J. A. (2009). The TRIM-NHL protein TRIM32 activates microRNAs and prevents self-renewal in mouse neural progenitors. *Cell* **136**, 913–25

95. Betschinger, J., Mechtler, K. & Knoblich, J. A. (2006). Asymmetric Segregation of the Tumor Suppressor Brat Regulates Self-Renewal in Drosophila Neural Stem Cells. *Cell* **124**, 1241–1253

96. Hammell, C. M. *et al.* (2009). NHL-2 Modulates MicroRNA Activity in Caenorhabditis elegans. *Cell* **136**, 926–938

97. Ecsedi, M. & Grosshans, H. (2013). LIN-41/TRIM71: emancipation of a miRNA target. *Genes Dev.* **27**, 581–9

98. Reinhart, B. J. *et al.* (2000). The 21-nucleotide let-7 RNA regulates developmental timing in Caenorhabditis elegans. *Nature* **403**, 901–906

99. Slack, F. J. *et al.* (2000). The lin-41 RBCC gene acts in the C. elegans heterochronic pathway between the let-7 regulatory RNA and the LIN-29 transcription factor. *Mol. Cell* **5**, 659–69

100. Pasquinelli, A. E. *et al.* (2000). Conservation of the sequence and temporal expression of let-7 heterochronic regulatory RNA. *Nature* **408**, 86–89

101. Kloosterman, W. P. *et al.* (2004). Substrate requirements for let-7 function in the developing zebrafish embryo. *Nucleic Acids Res.* **32**, 6284–91

102. Schulman, B. R. M., Esquela-Kerscher, A. & Slack, F. J. (2005). Reciprocal expression of lin-41 and the microRNAs let-7 and mir-125 during mouse embryogenesis. *Dev. Dyn.* **234**, 1046–54

103. Lancman, J. J. *et al.* (2005). Analysis of the regulation of *lin-41* during chick and mouse limb development. *Dev. Dyn.* **234**, 948–960

104. Lin, Y.-C. *et al.* (2007). Human TRIM71 and its nematode homologue are targets of let-7 microRNA and its zebrafish orthologue is essential for development. *Mol. Biol. Evol.* **24**, 2525–34

105. Rybak, A. *et al.,* (2009). The let-7 target gene mouse lin-41 is a stem cell specific E3 ubiquitin ligase for the miRNA pathway protein Ago2. *Nat. Cell Biol.* **11**, 1411–1420

106. Chen, J., Lai, F. & Niswander, L. (2012). The ubiquitin ligase mLin41 temporally promotes neural progenitor cell maintenance through FGF signaling. *Genes Dev.* **26**(8):803-15

107. Chen, Y. L. *et al.* (2013). The stem cell E3-ligase Lin-41 promotes liver cancer progression through inhibition of microRNA-mediated gene silencing. *J. Pathol.* **229**, 486–496

108. Cecco, L. De *et al.* (2014). Identification of a gene expression driven progression pathway in myxoid liposarcoma. *Oncotarget* **5**, 5965

109. Ren, H. *et al.* (2018). E3 ubiquitin ligase tripartite motif-containing 71 promotes the proliferation of non-small cell lung cancer through the inhibitor of kappaB-α/nuclear factor kappaB pathway. *Oncotarget* **9**, 10880–10890

110. Schulman, B. R. M. *et al.* (2008). The let-7 microRNA target gene, Mlin41/Trim71 is required for mouse embryonic survival and neural tube closure. *Cell Cycle.* **7**(24):3935-42

111. Furey, C. G. *et al.* (2018). De Novo Mutation in Genes Regulating Neural Stem Cell Fate in Human Congenital Hydrocephalus. *Neuron* **99**, 302-314.e4

112. Löer, B. *et al.* (2008). The NHL-domain protein Wech is crucial for the integrin–cytoskeleton link. *Nat. Cell Biol.* **10**, 422–428

113. Mitschka, S. *et al.* (2015). Co-existence of intact stemness and priming of neural differentiation programs in mES cells lacking Trim71. *Sci. Rep.* **5**, 11126

114. Tocchini, C. & Ciosk, R. (2015). TRIM-NHL proteins in development and disease. *Semin. Cell Dev. Biol.* **47**–**48**, 52–59

115. Loedige, I. *et al.* (2013). The mammalian TRIM-NHL protein TRIM71/LIN-41 is a repressor of mRNA function. *Nucleic Acids Res.* **41**, 518–32

116. Li, Y. P. *et al.* (2019). A TRIM71 binding long noncoding RNA Trincr1 represses FGF/ERK signaling in embryonic stem cells. *Nat. Commun.* **10**,

117. Nguyen, D. T. T. *et al.* (2017). The ubiquitin ligase LIN41/TRIM71 targets p53 to antagonize cell death and differentiation pathways during stem cell differentiation. *Cell Death Differ.* **24**, 1063–1078

118. Kumar, M. S. *et al.* (2007). Impaired microRNA processing enhances cellular transformation and tumorigenesis. *Nat. Genet.* **39**, 673–677

119. Neumüller, R. A. *et al.* (2008). Mei-P26 regulates microRNAs and cell growth in the Drosophila ovarian stem cell lineage. *Nature* **454**, 241–245

120. O'Farrell, F. *et al.* (2008). Regulation of the *Drosophila lin-41* homologue *dappled* by *let-7* reveals conservation of a regulatory mechanism within the LIN-41 subclade. *Dev. Dyn.* **237**, 196–208

121. Carvajal, L. A. *et al.* (2012). E2F7, a novel target, is up-regulated by p53 and mediates DNA damage-dependent transcriptional repression. *Genes Dev.* **26**, 1533–45

122. de Bruin, A. *et al.* (2003). Identification and characterization of E2F7, a novel mammalian E2F family member capable of blocking cellular proliferation. *J. Biol. Chem.* **278**, 42041–9

123. Ordóñez-Morán P. *et al.* (2015). HOXA5 counteracts stem cell traits by inhibiting Wnt signaling in colorectal cancer. *Cancer Cell* **28**:815–29.

124. Luisi, S. *et al.* (2005). Inhibins in female and male reproductive physiology: role in gametogenesis, conception, implantation and early pregnancy. *Hum. Reprod. Update* **11**, 123–135

125. Deng, S. *et al.* (2007). Plexin-B2, but not Plexin-B1, critically modulates neuronal migration and patterning of the developing nervous system in vivo. *J. Neurosci.* **27**, 6333–47

126. Aeschimann, F. *et al.* (2017). LIN41 Post-transcriptionally Silences mRNAs by Two Distinct and Position-Dependent Mechanisms. *Mol. Cell* **65**, 476-489.e4

127. Harris, D. T. & Horvitz, H. R. (2011). MAB-10/NAB acts with LIN-29/EGR to regulate terminal differentiation and the transition from larva to adult in C. elegans. *Development* **138**, 4051–62

128. Kwon, S. C. *et al.* (2013). The RNA-binding protein repertoire of embryonic stem cells. *Nat. Struct. Mol. Biol.* **20**, 1122–1130

129. Treiber, T. *et al.* (2017). A Compendium of RNA-Binding Proteins that Regulate MicroRNA Biogenesis. *Mol. Cell* **66**, 270-284.e13

130. Castello, A. *et al.* (2012). Insights into RNA Biology from an Atlas of Mammalian mRNA-Binding Proteins. *Cell* **149**, 1393–1406

131. Welte, T. *et al.* (2019). The RNA hairpin binder TRIM71 modulates alternative splicing by repressing MBNL1. *Genes Dev.*

132. Sheth, U. & Parker, R. (2003). Decapping and Decay of Messenger RNA Occur in Cytoplasmic Processing Bodies. *Science* **300**, 805

133. Kulkarni, M., Ozgur, S. & Stoecklin, G. (2010). On track with P-bodies. *Biochem. Soc. Trans.* **38**, 242–251

134. Sun, X. *et al.* (2016). The insights of Let-7 miRNAs in oncogenesis and stem cell potency. *J. Cell. Mol. Med.* **20**, 1779–88

135. Johnson, C. D. *et al.* (2007). The let-7 MicroRNA Represses Cell Proliferation Pathways in Human Cells. *Cancer Res* **67**, 7713–7735

136. West, J. A. *et al.* (2009). A role for Lin28 in primordial germ-cell development and germ-cell malignancy. *Nature* **460**, 909–913

137. Feng, C. *et al.* (2012). Lin28 regulates HER2 and promotes malignancy through multiple mechanisms. *Cell Cycle* **11**, 2486–2494

138. Guo, Y. *et al.* (2006). Identification and characterization of lin-28 homolog B (LIN28B) in human hepatocellular carcinoma. *Gene* **384**, 51–61

139. Urbach, A. *et al.* (2014). Lin28 sustains early renal progenitors and induces Wilms tumor. *Genes Dev.* **28**, 971–82

140. Lee, S. H. *et al.* (2014). The ubiquitin ligase human TRIM71 regulates let-7 microRNA biogenesis via modulation of Lin28B protein. *Biochim. Biophys. Acta - Gene Regul. Mech.* **1839**, 374–386

141. Yin, J. *et al.* (2016). TRIM71 suppresses tumorigenesis via modulation of Lin28B-let-7-HMGA2 signaling. *Oncotarget* **7**, 79854–79868

142. Phan, D. *et al.* (2019). Trim71 Links an Ancient MicroRNA Pathway to Neural Stem Cell Development and Human Congenital Hydrocephalus. Trends Mol. Med. **25**(6):467-469

143. Waterhouse, A. *et al.* (2018). SWISS-MODEL: Homology modelling of protein structures and complexes. *Nucleic Acids Res.* **46**, W296–W303

144. Emsley, P. & Cowtan, K. (2004). Coot: Model-building tools for molecular graphics. *Acta Crystallogr. Sect. D Biol. Crystallogr.* **60**, 2126–2132

145. Brown, A. S., Mohanty, B. K. & Howe, P. H. (2015). Computational Identification of Post Translational Modification Regulated RNA Binding Protein Motifs. *PLoS One* **10**, e0137696

146. Kastritis, P. L. & Bonvin, A. M. J. J. (2013). On the binding affinity of macromolecular interactions: Daring to ask why proteins interact. *J R Soc Interface.* **10**(79):20120835

147. Heo, I. *et al.* (2009). TUT4 in Concert with Lin28 Suppresses MicroRNA Biogenesis through Pre-MicroRNA Uridylation. *Cell* **138**, 696–708

148. Cuevas, E. *et al.* (2015). Lin41/Trim71 is essential for mouse development and specifically expressed in postnatal ependymal cells of the brain. *Front Cell Dev Biol.* **3**:20

149. Torres-Fernández, L. A. *et al.* (2019). The mRNA repressor TRIM71 cooperates with Nonsense-Mediated Decay factors to destabilize the mRNA of CDKN1A/p21. *Nucleic Acids Res.* **pii:** gkz1057

150. Niculescu, A. B. *et al.* (1998). Effects of p21(Cip1/Waf1) at both the G1/S and the G2/M cell cycle transitions: pRb is a critical determinant in blocking DNA replication and in preventing endoreduplication. *Mol. Cell. Biol.* **18**, 629–43

151. Schmidt, M.-J., West, S. & Norbury, C. J. (2011). The human cytoplasmic RNA terminal U-transferase ZCCHC11 targets histone mRNAs for degradation. *RNA* **17**, 39

152. Chang, Y.-F., Imam, J. S. & Wilkinson, M. F. (2007). The Nonsense-Mediated Decay RNA Surveillance Pathway. *Annu. Rev. Biochem.* **76**, 51–74

153. Pehz, S. W., Brown, A. H. & Jacobson, A. (1993). mRNA destabilization triggered by premature translational termination depends on at least three cis-acting sequence elements and one trans-acting factor. *Genes Dev.* **7**(9):1737-54

154. Lejeune, F., Li, X. & Maquat, L. E. (2003). Nonsense-Mediated mRNA Decay in Mammalian Cells Involves Decapping, Deadenylating, and Exonucleolytic Activities. *Mol. Cell* **12**, 675–687

155. Brogna, S. & Wen, J. (2009). Nonsense-mediated mRNA decay (NMD) mechanisms. *Nat Struct Mol Biol.* **16**(2):107-13

156. Isken, O. & Maquat, L. E. (2008). The multiple lives of NMD factors: Balancing roles in gene and genome regulation. *Nature Reviews Genetics* **9**, 699–712

157. Maquat, L. E., Tarn, W. Y. & Isken, O. (2010). The pioneer round of translation: Features and functions. *Cell* **142**, 368–374

158. Rufener, S. C. & Mühlemann, O. (2013). EIF4E-bound mRNPs are substrates for nonsense-mediated mRNA decay in mammalian cells. *Nat. Struct. Mol. Biol.* **20**, 710–717

159. Chakrabarti, S. *et al.* (2014). Phospho-dependent and phospho-independent interactions of the helicase UPF1 with the NMD factors SMG5-SMG7 and SMG6. *Nucleic Acids Res.* **42**, 9447–60

160. Karam, R., Lou, C.-H., Kroeger, H., Huang, L., Lin, J. H. & Wilkinson, M. F. (2015). The unfolded protein response is shaped by the NMD pathway. *EMBO Rep.* **16**, 599–609

161. Yepiskoposyan, H. *et al.* (2011). Autoregulation of the nonsense-mediated mRNA decay pathway in human cells. *RNA* **17**, 2108–2118

162. Brumbaugh, K. M. *et al.* (2004). The mRNA Surveillance Protein hSMG-1 Functions in Genotoxic Stress Response Pathways in Mammalian Cells. *Mol. Cell* **14**, 585–598

163. Azzalin, C. M. & Lingner, J. (2006). The human RNA surveillance factor UPF1 is required for S phase progression and genome stability. *Curr. Biol.* **16**, 433–9

164. Luo, H. *et al.* (2016). SMG7 is a critical regulator of p53 stability and function in DNA damage stress response. *Cell Discov.* **2**, 15042

165. Janke, R. *et al.* (2016). Nonsense-mediated decay regulates key components of homologous recombination. *Nucleic Acids Res.* **44**, 5218–5230

166. Mendell, J. T. *et al.* (2004). Nonsense surveillance regulates expression of diverse classes of mammalian transcripts and mutes genomic noise. *Nat. Genet.* **36**, 1073–1078

167. Viegas, M. H. *et al.* (2007). The abundance of RNPS1, a protein component of the exon junction complex, can determine the variability in efficiency of the Nonsense Mediated Decay pathway. *Nucleic Acids Res.* **35**, 4542–51

168. Amrani, N. *et al.* (2004). A faux 3'-UTR promotes aberrant termination and triggers nonsense-mediated mRNA decay. *Nature* **432**, 112–118

169. Tani, H. *et al.* (2012). Identification of hundreds of novel UPF1 target transcripts by direct determination of whole transcriptome stability. *RNA Biol.* **9**, 1370–1379

170. Kim, K. M., Cho, H. & Kim, Y. K. (2012). The upstream open reading frame of cyclin-dependent kinase inhibitor 1A mRNA negatively regulates translation of the downstream main open reading frame. *Biochem. Biophys. Res. Commun.* **424**, 469–475

171. Singh, G., Rebbapragada, I. & Lykke-Andersen, J. (2008). A Competition between Stimulators and Antagonists of Upf Complex Recruitment Governs Human Nonsense-Mediated mRNA Decay. *PLoS Biol.* **6**, e111

172. Ivanov, P. V. *et al.* (2008). Interactions between UPF1, eRFs, PABP and the exon junction complex suggest an integrated model for mammalian NMD pathways. *EMBO J.* **27**, 736–747

173. Kahle, K. T. *et al.* (2016). Hydrocephalus in children. *Lancet* **387**, 788–799

174. Munch, T. N. *et al.* (2012). Familial aggregation of congenital hydrocephalus in a nationwide cohort. *Brain* **135**, 2409–15

175. Bothwell, S. W., Janigro, D. & Patabendige, A. (2019). Cerebrospinal fluid dynamics and intracranial pressure elevation in neurological diseases. *Fluids Barriers CNS.* **16**(1):9

176. Baron-Benhamou, J. *et al.* (2004). Using the lambdaN peptide to tether proteins to RNAs. *Methods Mol Biol.* **257**:135-54.

177. Abranches, E. *et al.* (2009). Neural Differentiation of Embryonic Stem Cells In Vitro: A Road Map to Neurogenesis in the Embryo. *PLoS One* **4**, e6286

178. Urbán, N. & Guillemot, F. (2014). Neurogenesis in the embryonic and adult brain: Same regulators, different roles. *Frontiers in Cellular Neuroscience* **8**,

179. Götz, M., Nakafuku, M. & Petrik, D. (2016). Neurogenesis in the developing and adult brain—similarities and key differences. *Cold Spring Harb Perspect Biol.* **8**(7). pii: a018853

180. Büssing, I., Slack, F. J. & Grosshans, H. (2008). let-7 microRNAs in development, stem cells and cancer. *Trends Mol. Med.* **14**, 400–9

181. Thornton, J. E. *et al.* (2012). Lin28-mediated control of let-7 microRNA expression by alternative TUTases Zcchc11 (TUT4) and Zcchc6 (TUT7). *RNA* **18**, 1875–1885

182. Choudhury, N. R. *et al.* (2014). Trim25 Is an RNA-Specific Activator of Lin28a/TuT4-Mediated Uridylation. *Cell Rep.* **9**, 1265–1272

183. Nowak, J. S. *et al.* (2014). Lin28a regulates neuronal differentiation and controls miR-9 production. *Nat. Commun.* **5**, 3687

184. Peter, M. E. (2009). Let-7 and miR-200 microRNAs: Guardians against pluripotency and cancer progression. *Cell Cycle* **8**, 843–852

185. Suzuki, H. I., Katsura, A. & Miyazono, K. (2015). A role of uridylation pathway for blockade of let-7 microRNA biogenesis by Lin28B. *Cancer Sci.* **106**, 1174–81

186. Rosa, A. & Brivanlou, A. H. (2013). Regulatory non-coding RNAs in pluripotent stem cells. *Int J Mol Sci.* **14** (7):14346–73

187. Jee, D. & Lai, E. C. (2014). Alteration of miRNA activity via context-specific modifications of Argonaute proteins. *Trends Cell Biol.* **24** (9): 546–53

188. Patranabis, S. & Bhattacharyya, S. N. (2016). Phosphorylation of Ago2 and Subsequent Inactivation of let-7a RNP-Specific MicroRNAs Control Differentiation of Mammalian Sympathetic Neurons. *Mol. Cell. Biol.* **36**, 1260–1271

189. Hu, Q. *et al.* (2019). Oncogenic lncRNA downregulates cancer cell antigen presentation and intrinsic tumor suppression. *Nat. Immunol.* **20**, 835–851

190. Abbas, T. & Dutta, A. (2009). p21 in cancer: intricate networks and multiple activities. *Nat. Rev. Cancer* **9**, 400–14

191. Hiyama, H., Iavarone, A. & Reeves, S. A. (1998). Regulation of the cdk inhibitor p21 gene during cell cycle progression is under the control of the transcription factor E2F. *Oncogene* **16**, 1513–1523

192. Liu, A. M. *et al.* (2011). Global Regulation on microRNA in Hepatitis B Virus-Associated Hepatocellular Carcinoma. *Omi. A J. Integr. Biol.* **15**, 187–191

193. Ye, Z. *et al.* (2015). Argonaute 2 promotes angiogenesis via the PTEN/VEGF signaling pathway in human hepatocellular carcinoma. *Acta Pharmacol. Sin.* **36**, 1237–1245

194. Cheng, N., Li, Y. & Han, Z.-G. (2013). Argonaute2 promotes tumor metastasis by way of up-regulating focal adhesion kinase expression in hepatocellular carcinoma. *Hepatology* **57**, 1906–1918

195. Kurosaki, T. & Maquat, L. E. (2016). Nonsense-mediated mRNA decay in humans at a glance. *J. Cell Sci.* **129**, 461–7

196. Silva, A. L. *et al.* (2008). Proximity of the poly(A)-binding protein to a premature termination codon inhibits mammalian nonsense-mediated mRNA decay. *Rna* **14**, 563–576

197. Kashima, I. *et al.* (2006). Binding of a novel SMG-1-Upf1-eRF1-eRF3 complex (SURF) to the exon junction complex triggers Upf1 phosphorylation and nonsense-mediated mRNA decay. *Genes Dev.* **20**(3):355-67

198. Safaee, N. *et al.* (2012). Interdomain allostery promotes assembly of the poly(A) mRNA complex with PABP and eIF4G. *Mol. Cell* **48**, 375–86

199. Williams, S. G. & Hall, K. B. (2014). Linkage and allostery in snRNP protein/RNA complexes. *Biochemistry* **53**, 3529–39

200. Lee, S. H. *et al.* (2014). Poly(A) RNA and Paip2 act as allosteric regulators of poly(A)-binding protein. *Nucleic Acids Res.* **42**, 2697–2707

201. Hong, K. Y. *et al.* (2017). The bent conformation of poly(A)-binding protein induced by RNA-binding is required for its translational activation function. *RNA Biol.* **14**, 370–377

202. Popp, M. W. & Maquat, L. E. (2018). Nonsense-mediated mRNA Decay and Cancer. *Curr. Opin. Genet. Dev.* **48**, 44–50

203. Nelson, J. O. *et al.* (2016). Degradation of Gadd45 mRNA by nonsense-mediated decay is essential for viability. *Elife* **5**, pii: e12876

204. Popp, M. W. & Maquat, L. E. (2015). Attenuation of nonsense-mediated mRNA decay facilitates the response to chemotherapeutics. *Nat. Commun.* **6**, 6632

205. Tarpey, P. S. *et al.* (2007). Mutations in UPF3B, a member of the nonsense-mediated mRNA decay complex, cause syndromic and nonsyndromic mental retardation. *Nat. Genet.* **39**, 1127–1133

206. Nguyen, L. S. *et al.* (2013). Contribution of copy number variants involving nonsense-mediated mRNA decay pathway genes to neuro-developmental disorders. *Hum. Mol. Genet.* **22**, 1816–1825

207. Alrahbeni, T. *et al.* (2015). Full UPF3B function is critical for neuronal differentiation of neural stem cells. *Mol. Brain* **8**, 33

208. McMahon, J. J., Miller, E. E. & Silver, D. L. (2016). The exon junction complex in neural development and neurodevelopmental disease. *Int. J. Dev. Neurosci.* **55**, 117–123

Acknowledgements

First of all, I would like to deeply thank Prof. Dr. Waldemar Kolanus, because he gave me much more than the opportunity to work in this project; he gave me help and support through all these years, he always looked after me and provided me with all kinds of opportunities for my career and my future. He gave me understanding in my bad days, and more importantly, he gave me trust in myself, as he always showed great interest, respect and consideration for my work. We have been a great team together.

I would also like to express my gratitude to Prof. Dr. Matthias Geyer, Prof. Dr. Günter Mayer and Prof. Dr. Christoph Thiele for their interest in my project and their contribution to it. I would like to express my acknowledgement as well to my dissertation's committee (Prof. Dr. Waldemar Kolanus, Prof. Dr. Michael Pankratz, Prof. Dr. Matthias Geyer and Prof. Dr. Ulf Meißner) for the evaluation of my work. Furthermore, I thank the ImmunoSensation Cluster of Excellence and Bayer Pharmaceuticals for the funding of this project.

I am really grateful to all the members of the LIMES institute, with special mention to the members of the Kolanus and Kiermeier labs, for providing a wonderful work atmosphere, for the stimulating scientific discussions, and more importantly, for their constant moral support and their sincere interest in my success and my wellbeing. I want to specially thank Dr. Karin Schneider and Dr. Sibylle Mitschka, who generated a great deal of knowledge in which my work is founded, and who mentored me in earlier years as I started working in this project. I will always be thankful to Dr. Bettina Jux, for all her help and support, and for really being an inspiring person, since I truly look up to her scientifically and personally. My acknowledgement also to the rest of the *TRIM-team*, Yasmine Port and Dr. Stefan Weise, as well as to my productive students Max Bille, Miki Uchima, Yubell Alvarez and Julia Windhausen, for all their contributions to the TRIM71 project. A big thanks goes also to Barbara Reichwein and Christa Mandel, since they have provided me with constant help of all kinds over these years. Angrit Namislo, for being a great "battle companion", despite both of us fighting quite different battles. Gertrud Mierzwa and Katharina Klein, for always bringing a breeze of good mood as they entered our lab. And last, but not least, Dr. Felix Eppler, Dr. Lorenz Fülle and Dr. Philipp Schlegel, for being much more than colleagues over the last years, for all their support and their love, and for all the fun in and out of the lab. Their friendship is the biggest treasure I got out of my time in the LIMES institute.

For everything I have and everything I am, I want to thank my family, especially my parents, who showed me the biggest love and support all over my life, and who always believed in me. They inspired me to work hard and never give up. But more importantly, they always encouraged me to be honest, fair, and good in my heart, and to always help and respect others. I am really lucky to have them.

Last, I want to thank my soul family: my friends (all M.As and OKTOPUS extraordinary people) and my wonderful boyfriend Lukas, all of them for being the best thing that ever happened to me, and for making of Germany my home. I am deeply grateful for everything I have enjoyed by their side, for everything I have learnt from each of them, and for everything still to come. Their love and the light they bring into my life is the true engine driving my inner strength. DANKE!